Theoretische Medizin und Biowissenschaften

der Medizinischen Fakultät

der Universität des Saarlandes, Homburg/Saar

Aus dem Bereich Molekulare Biophysik

Investigation of calcium signatures in human CD4$^+$ T cells with a focus on modulation of differentiation by plasma membrane ATPases

DISSERTATION

TO FULFILL THE REQUIREMENTS FOR THE DEGREE OF

"DOCTOR RERUM NATURALIUM" (DR. RER. NAT.)

der Medizinischen Fakultät

der UNIVERSITÄT DES SAARLANDES

2020

By Maylin Merino Wong

Born on 15th of November 1988 in Havana, Cuba

List of Contents

1 Summary

The immune system is optimized to provide protection against pathogens while maintaining immune tolerance to self-antigens. During the establishment of an immune response, components of the innate system are essential for the early constraint of the infection and for orchestrating activation, expansion and differentiation of cells of the adaptive immune system. T cells of the adaptive immune system represent a stronger mean of defense with increased protection during recall responses. In this regard, the establishment of the adaptive immune response relies on the activation and programing of naïve T cells into effector cells after proper cognate antigen recognition, which allows the primed T cells to proliferate and differentiate into cells with a variety of functions needed to fight against the pathogen. Following pathogen clearance, the majority of effector cells die, leaving behind different memory T cell subsets. These memory cells are different in their functions and migratory properties, thereby mediating rapid and specific immune responses upon re-infection. One of the most important mediators of T cell activation is the second messenger Calcium ion (Ca^{2+}), which control complex and essential effector functions such as proliferation, differentiation, metabolism, cytokine secretion and cytotoxicity. In this regard, inadequate Ca^{2+} regulation can lead to various autoimmune, inflammatory and immunodeficiency syndromes.

In the first part of this work, we studied the Ca^{2+} profiles of human T helper subtypes and proposed different mechanisms that may contribute to their Ca^{2+} differences in phenotypes following store operated Ca^{2+} entry (SOCE). We also investigated the Ca^{2+} profiles of regulatory T cells and found out that *in vivo* regulatory T cells, as the *in vitro* regulatory T cells, showed the highest Ca^{2+} SOCE peak. Our results indicate that a lower expression of Orai2 in regulatory T cells than in conventional T cells may contribute to the higher Ca^{2+} peak. Interestingly, memory T cells polarized into Th17 cells showed the highest expression of *ATP2B4* among the $CD4^+$ T helper subtypes, which lead us to investigate the role of PMCAs in fate decisions within the $CD4^+$ T cell compartments.

In the second part of this work, we show how plasma membrane Ca^{2+} ATPase isoform 4 (PMCA4) regulates the levels of intracellular Ca^{2+} within the $CD4^+$ T cell compartment. Modulation of PMCA either by allosteric inhibition of PMCA4 pump activity through pharmacological inhibition or siRNA-mediated downregulation increased SOCE in memory but not in naïve $CD4^+$ T cells. Importantly, downregulation of PMCA4 in naïve $CD4^+$ T cells, followed by polyclonal stimulation, decreased the percentage of primed cells expressing effector markers upon activation indicating a role of PMCA during the effector phase of the T cell response. Furthermore, we showed for the first time that PMCA4 is differentially expressed in human $CD4^+$ T cell compartments which resulted in distinct store operated Ca^{2+} entry profiles. Along this line, PMCA4 was increasingly up-regulated in the order naïve, central memory (CM) T cells, effector memory (EM) and effector memory RA positive ($EMRA^+$) T cells, which corroborated its role in memory fate decisions during T cell responses. On the other hand, analysis of calcium signals after disturbing mitochondrial function in naïve and memory T cells in both resting and under activation with a polyclonal stimulus, showed that memory cells rely more on PMCA4 for controlling the amplitude and dynamic of SOCE, while naïve T cells make preferential use of mitochondrial Ca^{2+} uptake to shape SOCE.

Summary

To unravel the underlying mechanism of regulation of expression of PMCA, in silico analysis of transcription factors binding to the promoter of the PMCA4 identified Yin Yang 1 (YY1) as a potential transcription factor. This prediction was further confirmed by chromatin immunoprecipitation (ChIP). Furthermore, time-dependent protein expression of YY1 and PMCA4, following activation of naïve T cells together with *in vitro* polarization into Th1 or regulatory T cells specific subtypes, revealed a dual role of YY1 in PMCA4 expression. In this regard, YY1 may act directly or indirectly as a repressor of PMCA4 during the Ca^{2+}-driven activation with the termination of its repressive activity once the cells are engaged to the memory lineage, thereby reestablishing the homeostatic Ca^{2+} levels needed for the culmination of immune response.

2 Introduction

2.1 CD4$^+$ T cell responses and memory formation

2.1.1 Origin and maturation of T lymphocytes

The cells of the immune system are derived from bone marrow-resident hematopoietic stem cells (HSCs) that give rise to a variety of progenitor populations generating all lineages of cells found in mature blood. In the bone marrow, HSC develop into a common myeloid progenitor (CMP) or a common lymphoid progenitor (CLP) (Orkin & Zon, 2008). The CMP gives rise to erythrocytes, platelets, basophils, eosinophils, monocytes and dendritic cells (DCs) (Akashi et al., 2000), whereas the CLP gives rise to B cells, T cells, natural killer cells and some DCs (Kondo et al., 1997). While the maturation of B cells from a CLP occurs mostly in the marrow and fetal liver before birth, precursors of T lymphocytes leave the fetal liver before birth and the bone marrow later in life and migrate to the thymus to complete their maturation. The majority of T cells harboring T cell receptors (TCR) with γδ chains arise from fetal liver HSCs, whereas cells harboring TCR with αβ chains from bone marrow-derived HSCs (Mold et al., 2010). Despite their different anatomical origin, the early events of maturation are similar. Most CLP express the C-C chemokine receptor type 7 (CCR7) and C-C chemokine receptor type 9 (CCR9), allowing their chemiotaxis from the bone marrow to the thymus attracted by their CC-chemokine ligand 19 (CCL19), CC-chemokine ligand 21 (CCL21) and CC-chemokine ligand 25 (CCL25). CCL19 and CCL21 are the ligands of CCR7 and are expressed by stromal cells, whereas CCL25 is the ligand for CCR9 and is expressed by medullary dendritic and cortical epithelial cells in the thymus (Uehara et al., 2002; Zlotoff et al., 2010). Due to the thymus does not contain self-renewing progenitors depends on the constant recruitment of precursors. The CLP entering the thymus differentiate into an early thymic progenitor (ETP) that localizes in the outer cortical region of the thymus and subcapsular sinus (Figure 1). The ETPs are multipotent cells with the ability to generate all lineages of lymphocytes. The final commitment to a specific T lineage depends on the transcriptional program triggers during signaling through several cell surface receptors expressed on ETPs. In these cells, the cleavage of surface Notch family proteins after interacting with its ligand on surrounding cells, induce migration of the cleaved intracellular portion of Notch proteins resulting in gene modulation (Dontje et al., 2006). For instance, Notch proteins collaborate with the transcription factor GATA-3a, Runx1 and E-box proteins, to commit developing lymphocytes to the T lineage (Carpenter & Bosselut, 2010; Dontje et al., 2006). These transcription factors induce downstream genes further required for the development of αβ T cells such as components of the pre-TCR and the VDJ recombination machinery. On the other hand, the cytokine interleukin-7 (IL-7), (produced by stromal fibroblasts in the bone marrow and by cortical epithelial cells in the thymus) is required for the proliferation of ETPs (Peschon et al., 1994; Plum et al., 1996), thereby increasing the number of progenitors of T cells that give rise to antigen-specific T cells after VDJ recombination. The ETP contains TCR genes in germline configuration, and does not express TCR, CD3, ζ chains, CD4 or CD8; therefore, are considered double negative (DN) and pro-T cells (cells in a pro-T cell stage). During the pro-T cell stage, recombination activating gene 1 and 2 (Rag1 and Rag2) are expressed and rearrangement at TCR β locus take places in a step-wise manner through sequential phenotypic stages from DN1 to DN3 (Carpenter & Bosselut, 2010). This process consists in the assembly of V, D and J gene

segments to produce rearranged V genes that encode the antigen-receptor variable region (V). Maximal variability is achieved by adding or removing nucleotides being joined together. In fact, it has been shown that repertoire of lymphocytes harboring distinct antigen specificity is around 10^7 or more (Cano R & Lopera H, 2013). Because of the deletion and untemplated addition of nucleotides during Rag mediated recombination, the majority of the rearrangements are out-of-frame and fail to produce genes encoding a functional protein (Carpenter & Bosselut, 2010). If a pro-T cell rearranges successfully its TCR-β chain gene, then the β chain is expressed on the surface in association with the invariant protein pre-Tα, CD3 and ζ proteins forming the pre-T cell receptor (pre-TCR). Only developing T cells that synthesize the TCR-β chain protein and assemble a pre-TCR can continue the maturation process, whereas cells that failed undergo programed cell death (Carpenter & Bosselut, 2010). The assembly of the pre-TCR provides signals for survival, proliferation, allow β chain allelic exclusion and drive the transition from the double-negative to the double-positive stage of thymocyte development (Carpenter & Bosselut, 2010; von Boehmer & Fehling, 1997). Following pre-TCR formation, the synthesis of α chain starts in $CD4^+CD8^+$ double-positive (DP) cells. A second increase in Rag gene expression at the late stage of pre-T cells promotes α gene recombination, which is characterized for only V to J rearrangement at the α chain locus. Contrary to the β chain locus, little or absent exclusion allelic has been shown for the α chain locus, making possible the co-existence of TCR-α receptors with different α chains but a unique β chain. In the double positive stage, the co-expression of TCR α chain, CD3 and ζ proteins lead to assembly of the complete TCR-αβ. As results of rearrangement of the TCR α gene, the TCR δ locus lying between V segments (common to both α and δ loci) and Jα segments is deleted, which commit the T cells to the αβ T cell lineage. Next, a process of negative and positive selection allows preserving useful cells and eliminating potentially harmful ones, as well as allow to the thymocytes to mature into $CD4^+$ or $CD8^+$ T cells. In the thymic cortex, DP thymocytes with randomly generated specificities interact with thymic epithelial cells (TEC) displaying a variety of self-peptides bound to the major histocompatibility complex (MHC) class I and class II (found in most of the vertebrates) or to the human leukocyte antigen (HLA) complex class I and class II (in humans). Therefore, DP T cells that do not find any "self-antigen-MHC-complex" die by apoptosis, whereas T cells that recognize this complex with intermediate affinity and avidity are rescued from apoptosis (Positive selection) (Figure 1). In parallel to this process DP cells develop into single positive CD4 or CD8 based on which MHC molecules (MHC class II or MHC class I molecules) are recognized by the TCR. Therefore, positive selection permits the commitment of the DP thymocytes towards a single T cell lineage that is restricted to MHC. Subsequently, SP cells enter the medulla of the thymus and interact with self-antigens presented by medullary thymic epithelial (mTEC) cells and DCs. T cells with TCRs recognizing with high affinity or avidity "self-antigen-MHC-complex" are deleted in a process known as negative selection (a process essential for central tolerance) (Figure 1) (von Boehmer & Melchers, 2010) or may develop into Regulatory T (reg T) cells, which harbor receptors with higher avidity for self than conventional MHC II-restricted cells (Bautista et al., 2009; Josefowicz & Rudensky, 2009). Thereby, negative selection assuring the destruction of potentially autoreactive cells while preventing autoimmunity (Anderson & Takahama, 2012). Cells that survive negative selection become naïve T cells that leave the thymus and become effector cells with specialized phenotypes after proper cognate peptide-MHC (cognate p-MHC) recognition inside the secondary lymph nodes (SLN).
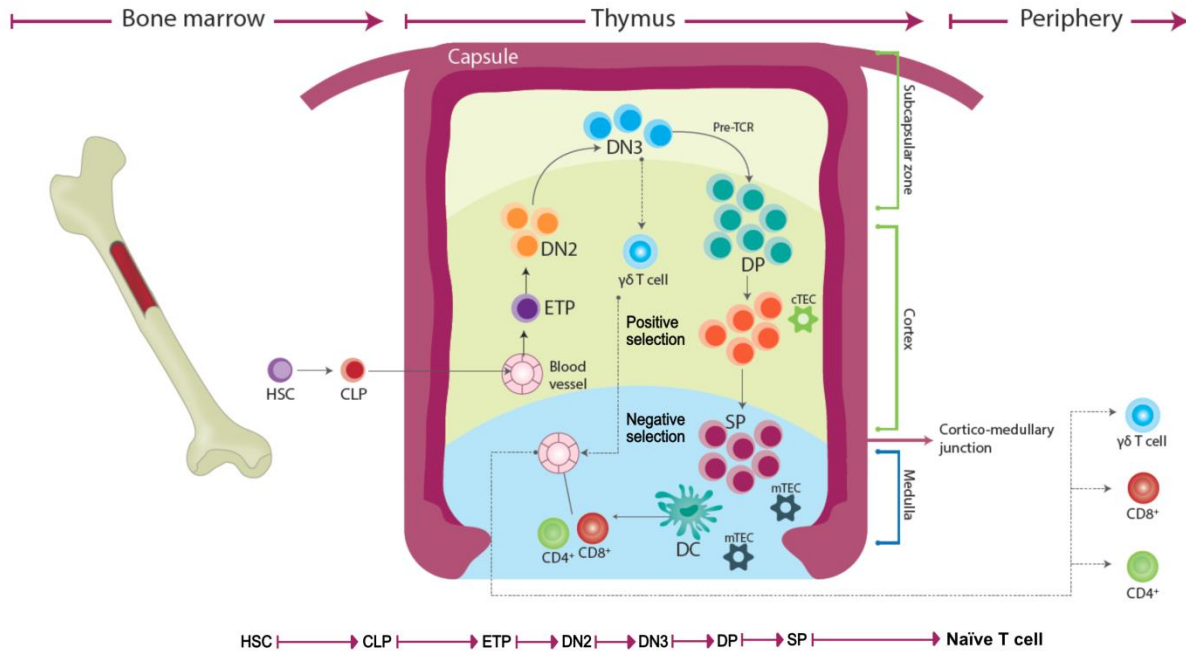
Figure 1: Overview of T cell development and maturation.
A subset of hematopoietic stem cells (HSC) in bone marrow initiates the transcription of recombination activating gene 1 and 2 (RAG1 and RAG2) and develops into common lymphoid progenitors (CLP). A small subset of the CLP migrates to the thymus via blood vessels to give rise to early thymic progenitors (ETP). Within the thymic cortex, ETP differentiate into double negative (DN) cells (CD4-CD8-). At the DN2 stage of development, cells express the Rag proteins to start T Cell Receptor (TCR) gene rearrangement, as well as proteins needed (CD3 chains, kinases and phosphatases) for TCR assembly and its downstream signaling. At DNA3 cells can follow divergent pathways, either they form αβ chains and give rise to CD4$^+$ or CD8$^+$ T cells with a αβ TCR or form γδ chains and give rise to γδ T lymphocytes. The expression of the β chain at this stage enables the expression of CD4 and CD8 double positive cells (DP). At this point, the DP cells with TCRs with intermediate affinity and avidity for self-peptides are selected. The epithelial cells of the thymic cortex (cTEC) present self-peptides in the context of the class I and class II HLA molecules. Only 1 to 5% of the DP cells harboring TCRs with intermediate affinity for self-peptides are programmed to survive, whereas cells that fail to recognize self-peptides-HLA complex undergo apoptosis. Positive selection also allows HLA restriction, cells that bind to HLA-I develop into CD4-CD8$^+$ and those that bind to HLA-II develop into CD4$^+$CD8-. Afterwards, single positive (SP) cells entering the medulla of the thymus go through negative selection. SP cells interact with a range of self-antigens presented by medullary thymic epithelial cells (mTEC) and dendritic cells (DCs) and those that bind with high avidity or affinity to self-peptides-HLA-I or self-peptides-HLA-II molecules die by apoptosis, guaranteeing that only non-reactive cells endure. Cells that pass negative selection mature into naïve T cells that leave the thymus and migrate through lymph nodes searching their cognate antigen to differentiate into effector T cells. Figure taken from (Cano R & Lopera H, 2013).

2.1.2   Activation and differentiation of human naïve CD4$^+$ T Cells

T cell responses are elicited inside the germinal centers of the lymph nodes (LN). There, the binding of cognate p-MHC on Antigen Presenting Cells (APC) to the T cell receptor complex on T cells initiates the signaling cascade that ends with the acquisition of effector functions on T cells. Optimal priming in CD4$^+$ T cells can last 1 to 2 days (Gasper et al., 2014) and requires not only antigen recognition but also cell-to

cell contact, co-receptors molecules, and cytokine signaling. Interactions between the co-receptors CD4 or CD8 and invariant parts of the p-MHC complex are needed to stabilize the TCR-agonist p-MHC complex on APC or target cells respectively, as well as for early signal transduction (Artyomov et al., 2010). On the other hand, the ligation of TCR and co-receptors is an indispensable step in the signaling cascade downstream TCR, but not enough to activate naïve T cells which require interactions through their stimulator molecules CD28 with CD80 (B7-1) and CD86 (B7-2) located on activated APC, triggering their optimal differentiation into effector cells and avoidance of anergy (Beyersdorf et al., 2015). Although some proteins downstream of the TCR pathway require stimulation through CD28 coreceptors, others are CD28 stimulation-independent, yielding a model in which CD28 co-stimulation amplifies TCR stimulation (Acuto & Michel, 2003). On the other hand, antigen recognition by T cells in conjunction with CD28 activation induces the expression of the ligand for CD40 (CD40L) on activated T cells. CD40L is generated rapid and transiently by activated T cells and interactions CD40L with CD40 on B cells are important for the differentiation, proliferation, immunoglobulin (Ig) isotype switching and generation of memory B cells (Elgueta et al., 2009). CD40L also engages CD40 on APC and may stimulate or increase the expression of B7 molecules on the APC, thereby increasing APC activation and the secretion of cytokines such as interleukin 12 (IL-12) that activate T cells. The binding of B7 to CD28 lowers the threshold sensitivity to p:MHC-TCR signalling (Riha & Rudd, 2010). Thus, B7 and CD40L pathways stimulate each other. Solid evidence has demonstrated that Ca^{2+} is the main messenger molecule inducing CD40L gene transcription. For instance, dephosphorylation of the nuclear factor of activated T-cells (NFAT) by the Ca^{2+}-dependent phosphatase calcineurin (CaN), leads to NFAT activation and its nuclear translocation. Next, nuclear NFAT cooperates with activating protein 1 (AP-1) to mediate CD40L transcriptional regulation (Fuleihan et al., 1994). In this line, Cyclosporine A (CsA), a potent inhibitor of CaN eliminates CD40L expression on normal T cells (Fuleihan et al., 1994). The emerging role of CD40L in immunity-associated inflammation implicates CD40L as a player in systemic lupus erythematous (SLE) (Desai-Mehta et al., 1996; Katsiari et al., 2002), rheumatoid arthritis (RA) (Berner et al., 2000; Harigai et al., 1999), in transplantation (Yu et al., 2001) and even in atherosclerosis (Mach et al., 1998; Schonbeck & Libby, 2001).

T cell activation is usually observed in a time scale of hours to days (Gasper et al., 2014). Lymphocytes constantly migrate from the blood to secondary lymphoid organs (SLO) and egress from SLO to the blood one or two times per day during homeostasis in search of cognate antigens (Girard et al., 2012). Post-thymic naïve T cells require IL-7 and self-p-MHC signals for their homeostatic survival. These interactions generate sub-mitogenic signals that keep the naïve T cells alive and in interphase (Boyman et al., 2009; Surh & Sprent, 2008). Thus, naïve T cells hardly divide and their frequency are kept after the onset of thymic atrophy at puberty (Tough & Sprent, 1994). Naïve lymphocytes enter the LN node via high endothelial venules (HEVs) or afferent lymphatic vessels and egress through cortical sinuses, medullary sinuses and the efferent lymphatic vessel in the medulla (Girard et al., 2012). The entry of circulating lymphocytes to the LN starts with the binding of the homing receptor L-selectin (CD62L), constitutively expressed on naïve T cells, to the endothelium of the HEVs (Yang, S et al., 2011). CD62L decelerates lymphocytes by interacting with ligands expressed on HEVs and subsequently a signaling cascade beginning with triggering of CCR7, expressed also constitutively in naïve T cells, leads to firm arrest and lymphocyte transmigration into the LN (Warnock et al., 1998). Therefore, the expression of these molecules on lymphocytes guarantees their binding to the LN. Recent evidence also suggested that naïve T cells have to home to SLN in order to

maintain a stable population size. In this line, a subset of glycoprotein gp381 stromal cells in secondary lymphoid organs, termed fibroblastic reticular cells, has been reported to be a major source of IL-7 and also the site of secretion of the CCR7 ligands: CCL19 and CCL21 (Link et al., 2007). Activation of naïve T cells after encountering the cognate p-MHC on the APC in the LN is followed by early and late surface expression of activation markers such as CD69 (very early), Transferring Receptor (CD71) (late), Interleukin-2 receptor alpha chain (CD25) (late) and Human Leukocyte Antigen-DR isotype (HLA-DR) (very late) (Reddy et al., 2004). The molecule CD69 is a type II membrane glycoprotein, member of the C-type lectin family and it is the earliest activation marker in T cells. CD69 expression is increased in a time dependent manner within 2-3 hours (Cosulich et al., 1987) reaching a peak around 12 hours (Reddy et al., 2004; Ziegler et al., 1994). Apart of TCR mediated activation, interferon-alpha/beta (IFN-α/β) and tumor necrosis factor-α (TNF-α) have been also shown to increase CD69 expression (Gonzalez-Amaro et al., 2013). The binding of CD69 to galectin-1 (Gal-1), the most well described ligand of CD69, on DCs negatively modulates the *in vitro* differentiation of T helpers-17 (Th17) cells (de la Fuente et al., 2014). Gal-1 also increases IL-10 secretion in T cells via activation of the aryl hydrocarbon receptor (AHR) pathway (Cedeno-Laurent et al., 2012). CD69 regulates the activator of Signal Transducer and activator of Transcription 5 (STAT5) and competition of STAT5 with Interleukin-6-dependent binding of STAT3 to IL-17 enhancer sequences inhibited Th17 responses (Martin et al., 2010). In fact, CD69 deletion exacerbated Th1 and Th17 responses after TCR activation (Yang, XP et al., 2011) and affected the number of Foxp3$^+$ reg T *in vitro* and *in vivo* in a cell transfer-induced colitis model (Radulovic et al., 2012). CD69 can also bind to the sphingosine 1-phosphate receptor type 1 (S1PR1) which induces S1PR1 internalization and degradation resulting in T cell retention in LNs (Bankovich et al., 2010; Shiow et al., 2006). Interestingly blocking S1P1R1 internalization has been shown to promote Th17 polarization and exacerbated autoimmune neuroinflammation (Garris et al., 2013). Other publications have shown a role of CD69 in metabolism such as amino acid uptake by interaction with amino acid transporter LAT1 though mammalian target of rapamycin complex 1 (mTORc1) activation (Cibrian et al., 2016).

Almost parallel to CD69 expression, IL-2 is produced within a few hours reaching a peak at 12 hours. TCR stimulation leads to AP-1 activation, which together with NFAT, join to composite regions in the IL-2 promoter (Muller & Rao, 2010). IL-2 signaling promotes expansion, survival and activation of T lymphocytes. IL-2-deficient mice develop severe autoimmunity with reduced fraction of regT and very high effector or conventional T cell fraction (Furtado et al., 2002). Unlike CD8 T cells, both naïve and memory CD4$^+$ T cells are resistant to proliferation induced by IL-2 in the absence of TCR activation (Gesbert et al., 2005). In CD4$^+$ T cells, TCR engagement results in downregulation of cyclin dependent kinase inhibitors (CDKIs) and upregulation of IL-2Rα (CD25) on the plasma membrane, which allows the entry into the cell cycle and increase the response to IL-2 (Gesbert et al., 2005; Liao et al., 2013). IL-2 signaling during priming also leads to late upregulation of interleukin-7 receptor α (IL-7rα or CD127) on the proliferating effectors, thereby favoring the survival of effector cells that are committed to the memory pool (Dooms et al., 2007).

CD25 is considered to be the most prominent cellular activation marker; its expression increases within 24 hours following TCR stimulation and can last for a few days (Jackson et al., 1990; Reddy et al., 2004). This activation event guarantees the entry, survival, proliferation and differentiation of T-cells into the LN. The majority of activated T cells inside the LN rapidly express a new array of selectins in order to migrate to

nonlymphoid tissues. For instance, selectin ligands on activated T cells bind to CD62P (P-selectin) and CD62E (E-selectin) expressed by endothelial cells in order to enter the skin (Bajnok et al., 2017).

The complex process of differentiation to effector cells within the LN is determined by the type of receptor activated on the APC which in turn depends on the nature of the antigen or threat, the load of antigen, the strength of interactions p-MHC-TCR, costimulatory signals between the APC and T cells and cytokines produced by APC and other innate cells during the ongoing infection. The early host-pathogen interactions result in an infection milieu that provides the proper cytokines to allow T helper differentiation. Cytokine signals help drive the CD4 lineage commitment by switching on specific transcriptional programs while maintaining other expressed to low levels. As a consequence of integration of signals coming from TCR and cytokine receptors, different effector T helper cells (Th1, Th2, Th9, Th17, Th22, Tfh (T follicular helper cells), iregT (induced regulatory T cells) are generated. The T helper cell subsets can be defined by the production of a set of specific cytokines and their transcription factor signatures. Briefly, the generation of different T helper subsets is explained. Intracellular pathogens such as virus bind to Toll like Receptors on DC to induce IL-12 secretion, which induced the expression of T- bet (master regulator of Th1) and production of interferon-γ (IFN-γ) (Biedermann et al., 2004). IL-12 and IFN-γ act together to induce T-bet expression, which results in additional IFN-γ amplifying the Th1 response. INF-γ stimulates macrophages to kill infected cells, as well as promotes the production of opsonizing antibodies (Sallusto, 2016; Sher & Coffman, 1992). On the other hand, extracellular pathogens such as parasites are cleared by Th2 cells. IL-4 promotes Th2 differentiation by activating STAT6 and subsequently GATA Binding Protein 3 (GATA-3) expression (master regulator of Th2) expression, thereby resulting in IL-4, IL-5 and IL-13 production (Th2 cytokine signature) (Zhang et al., 1997). Th2 cells also stimulate the production of IgE, and recruit eosinophils and mast cells to fight against extracellular pathogens. Another subtype is the Th17; its main function is the recruitment of leucocytes such as neutrophils to fight against extracellular bacteria and fungi. Signaling through STAT3 leads to the expression of the retinoic acid receptor-related orphan nuclear receptor $\gamma\tau$ (ROR-$\gamma\tau$) (Th17 master regulator) and their key cytokines IL-17A-F, IL-21 and IL-22 (Ivanov et al., 2006; Yang et al., 2008). Notably, Th17 have been involved in the pathogenesis of several autoimmune diseases (Infante-Duarte et al., 2000). A new subset, known as Th9, is the main source of IL-22. The cytokines IL-4 and TFG-β promote Th9 differentiation with a transcriptional program characterized by the expression of GATA-3, IRF-4 and PU.1 (Anuradha et al., 2013; Staudt et al., 2010). This subset, as the Th2, is generated against extracellular pathogens (Anuradha et al., 2013). One of the most recently discovered subtypes is the Th22, involved in wound repair and maintenance of tissue homeostasis (Eyerich et al., 2009). Th22 cells produce IL22 but not IL-17, which makes them functional different to Th17 cells. The cytokines IL-6 and TNF-α are required for Th22 differentiation (Duhen et al., 2009), as well as the AHR (Trifari et al., 2009). So far, its master regulator remains unknown.

Within the germinal center in the follicles localize with B cells a subset known as Tfh. They originate not only from naïve CD4^{+} T cells upon stimulation with IL-21 and IL-12, but also from activated T cell subtypes without terminal lineage commitment. The high expression of surface molecule CXCR5 on these cells facilitate their migration into the B cell follicles where they establish contacts with B cells (Forster et al., 1996). The generation of these cells rely on the engagement of ICOS in T cells with ICOSL in B cells within the germinal centers. These cells express the B cell lymphoma-6 (BCL-6) (Choi et al., 2013) as its main

transcriptional factor and the main cytokine that they produce is IL-21 (Bryant et al., 2007), which is required for the development of the germinal centers and the generation of plasma B cells (Ozaki et al., 2004).

Importantly, the balance between inflammation and tolerance is maintained by a subset of T cells with suppressive properties known as regulatory T cells (Sakaguchi et al., 1995). These cells are divided in natural regulatory T cells (nregT) and inducible regulatory T cells (iregT). The nregT develop in the thymus upon recognition of self-antigens and its master regulator is the transcription factor forkhead FoxP3 (Fontenot et al., 2003), whereas the iregT generate from naïve CD4$^+$ T cells upon particular conditions of antigen stimulation and cytokine milieu, FoxP3 expression is inducible in this cells. The iregT can be further divided in Tr1 (Groux et al., 1997) and Th3 (Doetze et al., 2000) regulatory T cells depending on whether they produce IL-10 or Transforming Growth Factor-β (TGF-β) respectively.

While it was believed that the T cell response was characterized by terminal differentiation of the T helper subtypes, it has been shown that most of the subsets show plasticity when influenced by cytokines within their microenvironment, mainly upon inflammatory conditions. In this line, upon inflammatory conditions Th17 cell producing INF-γ (Th17/Th1) (Bending et al., 2009), Th17 producing IL-10 and regT cells producing Th17-like cells (in the presence of IL-2 and IL1-β) (Deknuydt et al., 2009) or IL-6 and TGF-β (Zhou et al., 2008) have been found. The subtypes Th1 and Th2 are considered less flexible, due to mutual exclusion of Th1 and Th2 master regulators. Nevertheless, some studies have shown Th2 lineage flexibility. Upon viral infections Th2 cells were able to produce both IL-4 and INF-γ (Hegazy et al., 2010). Also they are able to adopt a Tfh phenotype by stimulation with IL-21 (Glatman Zaretsky et al., 2009). In addition, Tfh showed the higher plasticity giving rise to Th1 and Th2 cells (Reinhardt et al., 2009).

After primary antigen encounter some subsets of T helper cells have the capacity to survive into memory cells and mount recall responses with stronger potential to fight the pathogen upon subsequent antigen exposure (Oestreich & Weinmann, 2012; Pepper & Jenkins, 2011). Although some general concepts about how memory CD4$^+$ is generated are widely accepted, different theories have been proposed in order to explain the variety of memory subtypes with different functions and lineage plasticity. The following section addresses fundamental aspects of CD4$^+$ memory formation.

2.1.3   CD4$^+$ immunological memory formation

2.1.3.1   Factors determining memory formation

The kinetic of T cell response has been reviewed elsewhere (Ahmed & Gray, 1996; Kaech et al., 2002). The integration of TCR signals, stimulatory molecules and cytokine local milieu determine the effector subset and the progeny of memory T cells that remain stable for years in given individual. The traditional memory paradigm relies on a lineal model of memory generation that proposed that the clearance of the pathogen is followed by a contraction phase where more of expanded T helpers die and only a few, approximately 5%, persist as a quiescent memory population for extended periods of time. The duration of the CD4 T cell contraction phase may occur over 1-2 weeks (Pepper & Jenkins, 2011) or up to 4 weeks (Whitmire et al.,

2009). During this process most of the expanded cells (90-95%) are programmed to die, thereby resulting in the cessation of the effector functions (Ahmed & Gray, 1996; Pepper & Jenkins, 2011). The magnitude of the contraction phase is determined by the ratio of pro-apoptotic and apoptotic signals that dictate the final fate of the effector population. One of the most important cytokines driving memory formations is IL-2, required for naïve T cells during early and late effector phases to efficiently generate memory T cells. Different roles of IL-2 on memory generation have been demonstrated. First, IL-2 induces upregulation of CD127 and its permanent expression, allowing a subset of effector T cells to compete for IL-7, necessary for long term memory survival (McKinstry et al., 2014). Second, IL-2 increases the expression of B cell lymphoma 2 (Bcl-2), an anti-apoptotic protein and decrease the expression of Bim (pro-apoptotic molecule). The ratio Bcl-2/Bim determines which effector cells are programed to die or survive during the memory checkpoint (Marrack & Kappler, 2004; McKinstry et al., 2014). Third, IL-2 reduces the expression of tumor necrosis factor-related apoptosis-inducing ligand (TRAIL), favoring survival of effectors and memory generation (Li et al., 2007; McKinstry et al., 2014). On the other hand, it has been proposed that interactions CD70 on APC with CD27 in effector T cells during the late effector phase improved memory generation mainly by enhanced IL-2 production (McKinstry et al., 2014). Therefore, not only p-MHC-TCR interactions but also signals through co-stimulatory molecules favor IL-2 production and therefore the fitness of some effector cells and memory generation. Following encounter with the same antigen, memory T cells go through a second expansion phase that is much faster than the primary expansion and followed by a contraction phase. Again, when the threat is eliminated, most of the cells die, leaving this time secondary effector memory T cells with enhanced functionality (Fuse et al., 2008; Razvi et al., 1995). Memory T cells are able to respond faster and more efficiently upon secondary exposure to previously encountered microbial pathogens because they have a lower activation threshold and are less co-stimulation dependent (MacLeod et al., 2010). Contrary to naïve T cells, which form CD40L de novo, memory T cells store preformed CD40L (Koguchi et al., 2012), allowing its rapid mobilization upon T cell activation. Furthermore, their frequencies are considerably higher than those of naïve T cells (Blattman et al., 2002; Farber et al., 2014), which increases both the probability of cognate antigen encounter and the number of effector cells (MacLeod et al., 2009). Importantly, loss of repressive chromatin modifications in memory T cells (Hashimoto et al., 2013; Komori et al., 2015; Nakayama & Yamashita, 2009), together with increased messenger ribonucleic acid (mRNA) stability (Jeltsch & Heissmeyer, 2016) and more efficient translation of cytokine mRNAs (Swanson et al., 2002), contribute to their robust and faster response. Unlike naïve T cells, which circulate between secondary lymphatic tissues and blood, memory T cells circulate between lymphatic, blood, and peripheral tissues (Mora & von Andrian, 2006).

Multiple studies have demonstrated that TCR signaling strength influences memory CD4 formation. TCR signaling strength depends on the affinity of the TCR heterodimer for antigenic p-MHC molecules, the concentration of antigen and co-stimulatory molecules (determine TCR signal amplification) and the duration of the TCR-pMHC interaction (determine signaling duration). Along this line, it has been demonstrated that high avidity clones gain a survival advantage over clones with low avidity (Lanzavecchia & Sallusto, 2002; Malherbe et al., 2004). However, studies by Williams et al, using a model of Lymphocytic Choriomeningitis virus (LCMV)-specific CD4$^+$ T cell clones with different avidity for p-MHCII, showed that the memory pool was favored mainly by prolonged interaction of TCR-p-MHCII interactions, with avidity having no significant role on memory formation (Williams et al., 2008). On the other hand, in *in*

vivo models some but not all CD4^{+} T cell clones present in the memory pool showed a notable primary response. In this study, Th1 cells harboring TCRs recognizing two closely related Listeria monocytogenes peptides were compared: one mounted a robust primary effector response but weaker secondary response, while the other responded meagerly during the primary challenge but more robustly during the secondary challenge (Weber et al., 2012). Furthermore, the precursor frequency of antigen-specific cells also determines the overall activation and fate of the precursor pool (Chu et al., 2010; Jenkins & Moon, 2012). For CD4^{+} T cells was observed that high precursor frequency can adversely impact memory formation, which was correlated with a decrease in the interactions p-MHC on DC and precursors CD4^{+} T cells (Celli et al., 2007).

Due to the differences observed in different experimental conditions, the paradigm of memory generation explained by only a linear generation model has been questioned and numerous models of CD4 memory formation have been proposed with the aim to unravel this diversity.

2.1.3.2   Models of CD4^{+} T cell memory generation and CD4^{+} T cell memory subsets

The linear model for memory formation (naïve to effector to memory) is widely accepted. Nevertheless, multiple studies have shown the existence of different CD4^{+} effector lineages with distinct tissue-trafficking specificities, effector responses, proliferative potential and plasticity among them, making this a complex and heterogeneous pool. While it is clear that effector T cells derived from naïve T cells, how these effector T cells give rise to the heterogeneous population of memory T cells is still a controversial field with some studies supporting that effector T cells give rise to memory cells (Ahmed & Gray, 1996; Lanzavecchia & Sallusto, 2002), while others consider that an effector response is not needed for memory generation (Arsenio et al., 2014; Chang et al., 2007). Based on accumulative experimental data, different models of memory generation have been proposed in order to account for the differences observed. These models take into account intrinsic and extrinsic factors such as the strength of the TCR stimulation and the cytokine milieu, analysis of epigenetic modifications, transcriptome profile of isolated memory T cell subsets, as well as the analysis of phenotypic and functional characteristics the *in vitro* generated or isolated memory subsets.

On the other hand, some unlikely possibilities such as the idea that short-lived effector and long-lived memory cells derive from different naïve T cell clones have been experimentally disproven by single cell adoptive transfer or barcoding approaches (Gerlach et al., 2013; Tubo et al., 2013). The Linear model (Figure 2a) assume that naïve T cells are activated by their cognate antigen and transiently become effectors. These effector T cells transiently express a large number of genes, which makes their phenotype hard to predict, but it is known that activation markers such as CD38 and HLA-DR (Odumade et al., 2012), CD69 and CD25 are overexpressed (Reddy et al., 2004) and sometimes co-expression of CD45RA and CD45R0 have been detected at high levels (Mahnke et al., 2013). In the contraction phase most of the effectors die and some activated T cells will persist into any of numerous memory subsets generated through successive development from naïve T cells (Ahmed & Gray, 1996; Kaech et al., 2002). Memory T cells have been proposed to be generated in the order Central Memory (CM) T cells, Effector Memory (EM) T cells and Effector Memory CD45 Revertants, named Terminal Effector (TE) T cells or sometimes Effector Memory

RA positive (EMRA) T cells (Durek et al., 2016; Kaech et al., 2002; Sallusto & Lanzavecchia, 2001), however this is still a subject of controversy because conversion of EM to CM has also been proposed (Moulton et al., 2006). The EMRA T cells are likely formed with repeated re-stimulation of memory T cells (Macallan et al., 2017). Another model known as the Bifurcate, Disparate or Asymetric model (Figure 2b) suggests that the fate decision is made very early in the immune response, with the first asymmetric cell division. After antigen recognition, a T cell divide into two daughter cells, the distal daughter cell turn into CM T cells, whereas the proximal daughter cell turn into EM and effector T cells, the latter undergoing apoptosis during antigen withdrawal (Arsenio et al., 2014; Chang et al., 2007). In this model memory cells are generated independently of effector cells. A third model, in which TCR signaling strength dictate the fate of the memory subsets generated was also proposed. This model suggest that strong antigenic or long p-MHC interaction favor EM over CM generation (Lanzavecchia & Sallusto, 2002). This model is based on experimental data supporting that naïve $CD4^+$ T cells primed with weak antigen proliferate but they do not develop effector functions, but they can migrate to LN, proliferate and differentiate in response to the antigen in *in vivo* transfer experiments. On the other hand, naïve T cells primed with strong antigen produced Th1 and Th2 cytokines, migrated to secondary tissue but not LN (Iezzi et al., 2001). In this model, if the cells do not establish a durable interaction p-MCH-TCR early during T cell priming die by neglect, whereas strong interactions p-MHC-TCR due to a high ratio APC/T cells lead to T cell deletion by activation induced cell death (AICD), as seen in a system where interaction APC/T cell have been evaluated (Stoll et al., 2002) (Figure 2c). In a fourth model, known as simultaneous model integrates aspects of the previous models. This model is based on data on memory generation from Th1 and Tfh subsets. The model proposed that the duration of TCR signaling strength accompanied by the cytokine microenvironment (IL-2, IL-12, and IL-21), as well as interactions between T cells and B cells within the follicles determine the fate of the memory subset generated (Figure 2d). Upon this condition, during the primary response naïve T cells can give rise to Th1 or Tfh cells depending on the TCR strength and the polarizing milieu. For instance, increased TCR signaling strength under exposure to varying concentrations of IL-12 generates cells with intermediate to high expression of T-bet and Blim-1, which the latter inhibiting BCL-6 expression. A higher ratio T-bet/BCL-6 favor the generation of short live Th1 effector cells with high expression of T-bet (Th1SLECs) and Th1 memory precursor cells with intermediate levels of T-bet (Th1MPC), the latter subset can give rise to EM or CM cells upon recall responses (Gasper et al., 2014). Indeed Th1 cells with EM and CM phenotype has been found (Pepper et al., 2010). Alternatively, weaker TCR signaling strength upon IL-2 limiting conditions, exposure to Il-21 and interaction with B cells (through ICOS signaling) induce a population of Tfh-like cells with high plasticity and the potential to give rise to EM, CM and Tfh memory T cells, which may generate Th1 cells or other T helper subsets upon recall responses (Figure 2d). On the other hand, evidence that other T helper subsets enter the memory pool is less abundant. *In vitro* polarization of $CD4^+$-purified OT-II cells into Th2 showed that two pools of cells $CD62L^+$ and $CD62L^-$ are generated, representing CM and EM respectively (Mackenzie et al., 2014). Furthermore, *in vitro* polarized Th2 cells from naïve TCR-transgenic cells survived long time following transfer into nonlymphophenic naïve recipients (Lohning et al., 2008). On the other hand, recently Vesely and colleagues showed evidences that Th17 cells are also able to enter the memory pool. From their experiments, Th17 cells produced after immunization with heat-killed Klebsiella gave rise to lung $CD4^+$ resident memory T cells, which were maintained in the lung by IL-7 producing lymphatic endothelial cells (Amezcua Vesely et al., 2019). Other model known as self-renewing

effector model has also been proposed. In this model, naïve T cells give rise to either CM or effector T cells with self-renewing potential. These cells can migrate to lymphoid tissues, where they proliferate and develop into EM T cells with the ability to migrate to sites of infection. In this model, TE or EMRA T cells are proposed to derive from EM T cells (Ahmed et al., 2009). Last but not least, a new subset of T memory stem cells (TSCM) has been identified in CD8$^+$ and CD4$^+$ T cell compartments (Gattinoni et al., 2017). These cells express naïve markers such as CD45RA, CCR7, CD62L and IL-7Rα, but unlike naïve cells, they express CD95, interleukin-2 receptor β (IL-2Rβ), chemokine C-X-C motif receptor 3 (CXCR3) and higher levels of lymphocyte function-associated antigen-1 (Gattinoni et al., 2011). Furthermore, mouse CD8$^+$ TSCM can produce CM and EM-like cells and have shown the highest reconstitution and antitumor capacity in adoptive transfer experiments (Gattinoni et al., 2011; Zhang, Y et al., 2005). Although human CD8$^+$ TSCM have been generated *in vitro* from naïve precursors through activation of the WNT-β-catenin signaling pathway or using inhibitors of glycogen synthase kinase-3β, experiments with CD4$^+$ TSCM are still lacking. Therefore, how these cells emerge during the immune response and their contribution to memory CD4 T cell formation are questions that remain to be addressed.

Although the exact mechanism of memory generation is not fully understood, the phenotypic characteristics and functional properties of this heterogeneous pool have been extensively studied. It is well known that EM T cells express low levels of CD62L and do not express CCR7, while CM T cells express CCR7 and CD62L and undergo homeostatic proliferation in lymphoid tissues. While naïve T cells migrate to the secondary lymphoid tissues, effector T cells migrate to peripheral tissues that are susceptible to pathogen attack. Generally, peripheral effector and EM T cells are post-mitotic cells with markers of terminal differentiation, lack of proliferative capacity and are unable to migrate back to secondary lymphoid tissues (Ahmed et al., 2009). Although CM T cells that remain in SLO resemble more naïve T cells regarding their trafficking, proliferative potential and decreased effector functions, their gene expression pattern of effector molecules is not consistently similar to that of naïve T cells. In this regard, CM T cells unlike EM cells produce to a lesser degree IL-4 and IFN-γ but more IL-2 and show enhanced proliferative capacity (Reinhardt et al., 2001; Wang et al., 2012). Thus, CM T cells upon subsequent encounter with cognate antigens in lymphatic tissues generate more rapidly a large pool of antigen-specific effector T cells, thereby allowing a faster and stronger immune response (Bradley et al., 1993). Furthermore, CD4$^+$ CM T cells confer more powerful B cell help, which leads to faster B cell proliferation, class switching, as well as increased antibody production (Fazilleau et al., 2007; Hale & Ahmed, 2015) .In agreement with the idea of TE cells arising from EM cells, IL-15 has been shown to expand a subset of CD45RA re-expressing EM cells known as TE (Lugli et al., 2010). CD45RA$^+$CCR7$^-$ TE cells are generally found in the CD8$^+$ compartment (Sallusto et al., 1999), remain CCR7$^-$CD62L$^-$, are often negative for CD27 and CD28 and own the shortest telomeres among T cells (Romero et al., 2007). TE cells express markers of senescence, including KLRG-1, CD57 (Brenchley et al., 2003; Henson & Akbar, 2009) and they show phosphorylation of histone H2AX (Di Mitri et al., 2011) and low proliferative and functional capacity (Geginat et al., 2003), indicating terminal differentiation.
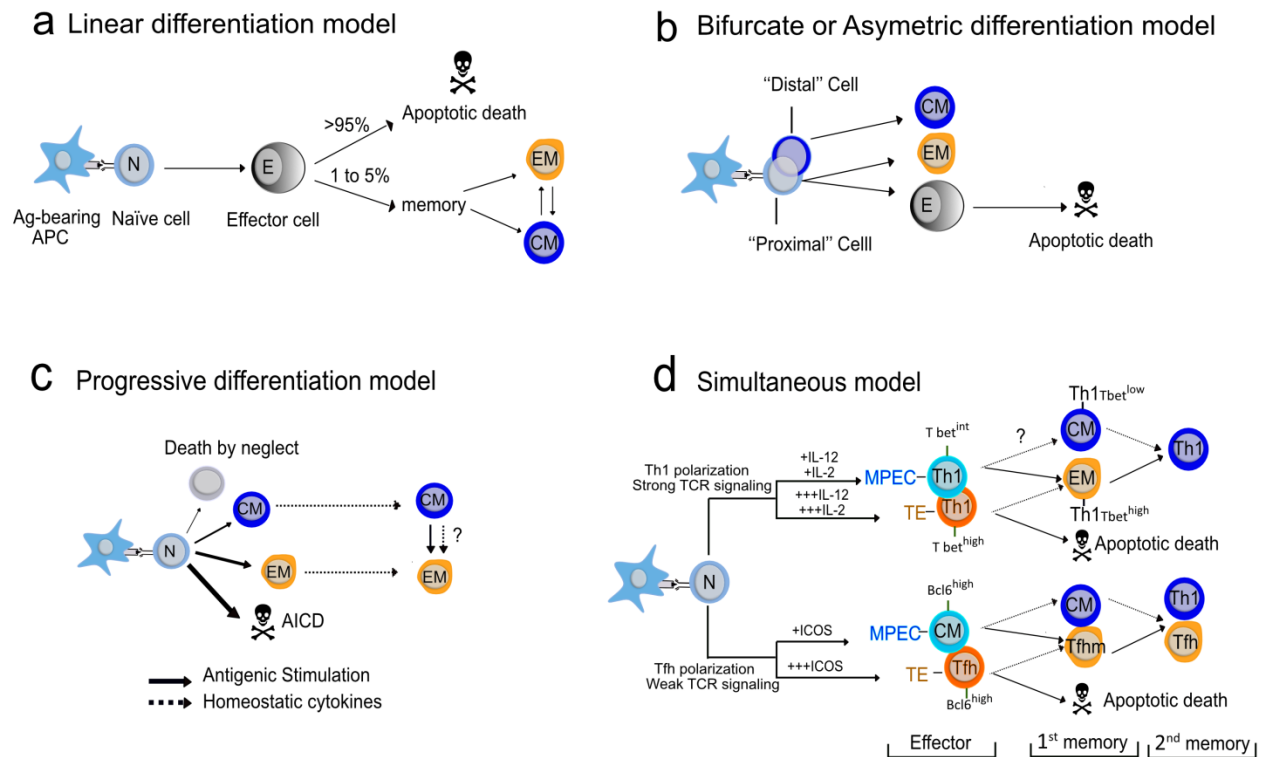
Figure 2: Models of memory CD4$^+$ generation.
(a) Linear differentiation model. In this model priming of naïve T cells with Antigen-bearing Antigen-Presenting Cells (Ag-bearing APC) give rise to effector T cells that proliferate and eradicate the pathogen. Upon Ag withdrawal 95% of the effector cells die leaving behind a small number of memory T cell subsets, that can be further divide in Effector Memory (EM) T cells and Central Memory (CM) T cells. It has been proposed that memory generation occurs sequentially from CM to EM, but also from EM to CM. **(b)** Bifurcate model of memory generation. In this model, T cell memory diversity is preceded by asymmetric generation of naïve T cells. During this process two cells are generated, with the proximal cell to the immune synapse giving rise to effector populations (Effector and EM T cells), whereas the distal cells give rise to CM T cells. **(c)** Progressive differentiation model. The duration and intensity of antigenic stimulation (represented by the thickness and length of the solid arrows) determine the fate of the memory population. The role of homeostatic cytokines in T cell differentiation is indicated by the dotted lines. AICD: activation-induced cell death. **(d)** Simultaneous model. This model proposed that strong TCR signaling along with varying IL-2 and IL-12 signaling induce high T-bet expression and Th1 differentiation. Continued interactions p-MHC-TCR and high IL-2 and IL-12 concentrations lead to terminal Th1 effector cell differentiation (TE-Th1Tbet^{high}) or Th1 memory precursors (MPEC-Th1 Tbet^{int}). The latter gives rise to both primary effector memory and primary central memory Th1. T helper follicular (Tfh) cell differentiation occurs upon sustained interaction of naïve T cells with B cells, which induce upregulation of BCL-6 that repress T-bet expression, favoring Tfh cell differentiation or CM T cell generation. After Ag withdrawal, cells undergo contraction and survival terminal Th1 or terminal Tfh retain lineage commitment and generate secondary Th1 or Tfh memory T cells respectively; whereas Th1 CM T cells and CM T cells generated from BCL6^{high} memory precursors are more flexible and generate different T helper subsets upon recall responses.

2.2 T cell metabolism as a regulator of activation and memory formation

Effector differentiation from naïve CD4$^+$ T cells entails dramatic reprograming of T cell metabolism to fulfill the demands of increased biosynthesis and energy utilization needed for proliferation and differentiation. During the contraction phase, survival CD4$^+$ T cells go through crucial points to develop into competent memory cells with long lasting time life and with capability to recover their proliferative and functional capacity upon antigen re-encounter. During this transition effector T cells shift from an active and greatly proliferative state to a resting and vigilant memory state (Pearce et al., 2013). This is accomplished through metabolic and epigenetic alterations occurring during differentiation of naïve CD4$^+$ T cells, which are metabolically quiescent and have low rates of nutrient uptake, glycolysis and biosynthesis. Naïve T cells use the glucose-derived pyruvate along with fatty acid and amino acid oxidation via TCA cycle in order to generate reducing equivalent to produce adenosine triphosphate (ATP) via oxidative phosphorylation (OXPHOS) inside the mitochondria (MacIver et al., 2013). Once the cells get activated, aerobic glycolysis and lipid biosynthesis rather than oxidation is increased. The switch to aerobic glycolysis, even in the presence of oxygen, is a characteristic not only of lymphocytes but also of highly proliferative cells such as cancer cells (Koppenol et al., 2011) which obtain the glycolytic intermediates for cell growth and division thought the conversion of pyruvate to lactic acid to prioritize efficient and rapid biosynthesis over efficient energy/ATP production (MacIver et al., 2013). In this line, depriving activated T cells from glucose impairs TCR induced proliferation and T cell mediated immunity (Gerriets et al., 2015). At the end of an immune response, the pool of remaining memory T cells has to return to lipid oxidation to generate efficient energy.

Naïve T cells maintain their basal energy requirements through cell-extrinsic signals. Both, the IL-7R and TCR, are important for this process. IL-7 is a pro-survival factor for early thymocytes, resting peripheral naïve and memory T cells. In fact, defects in this pathway can induce severe combined immunodeficiency in mice and humans (Tan et al., 2001). For instance, IL-7 is important for phosphorylation of STAT5, as well as regulates glucose uptake through the activation of the PI3K/Akt/mTOR exe (Pallard et al., 1999; Wofford et al., 2008). IL-7 signaling is also important for the expression of the anti-apoptotic protein BCl-2 (Maraskovsky et al., 1997). After T cell activation, metabolism requirements increase to fulfill the biosynthesis of different cellular constituents such as proteins, lipid membranes and nucleic acids. One of the most important transcriptional regulators upon TCR activation is the myelocytomatosis oncogene transcription factor c-Myc. In T cells, c-Myc is rapidly induced in response to p-MHC-TCR signals and its expression is kept by costimulatory receptors and cytokines such as IL-2 throughout the proliferative response (Lindsten et al., 1988; Preston et al., 2015). Besides, high c-Myc expression is only maintained in proliferating T cells with high rate of aminoacid uptake, and when protein synthesis or aminoacid uptake are limited C-Myc expression declines rapidly (Preston et al., 2015). Some of the different processes regulated by c-Myc in activated T cells are glutamine and glucose metabolism, as well as mitochondrial biogenesis. Particularly, c-Myc can induce the expression of all glycolytic genes, including the glucose transporter type 1 (Glut1), lactate dehydrogenase A (LDHA), hexokinase 2 (HK2), pyruvate kinase muscle isozyme M2 (PKM2) (Dang et al., 2009), glutaminase and the glutamine transporters SLC3a2, SLC5A1 and SLC7A1 (Gao et al., 2009; Wise et al., 2008). The transcription factor c-Myc also promotes T cell growth and entry into the cell cycle (Lindsten et al., 1988; Wang et al., 2011). In this regard, acute genetic deletion

of c-Myc prevented the expression of glutaminolytic and glycolytic genes in stimulated T cells, which resulted in a lack of proliferation of c-Myc-defficient T cells. Also, c-Myc is crucial for T cells to generate α-ketoglutarate via glutaminolyisis upregulation (Wang et al., 2011), which may be important not only in aerobic glycolyis to feed the TCA cycle but also to allow the citrate, generated through glycolysis, to exit the mitochondria to be employ in biosynthesis of lipids. Furthemore, α-ketoglutarate is a precursor for polyamine synthesis, with the latter having an important role in DNA synthesis (Wang et al., 2011).

Another important metabolic trigger is the signaling through CD28, which enhances glycolysis through the activation of PI3K/ Akt/ mTOR exe, promoting effector differentiation and clonal expansion (Frauwirth et al., 2002). Akt not only promotes Glut1 cell surface expression but also increases glycolytic rate through direct phosphorylation of glycolytic enzymes. For instance, HK2 activity is increased by Akt- dependent phosphorylation (Miyamoto et al., 2008). Besides, Akt-dependent activation of mTORC1 further stimulates aerobic glycolysis, as well as integrate pathways to enhance cell growth through lipid synthesis (Chi, 2012). This is coordinated with an Akt/mTORC1-dependent decrease in expression of the enzyme Carnitine palmitoyl transferase I (CPT1), a rate-limiting factor in long-chain fatty acid oxidation. Reduced CPT1 activity affects fatty acid oxidation, thereby preserving them for cell growth rather than energy generation (Porstmann et al., 2008). The mTORC1 complex have been target using the immunosuppressant rapamycin, which prevents glycolysis upregulation on activated T cells and inhibits T cell proliferation inducing anergy (Powell & Delgoffe, 2010).

Despite the glycolytic nature of T cell activation, activated T cells also upregulate OXPHOS. Chang et al showed that the extracellular acidification rate (ECAR), an indicator of aerobic glycolysis, and the oxygen consumption rate (OCR), an indicator of OXPHOS, of *in-vitro* and *in-vivo* activated T cells are higher than in naïve T cells, indicating that activated T cells use both aerobic glycolysis and OXPHOS. Besides inhibition of ATP synthase with olygomycin impaired the proliferation and activation of T cells and activated cells cultured in the presence of galactose to enforce respiration were able to proliferate albeit to a lesser extension as in the presence of glucose. When these cells were culture in the presence of galactose plus olygomicin did not proliferate and die, suggesting an important role of OPXHOS. The author showed that aerobic glycolysis is important for effector functions such as INF-γ production by T cells (Chang et al., 2013; Sena et al., 2013).

Furthermore, mitochondrial Reactive Oxygen Species (ROS) can augment NFAT activity needed for IL-2 production, as well as one carbon metabolism to support purine and thymidine synthesis (Sena et al., 2013), which highlights the importance of ROS for T cell activation. Hence, effector T cells that have diminished cell size, make less use of aerobic glycolysis, show reduced Akt or mTOR activity and a lesser mitochondrial membrane potential are more metabolically fit to mature into a long-lived memory T cell with CM cell features (Crompton et al., 2015; Pearce et al., 2009). Besides, studies using mice have shown that memory T cell formation relies on the transition from a highly anabolic state in effector cells to a more quiescent and catabolic state in memory cells; in which the shift from glycolysis to OXPHOS is essential (van der Windt & Pearce, 2012) (Pearce et al., 2009). Memory T cells have distinct mitochondrial morphology from effector T cells, for instance CM cells and IL-15 derived memory T cells have tighter cristae formation (Buck et al., 2016), which has been linked to more efficient OXPHOS (Cogliati et al., 2016). Likewise, memory T cells exhibit more fused mitochondria networks than effector T cells, with the latter showing more isolated or

punctate mitochondria (Buck et al., 2016). In this line, T cells lacking the optic atrophy 1 protein, an inner mitochondrial membrane protein, had defective memory T cell development due to loose cristae. Besides, mitochondrial remodeling of cultured T cells induced more fused mitochondria and subsequently T cells with memory-like characteristics and anti-tumour functions as seen after their adoptive transfer *in vivo*. Further supporting this concept, loss of methylation controlled j protein, a negative regulator of mitochondrial respiratory chain efficiency, results in augmented mitochondrial metabolism in effector T cells, increased cell survival during the contraction phase and subsequent improved T cell antiviral protective immunity (Champagne et al., 2016). Although, memory T cells use mostly mitochondrial metabolism, as seen by the preferential use of OXPHOS over aerobic glycolysis, a study showed that CM cells from CD8$^+$ T cells may be more reliant on mitochondrial OXPHOS than EM cells (Ecker et al., 2018; Phan et al., 2016).In addition, increasing aerobic glycolysis in mice affected the generation of CM T but enhanced EM T cell formation (Sukumar et al., 2013), indicating that the ratio OXPHOS/ glycolysis may impact and even control subset differentiation.

The above evidences show that metabolic reprograming of naïve T cells following antigen encounter is indispensable for proliferation, effector functions and memory fate commitment.

2.3   TCR signaling and downstream pathways

The TCR is a heterodimer composed for αβ or γδ chains and is the central receptor required for T cell activation (Abraham & Weiss, 2004). These heterodimers are associated with a CD3 signaling hexamer formed by one homodimer of ζ-chains (CD3ζζ) and two heterodimers formed by ε and γ or δ chains (CD3εγ or CD3εδ). The CD3 chains contain cytosolic immunoreceptor tyrosine-based activation motifs (ITAMs) that allow TCR signal transduction inside the cell. Upon TCR activation, tyrosine kinases (PTKs) of the Src family, in particular Lck and Fyn (associated to CD4/CD8 co-receptors or the TCR), phosphorylate the tyrosine residues in the ITAMs. Tyrosine phosphorylation of CD3ζ chain provides the binding site for ζ-chain-associated protein kinase of 70 kDa (ZAP-70) via its SH2 domain. Subsequently ZAP70 becomes activated by Lck or Fyn-dependent phosphorylation of its tyrosine residues (Zhang et al., 1998). One of the most relevant ZAP-70 targets is the transmembrane adapter protein linker for the activation of T cells (LAT), which acts as docking sites for effector enzymes containing SH2 domains such as phospholipase Cγ (PLC-γ). LAT has nine tyrosine residues which becomes rapidly phosphorylated upon TCR engagement. Phosphorylated tyrosine residues serve as binding sites for proteins such as PLC-γ1, the p85 subunit of phosphoinositide 3-kinase (PI3K) and the adapter proteins: growth factor receptor-bound protein 2 (GRB2) and GRB2-related adapter downstream of Shc (Gads). Other important protein involved in TCR signaling is SLP-76, which is recruited to activated LAT via their binding partner Gads. In this line, some elegant studies have shown that cells lacking LAT or SLP-76 fail to transduce TCR signals, which resembles the phenotype of Syk/ZAP-70 or Lck/Fyn double-deficient T cells (Koretzky et al., 2006; Liu et al., 1999).

TCR activation leads to the activation of PI3K signaling pathway, which is important for T cell activation and combine numerous receptor pathways. In naïve T lymphocytes, low levels of phosphatidylinositol (3,4,5)-trisphosphate (PtdIns (3,4,5)P3 or PIP3) are maintained by IL-7 signaling, which are increased in

response to TCR triggering. PI3K is the enzyme in charge of phosphorylates phosphatidylinositol-4,5-bisphosphate (PtdIns-4,5-P2 or PIP2) to form PIP3. PIP3 produced upon TCR clustering binds to PH domains in TEC family kinases (Itk and Btk, GEFs for Rho family GTPases) to promote activation of PLC-γ and subsequent hydrolysis of PIP2, which results in release of soluble inositol 1,4,5-trisphosphate or inositol trisphosphate (InsP3 or IP3) to initiate Ca^{2+} mobilization and accumulation of dialcylglycerol (DAG) in the plasma membrane, with the latter activating protein kinase C (PKC) isoforms to the inner membrane of the cell. On the other hand, PIP3 not only binds to the TEC family kinases but also to the kinases PDK1 and AKT (also known as PKB) (Hemmings & Restuccia, 2012). PDK1-mediated phosphorylation of Akt, in its catalytic domain, activates the enzyme. Activated AKT migrates to the nucleus, where it phosphorylates FOXO transcription factors, thereby promoting their nuclear exclusion and inhibition (Hay, 2011; Ouyang & Li, 2011). FOXO proteins regulate the expression of the zinc-finger transcription factor KLF2, required for T cells to control the expression of chemokine receptors and adhesion molecules important for traffic to secondary lymphoid tissues (Hedrick, 2009; Lorenz, 2009). AKT can also activates mTORC1 via a Rheb-GTPase proteins (Huang & Manning, 2009). The mTORC1 exe integrates antigen, cytokine receptors and nutrients signals to orchestrate T cell differentiation (Powell & Delgoffe, 2010). In this line, mTORC1 regulates important genes encoding cytolytic molecules, effector cytokines, as well as chemokine and adhesion receptors (Sinclair et al., 2008). Some phosphatases, such as PTEN and SHIP dephosphorylate PIP3 and therefore are considered negative regulators of the PI3K pathway (Harris et al., 2008).

InsP3 binds to the InsP3 receptor (InsP3R) in the membrane of the endoplasmic reticulum (ER) to initiate release of Ca^{2+} from ER (main Ca^{2+} store). The decrease in ER Ca^{2+} stores activates store-operated calcium release-activated Ca^{2+} (CRAC) channels in the plasma membrane (Lewis, 2001; Parekh & Penner, 1997) increasing the $[Ca^{2+}]_i$ for a period of minutes to hours (potentially days). As a consequence of Ca^{2+} influx, several Ca^{2+}-dependent proteins and pathways are activated, such as the serine/threonine phosphatase CaN and its downstream target transcription factor NFAT, Ca^{2+}-CaM dependent protein kinase (CaMK) and its target cyclic AMP-responsive element-binding protein (CREB), myocyte enhancer factor 2 (MEF2) and nuclear factor kappa-light-chain-enhancer of activated B cells (NF-κB). Calcineurin-NFAT is one of best characterized signaling pathways. Increases in $[Ca^{2+}]_i$ result in binding of Ca^{2+}-Calmodulin (Ca^{2+}-CaM) to CaN and triggering of its phosphatase activity (Crabtree & Olson, 2002). CaN in turn dephosphorylates NFAT proteins unmasking their nuclear localization sequence (NLS), followed for a rapid translocation of NFAT proteins into the nucleus. Furthermore, CaN masks NFAT nuclear export signals (NES) and maintains NFAT in its dephosphorylated form, thereby guaranteeing nuclear retention of NFAT (Crabtree & Olson, 2002; Macian et al., 2001). Regulation of gene expression by NFAT is highly dependent on maintained Ca^{2+} influx and CaN activity. In conditions where $[Ca^{2+}]_i$ levels decrease or after incubation of T cells with CsA (a potent CaN inhibitor), rapid rephosphorylation of NFAT is observed. Protein kinases such as PKA and GSK3 rephosphorylate NFAT and expose its NES, which triggers its immediate nuclear export. On the other hand, some cytosolic kinases keep NFAT from moving to the nucleus by either masking the interaction sites of NFAT with CaN or by disrupting the NLS (Beals et al., 1997; Katzav, 2004).

On the other hand, PLC-γ-mediated hydrolysis of PIP_2 produces DAG which binds with high affinity to the Ras/Rap guanyl-releasing protein (GRP) family of guaninenucleotide exchange factors (GEFs), to protein

kinase C (PKC) and protein kinase D (PKD). PKC signaling is essential for efficient TCR-induced cytokine production and PKC-mediated phosphorylation of RapGEF2 essential for GTPaseRap1 activation, which controls the activity of the integrin LFA1 and hence lymphocyte adhesion (Kinashi & Katagiri, 2005). Another important target of DAG/PKC is the Ras guanyl nucleotide-releasing protein (RasGRP), which is recruited to the membrane through a DAG-binding domain and activates a guanine nucleotide-binding protein known as Ras. The activation of Ras results in the activation of the serine-threonine kinase Raf-1 that subsequently activates mitogen-associated protein kinases (MAPKs), among them Erk1and Erk2 (extracellular signal-regulated kinase 1 and 2 respectively). The Raf/MAPK/ERK pathway controls the levels of the transcription complex c-Jun/c-Fos, known as AP-1, as well as CD69 expression (D'Ambrosio et al., 1994).

The second major intracellular pathway triggered by DAG activates a PKC family member known as PKCθ, wich binds to DAG through its lipid-binding domain. PKCθ deficient T cells fails to induce IkB degradation upon T cell activation, which leads to cytosolic NF-κB retention. Upon resting conditions NF-κB is forming a complex with its inhibitor IκB and therefore it remains in the cytosol. During T cell activation, IκB is targeted by the IκB kinase (IKK) complex , ubiquitinylated and subsequently degraded, thereby allowing NF-κB nuclear translocation and the transcriptional expression of NF-κB-dependent-genes, some of them involved in the survival, homeostasis and function of activated T lymphocytes (Schulze-Luehrmann & Ghosh, 2006; Sommer et al., 2005).

2.4 Ca^{2+} signaling in T cells

2.4.1 Store Operated Ca^{2+} entry (SOCE)

In a variety of non-excitable cells, Ca^{2+} is released from the ER through inositol 1,4,5-trisphosphate receptors (InsP3R) and ryanodinereceptors, while extracellular Ca^{2+} can enter from several channels. Among these channels Ca^{2+} release-activated Ca^{2+} (CRAC) channels in the plasma membrane that open after intracellular Ca^{2+} store depletion, remain the most well described Ca^{2+} influx pathway in lymphocytes (Lewis, 2001; Parekh & Penner, 1997). The main components of the SOCE machinery are ORAI and STIM proteins. There are three ORAI isoforms expressed in human T cells (ORAI1-ORAI3). Although they possess similar functional properties in overexpression systems, they are different in their tissue expression pattern, pharmacological properties and inactivation characteristics (DeHaven et al., 2007; Lis et al., 2007). ORAI1 localizes in the plasma membrane and appears to be the predominant isoform mediating SOCE in lymphocytes (Feske, 2007; Hogan et al., 2010). Transcript levels of murine *ORAI1* are specifically abundant in cells of the immune system, while *ORAI2* transcripts are elevated in the spleen, lung, brain and small intestine, whereas *ORAI3* transcripts are high in various solid organs (Prakriya & Lewis, 2015). Expression of *ORAI2* is also reported in dendritic cells, macrophages, mast cells (Hoth & Niemeyer, 2013), regT (Kircher et al., 2018) and it is higher in naïve T cells than in effector T cells (Hoth & Niemeyer, 2013). ORAI1 constitutes the major pore-forming subunit of the CRAC channel. ORAI1 N and C-termini are cytoplasmic. The C-terminus of ORAI1 has a coiled-coil (CC) domain that contains a binding site for STIM1 and the N-terminus include two inhibitory phosphorylation sites and a calmodulin binding domain (CaM-BD) (Kawasaki et al., 2009; Mullins et al., 2009). On the other hand, STIM molecules are single-pass transmembrane proteins into the ER membrane. Their N-terminus localizes in the ER lumen and contains a

EF-hand Ca^{2+} binding domain that senses the levels of Ca^{2+} in the ER (Figure 3). Mutations in the EF-hand domain of STIM that compromised Ca^{2+} binding resulted in constitutive Ca^{2+} influx in the absence of ER Ca^{2+} store depletion (Liou et al., 2005; Zhang, SL et al., 2005). The C-terminus of STIM1 contains the second and third coiled-coil domains (CC2 and CC3), which are part of a minimal CRAC channel activation domain known as CAD, SOAR (STIM Orai-activating region), OASF (Orai1-activating small fragment) (Kawasaki et al., 2009; Park et al., 2009) (Figure 3), which binds directly to Orai1 to activate CRAC channels. Purified CAD/SOAR/OASF is enough to activate Orai1 in cells with full Ca^{2+} ER stores (Park et al., 2009).

SOCE is initiated in T cells after engagement of p-MHC on APC to the TCR complex in T cells inducing cleaves of PIP2 into IP3 and DAG (Figure 3). The former binds to IP3R in ER membrane leading to store depletion. Ca^{2+} depletion from ER stores (~0.5-1mM) is rapidly sensed by the EF-hand domains of STIM proteins (Cahalan & Chandy, 2009; Liou et al., 2005), inducing their activation, oligomerization and redistribution into discrete puncta located in junctional ER sites that are as close as 10 to 25nm from to plasma membrane (Luik et al., 2008) (Figure 3). In these puncta, ORAI1 channels are allosterically activated by direct interaction of the CAD domain of STIMs with both N- and C-terminal regions of ORAI1 (Luik et al., 2006) (Figure 3). Interestingly, a mutation on STIM1 resulted in a mutant protein (amino acid 1-440), that was able to form puncta and bind to ORAI1, but failed to induce SOCE following store depletion (Park et al., 2009). Therefore, clustering and activation of CRAC channels are detachable mechanisms. In T cells, STIM1 and ORAI1 play important roles. Both STIM1 and ORAI1 translocate to the immunological synapse between APC and T cells, co-localizing with TCR, costimulatory molecules and tyrosine-phosphorylated molecules (Lioudyno et al., 2008; Quintana et al., 2011). This interface coincides with local Ca^{2+} influx from the extracellular space (Quintana et al., 2011). Colocalization of these molecules at the contact site between T cell and APC is crucial to increase and sustain local Ca^{2+} influx in the vicinity of immunological synapse.

Several lines of evidence highlight the importance of SOCE in T cells. For instance, TCR-dependent Ca^{2+} influx and store operated Ca^{2+} influx are not additive and their corresponding currents properties are alike (Premack et al., 1994; Zweifach & Lewis, 1993). In addition, SOCE was abolished in T cells of immunodeficient patients with inherited mutations of the *ORAI1* gene (Feske et al., 2005; Partiseti et al., 1994), as well as in *in vitro* polarized CD4$^+$ and CD8$^+$ cells of knockout mice lacking Orai1 or knock-in mice expressing the non-functional Orai1-R93W mutant protein (McCarl et al., 2010; Vig et al., 2008). On the other hand, STIM1 is considered to play a main role as activator of the CRAC channel whereas STIM2 play a lesser albeit important role in T-lymphocytes. In murine T cells, STIM1 is constitutive expressed in naïve T cells while STIM2 expression is only increased during differentiation into T helper cells *in vitro*. The oligomerization kinetics is also different with STIM2 responding to smaller decrease in ER Ca^{2+} (Brandman et al., 2007) and with a ~3.5-4 times slower unfolding of the EFh-SAM domain than STIM1 (Stathopulos et al., 2009). On the other hand, STIM1 senses the depletion of ER Ca^{2+} stores and activates SOCE early during the immune response, whereas STIM2 sensitivity to initial Ca^{2+} depletion is smaller. Nevertheless, STIM2 acts in resting cells with Ca^{2+}-full stores to regulate basal Ca^{2+} influx, as well as throughout the late stages, when Ca^{2+} store refilling is taking place. At this point, STIM1 becomes inactive by rebinding of Ca^{2+}, while STIM2 is still active due to the its lower EF-hand affinity for Ca^{2+}, that permits

mild oligomerization of STIM2 in resting ER Ca^{2+} concentrations (Brandman et al., 2007; Oh-hora & Rao, 2008). Therefore, STIM1 seems to have a main role during strong TCR stimulation leading to significant store depletion, while STIM 2 may be more related to weaker stimulus inducing partial store depletion (Shaw & Feske, 2012). Loss of function mutation in STIM1 in human patients or STIM deletion in mice abolished almost completely SOCE. In contrast, STIM2 deletion had no significant effect on SOCE peak but impaired sustained Ca^{2+} influx, important for maintained nuclear NFAT activity and both IL-2 and INF-γ production (Oh-hora & Rao, 2008). Only STIM1$^{-/-}$STIM2$^{-/-}$ in mice completely abolished SOCE in T and B cells, highlighting the role of STIM2. In this way, all mutations affecting CRAC channels and SOCE result in CRAC channelopathy, defined by severe immunodeficiency, autoimmunity, congenital myopathy with atrophy of type II muscle fibers and ectodermal dysplasia with anhydrosis and a dental enamel calcification defect (Feske, 2010). On the other hand, differentiation of mouse Th17 cells requires SOCE and SOCE deficient T cells have failed to induce autoimmunity in a mouse model for ulcerative colitis and Crohn's disease inflammatory bowel disease (IBD) (McCarl et al., 2010) and a mouse model for multiple sclerosis (experimental autoimmune encephalomyelitis) (Ma et al., 2010), in both Th17 cells played an important role during the pathogenesis of the disease. On the other hand, gain-of-function mutations in ORAI1 and STIM1 have also been described. These mutations lead to constitutive and increased CRAC channel activation and distinct syndromes. A mutation in exon 7 of STIM1 (c.910C>T) produces a single amino acid change, STIM1 p.R304W in the C-terminus of STIM1, leading to two different syndromes; Stormorken syndrome and York platelet syndrome, both characterized by bleeding tendency due to thrombocytopenia and platelet defects, among others symptoms. In lymphocytes from patients with Stormorken syndrome constitutive activation of STIM1 without store depletion in the absence (Morin et al., 2014) or presence (Misceo et al., 2014) of Ca^{2+} extracellular was shown, but the exact molecular mechanism is not well understood. Other mutation on STIM1 (STIM1 p.D84G mutation), located in the EF hand Ca^{2+} binding domain of STIM1, causes a non-syndromic TAM and Stormorken-like syndrome. The Stormorken-like syndrome resembles clinically the Stormorken syndrome but lacks miosis as a clinical symptom. Myoblast generated from patients with this mutation also shown high basal Ca^{2+} levels in the absence of extracellular Ca^{2+} and strong Ca^{2+} influx after Ca^{2+} addition to the extracellular medium without previous store depletion(Bohm et al., 2013). Furthermore, gain of functions mutation on ORAI1 have been found which also leads to constitutive CRAC channel activation in the absence of store depletion in patient myotubes (Endo et al., 2015). These mutations result in two missense mutations in ORAI1, c.292G>A and c.412C>T, that lead to single amino acid substitutions in the first (ORAI1 p.G98S) and second (ORAI1 p.L138F) transmembrane domain of ORAI1 (Endo et al., 2015).

2.4.2   Other Ca^{2+} permeable ion channels in T cells

Besides SOCE, other channels contribute to the net Ca^{2+} influx in T lymphocytes. These channels are L-type voltage-gated Ca^{2+}, K^+ channels, ATP-responsive purinergic P2 receptors, transient receptor potential (TRPC) channels, TRPV channels and some TRPM channels (Feske, 2007; Scharenberg et al., 2007).
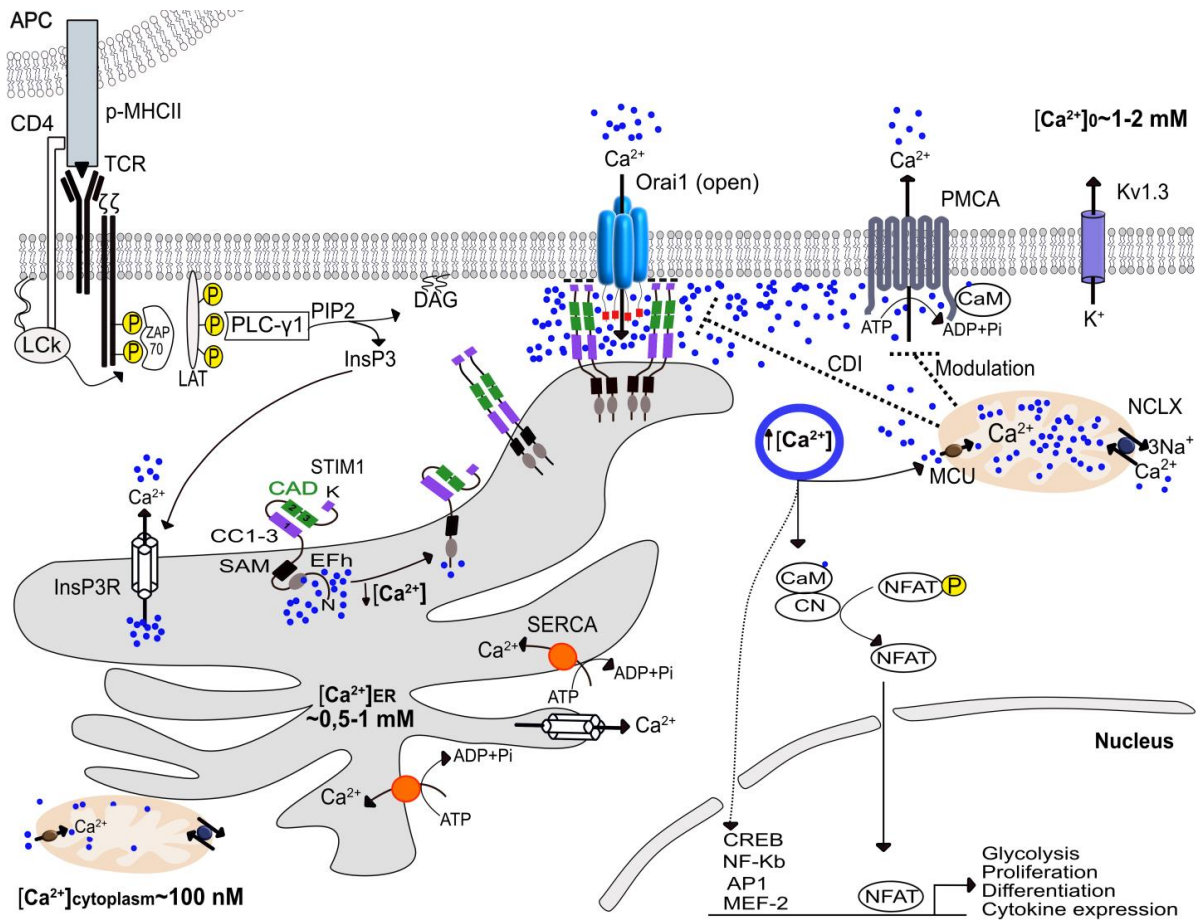
Figure 3. Ca^{2+} influx pathways in T cells.
The binding of peptide-MHCII (p-MHCII) to the T cell receptor (TCR) induces downstream activation of tyrosine kinases, such as LCK and ZAP70, resulting in tyrosine phosphorylation and activation of Phospholipase C-γ1 (PLC-γ1). PLC-γ1 hydrolyzes the membrane phospholipid PIP2 into InsP3 and DAG. InsP3 binds to InsP3 receptors (IP3R) in the ER membrane, releasing Ca^{2+} from ER stores. The fall in ER $[Ca^{2+}]_i$ is sensed by the EF hand domain in STIM1 resulting in unfolding of the STIM1 N-terminus and multimerization. STIM1 multimers translocate to ER-plasma membrane junctions and form clusters or puncta, in which ORAI1 channels are recruited. A minimal CRAC channel activation domain (CAD) located in the C-terminus of STIM1 (green boxes) is sufficient to bind and activate ORAI1 and SOCE. The CAD domain has two coiled (CC) domains, which interact with a CC domain in the C-terminus (red boxes) and N-terminal regions (not shown) of ORAI1. The Ca^{2+} influx elevates $[Ca^{2+}]_i$ and activates the calcineurin (CN)-NFAT pathway. NFAT induces gene transcription in cooperation with other transcription factors (AP-1, NK-β among others), resulting in a metabolic switch, proliferation, differentiation and cytokine expression. Upon TCR activation, some mitochondria translocate and localized beneath to the mouth of ORAI1 channels, which allows them to take large amount of incoming Ca^{2+} and maintain channel activity by preventing its Ca^{2+}-dependent inhibition (CDI). Mitochondria can also dissipate the high Ca^{2+} micro-domains close to PMCA, thereby reducing the Ca^{2+}-microdomain dependent modulation of PMCA, Ca^{2+} extrusion and preserving Ca^{2+} for signaling. Abbreviations: SAM, sterile-alpha motif CaM: calmodulin. Figures shown in (Feske et al., 2012) were taken as basis for this figure.

Introduction

The K^+ channels provide the electrical driving force for Ca^{2+} entry by regulating the negative membrane potential (Vm). The depolarizing inward Ca^{2+} current through CRAC channels is counterbalanced by K^+ required for efficient signal transduction (Cahalan & Chandy, 2009). The predominate K^+ channels regulating membrane voltage (Vm) in lymphocytes are the voltage-activated K^+ channel (Kv1.3) (Attali et al., 1992; Beeton et al., 2006; Grissmer et al., 1990) and the Ca^{2+} activated K^+ channel (KCa3.1) (Grissmer et al., 1993; Partiseti et al., 1992). The Kv1.3 channel contains voltage sensors to sense depolarization of the membrane potential, while KCa3.1 opens after biding of Ca^{2+} to CAM, which is constitutively bound to the channel (Xia et al., 1998). KCa3.1 channel activity is regulated by the class II PI3K , whose function among others, is to increase the concentration of plasma membrane PI(3)P (Srivastava et al., 2006). The contribution of Kv1.3 and KCa3.1 to Ca^{2+} influx in T cells depended on their expression levels and state of activation. For instance, resting naïve human T lymphocytes mainly express Kv1.3 channels and Kv1.3 channels contribute to the overall activation of naïve T cells (Leonard et al., 1992), whereas activated T cells upregulate KCa3.1, which play an important role in TCR-stimulated Ca^{2+} influx and proliferation (Fanger et al., 2000). Besides, EM and CM cells have preferential use of K^+ channels (Cahalan & Chandy, 2009; Srivastava et al., 2006). In this line, EM cells at the inflammation sites particularly upregulate Kv1.3 and produce IFNγ, IL-5 and IL-4 , while CM cells in mucosal lymphoid organs and lymph nodes upregulate KCa3.1 upon activation (Beeton et al., 2006).

Voltage-gated Ca^{2+} channel (Cav channels) are found mostly in excitable cells, such as neurons and muscle cells and induce Ca^{2+} influx after membrane depolarization. In human T cells, all members of the L-type family of CaV (CaV1.1, 1.2, 1.3 and 1.4) are expressed, as well as their regulatory β3 and β4 subunits (Badou et al., 2006; Kotturi & Jefferies, 2005). T cells lacking β3 or harboring a mutation in β4 gene showed impaired Ca^{2+} influx after TCR stimulation but not after thapsigargin treatment (Badou et al., 2006). However, it has been suggested that membrane depolarization does not activate Cav channels in T cells and that alternative gating mechanisms for Cav channels may exist in T cells. It has been proposed that a giant scaffold PDZ protein known as AHNAK1 controls Ca^{2+} entry in T cells (Matza et al., 2008). It is believed that AHNAK1 interacts with the β regulatory subunit of Cav1.1 channels to determine Cav1.1 plasma membrane localization. AHNAK1-deficient mice show altered Ca^{2+} influx, proliferation, and cytokine secretion. However, it remains unknown the molecular mechanism by which AHNAK1 controls Cav channel gating.

TRP channels are six-transmembrane cation-permeable channels that regulate intracellular levels of Na^+, Ca^{2+} and Mg^{2+}. Both Jurkat T cell lines and human T lymphocytes express functional TRPC1, TRPC3, TRPC6, TRPV6, TRPM2, TRPM4 and TRPM7 (Gamberucci et al., 2002; Philipp et al., 2003). The majority of TRP channels are permeable and non-selective to some cations such as Ca^{2+} and Na^+. TRPM2 is one of the most studied TRP channels in T cells. TRPM2 is a non-selective Ca^{2+} permeable channel that is activated by intracellular second messengers such as ADP-ribose (ADPR), cyclic ADPR (cADPR) nicotinamide adenine dinucleotide (NAD^+) and hydrogen peroxide (H_2O_2), (Massullo et al., 2006; Perraud et al., 2001). Upon TCR activation, ADPR activates the channel by binding to the channel's enzymatic Nudix domain, whereas cADPR either directly gate the channel at concentrations above 100 µM or increases the sensitivity of the channel to ADPR at concentrations below 10 µM. Therefore, both ADPR and cADPR can contribute to Ca^{2+} influx via TRPM2 in T cell lines. On the other hand, H_2O_2 produced during inflammatory pathologies

induces Ca^{2+} influx trough TRPM2 channels, thereby contributing to ROS-induced pathologies (Di et al., 2011).

Seven P2X receptors (P2X1-P2X7) are ATP-gated channels with significant Ca^{2+} permeability. Each P2X receptor forms either homomeric or heteromeric P2X receptors. P2X1, P2X2, P2X6 and P2X7 subunits are found in T cells. Extracellular ATP activates the channel resulting in Ca^{2+} influx (Khakh, 2001). Furthermore, TCR activation leads to rapid release of ATP, which activates P2X7 receptors. Activation of P2X7 results in Ca^{2+} influx and calcineurin-dependent pathways, T and B cell proliferation and IL-2 production (Woehrle et al., 2010). This autocrine activation seems to activate T cells through Ca^{2+} influx (Yip et al., 2009).

These results point out the important role of non-store-operated Ca^{2+} channels regulating Ca^{2+} influx and $[Ca^{2+}]_i$ in T cells. Nonetheless, TRP- or P2X receptor-deficient mice do not shown major abnormalities of T cell development and functions (Solle et al., 2001).

2.5   Mechanisms of Calcium Clearance in T Cells

Ca^{2+} is involved in almost all aspects of cell life such as excitability, exocytosis, motility, transcription and programmed cell death. Therefore, cells evolve all types of mechanisms that allow them to integrate and transduce Ca^{2+} rise, while avoiding Ca^{2+} overload induced cell death. In lymphocytes, Ca^{2+} signal can adopt different patterns, from spikes to oscillations to sustained plateaus, depending on the needs of cell (Berridge & Dupont, 1994; Dolmetsch et al., 1998). For instance, the spike and plateau phases activate different downstream pathways implied in B cell activation (Dolmetsch et al., 1998). In lymphocytes, SOCE is considered the main Ca^{2+} entry pathway in T cells, which is tightly controlled directly or indirectly by Ca^{2+} extrusion mechanisms on plasma membrane such as ATPases and Na^+/Ca^{2+} exchanger, as well as through K^+ channels, mobile Ca^{2+} buffers and organelles such as mitochondria and ER. The combined action of these Ca^{2+} regulatory mechanisms controls the time course and amplitude of Ca^{2+} signals. Regardless of the several studies to unravel the role of Ca^{2+} sources in T cell signaling, mechanisms that clear cytosolic Ca^{2+} also determine the amplitude, duration and outcome of Ca^{2+} signals.

2.5.1   Plasma Membrane Calcium ATPases (PMCAs)

2.5.1.1   General properties of PMCAs

Plasma membrane Ca^{2+}-ATPases (PMCAs) are tightly regulated Ca^{2+} extrusion pumps that provide fine-tuning of intracellular calcium concentrations. There are four expressed isoforms in mammalian tissues (PMCA1, PMCA2, PMCA3 and PMCA4), each encoded by a different gene (*ATP2B1-ATP2B4*) on chromosomes 12q21.3, 3p25.3, Xq28, and 1q32.1 in humans respectively. Alternative RNA splicing at sites A and C in PMCA protein structure, leads to the production of multiple splice variants for each PMCA isoform (Strehler, 2013) (Figure 4). Over 30 different PMCA splice forms can thus be generated for each PMCA isoform. PMCA1 and PMCA4 are ubiquitous, whereas PMCA2 and PMCA3 are more tissue-

specific with a higher prevalence in nervous system and skeletal muscle. Absence of PMCA1 in mice results in embryolethality, loss of PMCA2 results in deafness and ataxia and loss of PMCA4, the main calcium efflux protein in sperms, leads to male infertility with few overt effects (Okunade et al., 2004; Prasad et al., 2007).

PMCAs are members of the large family of P-type ion pumps, which form a phosphorylated intermediate during the reaction cycle. Contrary to SERCA pump, which transport $2Ca^{2+}$ ions per ATP hydrolyzed, the PMCA pump hydrolizes 1ATP molecule per Ca^{2+} ion transported (Niggli et al., 1981). PMCAs are single polypeptides containing between 1100 to 1250 amino acids and with a molecular mass of 125 to 140 kDa. They contain 10 membrane-spanning segments and their N-terminal and C-terminal are located in the cytosolic side, as the two major intracellular loops (Di Leva et al., 2008) (Figure 4). The first intracellular loop has been proposed to mediate long-range transmitting conformational changes during the transport cycle and is called actuator domain (A domain). The second one is the major catalytic domain containing the nucleotide-binding (N domain) and catalytic phosphorylation domain (P domain). The N-domain binds ATP to act as a kinase phosphorylating its own P domain (Toyoshima et al., 2000) (Figure 4). In addition, an invariant aspartate residue located in P-domain is transiently phosphorylated during ATP hydrolysis, which is the hallmark of the P-type ATPase family (Palmgren & Nissen, 2011). The long C-terminal tail is crucial for pump regulation, this contains an auto-inhibitory and a CaM-BD, which partially overlaps with the auto-inhibitory domain (Di Leva et al., 2008) (Figure 4). The auto-inhibitory domain interacts not only with the first cytosolic loop, but also with the catalytic core of the pump (Falchetto et al., 1991), to maintain the PMCA in a relatively inactive state at low $[Ca^{2+}]_i$ (Figure 4). A crystal structure of the autoinhibited state of the enzyme showed that its C-terminal regulatory domain interacts with the catalytic core, avoiding substrate and ATP access in the absence of Ca^{2+}-CaM. The elevation in the cytoplasmic Ca^{2+} results in an increase in the formation of Ca^{2+}-CaM bound to the CaM-BD in the C-terminal of the pump, displacing it from its binging to its catalytic part and subsequently removing the autoinhibition of the pump (Goldberg et al., 1996) (Figure 4). While unstimulated PMCA pumps have poor affinity for Ca^{2+}, the binding of Ca^{2+}-CaM leads to a decrease of the Kd for Ca^{2+} from 10-20 µM to less than l µM (Carafoli et al., 1992; Enyedi et al., 1987). A second CaM-BD with much lower affinity for CaM has also been identified (Tidow et al., 2012), which is located downstream of the high affinity one in some splicing variants, supporting the idea that alternative splicing might be a general mechanism for PMCAs in mediating fine-tuning Ca^{2+} signaling.

The activity of PMCAs is also influenced by the phospholipid composition in the surrounding plasma membrane, in this regard, acidic phospholipids and polyunsaturated fatty acids activate the pump by binding to two distinct regions: one is the CaM-BD (Brodin et al., 1992), and the second region is situated in the first cytosolic loop of the pump (Brini et al., 2010) Polyphosphoinositides in particular, are the most potent stimulators of PMCAs (Niggli et al., 1981). Acidic phospholipids are capable to reduce the Michael constant (Km) of the Ca^{2+}- CaM (0.4 ~ 0.7 mM) to as low as 0.3mM, would render PMCAs insensitive to Ca^{2+}-CaM stimulation (Missiaen et al., 1989; Niggli et al., 1981).In contrast, CaM doesn't exert the same effect on acidic phospholipids, meaning acidic phospholipids are capable of further reducing the Km of the Ca^{2+}-CaM stimulated pump (Niggli et al., 1981).
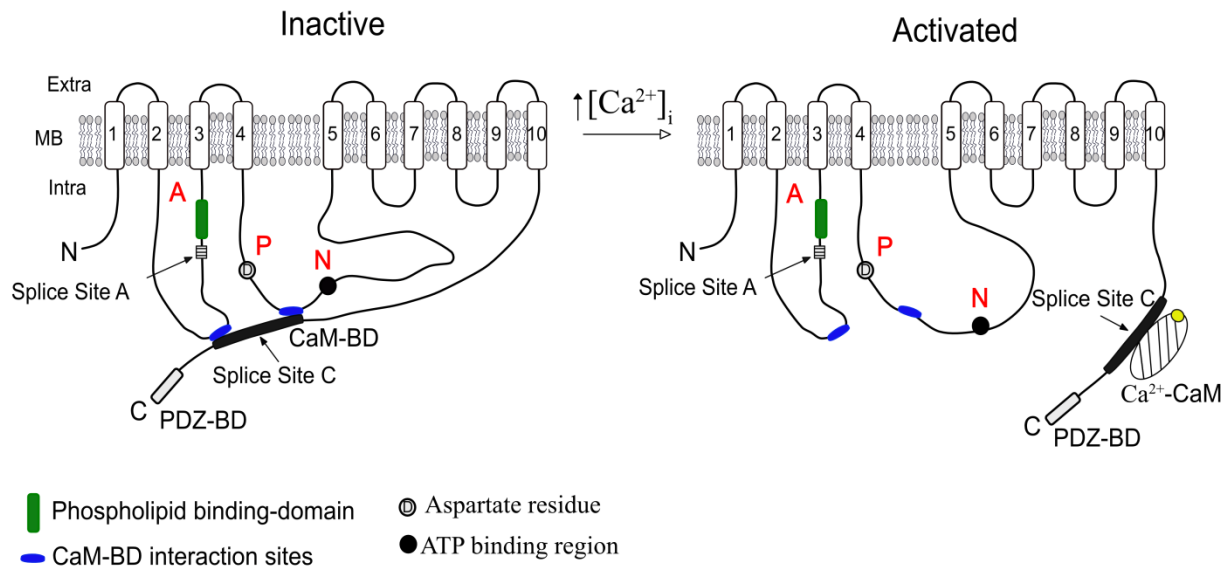
Figure 4: Model of the PMCA in its autoinhibited form (left) and upon stimulation (right).
Binding of Ca^{2+}-CaM onto the COOH terminal of the pump induces a conformational change in the pump structure (right). The PMCAs are thought to consist of 10 transmembrane segments, and their NH2 (N) and COOH (C) terminal regions localize to the cytoplasm. The conserved aspartate residue (D), that form the phosphorylated intermediate during the reaction cycle, phospholipid binding-domain, the calmodulin-binding domain (CaM-BD) and the CaM-BD interaction sites located on the intracellular loops are indicated. The first intracellular loop is called actuator domain (A). The second intracellular loop is the major catalytic domain containing the phosphorylation domain (P) and the nucleotide-binding domain (N). The sites on the protein that can be affected due to splicing at sites A and C are shown. The PDZ domain binding/putative COOH-terminal targeting domain is drawn as a rectangle at the C-terminus. Furthermore, the first and major catalytic loop are represented differently in the inhibited (left) and stimulated (right) state to indicate conformational changes induced by the binding of Ca^{2+}-CaM (hatched oval) to the autoinhibitory CaM-BD. Figure modified from (Strehler & Zacharias, 2001).

2.5.1.2 PMCA transcriptional control and interaction partners

The transcriptional regulation of PMCA genes remain poorly understood, but they are differentially regulated during distinct embryonic development, as well as in different tissues in response to different stimulus (Ritchie et al., 2011). ATP2B1 is expressed early on during embryogenesis and it's kept during the whole organism life. In this line, germ line knockdown of both copies of ATP2B1 is embryonic lethal. In spite of its almost constitutively expression, ATP2B1 have been shown to be regulated by different transcription factors. In mouse vascular smooth cells, the early response transcription factor c-Myb repressed ATP2B1 transcriptional expression during the G1/S phase of the cell cycle (Afroze & Husain, 2000). Early studies of the ATP2B1 gene showed that its transcriptional control is mediated by Protein Kinase C and protein Kinase A, both mediators of hormone-induced second messenger (Ca^{2+}-cAMP), that may act through transcriptions factors as CREB. ATP2B1 transcriptional control is also mediated by vitamin D,1,25 (OH)2 D3, which strongly induces PMCA expression in the osteoblast, small intestine and kidney distal tubules (Glendenning et al., 2001; Kip & Strehler, 2004; Pannabecker et al., 1995). On the other hand,

little is known about transcriptional regulation of the ATP2B4 gene. In this regard, few studies have shown that c-Myc binds directly to a regulatory region of the ATP2B4 promoter to mediate transcriptional downregulation of PMCA4b during B cell differentiation (Habib et al., 2007). Induction of PMCA4b has also been demonstrated in duodenum cells in response to the synthetic anti-inflammatory steroid, dexamethasone (Kim et al., 2009). Besides, splicing on site A and C on PMCAs results in functional changes of the PMCAs, which depend on the cell type and differentiation stage.

In addition to containing the Ca^{2+}-CaM binding site, the COOH-terminal region of the Ca^{2+} pumps is target of phosphorylation by protein kinases A and C (Carafoli, 1994; Penniston & Enyedi, 1998) and target of calpain proteases (Carafoli, 1994). The C-terminal sequence of the b- and most c- and d- splice variants of all PMCAs can bind to PDZ domain-containing proteins, which include members of the Ca^{2+}-CaM-dependent serine protein kinase (CASK), membrane-associated guanylate kinase (MAGUK) family, Na^+/H^+ exchanger, neuronal nitric oxide synthase (nNOS), LIM family protein CLP36, homer protein Ania-3, PMCA-interacting single-PDZ protein (PISP) and regulatory factor 2 (NHERF2) and (Stafford et al., 2017). Additional proteins were shown to bind to the N-terminal tail or distinct regions of the intracellular loops of some PMCAs such as RASSF-1(Armesilla et al., 2004), CaN (Buch et al., 2005) and α1-syntrophin (Williams et al., 2006). Most of the differences among isoforms and splice variants are located in their COOH-terminal tail, making this region a good target of differential phosphorylation. For instance, PKA phosphorylates Ser-1178 in hPMCA1b within the sequence KRNSS increasing pump activity and similar sequence (KQNSS) has been found in only other PMCA isoform (PMCA2b) (James et al., 1989), suggesting that only certain PMCA isoforms are target of PKA phosphorylation. On the other hand, Enyedi et al. showed that PKC affected a region of 20 residues located downstream of the CaM-BD, that overlaps with the autoinhibitory domain of the pump. Phosphorylation by PKC released the inhibition conferred by that region, but only partially stimulated PMCA4. Nevertheless, PMCA pump only showed full activity in the absence of the inhibitory effect of the CaM-BD site. These results reinforce *in vivo* data showing that PKC moderately stimulates the pump, but enhances the effect of Ca^{2+}-CaM on PMCA activation (Smallwood et al., 1988). Besides, it has been shown that tyrosine phosphorylation on PMCA in human platelets causes PMCA downregulation (Dean et al., 1997). It is believed that PMCA can direct its partner proteins to a particular sub-domain with low calcium levels reducing their activity. For instance, it has been proposed that PMCA4b tether nNOS to low calcium micro-environment, which results in significant inhibition of nNOS activity and nitric oxide synthesis (Schuh et al., 2001). PMCA interacts with CaN and leads to inhibition of the CaN-NFAT activity (Buch et al., 2005; Wu et al., 2009). Baggott and colleagues showed that PMCA4 deficient mouse lung endothelial cells (MLEC) exhibited increased NFAT activation following stimulation (Baggott et al., 2014); and in PC12 cells downregulation of PMCA2 or PMCA3 induced a permanent increase in the intracellular Ca^{2+} levels in resting cells and subsequent activation of NFAT1 (NFATc2) and 3 (NFATc4), as well as reduction of dopamine secretion (Kosiorek et al., 2014). An opposite role of PMCA4 on NFAT activity has been shown in vascular smooth muscles cells (VSMC), where PMCA4b knockout VSMCs decreased NFATc3 expression (Afroze et al., 2014). On the other hand, the release of cytochrome C from the mitochondria along with the activation of both caspases and calpains may induce cleavage and PMCA inactivation (Schwab et al., 2002) through internalization and degradation of the protein (Chami et al., 2003). Interestingly, caspase-3-mediated cleavage of PMCA4b generates a

fragment of approximately 120 kD lacking the autoinhibitory domain and showing constitutive activity (Paszty et al., 2007).

Recently, using high-resolution functional proteomics combined with multi-epitope and knockout controlled affinity purification, Schmidt et al. identified two Ig domain-containing proteins: neuroplastin (NPTN or Np) and basigin (also known as CD147 or EMMPRIN), as essential auxiliary subunits of PMCAs. The authors showed that native PMCAs form heteromeric complexes consisting of two pore-forming PMCA1-4 subunits and two of the single-span membrane proteins (neuroplastin or basigin). Formation of a complex of neuroplastin or basigin with PMCAs 1-4 occurred in the endoplasmic reticulum and it was essential for the stability of the pump , as well as for its successful delivery to the cell surface (Schmidt et al., 2017). In the rodent brain, neuroplastin exists as two splice variations highly glycosylated, Np65 and Np55, which differ by a single Ig domain at the extracellular N-terminus of the protein, resulting in molecular weights of 40 and 28 kDa as indicated after deglycosylation (Korthals et al., 2017). While in mouse brain Np65 and Np55 could be detected, in mouse T lymphocytes NPTN55 is the only variant and its expression is increased after activation of purified lymphocytes on immobilized anti-CD3/anti-CD28 antibodies (Korthals et al., 2017).

2.5.1.3   Regulation of intracellular Calcium levels by PMCAs

Two Ca^{2+} extrusion mechanisms operate in Jurkat T cells: the PMCA and the Na^+/Ca^{2+} exchanger (Balasubramanyam et al., 1993; Gardner & Balasubramanyam, 1996). PMCAs provide the dominant mechanism for Ca^{2+} clearance in human T cells (Balasubramanyam et al., 1993) and while some publications have shown a contribution of Na^+/Ca^{2+} exchanger (Balasubramanyam et al., 1993; Gardner & Balasubramanyam, 1996), other publications state that their contribution to Ca^{2+} clearance is not significant in Jurkat T cells (Bautista et al., 2002), in human T cells and the human T cell clone P28 (Donnadieu & Trautmann, 1993). After an increase in $[Ca^{2+}]_i$, PMCA activity rise in two phases: a rapid increase in pump activity occurs due to increased Ca^{2+} occupancy of the pump's transport site (Bautista & Lewis, 2004) a subsequently a several-fold further increase happens over tens of seconds when $[Ca^{2+}]_i$ exceeds several hundred nanomolar (Bautista et al., 2002). Bautista and colleagues experiments showed that increasing the capacitative Ca^{2+} entry (CCE) from 15 to 40s in Jurkat T cells, reduced the initial time constant of recovery after Ca^{2+} removal and that PMCA modulation augmented further PMCA activity by increasing both the affinity (reduced Km) and the maximal rate of the PMCA (Vmax) (Bautista et al., 2002). This modulation has been shown to be reversed slowly with a time constant of 400s after $[Ca^{2+}]_i$ returns to basal levels, giving the pumps a "memory" of the $[Ca^{2+}]_i$ rise. By slowly up-regulating activity, the pump fine tunes its activity to equilibrate Ca^{2+} influx and extrusion rate, and reach steady $[Ca^{2+}]_i$ plateau, even at micromolar levels of $[Ca^{2+}]_i$, which exceeds the Km for the pump (200 nM). Thus, PMCA modulation is important for the stability and dynamic of Ca^{2+} signaling in T lymphocytes by stimulating extrusion and increasing PMCA activity to respond dynamically to higher Ca^{2+} load avoiding toxic levels of $[Ca^{2+}]_i$. In this line, cardiac and hair cells generating rapid signaling, express an quick modulated isoform, PMCA2a, while Jurkat T cells engaged in slower signals, mostly express a isoform with slow modulation, PMCA 4b (Caride et al., 2001).

2.5.2   Regulation of intracellular Calcium levels by Mitochondria

Mitochondria are the main machinery for ATP production and essential regulators of Ca^{2+} signaling in several types of cells. Mitochondrial uptake of Ca^{2+} through the mitochondrial Ca^{2+} uptake/uniport in the inner membrane (mtCU) (Gunter & Pfeiffer, 1990) is driven by the large negative mitochondrial membrane potential. The accumulated Ca^{2+} inside the mitochondrial matrix is released slowly through an antiporter by exchanging Ca^{2+} with Na^+, known as NCLX (Na^{2+}/Ca^{2+}exchanger) (Demaurex et al., 2009). This mechanism that maintain mtCU-induced Ca^{2+} accumulation while preventing matrix Ca^{2+} overload, avoid apoptosis due to accumulation of mitochondrial Ca^{2+} (Palty et al., 2010). The low affinity of mtCU for Ca^{2+} (Kd of 10-15 µM) under physiological conditions, is overcome for the ability of mitochondria to localize at microdomains of high Ca^{2+} or by interactions at interface between ER and mitochondria through mitochondrial-associated ER membranes (MAMs), which allows Ca^{2+} elevations being transmitted to mitochondria (Duchen et al., 2008). In this line, the apparent Ca^{2+}-sensitivity of the mitochondrial calcium uniporter 1 (MICU1) of approximately 4-5 µM (Waldeck-Weiermair et al., 2015) coincides quite well with the ion concentrations at the contact sites between the ER and mitochondria (Giacomello et al., 2010). However, higher affinity mitochondrial Ca^{2+} uptake has been observed in many studies (Santo-Domingo & Demaurex, 2010). The regulation of mitochondrial processes within microdomains relies on the dynamic morphology and motility of mitochondria. These organelles are able to adapt their morphology and spatio-temporal properties by branching, fission and fusion events to respond accordingly to the cell needs (Frieden et al., 2004). Besides, mitochondria can stablish stabile interactions with plasma membrane and ER proteins through plasma membrane-associated membranes (PAM), which are microdomains of the plasma membrane interacting with the ER and mitochondria and allow the interchange of proteins, lipids, and metabolites among these organelles (Koziel et al., 2009). The modulatory role of mitochondria on SOCE has been widely demonstrated; Hoth et al, have shown that the TG-insensitive store (mitochondria) regulates SOCE Ca^{2+} signals by sensing local Ca^{2+} elevations near to CRAC channels. This TG-insensitive store played an essential role sustaining high rate of Ca^{2+} entry and a high $[Ca^{2+}]_i$ plateau after Tg-induced SOCE (Hoth et al., 1997; Quintana et al., 2007). This store showed a high capacity without no saturation signs to $[Ca^{2+}]_i$ higher than 1.8 µM, as well as a Ca^{2+}-dependence on loading Ca^{2+}. The Ca^{2+} dependence appeared to be biphasic, so that low $[Ca^{2+}]_i$ induced low rate of uptake, whereas higher $[Ca^{2+}]_i$ produced a faster nonlinear rate (Hoth et al., 1997). In agreement with these results, others have shown that Ca^{2+} uptake by mitochondria occurs within 8-10s at physiological levels of $[Ca^{2+}]_i$ and using the fluorescent indicator rhod-2 or mitochondrially targeted proteins like aequorin, rapid uptake was detected after activation of IP3-sensitive Ca^{2+} stores (Rizzuto et al., 1993). Bautista et al also evaluated the role of mitochondria to SOCE. From their results, inhibiting mitochondrial Ca^{2+} uptake with antimycin plus oligomycin changed the time recovery after 40s Ca^{2+} pulse, to a single exponential decay with a time constant value that was between the fast and slow time constant values obtained under control conditions. They attributed their results to the capacity of mitochondria to take calcium up during increased Ca^{2+} influx and release it when the $[Ca^{2+}]_i$ falls below 400 nM (Bautista et al., 2002; Colegrove et al., 2000; Hoth et al., 1997). From all these results is clear that mitochondria affect the time course of Ca^{2+} recovery.

On the other hand, Quintana and colleagues showed that under physiological conditions; for instance, after immune synapse formation (IS), mitochondrial control of Orai channels is more efficient due to sustained

global Ca^{2+} signals are significantly bigger than in the presence of Tg-mediated SOCE. This was possible to the redistribution of mitochondria to less than 200nm from the plasma membrane and accumulation of mitochondria beneath the IS (Figure 3). Besides, this effect is enhanced due to accumulation of STIM1, Orai1 and PMCA at the IS. In this way, mitochondria at the IS dissipates the high Ca^{2+} micro-domains and increases global Ca^{2+} by buffering Ca^{2+} deep into the cytosol, as well as reduces the Ca^{2+}-microdomain dependent modulation of PMCA, resulting in enhanced global Ca^{2+} signals needed for NFAT activation and differentiation of T cells (Figure 3). In contrast, in absence of IS, mitochondria are located further away from plasma membrane as at the IS, which make local Ca^{2+} signal higher and global Ca^{2+} signal smaller. This induces slow Ca^{2+}-dependent Orai channel inactivation and increases PMCA4 activity, resulting in less efficient NFAT activation (Quintana et al., 2011).

Due to the amplitude and shape of the SOCE are strongly influenced by the buffering capacity of mitochondria, analyzing mitochondrial function during activation and differentiation of lymphocytes may provide new insights and a better understanding on how this complex process takes place.

2.5.3 Calcium Regulation by SERCA

Sarco-endoplasmic reticulum Ca^{2+}-ATPases (SERCA) pumps excess Ca^{2+} from the cytosol into the ER lumen. They are the main intracellular Ca^{2+} storage organelle, with a steady-state Ca^{2+} concentration of approximately 1mM, close to extracellular concentrations, and with significant heterogeneity in Ca^{2+} levels among its different regions (Rizzuto et al., 2012). Low-affinity, high-capacity buffers like calsequestrin and calreticulin soak up the incoming Ca^{2+}, increasing the storage and Ca^{2+} buffering capacity of the ER (Mekahli et al., 2011). Ca^{2+} release from the ER predominantly occurs via the IP3R and the ryanodine receptor (RyR) (Mekahli et al., 2011) and their contribution to cytosolic Ca^{2+} clearance is minimum in T cells (Bautista et al., 2002; Dolmetsch & Lewis, 1994); nonetheless, SERCA is an essential component of the Ca^{2+} signaling machinery in T lymphocytes. Some SERCA isoforms such as SERCA2b and SERCA3 are expressed in T cell lines and human T cells, and their expression vary with the activation state of the cell. Treatment with phorbol-ester and ionomycin resulted in a two-fold upregulation of SERCA2b, while SERCA3 drops by 90% in approximately 1 to 3 days (Launay et al., 1997). Although the repercussion of these changes are not understood, they may be determined by the relative localization of the SERCA isoforms and their close positioning to stores implied in gating CRAC channels. On the other hand, it is clear that SERCA controls Ca^{2+} signaling through ER store refilling and therefore SOCE, but it doesn't have a direct role in Ca^{2+} clearances unless mitochondria is present. In experiments by Bautista et al, ER store refilling retarded the slow phase of Ca^{2+} clearance rate only after prolonged periods of Ca^{2+} influx (40s), effect that was abolished when mitochondria function was impaired with antimycin A1 plus oligomycin, highlighting the role of ER mediated-store refilling only in the presence of functional mitochondria. Inhibition of both mitochondria and SERCA abolished the slow phase of Ca^{2+} clearance. The authors explained these findings to the communication network between SERCA and mitochondria, with the latter releasing Ca^{2+} that is take up by SERCA and later is released through IP3R located on the ER membrane, thereby slowing the slow phase of Ca^{2+} clearance (Bautista et al., 2002). Taken together, we can conclude that PCMA is the main Ca^{2+} extrusion mechanism in Jurkat T cells and that it is entirely responsible for

controlling Ca^{2+} clearance in the absence of functional SERCA and mitochondria. The spatiotemporal Ca^{2+} signals induced after p-MHC-TCR engagement are integrated in a more complex network that lead to the polarization and accumulation of SOCE and Ca^{2+} related proteins at the IS, decreasing the local Ca^{2+} signals while increasing global Ca^{2+} and therefore the activation state of T-cells.

2.6   Yin Yang 1 transcription factor: Structure and function

Yin Yang 1 (YY1) was discovered as a transcription factor that may act as activator or repressor of its target genes, depending on the presence or not of the viral oncoprotein E1A, hence its name Yin Yang 1. YY1 belongs to the zinc-finger transcription factor family and is a member of the polycomb group (PcG) protein complexes. As a part of the PcG complex, YY1 acts as the DNA targeting subunit of PcG complex, maintaining repressed transcriptional states (Atchison et al., 2003). Studies have shown its role as a transcriptional repressor, activator, or an initiator element binding protein required in dissimilar cellular processes, such as embryogenesis, differentiation, development, proliferation, tumorigenesis, and apoptosis (Gordon et al., 2006). While mice with complete ablation of the YY1 gene died at embryonic stage, mice lacking one YY1 allele showed significant growth delay and developmental abnormalities (Donohoe et al., 1999).

The YY1 gene contains five highly conserved exons encoding a protein with 414 amino acid residues and an predicted molecular weight of 44 kDa, but running in SDS-polyacrylamide gel at around 68 kDa due to posttranslational modifications (Galvin & Shi, 1997; Gordon et al., 2006). The C-terminus domain of YY1 (aa 298-397) (Galvin & Shi, 1997; Shi et al., 1991) contains four C2H2-type zinc-finger that binds to the DNA to repress their target genes. Other domain, rich in glycine residues, located between amino acids 157 and 201 also possess transcriptional repression activity. Two intriguing consensus motif are found within the gliycin-rich motif at amino acids position 176-182 (GxxxxGK) and 189-195 (GxGxxG), but less is known about their contribution to transcriptional repression. On the other hand, the N-terminal region of YY1 acts as a potent activation domain. This region contains 2 clusters: an acidic cluster (aa 43-53) composed by 11 acidic amino acids and 1 histidine-cluster (aa 70-80) formed by 11 consecutive histidines. (Shi et al., 1991).

YY1 can regulate several genes, many of them involved in cancer growth and progression, such as c-Myc, E1A, ERBB2, c-fos and p53.3,4 (Gordon et al., 2006; Sui et al., 2019). Different models of transcriptional regulation by YY1 have been suggested based on experimental data. For instance, it has been suggested that competition of YY1 with activators in overlapping binding sites decreases promoter activity resulting in gene-specific repression of transcription. Other theory proposes that YY1 negatively regulates nearby promoter-bound activators (Galvin & Shi, 1997). On the other hand, transcriptional activation has been suggested though displacement of YY1 by transcriptional activators, an example of this is the displacing of YY1 by NF-kB increased expression, which relieves its repressive effect (Lu et al., 1994). Others have proposed that YY1 can repress their target genes via direct physical binding; for instance, the YY1 zinc-finger motifs interacted with the basic leucine zipper region (bZIP) on the bound CREB protein to the c-fos promoter (Guo et al., 1997). Moreover, Galvin and Shi have argued against the DNA-binding model, they

showed that YY1 interferes with the communication of CREB independently of physical interactions with DNA, which resulted in a delayed CREB-mediated activation (Galvin & Shi, 1997). Other models exemplify the ability of YY1 to recruit co-repressors that facilitate transcriptional repression or induce condensation of chromatin or chromatin remodeling to support YY1-mediated DNA interaction and repression (Thomas & Seto, 1999). YY1 also repress two important cofactors involved in viral regulation, interferon beta (IFN-β) and gamma (IFN-γ). In this line , YY1 binds to the *IFNB* promoter to either activate or repress transcriptional activity of *IFNB*, based on its interaction with HDACs, (Weill et al., 2003). YY1 has been shown to bind to two sites of the *IFNG* promoter inducing repression of basal *IFNG* transcription by either activating the BE silencer element in cooperation with an AP2-like nuclear protein or by blocking AP1 interactions with DNA (Ye et al., 1996).

While the C-terminal of YY1 plays a role in nuclear retention, its N-terminal domain allows low affinity association into the nucleus, and it is not needed for nuclear retention. Last but not least, YY1 is regulated by multiple types of post-translational modifications including poly ADP-ribosylation, acetylation, P-linked glycosylation. S-nitrosylation, sumoylation, phosphorylation, methylation and ubiquitination, as well as it is target of caspases. For instance, YY1 methylation by SET7/9 at two lysine residues was shown important for its *in vitro* DNA binding activity in culture cells, impacting cell proliferation (Zhang et al., 2016). In addition, phosphorylation of YY1 by CK2α at serine 118 in the transactivation domain of YY1, proximal to the caspase-7 cleavage site, protects from apoptosis, whereas knockdown of CK2α enhanced YY1 cleavage under apoptotic conditions (Riman et al., 2012). Two other groups have shown almost at the same time the importance of ubiquitination as an essential mechanism regulating YY1 activity. They showed that Smurf2 Ubiquitin ligase ubiquitinates YY1 and targets it to degradation (Jeong et al., 2014; Ramkumar et al., 2013). The different roles that YY1 plays according to the context and stage of differentiation of the cells, along with the tight regulation at translational level, make YY1 a complex and versatile transcription factor with a wide spectrum of functions.

In the current work, we demonstrated that YY1 binds to the PMCA4 promoter and may regulate the fate of naïve T cells upon activation and memory generation.

3 Materials

3.1 Antibodies

Table 1: Primary and secondary antibodies used for Western Blot and Chromatin Immunoprecipitation

Antibodies	Class/Clone	Host/Isotype	Supplier	Catalog number	Dilution
Primary Antibodies					
Anti-PMCA4 ATPase	Monoclonal JA9	Mouse IgG1	Thermofisher	MA1-914	1:500
Anti-Orai1	Polyclonal	Rabbit	Sigma	O8264	1:1000
Anti-STIM1	Polyclonal	Rabbit IgG	Proteintech	11565-1-A	1:1000
Anti-STIM2	Polyclonal	Rabbit	Sigma	S8572	1:1000
Anti-YY1	monoclonal D5D9Z	Rabbit	Cell Signaling	46395S	1:1000(WB) 1:50 (ChIP)
Anti-GAPDH	Monoclonal 14C10	Rabbit	Cell Signaling	2118	1:2000
Anti- ß-actin	Monoclonal AC15	Mouse IgG1	Abcam	ab6276	1:1000
Anti-NFAT1	Polyclonal	Rabbit	Cell Signaling	4389	1:1000 (WB) 1:50 (ChIP)
Go-ChIP-Grade™ Isotype Ctrl	Polyclonal 29108	Rabbit IgG	Biolegend	910806	1:100
Mouse IgG, k isotype control	Monoclonal	Mouse IgG1	Biolegend	401401	1:100
Secondary Antibodies					
anti-Rabbit IgG HRP-linked F(ab')$_2$	-	Donkey	GE Healthcare	NA9340	1:25000
anti-Mouse IgG HRP-linked whole Ab	-	Sheep	GE Healthcare	NA931	1:5000

Materials

Table 2: Primary antibodies used in flow cytometry

Antigen	Fluorophore	Supplier	Order number
CD4	PerCP-Cy5.5	Biolegend	300530
CD127 (IL-7Ra)	Alexa Fluor® 700	Biolegend	351344
CD25	FITC	Biolegend	302604
CD45RO	PE-Cy7	Biolegend	304230
CD197(CCR7)	Alexa Fluor® 647	Biolegend	353218
CD45RA	PE	Biolegend	304108
CD62L	Pacific Blue	Biolegend	304826
CD69	Pacific Blue	Biolegend	310919
CD154	APC	Biolegend	310809
human TruStain FcXtm	-	Biolegend	422302
IFN-γ	FITC	BD	561053
T-Bet	Brilliant Violet™ 421	BD	563318
GATA3	PE-Cy™7	BD	560405
IL-17A	PE	BD	560486
FoxP3	PE	BD	560046
ROR-γt	Alexa Fluor® 647	BD	563620
IL-4	Alexa Fluor® 647	BD	500712

3.2   DNA oligos

Table 3: DNA oligos used in qPCR, PCR and transient knockdown

Identifier	Primer sequence or order number/ Supplier
ATP2B4 variant a (CCDS 3097.7) + variant b (CCDS 1440.1)	F 5'-AGGCGAGGTAGAGCAAGAAAAG-3' R 5'-GTGTGCTTGTCAGTGGGAGAA-3'

Materials

Identifier	Primer sequence or order number/ Supplier
ATP2B4 variant a (CCDS 3097.7)	F 5'-AACCGTATCCAGACTCAGATCG-3' R 5'-CAAGGTGTTGACCCATGTTCTG-3'
ATP2B4 variant b (CCDS 1440.1)	F 5'-TCCAGACTCAGATCAAAGTGGT-3' R 5'-ATGCTTTCGTGGAGGGAACT-3'
Interferon gamma (INFG)	F 5'-TGTCCAACGCAAAGCAATAC-3' R 5'- TCGACCTCGAAACAGCATCT-3'
Foxp3	F 5'-CAAGTTCCACAACATGCGAC-3' R 5'-CTGAAGAAGGCAAACATGCG-3'
TBP	F 5'-CGGAGAGTTCTGGGATTGT-3' R 5'-GGTTCGTGGCTCTCTTATC-3'
STIM1	F 5'-CAGAGTCTGCATGACCTTCA-3' R 5'-GCTTCCTGCTTAGCAAGGTT-3'
STIM2	F 5'-GTCTCCATTCCACCCTATCC-3' R 5'-GGCTAATGATCCAGGAGGTT-3'
Orai1	F 5'-ATGAGCCTCAACGAGCACT-3' R 5'-GTGGGTAGTCGTGGTCAG-3'
Orai2	F 5'-TGGAACTGGTCACCTCTAAC-3' R 5'-GGGTACTGGTACTGCGTCT-3'
Orai3	F 5'-GTACCGGGAGTTCGTGCA-3' R 5'-GGTACTCGTGGTCACTCT-3'
TRPM2	F 5'-GAACTCTAACCTGCACGCCT-3 R 5'-GAGGAGGGTCTTGTGGTTCG-3'
PTK2	F 5'-GTGCTCTTGGTTCAAGCTGGA-3' R 5'-GCAAGATGTGTGGGATTGCAG-3'
CACNA2D2	F 5'-AGCTGGTTCCAAGCAGACC-3' R 3'-CGTTTACCGAGCCGAAGTAG-5'
TRPC1	F 5'-GCGTGCGACAAGGGTGAC-3' R 5 '-ACAGCATTTCTCCCAAGCACAT-3'
CAMK2D	F 5'-GAAGCTGATGCCAGTCATTGTA-3' R 5'-TGACTTCAGGTCCCTGTGAA-3'
PMCA4 promoter region primers	F 5'-CACCACCGTGCCAGCTAA-3' R 3'-GAAGGGTGCTAGTTGGACA-5'
Hs_YY1_1 SG QuantiTect Primer Assay	QT00052738/ Qiagen
Hs_ATP2B1 QuantiTect Primer Assay	QT00087045/ Qiagen
Hs_ATP2B2 QuantiTect Primer Assay	QT00046123/ Qiagen
Hs_ATP2B3 QuantiTect Primer Assay	QT00090643/ Qiagen
Hs_TBP_1_SG QuantiTect Primer Assay	QT00000721/ Dharmacon
Hs_TRPC3_1_ SG QuantiTect Primer Assay	QT00025025/ Qiagen

Identifier	Primer sequence or order number/ Supplier
Hs_TRPC6_1_ SG QuantiTect Primer Assay	QT00037660/ Qiagen
Accell Human ATP2B4 siRNA' SMART pool	E-006118-0005/ Dharmacon
Accell Human Control siRNA Kit	K-005000.R1-01/ Dharmacon

3.3 Cytokines and neutralizing antibodies

Table 4: Polarizing cytokines and neutralizing antibodies

Reagent	Supplier	Product number
Human IL-12, premium grade	Miltenyi Biotech	130-096-705
Human IFN-g1b, premium grade	Miltenyi Biotech	130-096-482
Human TGF-ß1, premium grade	Miltenyi Biotech	130-095-066
Human IL-2, premium grade	Miltenyi Biotech	130-097-748
Human IL-23, research grade	Miltenyi Biotech	130-095-758
Human IL-1B, premium grade	Miltenyi Biotech	130-093-897
Human IL-4, premium grade	Miltenyi Biotech	130-093-917
Human Anti-IL-4 pure, functional grade	Miltenyi Biotech	130-095-753
Human Anti-IL-12 pure, functional grade	Miltenyi Biotech	130-095-755
Human Anti-IL-10 pure, functional grade	Miltenyi Biotech	130-096-041
Human Anti-IFN-γ pure, functional grade	Miltenyi Biotech	130-095-743

3.4 Key chemicals

Table 5: Key chemicals and reagents

Key Chemicals	Supplier	Product/Order number
Ammonium persulfate (APS)	Sigma Aldrich	248614-56
Albumin from bovine serum (BSA)	Thermo Fisher Scientific	C3100MP

Materials

Key Chemicals	Supplier	Product/Order number
Calcium chloride solution (CaCl$_2$)	J.T. Baker	0504
Complete Protein Inhibitor	Merck	05892791001
Dimethylsulfoxid (DMSO)	Sigma Aldrich	D4540-100ML
Ethylenediaminetetraacetic acid (EDTA)	Sigma Aldrich	E9884
Ethanol	Sigma Aldrich	32205
Fetal calf serum (FCS)	Thermo Fisher Scientific	10270-106
Methanol	Fisher Chemical	M3950
Natriumazid (NaN3)	Sigma Aldrich	S8032
Isopropanol	Sigma Aldrich	19516
Sodium chloride solution (NaCl)	Sigma-Aldrich	S9888
Penicillin/Streptomycin	Sigma Aldrich	P4333-100ML
4-(2-hydroxyethyl)-1 piperazineethanesulfonic acid HEPES	Sigma	H7523
Precision Plus Protein Dual Color	Bio-Rad	161-032
Sodium dodecyl sulphate (SDS)	Acros organics	327315000
N,N,N',N' Tetramethylethylendiamin (TEMED)	Sigma Aldrich	T9281
Tween-20	Sigma Aldrich	P1379
β-Mercaptoethanol	Acros Organics	125472500
Agarose Broad Range T846.3	Carl Roth GmbH	T846.3
Chloroform 99 % (500 ml)	Sigma	C-2432
Diethylpyrocarbonat (DEPC)	Sigma	D5758
Fura-2AM	Invitrogen	F1221
Ionomycin (1mg)	Calbiochem	407950

Materials

Key Chemicals	Supplier	Product/Order number
Poly-L-ornithine hydrobromide	Sigma	P3655
Thapsigargin (Tg)	Invitrogen	T7458
Trizol Reagent	Invitrogen	15596-026
Peroxidase from horseradish	Serva	31943
Propidium Iodide (PI)	VWR	BTIU40016

3.5 Solutions

Table 6: Standard solutions and media composition

Solutions	Composition/ Catalog number
Key Solutions for Western Blots	
RIPA lysis buffer 1x	50 mM Tris 150 mM NaCl 0.1% SDS 1% NP40 0.5% Sodium deoxycholate in PBS; pH 7.5
DM lysis buffer 1x	20 mM Tris 10 mM KCL 10% glycerin (v/v) 0.5% n-Dodecyl β-D-maltoside (DMM) in PBS; pH 7.4
Laemmli buffer 5x	125 mM Tris pH 6.8 2.5% SDS 0.1% Bromphenol blue 60% Glycerin 25% β-Mercaptoethanol
Stacking buffer	0.5 M Tris-HCl 0.4% SDS in H_2O dest; pH 6.8

Materials

Solution	Composition/ Catalog number
Separating buffer	1.6 M Tris-HCl 0.4% SDS in H_2O dest; pH 8.8
Electrophoresis running buffer	25 mM Tris 190 mM glycine 0.1% SDS in H_2O dest; pH 8.3
Blotting buffer	20% Methanol 1% SDS 250 mM Tris-HCl 1.92 M Glycin in H_2O dest; pH 8.3
Tris-buffered saline with Tween 20 10x (TBST 10x)	5 mM Tris-HCl 1.5 mM NaCl in H_2O dest; pH 7.5
Tris-buffered saline with Tween 20 1x (TBST 1x)	0.1% Tween 10% TBS 10x in H_2O dest; pH 7.5
Preparation of primary antibody for Western Blot	1% BSA 0.02% NaN3 in PBS
Preparation of secondary antibody for Western Blot	5% skimmed milk in TBST 1x

Ringer solutions (Physiological solutions for Ca^{2+} imaging)

Ringer solution without Ca^{2+}	145 mM NaCl 4 mM KCl 10 mM Glucose 10 mM HEPES 2 mM $MgCl_2$ 1 mM EGTA Osmolarity: ~310 mosm; pH 7.4

Materials

Solutions	Composition/ Catalog number
Annexin binding buffer 10x	0.1 M Hepes 1.4 M NaCl 25 mM $CaCl_2$ solution in H_2O dest; pH 7.4
Buffers for ChIP Assay	
Coupling buffer (to conjugate Abs to protein A/G agarose beads)	0.01 M sodium phosphate 0.15 M NaCl pH 7.2
Lysis buffer used after fixation and crosslinkers of proteins	20 mM Tris 100 mM KCl 10% glycerine (v/v) 0.5% n-Octyl-β-D-glucopyranoside
Binding buffer	20 mM Tris, 100 mM KCl 10% glycerine (v/v)
Low-salt buffer	50 mM Tris/HCl 150 mM NaCl 0.1% SDS 0.1% NaDoc 1% Triton X-100 1 mM EDTA
High-salt buffer	50 mM Tris/HCl 500 mM NaCl 0.1% SDS 0.1% NaDoc 1% Triton X-100 1 mM EDTA
LiCl buffer	10 mM Tris/HCl 250 mM LiCl 0.5% IGEPAL CA-630 0.5% NaDOC 1 mM EDTA

<div align="center">Materials</div>

Solution	Composition/ Catalog number
TE buffer	10 mM Tris/HCl 1 mM EDTA
Dulbecco's Phosphate Buffered Saline (1x) (DPBS)	14190-094 Invitrogen/Gibco
Hank's BSS (1x) (HBSS)	H15-009 PAA Laboratories
LSM 1077 Lymphocyte Separation Media (Ficoll)	C-44010 PromoCell
AIM-V Medium	Thermo Fisher Scientific

3.6   Key kits, devices and special laboratory equipment

Table 7: Key kits, devices and special laboratory equipment

Kits /Devices	Supplier	Catalog number
BCA Protein Assay Kit	Thermo Fisher Scientific	23225
Clarity Western ECL	Bio-Rad	1705060
Negative CD4$^+$ Isolation Kit	Miltenyi Biotec	130-096-533
MitoProbe DilC1 assay kit	Thermoscientific	M34151
Super ScriptTMII Reverse Transcriptase	Life technologies	18064-014
Zombie Aqua Fixable Viability Kit	Biolegend	423101
QuantiTect SYBR Green Kit	Qiagen	204145
MitoTracker-Red	Thermoscientific	M22425
MACS SmartStrainers, 30 µM	Miltenyi	130-098-458
RNeasy Plus Micro kit (50)	Qiagen	74034
RNeasy Plus Mini Kit (50)	Qiagen	74134
Protein A/G Plus Agarose, 2ml	Santa Cruz Biotechnology	Sc-2003
PVDF Membranes	Merck	IPVH 0001
Falcon® 96-Well flat bottom for cell culture	VWR	353219
Zombie NIR™ Fixable Viability Kit	Biolegend	423105

Materials

Kits /Devices	Supplier	Catalog number
BD Fixation/Permeabilization Solution Kit	BD	554714
G3 Human gene expression v3 microarray	Agilent	5188-5242/5973-1507/5188-5242A
ChemiDoc TM XRS	Bio-Rad	-
CO2 Inkubator Heracell 150i	Thermo Fisher Scientific	-
CO2 Inkubator Heraeus	Thermo Fisher Scientific	-
Infinite M200 Pro	Tecan	-
pH Elektrode Accumet Basic	Thermo Fisher Scientific	-
CFX96TM Real-Time System C1000TM Thermal Cycler	BioRad	-
Cell Observer Primo Vert	Zeiss	-
NanoDrop One Spectrophotometer	Thermo Scientific™	-
FACSVerse™	BD Biosciences	-
Qsonica Sonicator Q700	Thermoscientific	-
FACSAria III	BD Biosciences	-

4 Methods

4.1 Isolation of PBMC from peripheral blood

Blood samples were collected from healthy donors in the Institute of Clinical Hemostaseology and Transfusion Medicine, Saarland University, Homburg. Research was approved by the local ethical committee (83/15; FOR2289-TP6, Niemeyer/Alansary). To isolate the PBMC, the LRS or Amicus chambers, containing residual blood from preparative hemapheresis kits were used as a source of PBMCs.

A 50 ml Leucosep tube was loaded with 17 ml LSM 1077 lymphocyte separation medium and centrifuged for 30 s (1000 g, RT) to allow the medium pass through the filter. The LSM 1077 lymphocyte separation medium is a Ficoll based separated solution composed by a hydrophilic polymer of sucrose which allows the separation of cells according to their own density during centrifugation. The LRS or Amicus chambers are flushed with approximately 30 ml of Hank's BSS and collected in the prepared Leucosep tube. Following the Leucosep tube containing the cells was centrifuged at 450 g at RT for 30 min, without brake and low acceleration (Acc.:1). After centrifugation, the PBMC were enriched in the white ring between the yellowish colored blood plasma and the colorless separation medium. The blood plasma was aspirated and discarded, while the white PBMC ring was transferred to a new 50 ml tube and filled up to 50 ml with Hank's BSS. After a further centrifugation step at 250 g for 15 min at RT, erythrocytes were lysed by incubating the cell pellet with 2 ml erythrocyte lysis buffer for 2 min. Erythrocytes debris were removed by washing with 50 ml of Hank's BSS at 200 g for 10 min at RT. The remaining PBMCs were resuspended in 20 ml PBS supplemented with 0.5% BSA and the cell suspension filtered using a 30 μm pore size strainer. Finally, the cell concentration was determined using the Z2 counter from Beckman Coulter and $0.4x10^6$ or $0.8x10^6$ PBMC were resuspended in AIMV medium at a final concentration of $5.92x10^6$ cells/ml and 2 ml of the cell suspension was added into each well of a 6 well plate and incubated overnight at 5% CO2 and 37ºc to allow the adherence of cells to the bottom of the plate.

4.2 Isolation of CD4$^+$ T cell subtypes from peripheral blood

4.2.1 Staining Procedure

Total CD4$^+$ T cells were isolated from the non-adherent fraction after overnight incubation of PBMCs either by FACS sorter or using a CD4$^+$ negative isolation Kit (Miltenyi, #130-096-533) followed by automated cell isolation system (Miltenyi, AutoMACS), according to the manufacturer's instructions. For isolation of CD4$^+$ specific subtypes, the enriched fraction containing mostly cells in suspension, were harvested in 50 ml tubes and centrifuged at 300 rcf for 10 min at 22°C. The pelleted cells were washed two times with 45 ml of cold PBS + 0.5% BSA, by moving the tube up and down slowly approximately 10 times, followed by centrifugation at 320 rcf for 5 min at 4°C. After the second washing, the PBMC were mixed with a blocking reagent specific for the Fc-receptors (human TruStain FcXtm) at a final dilution of 1/50 and incubate for 10 min at RT. This step prevents the binding of Fc-receptors on remaining APCs to the antibodies used for cell staining. Next, without washing a mix of fluorescent-conjugated monoclonal antibodies specific for cluster

of differentiations (CD) expressed on CD4$^+$ subtypes, was added to a final dilution of 1:40, mixed well and incubated for 45 min in ice protected from light. The mix of antibodies used varies depending on the target population to sort (Table 8). Afterward, 45 ml of PBS+0.5% BSA was added to the cells and washed by moving the tube up and down slowly approximately 10 times followed centrifugation at 320 rcf for 5 min at 4°C. This washing step was performed two times more as described before. After washing, the cells were resuspended in 4 ml of PBS+0.5% BSA and the cell suspension passed through a 30 or 40 μM cell strainer in order to get rid of agglomerates formed due to cell debris. The filtrated cells were directly collected in 4 ml sterile FACS tubes and subsequently Propidium Iodide (PI) was added to a final concentration of 1 μg/ml to the suspension cells. Post sorted CD4$^+$ T cell subtypes were seeded at density of 2×10^6 cells/ml in AIMV medium containing 1% Pen/Strep and cultured for at least 24 h before conducting experiments. The medium culture of regulatory T cells was also supplemented with 10ng/ml of recombinant human IL-2.

Table 8: Mix of antibodies used for sorting CD4$^+$ T cell subtypes out of PBMC

Subtypes	Antibodies
Total CD4$^+$: (CD4$^+$CD127$^+$)	CD4-PerCP-Cy5.5
Naïve: (CD4$^+$CD127^{high}CD25$^-$CD45RO$^-$)	CD127-Alexa Fluor® 700
Memory: (CD4$^+$CD127^{high}CD25$^-$CD45RO$^+$)	CD25-FITC
RegT: (CD4$^+$CD127^{low}CD25$^-$CD45RO$^+$)	CD45RO-PE-Cy7
Naïve: (CD4$^+$CD127^{high}CD25$^-$CD45RO$^-$CCR7$^+$)	CD4-PerCP-Cy5.5
EM: (CD4$^+$CD127^{high}CD25$^-$CD45RO$^+$CCR7$^-$)	CD127-Alexa Fluor® 700
CM: (CD4$^+$CD127^{high}CD25$^-$CD45RO$^+$CCR7$^+$)	CD25-FITC
EMRA: (CD4$^+$CD127^{high}CD25$^-$CD45RO$^-$CCR7$^-$)	CD45RO-PE-Cy7
	CCR7-Alexa Fluor® 647

4.3 Flow Cytometry and Fluorescence Activated Cell Sorting analysis

4.3.1 The principle of Flow Cytometry

In flow cytometry the sample is hydrodynamically focused in the core stream and single cell or particle passed through an analytical laser beam source for interrogation. Once a fluorescent sample is intercepted by the lasers, an optical-to-electronic system registers the light scattered and fluorescence emitted from the cells or particles, thereby allowing drawing conclusions about the properties of the cells. Cellular components such as cell membranes, granular material, nucleus, as well as cell shape and surface topography contribute to the scattering of the light. Hence, forward scatter light (FSC) is a measure of diffracted light that is proportional to the cell-surface area or size of cell or particles and is measured along the path of the laser beam in the forward direction. On the other hand, sideward scatter light (SSC) represents refracted and reflected light product of a change in the index of refraction at any cell interface and it is recorded at 90 degrees to the laser beam, being proportional to cell granularity or internal complexity. In

addition to size and granularity analysis, flow cytometry facilitates expression analysis by labeling samples with a mix of fluorescent-labeled antibodies specific for different epitopes, simultaneously allowing the identification of complex populations harboring specific expression patterns.

On the other hand, Fluorescent Activated Cell Sorting (FACS) shares the same principle as flow cytometry, but unlike flow cytometry, samples that were interrogated by the laser beam are not subsequently discarded to the waste but rather separated and further processed. In this regard all FACS equipment are equipped with a sorting feature that allows to sort populations after the population of interest have been defined on a data acquisition plot. Once a target particle is detected, an electrical charge is applied to the stream so that the droplet containing that particle breaks off from the stream. Subsequently, the charged droplet passes by two strongly charged (2000-6000 volts) deflection plates and depending on the droplet's charge polarity, the droplet is deflected to the left or right. Uncharged droplets are left unaffected and directed from the straight stream to the waste aspirator. In order to guarantee the precision of the sorting process, the drop delay (time between particle interrogations and droplet breakoff point) should be calculated and kept constant during the whole sorting procedure. Other parameters such as the flow rate, sort precision mode among others determine the efficiency and purity of the sorted populations.

In the context of this work, two flow cytometers were used for the analysis of cells; a BD FACSVerse™ Flow Cytometer for flow cytometry analysis and BD FACSAria™ III Sorter for isolation and separation of interested populations.

4.3.2   FACSVerse cytometer

Flow cytomery analysis of cells was done using a FACSVerse flow cytometer by Becton Dickinson and BD FACSuite™ software equipped with three lasers; a blue laser: 488 nm, filters: 530/30, 575/26, 670/14, 695/40, 780/60; a red laser (640 nm), filter: 660/20, 780/60; violet laser: 405 nm, filter: 450/40, 525/50). The measured data were displayed either in a histogram as percentages, the median fluorescence intensity (MFI) of a population or as a dot plot where individual fluorescent values for each cells are plotted. For quantification, gates were set to define cellular populations based on the measured expression of surface markers characteristic of each, as mentioned in the result section. The analysis of the data was carried out using the FlowJo software 10.0.7.

4.3.3   FACSAria III sorter cytometer

The sorting of $CD4^+$ subtypes was performed on a FACSAria III sorter cytometer at the Core Facility Cytometry of the Physiology department, Centre for Integrative Physiology and Molecular Medicine, Saarland University. The FACS Sorter was integrated with a FACSDiva software version 6.1.3 and equipped with 4 lasers, allowing the detection up to 11 different colors. The four lasers consist on a blue (B) laser: 488 nm, filter 503/30, 695/40; red (R) laser: 633 nm, filters: 660/20, 730/45, 780/60; near ultra violet (nUV) laser: 375 nM, filters: 510/50,450/40 and yellow and green (Y/G) laser: 561 nM, filters: 582/15, 670/14, 610/20, 780/60. The configuration selected for sorting was (3B-3R-2nUV-4YG) and the nozzle size

used 70 μM. Before starting, the FACS machine was prepared for aseptic sorting and the drop delay was automatically calculated using fluorescent Acudrop BD beads before running each sorting. After successful drop delay calculation, proper compensation was done and cells were sorted at 4°c at 10000 events/s reaching sort efficiency higher than 95% in most of the cases. The purity of the cells was further confirmed post-sorting and it was more than 99%.

4.3.4   Post sorting analysis of sorted CD4+ T cell compartments

Post sorting analysis of CD4+ compartment was done immediately after sorting of the CD4+ compartments. Briefly $0.2x10^6$ cells were washed in FACS buffer two times at 320 g for 5 min at 4°c and 50 μl of a mix of monoclonal antibodies specific for CD4, CD45RO, CD45RA and CCR7 was added at a final dilution of 1:40. Following, cells were incubated for 25 min on ice protected from light. After staining cells were washed two times with 2 ml FACS buffer and re-suspended in 400 μl FACS buffer and analyzed by flow cytometry using a FACSVerse (BD) flow cytometer.

4.3.5   Analysis of compartment distribution and activation markers by flow cytometry

Approximately $0.2x10^6$ siRNA-transfected and stimulated cells were harvested in 4 ml FACS tubes and right after 1 ml of PBS was added to the tubes. The suspension cells were subjected to the magnetic field of magnetic separator (DynaMag Miltenyi), in order to remove the anti-CD3/CD28 magnetic beads. The non-bound fraction was then collected in a new 4 ml FACS tubes and washed to times with 2 ml of PBS by centrifugation at 320g for 5 min and 4°C. Next, cells were stained with 25 μl of viability dye (Zombie Aqua Fixable Viability Kit, Biolegend) to a final dilution 1:1000 at room temperature (RT) and protected from light. Cells were washed two times with 2 ml FACS buffer by centrifugation at 320 g for 5 min at 4°C. Subsequently, a 25 μl mix of monoclonal antibodies specific for CD4 (dilution 1/40), CD45RO (dilution 1/40), CCR7 (dilution 1/40), CD62L (dilution 1/100), CD25 (dilution 1/40) or a mix of monoclonal antibodies specific for CD69 (dilution 1/100) and CD154 (dilution 1/40) were added and incubated for 25 min on ice protected from light. After staining, cells were washed two times with 2 ml FACS buffer and re-suspended in 400 μl FACS buffer and analyzed by flow cytometry using a FACSVerse (BD) flow cytometer.

4.3.6   Mitochondrial staining

4.3.6.1   Active membrane potentials staining (DilC1 Staining)

For analysis of active membrane potentials, $0.2 x10^6$ cells/ml were incubated or not with CCCP to a final concentration of 50 μM in warm phosphate-buffered saline and incubated at 37°C and 5% CO2 for 5 min. Next, DiIC1 was added to a final concentration of 50 nM and cells were incubated at 37°C, 5% CO2 for additional 20 min. DilC1 stained cells were washed once with 2 ml of warm phosphate-buffered saline and the DiIC1(5)-stained cells resuspend in 50 μl of 1x annexin binding buffer followed by addition of 2.5 μl annexin V conjugate (annexin V-Alexa Fluor® 488 conjugate, V13241) and 0.5 μl of a 100 μg/ml propidium

iodide solution. Samples were incubated at 37°C, 5% CO2 for additional 15 min. After incubation 400 µl annexin binding buffer were added into each tube and samples were analyzed on a FACSVerse Cytometer.

4.3.6.2   Mitochondria size staining

For analysis of mitochondria size, 0.2×10^6 cells were resuspended gently in 1 ml of prewarmed (37°C) staining solution containing the MitoTracker-Red probe at a final concentration of 25 nM and incubated under growth conditions at 37°C, 5% CO2 for 20min. After incubation, the MitoTracker-Red-stained cells were washed once with 2 ml of warm phosphate-buffered saline and the MitoTracker-Red-stained cells resuspended in 50 µl of 1x annexin binding buffer followed by addition of 2.5 µl annexin V conjugate (annexin V–Alexa Fluor® 488 conjugate) and 0.5 µl of a 100 µg/ml propidium iodide solution. Samples were incubated at 37°C, 5% CO2 for additional 15 min. After incubation 400 µl annexin binding buffer was added into each tube and samples were analyzed on a FACSVerse cytometer.

4.4   *In vitro* polarization of naïve CD4+ T cells into CD4+ T helper subtypes

The *in vitro* polarization of naïve CD4+ T cells was done according to the protocol previously developed in our group (Kircher et al., 2018). Briefly, 2×10^6 cells/ml in AIMV medium without FCS but containing 1% Pen/Strep were seeded in 12 well flat bottom plates and stimulated with anti-CD3/CD28 coated expander beads (Dynabeads® Human T-Activator CD3/CD28) for 7 days to 1:10 bead: cell ratio under control non-polarized cells (Th0) or polarized conditions. Th0 were cultured with anti-INFγ (20 µg/ml), anti-IL4 (10 µg/ml) and IL-2 (10 ng/ml); Th1 with IL-12 (20 ng/ml), INFγ (5 ng/ml), anti-IL4 (10 µg/ml) and IL-2 (10 ng/ml); regulatory T cells (regT) with TGF-β1 (5 ng/ml), anti-INFγ (20 µg/ml) and IL-2 (10 ng/ml); Th2 with anti-INFγ (20 µg/ml), anti-IL-12 (10 µg/ml), anti-IL10 (10 µg/ml), IL-2 (10 ng/ml) and IL-4 (30 ng/ml) and Th17 with L-6 (30 ng/ml), IL-1β (10 ng/ml), IL-23 (100 ng/ml), anti-INFγ (20 µg/ml), anti-IL4 (10 µg/ml) and TGF-β1 (0.1 ng/ml).

4.5   Intracellular staining of cytokines and transcription factors

At the end of polarization period, 0.25×10^6 to 0.5×10^6 cells were re-stimulated with 5 ng/ml PMA and 500 ng/ml ionomycin for 4 h in presence of Golgistop (according to manufacturer's instructions, BD). Next, cells were harvested and the antiCD3/CD28 beads removed. After washing two times the cells with PBS, cells were stained with a viability dye (Zombie NIR Fixable Viability Kit, Biolegend) at a final dilution of 1:1000 for 20 min at RT, followed by surface staining for CD4 and eventually fixed and permeabilized using commercial buffer (BD FixPerm Solution). Antibodies used for staining were supplied from Becton Dickinson and are shown in (Table 2). Flow cytometric analysis was performed using a FACSVerse cytometer.

4.6   Microarray analysis of Th0, Th1 and regT subtypes

To perform a microarray gene expression of Th0 and regT subtypes, naïve T cells from 5 donors were polarized into Th1 or regT subtypes as previously described (section 4.5) and total RNA was isolated using Trizol as explained in section 4.8.1. The quality of the isolated RNA was insured by measuring the RNA integrity number (RIN) using Agilent 2100 Bioanalyzer (Agilent Biotechnologies). Expression analysis was performed using Gene Expression Hybridizaiton Kit (5188-5242-A), (Agilent Biotechnologies). RNA processing and microarray hybridization were performed at the Department of Human Genetics of the University Hospital of Saarland, Prof. Dr. Eckart Meese's lab with the help of Dr. Nicole Ludwig. The RNA was amplified and labeled using a G3 Human gene expression v3 microarray (Agilent), following the manufacturer's instructions. Analysis of the microarray data was done in collaboration with the Department of Clinical Bioinformatics, University of Saarland, Prof. Dr. Andreas Keller's lab with the help of Dr. Mustafa Kahraman and also using Advaita Bioinformatics/iPathwayGuide software (Advaita, Plymouth, MI, USA) (Ahsan & Draghici, 2017). Volcano Plots were built using the negative log (base 10) of the adjusted p-value (obtained using a False Discovery Rate approach) and log (base 2) of the fold change in gene expression. Most differentially expressed genes were selected using thresholds of 0.6 for expression change and 0.05 for significance. For gene ontology analysis, p-value correction was done using the elim and weight pruning method, that eliminates duplicates or redundant entrances (Alexa et al., 2006).

4.7   Transfection

For downregulation of PMCA, 2×10^5 cells were seeded in 96-well plate in Accell siRNA Delivery Media (ADM, Horizon) supplemented with 10 ng/ml of recombinant IL-2 and transfected with 1 μM accell siRNA targeting ATP2B4 (Accell Human ATP2B4 siRNA - SMARTpool, E-006118-00-0005, Horizon) or non-silencing control RNA (Accell Non-targeting Pool, D-001910-10-05, Horizon) in 100 μl final volume according to the manufacturer's instructions. Seventy-two hours later cells were harvested for mRNA or functional analysis (see sections compartment distribution and SOCE measurement).

4.8   RNA isolation and cDNA synthesis

For Isolation of total RNA from cells two methods were used depending on the number of available cells. In the cases where more than 2×10^6 cells were available, isolation was done using Trizol reagent whereas for smaller numbers of cells we used RNeasy Plus Micro kit from Qiagen (up to 5×10^5 cells) or the RNeasy Mini Kit Qiagen (from 1×10^6 cells) following the manufacturer's instructions.

4.8.1   Trizol isolation of total mRNA

Total RNA from CD4$^+$ T cells were isolated using 800 μl of Trizol reagent containing Phenol and Guanidiniumthiocyanate. Samples were stored at -80°C in Trizol prior to further handling. Upon use, cells were thawed at RT and centrifuged at 12000 g for 10 min at 4°C to remove the cell debris. Cell lysis and

digestion of endogenous RNAses are achieved by adding guanidine thiocyanate solution. The supernatant was further incubated at RT for 5 min and 200 µl chloroform were added and mixed with vigorous shaking, then samples were incubated for 2 to 3 min at RT and centrifuged at 12000 g for 15 min at 4°C. After centrifugation, three liquid layers were detectable; where the upper aqueous layer contained the RNA, the intermediate layer DNA and the lower organic layer proteins. The RNA-containing fraction was transferred to a fresh tube and was pulled down by addition of 1 µl glycogen (Invitrogen) and 500 µl isopropanol followed by incubation at RT for 10 min. After centrifugation at 1200 g for 10 min at 4°c the supernatant was removed and RNA was washed with 1 ml ethanol 75% in DEPC-treated H_2O. RNA pellets were dried, suspended in 10 µl DEPC-treated H_2O. The integrity of the RNA was confirmed by a 2% agarose gel. RNA concentration was determined using a 1 µl of siRNA using a nanoDrop One Spectrophotometer. The ratio of absorbance 260 to 280 and 260 to 230 were used to determine purity of the total mRNA. The ratio of absorbance 260 to 280 indicates contaminants that absorb at 280 nm such as proteins, whereas the ratio of absorbance 260 to 230 nm indicates contaminants that absorb at 230 nm such as guanidine thiocyanate (GTC), guanidine hydrochloride (GuHCl), EDTA, non-ionic detergents like Triton™ X-100, some proteins and phenol.

4.8.2   RNA isolation using kits

mRNA samples derived from CD4$^+$ naïve and memory T cell populations, as well as CD4$^+$ T cell compartments were isolated using either RNeasy Plus Micro kit or the RNeasy Mini Kit from Qiagen. The lysis of the cells was done with buffer RLT provided in the kit by vortexing for 1 min. Samples were either stored at -80°c or immediately processed following manufacturer's instructions.

4.8.3   cDNA synthesis

The synthesis of complementary DNA (cDNA) from an RNA sequence of a particular gene is achieved by reverse transcription. This step is important in order to generate a template for further amplification by real time PCR. Synthesis of cDNA was carried out using a standard PCR-cycler with 0.2 to 0. 8 µg of total mRNA. In a first step, annealing was achieved by adding 1 µl oligo-dT-primers (0.5 µg/µl) and 1 µl of mixture of dNTPS for strand synthesis. Following heating at 65°C for 5 min; 1 µl DTT (0.1 M), 4 µl 5x first strand buffer and 1 µl RNAse OUT (RNAse out Kit) were added and subsequently heated for another 2 min at 42°C. Amplification was performed in a final step, where 1 µl Supercript II Reverse Transcriptase was added following incubation at 42°C for 50 min. Next, the temperature was increased to 72°C for 15 min to promote complete synthesis of all PCR products and the procedure ended with a cool down (4°C). PCR mixes without mRNA were used as general control for extraneous nucleic acid contamination.

4.9   Quantitative (real-time) polymerase chain reaction (qRT-PCR)

The cDNA obtained from reverse transcription is employed as template for quantitative PCR. Contrary to conventional PCR, in each real-time PCR cycle the resulting DNA products are monitored in a real-time

manner by measuring the fluorescence generated by intercalating DNA-dye such as SYBR green or by sequence-specific probes. In each cycle the fluorescence is recorded and when a fluorescent signal crosses the fluorescence threshold value (set as approximately 10 times the standard deviation of the fluorescence value of the baseline) a threshold cycle (Ct) is generated. This Ct is defined then as the cycle number at which the fluorescent signal of the reaction crosses the threshold. Once the amplification reaction is completed, the template is melted to determine non-specific bindings. As the temperature of the reaction rises, a melting curve is generated. This melting curve represents the fluorescence measured when double-stranded DNA, labeled with fluorescent molecules, dissociates or "melts" into single-stranded DNA (ssDNA). This is a straightforward way to check the presence of primer-dimer artifacts and to ensure reaction specificity.

Table 9: PCR conditions for quantitative real-time PCR

Step	Time	Temperature	
Initial heat activation for HotStar Taq DNA Polymerase	15 min	95°C	
Denaturation	30 sec	95°C	
Annealing	30 sec	58°C	45 cycles
Extension	30 sec	72°C	
Plate Read			
Denaturation	30 s	95°C	
Melt curve	5 s	65°C-95°C, increment 0.5°C	

In this work, the cDNA obtained from reverse transcription was amplified by using specific primer pairs for the genes of interest. Specific primers for the detection of *STIM1-2*, *Orai1-3*, *ATP2B4*, *ATP2B4a* and *ATP2B4b* as well as *YY1* were used (primer sequences are listed in Table 3). The protocol for DNA amplification is shown in Table 9 and consists of three temperature steps: the procedure starts with an increase in temperature that allows the template, as well as further resulting amplicons being denaturalized, the second step provides the optimal annealing temperature for binding of the primers to their complementary sequence, and the third step allows the binding of DNA polymerase to its DNA template and DNA synthesis. To quantify the level of gene expression the QuantiTect SYBR Green PCR Kit from Qiagen was used, which provides all the components necessary for the amplification such as HotStarTaq® DNA Polymerase and SYBR Green among others. SYBR Green dye intercalates to double strand DNA giving a fluorescence signal proportional to the amount of cDNA on the samples. The analysis of the PCR results is based on the $2^{-\Delta CT}$ method (Garson et al., 2009; Livak & Schmittgen, 2001). The expression of target genes was normalized to the reference gene TATA-box binding protein (TBP), and in most of the cases a second reference gene RNA Polymerase (RNAPol) was used. All templates were tested in duplicates or triplicates.

4.10 Western Blot

Western blot (Immunoblotting) technique was used to determine PMCA, STIM, Orai1 and YY1 protein levels. For quantification of protein content, cell lysates were produced using a lysis buffer 1x (develop in the group of Prof. David Mick, Center of Human and Molecular Biology (ZHMB), Saarland University) supplemented with a cocktail of protease inhibitors (here named DM Lysis buffer 1x) while shaking at approximately 400 rpm during overnight incubation at 4°C. The next day, lysates were stored at -80°C till sample processing or immediately sonicated with a Qsonica Sonicator Q700 (Thermoscientific) for 3 minutes under the following conditions: 5% amplitude, laps 15 min, pause 10 min. Later, samples were centrifuged at 15000 rpm for 20 min at 4°C to get rid of debris and protein determination was done by bicinchoninic acid (BCA) protein assay following the manufacturer's instructions. After protein quantification, 10 to 50 µg of proteins were diluted in Laemmli buffer 1x and denaturalized at 65°C for 15 min. Denaturalized samples and dual color marker were separated in a discontinuous SDS-PAGE gel (5 or 7% stacking gel and 10 or 15% separating gel) at constant voltage of 150 mV in 1xSDS-running buffer. The ionic detergent SDS binds to proteins, to create negatively charge complexes, that are separated based on their size during electrophoresis. All buffers used are shown in Table 6 with single reagents indicated in Table 5. Separated proteins were blotted onto nitrocellulose membranes at constant current of 350 mA for 90 min in blotting buffer. The transfer is essential for exposure of epitopes on the membrane surface where binding of the detecting antibody is feasible. The membranes were blocked in 5% skimmed milk in PBS-T for one hour to avoid unspecific binding of antibodies in the successive steps. Membranes were incubated with the primary antibody overnight at 4°C. After overnight incubation, the membranes were washed three times with PBS-T and incubated with the pertinent secondary antibody at RT for one hour. The membranes were washed again four times with PBS-T and a final washing step with TBS. Antibody bound protein fractions were detected with the ECL chemiluminescent solution in the ChemiDocTM XRS system. Different exposure times were used depending on the primary antibody. To quantify protein levels, membranes were treated with a primary antibody against the house-keeping protein GAPDH or β-actin. The quantitative analysis of protein levels was based on the volume of the bands, which takes into account that the density of a given band is measured as the total volume under the three-dimensional peak (length and width=area plus chemiluminescent signal emitted from the blot=peak hight (3rd dimensional peak). The background subtraction was done by using rolling disk background subtraction. Quantification was done using the Image Lab software (Bio-Rad).

4.11 Single cell Ca^{2+} imaging

4.11.1 Principle

T cells were loaded in suspension with 1 µM Fura-2AM in AIMV medium at room temperature for 25-30 minutes and seeded on 0.1 mg/ml poly-ornithine coated glass coverslips. Fura-2AM is a polyaminocarboxylate fluorophore that binds divalent ions such as Ca^{2+} and is conjugated to an acetoxymethylester-group (AM). The AM-group enables the dye to permeate into cells where it is hydrolyzed by esterases in the cytosol to yield Fura-2. Fura-2AM is a ratiometric calcium indicator with high affinity for Ca^{2+} and UV light excitable. The ratiometric characteristics of the dye rely on two

absorption spectral peaks at 340 and 380 nm and one emission peak at 510 nm. Addition of Ca^{2+} increases the fluorescence of Fura-2AM when excited at 340nm and decreases the fluorescence from excitation at 380 nm. Therefore, after background subtraction, the intensity of emitted light recorded with 340 nm excitation divided by the intensity of emitted light recorded with 380 nm can be presented as a 340/380 ratio and reflects changes in $[Ca^{2+}]_i$, as well as allows to cancel out variations in dye loading. As described by Grynkiewicz and colleagues, the ratio values of Fura-2AM obtained after excitation at the two wavelengths can be converted to a Ca^{2+} concentration if the minimal and maximal $[Ca^{2+}]_i$ values using the cell type under study are determined using a specific equipment combination in a process called calibration using the following equation:

Equation 1: $$Calcium\ (nM) = Kd(Fura)\ x\ \frac{(R\text{-}Rmin)}{(Rmax\text{-}R)}\ x\ \frac{Fmax}{Fmin}$$

where R is the ratio value of the background corrected fluorescence registered from cells during the experiment; Rmin is the fluorescence ratio (F340/F380) in the absence of extracellular calcium and under conditions where intracellular Ca^{2+} stores have been depleted for 30 min with Tg and ionomycin and Rmax is the fluorescence ratio (F340/F380) at 20 mM Ca^{2+} and thus at the maximal $[Ca^{2+}]_i$ in the plateau state. Fmax represents the fluorescence of Fura-2AM in 0 mM Ca^{2+} and thus free Fura-2AM at 380 nm and Fmin the fluorescence in 20 mM (in the plateau state) at 380 nm. K is the dissociation constant of Fura-2 for Ca^{2+} at 37°C (224 nM) (Grynkiewicz et al., 1985).

4.11.2 Method

T cells were loaded in suspension with 1 μM Fura-2AM in AIMV medium at room temperature for 20-25 min, briefly centrifuged, resuspended in 0.5 mM Ca^{2+} ringer solution and seeded on glass coverslips previously coated with 0.1 mg/ml poly-ornithine. Coverslips were placed into a measuring chamber, connected to a perfusion system and data was recorded using a set-up composed of an inverted microscope with a 20x objective lens, an infrared lamp, a xenon-lamp with control unit (Polychrome V monochromator) and a CCD camera. The microscope was equipped with a dichroic (DC) mirror or beam splitter (LP 410) for Fura-2AM measurements. The standard measuring protocol known as store depletion protocol included perfusion of solutions with different calcium concentrations (Ringer's solutions) (Table 6) in the presence of Tg to inhibit SERCA and achieve store depletion and therefore CRAC channel activation. The protocols started with perfusion of a 0.5 mM Ca^{2+} solution, which allows measuring basal Ca^{2+} concentrations, following 0 mM Ca^{2+} solution, which allows Ca^{2+} to be pumped out of the cells and the remaining being chelated by EGTA. Full SOCE activation was measured by perfusing a 0 mM Ca^{2+} solution containing Tg for 10 min followed by a 0.5 mM Ca^{2+} solution plus Tg in order to estimate the Ca^{2+} influx via activated Orais channels. SOCE was stopped by a 0 mM Ca^{2+} solution plus Tg, which allows measurement of only Ca^{2+} extrusion. Where indicated cells were treated with 1 μM CCCP or 5 μM or 20 μM Caloxin-1C2 acutely together with the 0.5 mM Ca^{2+} ringer solution. Images were analyzed using the TillVision software followed by Igor software. Analyzed parameters include: maximum $[Ca^{2+}]_i$ (Peak), steady state $[Ca^{2+}]_i$ analyzed as

the average $[Ca^{2+}]_i$ 25 s before removal of $[Ca^{2+}]_o$ (Plateau) and the fraction of retained $[Ca^{2+}]_i$ (Plateau/Peak) calculated for each cell independently.

For the analysis of the efflux rates, cells within 200 nM or 500 nM $[Ca^{2+}]_i$ peak or $[Ca^{2+}]_i$ plateau (iso-cells) were grouped and the inverse of the time constants (rate constant) of single cells were calculated by fitting single or double exponential decay to the decline in $[Ca^{2+}]_i$ after maximal store depletion or after Ca^{2+}_0 removal. Where indicated, the fitting was performed after averaging iso-cell traces and fitting the average curves to double exponential decays, the decay rates were represented as time constants then.

4.12 Transcription factors binding site (TFBS) analysis

A 5000 base pair long sequence upstream to the start codon of ATP2B4 was used for as a potential promoter sequence for ATP2B4. Prediction of transcription factor potentially regulating PMCA4 was done using the algorithms provided by three different databases: ChIP-Seq (Ambrosini et al., 2016), HOCOMOCO (Kulakovskiy et al., 2018) and Promo V3 (Messeguer et al., 2002). Identification of transcription factor binding sites (TFBS) was done by Ensembl Transcription Factor tool (Ensembl Regulatory Build) (Zerbino et al., 2015) and making use of the matrix-based transcription factor binding site in JASPAR database (Fornes et al., 2020). Results obtained from the independent databases were subject to Venn analysis using the online tool Venny 2.1 (Oliveros, 2007) to detect common results (Table 10).

4.13 Chromatin Immunoprecipitation (ChIP)

To test binding of transcription factors to PMCA4b promoter region, antibodies against transcription factors (YY1 or NFAT, 3 μg each) or isotype control antibodies (rabbit IgG or mouse IgG respectively) were coupled to protein A/G agarose beads in coupling buffer (0.01 M sodium phosphate, 0.15 M NaCl, pH 7.2) overnight at 4°C and then cross-linked to the beads using 5 mM of the cross-linker BS3. In parallel, human CD4+ T cells were harvested, washed and then cross-linked with PBS containing 5 mM of the cross-linker DSP and 3% PFA for 20 min at 4°C. Excess crosslinker and PFA were quenched by 125 mM Glycine in PBS. Cell pellets were lysed in 20 mM Tris, 100 mM KCl, 10% glycerine (v/v), 0.5% n-Octyl-β-D-glucopyranoside. Finally, lysates were subjected to chromatin shearing with Qsonica Sonicator Q700 in total processing time of 4 min, 20 s laps of 40% amplitude and 10 s pauses. Clear lysates were diluted to 1 ml with binding buffer (20 mM Tris, 100 mM KCl, 10% glycerine (v/v)). An aliquot of 50 μl was kept as an input control. Lysates were incubated with preclearing beads (isotype IgG bound beads) for 3 h at 4°C, unbound lysate was allowed to bind to control IgG (a fresh aliquot of isotype IgG bound beads) for 3 h at 4°C and finally, unbound lysate was bound to chromatin IP beads (transcription factor bound beads) for 3 h at 4°C. Beads collected at different steps were washed with standard low salt, high salt, LiCl buffer and finally with TE according to Thermoscientific protocol. Finally, DNA was eluted with 1% SDS in 100 mM NaHCO3, purified using DNA purification kit (Qiagen) and used as template to test for binding of the PMCA4b promoter region using Q5 hot start polymerase (NEB biolabs) and the primers: forward 5-

CACCACCGTGCCAGCTAA-3', reverse 3-GAAGGGTGCTAGTTGGACA-5. Amplicons were visualized by DNA agarose and identity was confirmed by Sanger sequencing.

4.14 Statistical analysis

For analysis of Ca^{2+} imaging data, 100-400 cells were measured per experiment and data shown represent the average of averages of independent measurements (n=5-18) obtained from 3-11 donors. Data is presented as mean ± S.E.M or SD. Data was tested for normal distribution. When comparing two groups, statistical significance was tested by performing unpaired two-tailed Student t-test for normally distributed data sets and Mann-Whitney test when samples are not normally distributed. Comparing more than two groups was done using Kruskall-Wallis one-way analysis of variance (ANOVA) for not normal distributed samples or conventional ANOVA when data showed normal distribution and equal variance. Asterisks indicate significant differences for different p values as follows: * $p<0.05$, ** $p<0.01$, *** $p< 0.001$. Statistical analysis was performed using Graphpad Prism and OriginPro Software.

5 Results

5.1 Characterization of Ca^{2+} profiles of human T helper subtypes

5.1.1 *In vitro* polarization using naïve $CD4^+$ T cells result in subtypes with specific cytokine signature and Ca^{2+} phenotypes

In the first phase of this project we characterized the Ca^{2+} profiles of human $CD4^+$ T helper subtypes (Th1, Th2, Th17 and regT). While the polarizing conditions for Th1 and regT cells were already stablished in our group (as mentioned in the methods section), polarization of Th17 and Th2 cells from total $CD4^+$ T cells was challenging, showing limited efficiency. With the goal to generate a higher number of IL-4 producing Th2 cells and IL-17 producing Th17 cells while reducing the number of non-specific cytokine producing cells, we investigated new experimental conditions. In order to optimize the Th17 polarizing conditions, we cultured total $CD4^+$ T cells with decreasing concentrations of TGF-ß1, an important inductor of regT cells and also needed for Th17 generation (Bettelli et al., 2006). Interestingly, low concentration of TGF-ß1 (between 0.1 and 1 ng/ml) induced the highest numbers of IL-17, Ror-γt and Ror-γt/IL-17 positive cells while decreasing the number of Foxp3 positive T cells in two donors (Figure 5d). Nevertheless, when we attempted polarization of Th17 from naïve $CD4^+$ T cells, neither IL-17 nor Ror-γT positive cells were detected (Figure 5c). Indeed, polarization of memory sorted $CD4^+$ T cells into Th17 cells using our previous stablished Th17 conditions and TGF-ß1 concentrations of 0.1 ng/ml resulted in stable and higher production of IL-17 producing cells (Figure 5c), as well as improved the efficiency of polarization by reducing donor to donor variability.

Henceforth, we sorted naïve and memory $CD4^+$ T cells to obtain the desired T helper's subtypes following the strategy shown in (Figure 10a). We attempted polarization of Th1, Th2 and regT out of naïve $CD4^+$ T cells, while Th17 cells were polarized from memory $CD4^+$ T cells. Control populations (Th0) were similarly stimulated but kept in non-polarizing medium. After 7 days of culture in the presence of polarizing cytokine cocktails and using different stimulation intensities (see material and methods) for each subtype, the generation of T helper subtypes was evaluated by intracellular staining of both cytokines and transcription factors characterizing each population, INF-γ for Th1, IL-4 for Th2, IL-17 for Th17 and the transcription factor FoxP3 for regT (Figure 5a and b). Under specific Th1 polarizing conditions the number of INF-γ producing cells was significantly higher than their correspondent cytokine levels in control conditions (Th01:10 and Th01:20) and Th2 and regT subtypes but not in Th0 1:50 and Th17 cells. The number of IL-4 producing cells was also significant higher in cells polarized under Th2 polarizing medium than in Th1, regT, Th17 subtypes and control conditions (Th01:10 and Th01:50). regT cells expressed significantly higher levels of the signature transcription factor FoxP3 than the other subtypes (Figure 5a and b). Th17 cells also showed a significant higher production of IL-17 as compared to the other subtypes, as well as INF- γ production (Figure 5a and b). The fraction of IL-17 positive cells originated from Ror-γt positive but INF-γ negative cells (Figure 5c). Importantly Th2 and Th17 cells were not significant different to their respective controls Th0 (Figure 5b).

Next, we characterized the calcium profiles of *in vitro* polarized cells using a Tg-store depletion protocol. The calcium profile of *in vitro* polarized cells using naïve CD4+ T cells was not different from that of *in vitro* polarized cells using total CD4+ T cells (Kircher et al., 2018). Th1 cells showed reduced both Ca^{2+} peak and Ca^{2+} plateau than control non-polarized but similarly stimulated Th0 (bead: cell ratio of 1:10) (Figure 6a and d).
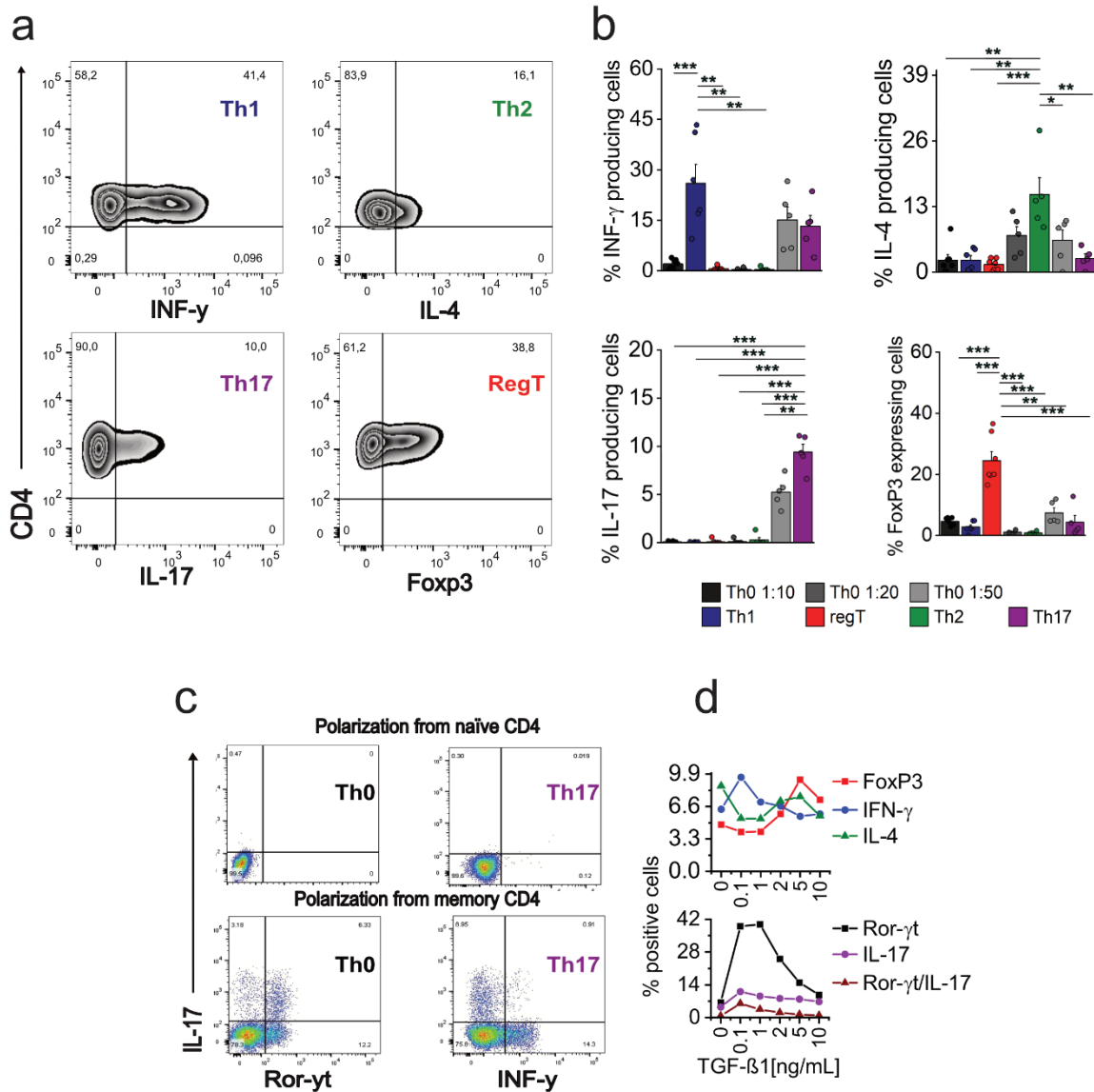

Figure 5: *In vitro* polarization using naïve CD4+ T cells results in subtypes with specific cytokine signature.
(a) Flow cytometry analysis of *in vitro* polarized T helper subtypes (Th1, Th2, Th17 and regT) after 7 days of polarization. (b) Quantification of cytokine expression in T helper subtypes and their corresponding controls (Th01:10, Th01:20 and Th01:50) from 5 to 6 donors. (c) Flow cytometry analysis of Il-17 and Ror-γt expression in *in vitro* polarized Th17 and control Th01:50 using either naïve CD4+ T cells or memory CD4+ T cells as starting population. (d) TGF-ß1 dose dependent effect on IL-17, INF-γ and IL4 production and FoxP3 and Ror-γt expression (representative of two experiments). Data represent mean ± SEM. Asterisks indicate significance at * p<0.05, ** p<0.01, *** p<0.001, using unpaired two-tailed Student t-test.

The regT exhibited the highest Ca^{2+} peak among the subtypes and control conditions, but its Ca^{2+} plateau was not significantly different from that of the Th0 stimulated with a bead: cell ratio of 1:10, but significantly different from those of the other subtypes (Figure 6a and d). The Ca^{2+} peak of Th2 cells was only significantly different from that of the regT, while its Ca^{2+} plateau was significantly different from that of Th0 stimulated with the bed: cell ratio of 1:50 and to that of the Th17 cells and regT (Figure 6b and d). Th17 cells exhibited the smallest Ca^{2+} signals and Ca^{2+} plateau among the subtypes. The Ca^{2+} peak of Th17 cells was only different from that of the regT cells and Th01:10, whereas the Ca^{2+} plateau was significantly different from that of the regT, Th2 and controls Th01:10 and Th01:20 (Figure 6c and d). Importantly, we did not detect significant differences in Ca^{2+} peak among control non-polarized cell stimulated at different bead: cell ratio intensities, but the Ca^{2+} Plateau of control non polarized Th01:50 cells, which derived from memory $CD4^+$ T cells were significantly different as compared to Th01:10 and Th01:20, with the two latest derived from naïve $CD4^+$ T cells.
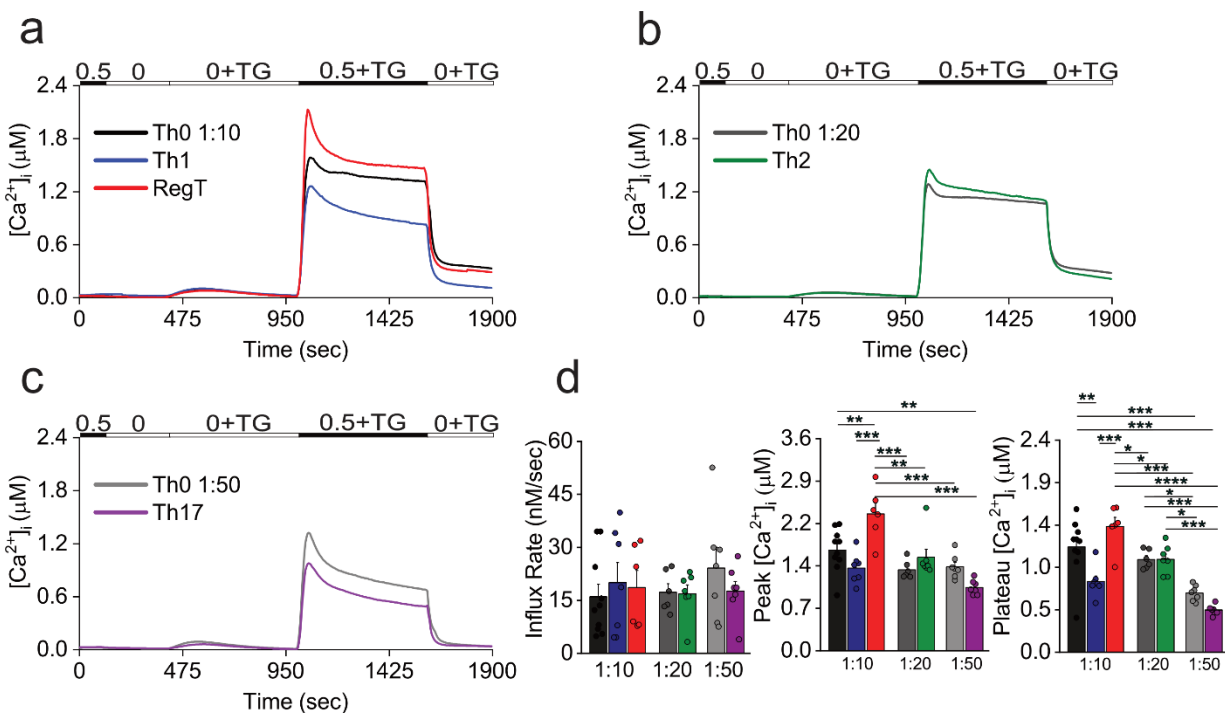

Figure 6: *In vitro* polarized $CD4^+$ subtypes have distinct SOCE phenotypes following Tg-induced activation.
(**a, b, c**) Average traces showing changes in $[Ca^{2+}]_i$ over time of *in vitro* polarized T helper subtypes and their corresponding controls in response to 0.5 mM Ca^{2+}_0 solution after Tg-induced store depletion. Data represent average obtained from 8 to 10 independent Ca^{2+} measurements (~100-300 cells), representative of 8 to 11 donors. (**d**) Corresponding statistics of $[Ca^{2+}]_i$ influx rate, $[Ca^{2+}]_i$ peak and $[Ca^{2+}]_i$ plateau. Data represent mean ± SEM. Asterisks indicate significance at * $p<0.05$, ** $p<0.01$, *** $p<0.001$, using one-way analysis of variance (ANOVA).

5.1.2 Transcriptome analysis of Th0, Th1 and regT subtypes identifies differentially expressed Ca^{2+} homeostasis relevant genes

Due to the finding that Th1 and regT showed the strongest differences in Ca^{2+} peak and plateau among the subtypes, our next goal was to study the underlying mechanisms leading to these differences in Ca^{2+} phenotypes. First, we evaluated some Ca^{2+} related genes using quantitative PCR (Figure 7f). Interestingly, no TRPC channels were differentially expressed, but PMCA4 was significantly increased in Th17 cells and increased expression was also detected in control Th01:50 and Th1 albeit no significant (Figure 7f). As the underlying mechanism may be challenging to unravel by evaluating only individual genes, we performed a transcriptome analysis (see material and methods) of Th0, Th1 and regT subtypes. The (Figure 7a) shows a hierarchical clustering of Th0, Th1 and regT polarized subtypes (5 replicates each), in which genes with similar expression pattern across replicates are clustered together, while samples are grouped into Th0, Th1 or regT based on their resulting gene cluster patterns. The range of expression levels of each gene is represented using a heatmap with a bar color scale at the top left of the graph (Figure 7a). As expected, the replicates were located within the same group (for Th0: red, Th1: blue and regT: green), with only one Th0 replicate being grouped within the Th1 group. Interestingly, clustering analysis revealed that Th0 and regT fall into the same cluster and are distant to Th1.

Next, we screened for differentially expressed genes in Th1 and regT subtypes. The (Figure 7b) shows two Volcano Plots, where significantly differentially expressed genes are shown towards the right or left of the threshold (0.6) used to select the differentially expressed genes. The volcano Plot of Th0 versus Th1 shows that 946 were differentially expressed out of a total of 24459 genes with measured expression. On the other hand, analysis of differently expressed genes in Th0 versus regT identified 470 differentially expressed genes out of a total of 24466 genes with measured expression. Next, we screened for signature genes of each subtypes. The (Figure 7c) shows that each subtype expressed either Th1 or regT signature genes. As expected, gene expression analysis of SOCE components (STIM1, STIM2 and Orai1-Orai3) confirmed that the main components of the SOCE pathway doesn't change among Th1 and regT subtypes.

In order to select the most relevant genes that potentially contribute to the observed differences in SOCE phenotypes between Th1 and regT subtypes, we performed a meta-analysis. The (Figure 7d) shows that 110 genes are not differentially expressed between the two subgroups (Th0 vs regT and Th0 vs Th1) and therefore they are not differentially expressed between Th1 and regT. However, 360 genes were uniquely differentially expressed in Th0 vs regT, while 836 genes in Th0 vs Th1. Having a number of genes that were uniquely differentially expressed in Th1 and regT subtypes, the next was to unravel the fraction of genes involved in cellular Ca^{2+} ion homeostasis. The (Figure 7e) shows a gene ontology meta-analysis of Ca^{2+} related genes that were differentially expressed in Th1 and regT groups. A total of 17 differentially expressed genes out of a total of 369 genes related to cellular Ca^{2+} ion hemostasis were identified in Th0 vs regT (pvalue=0.018), while 30 differentially expressed genes out 369 genes related to cellular Ca^{2+} ion hemostasis were identified in Th0 vs Th1 (pvalue=0.269). From these ATP2B4, P2RX5 and TRPM2 were exclusively differentially expressed in Th0 vs Th1 and showed the highest fold change among the total genes.
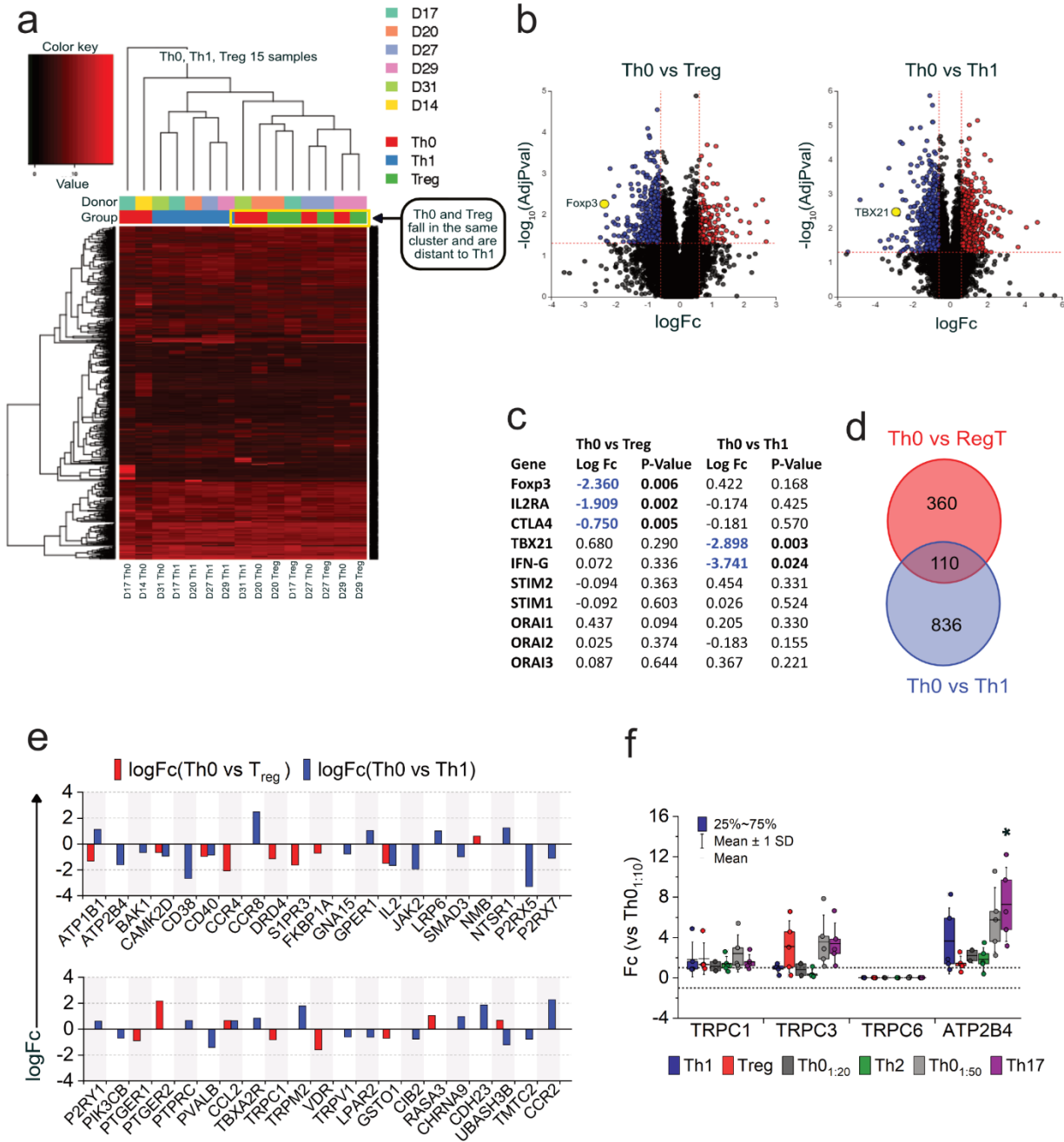
Figure 7: A microarray data analysis of Th0, Th1 and regT subtypes identifies relevant Ca²⁺ genes.
(**a**) Hierarchical cluster of genes and sample replicates (Th0, Th1 and regT) from 5 donors. (**b**) Volcano Plots of Th0 vs regT and Th0 vs Th1 obtained using a threshold of 0.05 for statistical significance (p-value) and a log fold change (logFC) of expression with absolute value of at least 0.6. (**c**) Log of the FC of signatures genes and SOCE components in regT and Th1 subtypes. (**d**) Meta-analysis of significantly differentially expressed genes in Th0/regT vs Th0/Th1. (**e**) Gene ontology meta-analysis of Ca²⁺ relevant genes. (**f**) Relative mRNA expression of TRPC1, TRPC3, TRPC6 and ATP2B4 in *in vitro* polarized T helper subtypes (4 donors) calculated by real time qPCR using the $2^{-\Delta\Delta Ct}$ method. Data in f represents mean ± SD. Asterisks indicate significance at * $p<0.05$, using one-way analysis of variance (ANOVA).

As ATP2B4 was significantly upregulated in Th17 cells that were polarized from memory CD4$^+$ T cells, and its expression seems to be also increased in Th1 cells (Figure 7e and f) and memory Th0 control (Figure 7f), we were particularly interested in unraveling the role of PMCA4 in the generation of subtype specific responses.

5.1.3   *In vivo* sorted regulatory T cells recapitulate *in vitro* polarization

To investigate if the Ca^{2+} phenotypes of *in vitro* polarized cells resemble those of *in vivo* differentiated cells regT, we sorted *in vivo* generated both regT and conventional or effector T cells (Tcon) out of PBMC, following the strategy shown in (Figure 8a). The purity of the sorted population was evaluated by intracellular staining of the master regulator of regT (FoxP3) and surface staining of IL-2R (CD25) (Figure 8b and c), which are constitutively expressed in regT. As expected, the number of FoxP3 and CD25 positive cells was significantly higher in sorted regT than in Tcon (Figure 8c). Interestingly, *in vivo* sorted regT showed SOCE with higher Ca^{2+} peak than conventional CD4$^+$ T cells, but unaltered plateaus. In contrast to *in vitro* polarized regT cells (Figure 7c), *in vivo* regT showed a reduced expression of Orai2 compared to Tcon, while no differences in other SOCE proteins was founded (Figure 8f). Next, we evaluated the expression, in *in vivo* sorted T cells, of some genes that were either differentially expressed or not in our microarray analysis of Th0 vs regT. In accordance with the gene expression profile of *in vitro* Th0 vs regT, TMEM63, PTK2 and CACNA2D2 were significantly downregulated in *in vivo* differentiated regT vs Tcon, while TRPC1, TRPM2 and ATP2B4 were not (Figure 9a).

Due to regT showed increased Ca^{2+} peak but reduced plateau and as we sow before, *in vitro* polarized cells using memory CD4$^+$ T cells showed the smallest plateau among the subtypes (Figure 7d), we wondered if the ratio naïve vs memory CD4$^+$ T cells is altered in regT vs Tcon. Surprisingly, the ratio of memory T cells vs naïve was significantly higher in regT than in Tcon (Figure 9b).

On the other hand, mitochondria has been shown to modulate SOCE in T cells by inhibiting the Ca^{2+} dependent inactivation of Orai channels (Hoth et al., 1997; Quintana et al., 2007). Therefore, we were interested in evaluating the role of mitochondria shaping SOCE in *in vivo* sorted regT. We use an uncoupler of mitochondrial oxidative phosphorylation, carbonyl cyanide m-chlorophenyl hydrazine (CCCP, 1 μM) to block mitochondrial Ca^{2+} uptake. Acute application of CCCP after Tg-induced store depletion led to a significant inhibition of SOCE plateau in both regT and Tcon, while the SOCE peak remained unaltered (Figure 9c-e). Interestingly, although mitochondria size of Tcon and regT were similar (Figure 9f), regT shows less active mitochondrial potential than Tcon (Figure 9g).

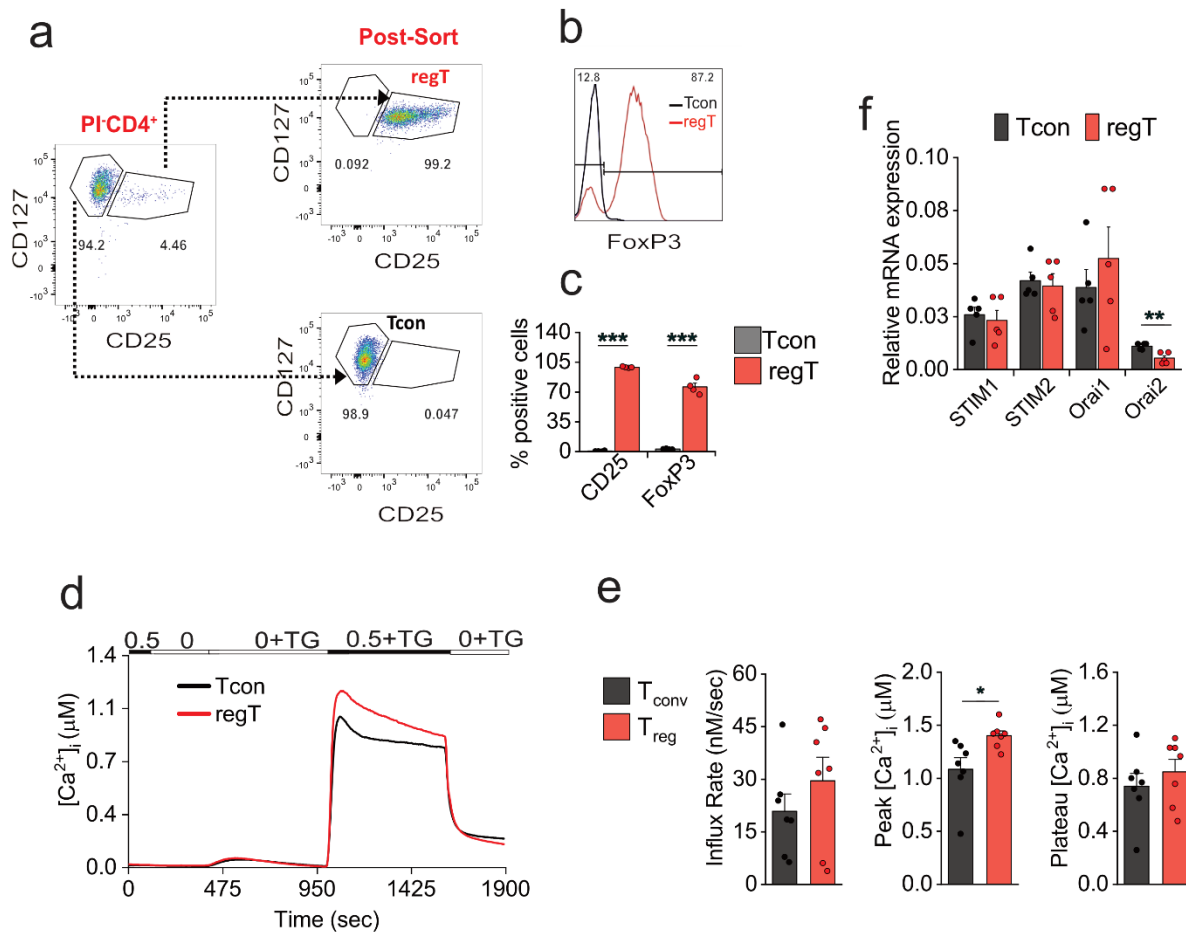**Figure 8: *In vivo* sorted regT cells recapitulate the phenotype of *in vitro* differentiated regT.**
(a) Representative flow cytometry image with gating strategy used to isolate regulatory T cells (regT) out of PBMC. Cells were gated from the singles/Lymphocytes/Propidium Iodide negative (PI⁻) gate and sorted as conventional T cells (Tcon (CD127^{high}CD25⁻)) and regT (CD127^{low}CD25⁺) by Fluorescence Activated Cell Sorting. Gating Strategy is shown in red color upper the plots. **(b)** Representative flow cytometry analysis of FoxP3 expression in Tcon and regT. **(c)** Quantification of FoxP3 and CD25 expression in Tcon and regT. **(d)** Average traces showing changes in $[Ca^{2+}]_i$ over time of Tcon and regT isolated as shown in (a) in response to 0.5 mM Ca^{2+}_0 solution after Tg-induced store depletion. Data represent average obtained from 7 independent Ca^{2+} measurements (~100-400 cells), representative of 6 donors. **(e)** Corresponding statistics of $[Ca^{2+}]_i$ influx rate, $[Ca^{2+}]_i$ peak and $[Ca^{2+}]_i$ plateau. **(f)** Quantification of the expression of SOCE genes (STIM1, STIM2, Orai1-Orai3) in Tcon and regT in cells sorted as in a. Data represent mean ± SEM. Asterisks indicate significance at * p<0.05, ** p<0.01, *** p<0.001, using unpaired two-tailed Student t-test.
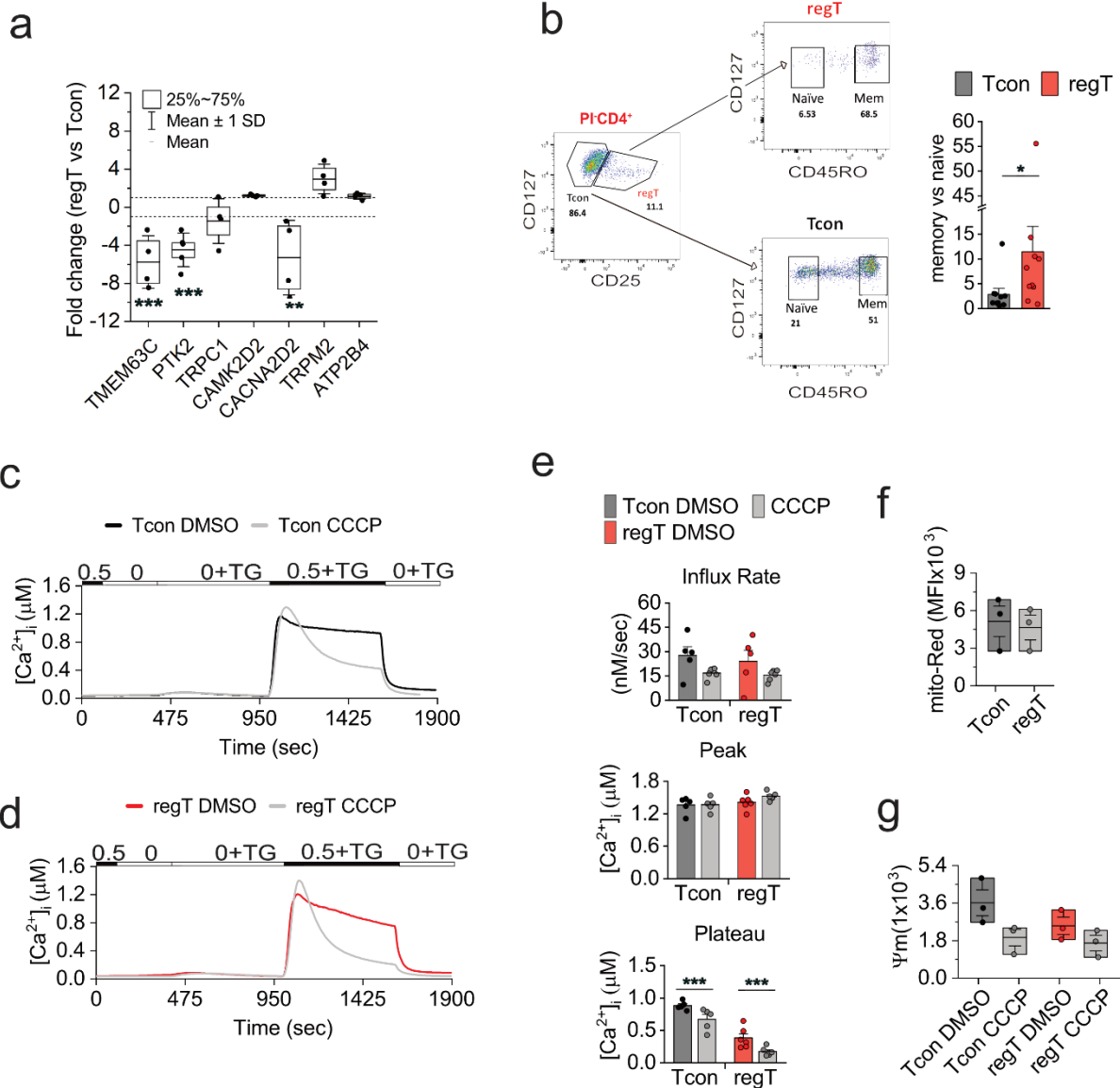
Figure 9: Ca^{2+} regulatory mechanisms in *in vivo* sorted regulatory T cells.
(a) Fold changes differences in gene expression of Ca^{2+} relevant genes in regulatory T cells (regT) vs conventional T cells (Ton) calculated by real time qPCR using the $2^{-\Delta\Delta Ct}$ method. Selected genes were taken from the gene expression microarray data of *in vitro* differentiated Th0 vs regT. **(b)** Representative flow cytometry analysis showing percentage of naïve and memory T cells in Tcon and regT and ratio of memoy vs naïve T cells in both Tcon and regT from 10 donors. **(c, d)** Average traces showing changes in [Ca^{2+}]$_i$ over time of Tcon and regT isolated in response to 0.5 mM Ca$^{2+}_0$ solution after Tg-induced store depletion. Data represent average obtained from 5 to 6 independent Ca^{2+} measurements (~100-400 cells), representative of 3 donors. **(e)** Corresponding statistics of [Ca^{2+}]$_i$ influx rate, [Ca^{2+}]$_i$ peak and [Ca^{2+}]$_i$ plateau. **(f)** Analysis of mitochondria size in naïve and memory resting and activated CD4$^+$ T cells using Mitotracker-Red. **(g)** Analysis of mitochondria potential (ΔΨm) in Tcon (balck) and regT (red) CD4$^+$ T cells stained with the mitochondrial membrane potential indicator DilC1. Data in b, e, f and g represents mean ± SEM. Asterisks indicate significance at * p<0.05, ** p<0.01, *** p<0.001, using unpaired two-tailed Student t-test.

5.2 Differential expression of PMCA4b results in distinct SOCE profiles in naïve and memory CD4^{+} T cells

In the first part of this work, we characterized SOCE profiles of *in vitro* polarized human CD4^{+} T cell subtypes and observed that polyclonal stimulation of naïve and memory cells with anti-CD3/CD28-coated beads, under non-polarizing conditions (control cells), showed differential SOCE profiles along with upregulation of PMCA4 in the activated memory cells (Kircher et al., 2018). Therefore, we were interested in unraveling the role of PMCAs during activation and differentiation of human CD4^{+} T cells. First, we sorted naïve (CD4^{+}CD127^{high}CD25^{-}CD45RO^{-}) and memory (CD4^{+}CD127^{high}CD25^{-}CD45RO^{+}) populations out of the human peripheral blood mononuclear cells (PBMCs) using the fluorescence activated cell sorting (FACS) strategy shown in (Figure 10a) that excluded regulatory T cells (CD4^{+}CD127^{low}CD25^{+}), which are able to suppress the expansion and differentiation of naïve and memory T cells *in vivo* (van Herwijnen et al., 2012) and *in vitro* (Venken et al., 2007). One day after sorting, we measured global Ca^{2+} signals following Tg-induced store depletion. The SOCE profile of naïve and memory T cells was different. The magnitude of the SOCE peak and the steady state plateau of naïve T cells were 13% and 45% higher than the corresponding values of memory T cells respectively (Figure 10b). This observation indicates that at relatively similar $[Ca^{2+}]_i$, memory T cells were able to clear more calcium that naïve T cells. As shown in (Figure 10c), both populations are not significant different in basal Ca^{2+} and influx rate, but there was a tendency to lower basal $[Ca^{2+}]_i$ and higher influx rates in memory T cells (Figure 10c). The plateau and the ratio plateau/peak were significantly reduced in memory compared to naïve T cells (Figure 10c). The higher plateau/peak ratio in naïve T cells indicates again a slower decay of Ca^{2+} signals. To have a direct estimate of the decay rate, taking into account that different $[Ca^{2+}]_i$ levels may influence the $[Ca^{2+}]_i$ clearance rates in T cells (Bautista et al., 2002; Bautista & Lewis, 2004), we binned the cells into groups of similar peak or plateau $[Ca^{2+}]_i$ (iso-cells) and calculated the decay rate constants of individual cells in presence or absence of Ca^{2+}_0 (Figure 10d and e). In both populations, the decay rates were dependent on $[Ca^{2+}]_i$ in agreement with (Bautista et al., 2002; Bautista & Lewis, 2004). The analysis of the rate constants of iso-cells, showed faster decay rates in memory compared to naïve T cells, independent of the $[Ca^{2+}]_i$. The number of cells showing peak $[Ca^{2+}]_i > 2\ \mu M$ or plateau $> 1.5\ \mu M$ was limited thereby hampering the statistical analysis.

To determine whether differential expression of SOCE components can account for the differences in Ca^{2+} profiles between naïve and memory cells, we analyzed their expression at mRNA and protein levels. None of SOCE proteins was significant differently expressed between naïve and memory CD4^{+} T cells, but a 47% increase in *STIM1* mRNA levels together with a 31% *Orai1* transcripts and 10% protein levels was observed in memory T cells (Figure 11a-c). Due to the spatiotemporal profile of Ca^{2+} signals in T cells dependent not only on Ca^{2+} entry pathways but also on the action of extrusion mechanisms on plasma membrane such as ATPases (Bautista et al., 2002; Bautista & Lewis, 2004), we evaluated the levels of transcripts of the fours PMCAs (ATP2B1-4) isoforms in total CD4^{+} T cells by real time qPCR. We detected transcripts of ATP2B1 and ATP2B4, with the latter showing a significantly higher expression level (Figure 11d). To identify the splice variant(s) expressed in CD4^{+} T cells, we designed splice-specific primers for ATP2B4a, ATP2B4b or a primer combination for both of them and analyzed the corresponding expression. The (Figure 11e) shows
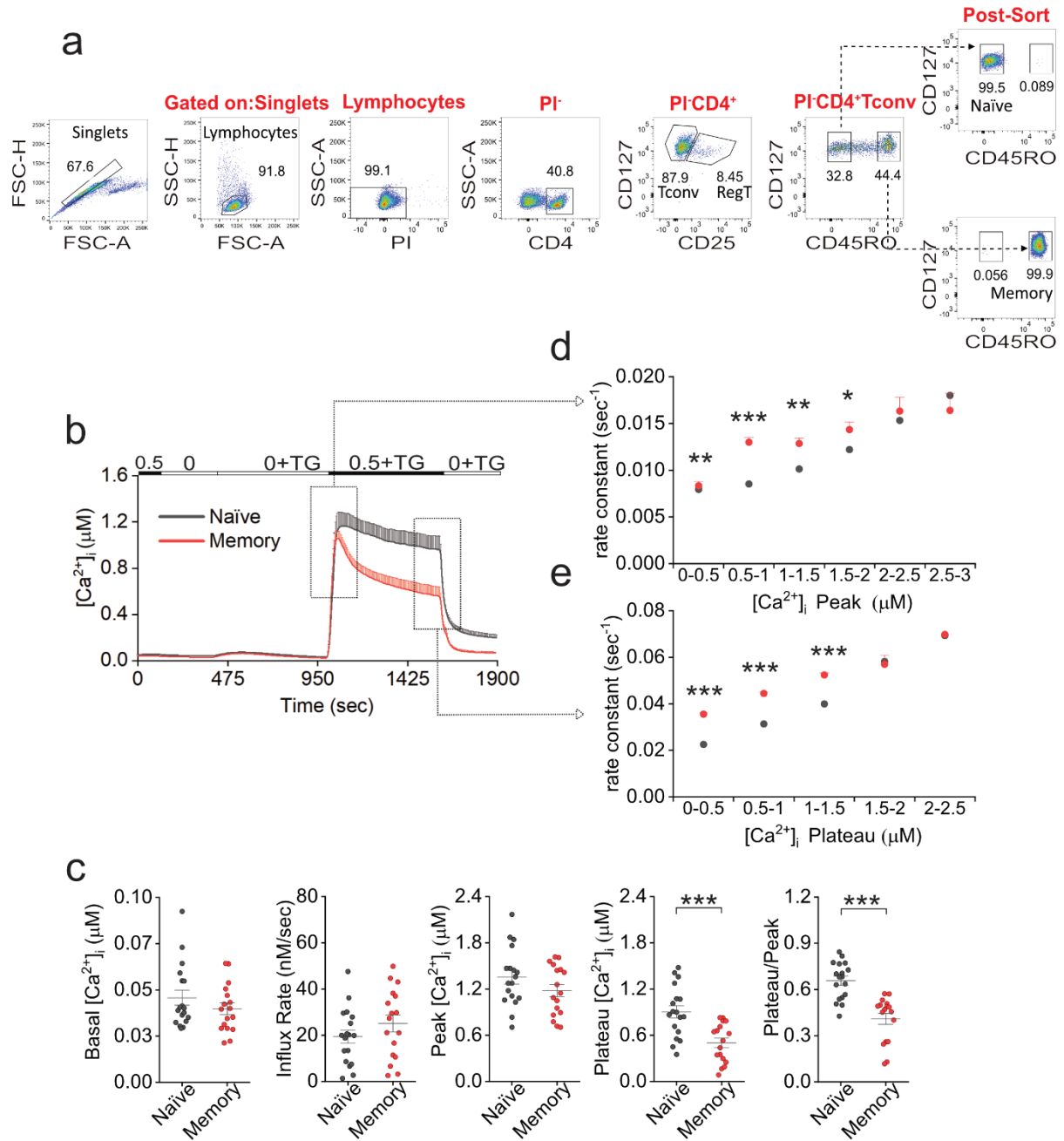
Figure 10: Naïve and memory CD4+ T cells have distinct SOCE profiles.
(a) Representative flow cytometry image with gating strategy used to isolate human naïve (CD4+CD127highCD25-CD45RO-) or memory (CD4+CD127highCD25-CD45RO+) T cells by Fluorescence Activated Cell Sorting. Gating Strategy is shown in red color upper the plots. **(b)** Average traces showing changes in $[Ca^{2+}]_i$ over time of naïve and memory CD4+ T-cells isolated as shown in (a) in response to 0.5 mM Ca^{2+}_0 solution after Tg-induced store depletion. Data represent average obtained from 18 and 17 independent Ca^{2+} measurements (~100-300 cells), representative of 11 donors. **(c)** Corresponding statistics of basal $[Ca^{2+}]_i$, Influx rate, $[Ca^{2+}]_i$ peak, $[Ca^{2+}]_i$ plateau and ratio Plateau/Peak. **(d, e)** Average rate constants values of iso-cells plotted against their respective $[Ca^{2+}]_i$ peak (d) or $[Ca^{2+}]_i$ plateau (e) intervals. Data represent mean ± SEM. Asterisks indicate significance at * $p<0.05$, ** $p<0.01$, *** $p<0.001$, using unpaired two-tailed Student t-test (c) or Kruskall-Wallis one-way analysis of variance (ANOVA) (d and e).

that ATP2B4b is the predominantly expressed splice variant in total CD4$^+$ T cells, in accordance with published results (Caride et al., 2001). To investigate whether naïve and memory cells have different expression of PMCA4 which possibly underlies the observed SOCE profiles we analyzed the expression of ATP2B4 in naïve and memory T cells using splice-specific primers (Figure 11f and g). Memory T cells expressed significantly higher levels of ATP2B4 than naïve T cells (Figure 11f). In addition, levels of detected PMCA4 proteins were significantly higher in memory T cells (Figure 11h and i). We could hardly detect ATP2B4a in naïve and memory sorted T cells (Figure 11g). These results implicate that ATP2B4b is the main isoform in naïve and memory CD4$^+$ T cells populations and it may cause the faster decay in memory T cells.
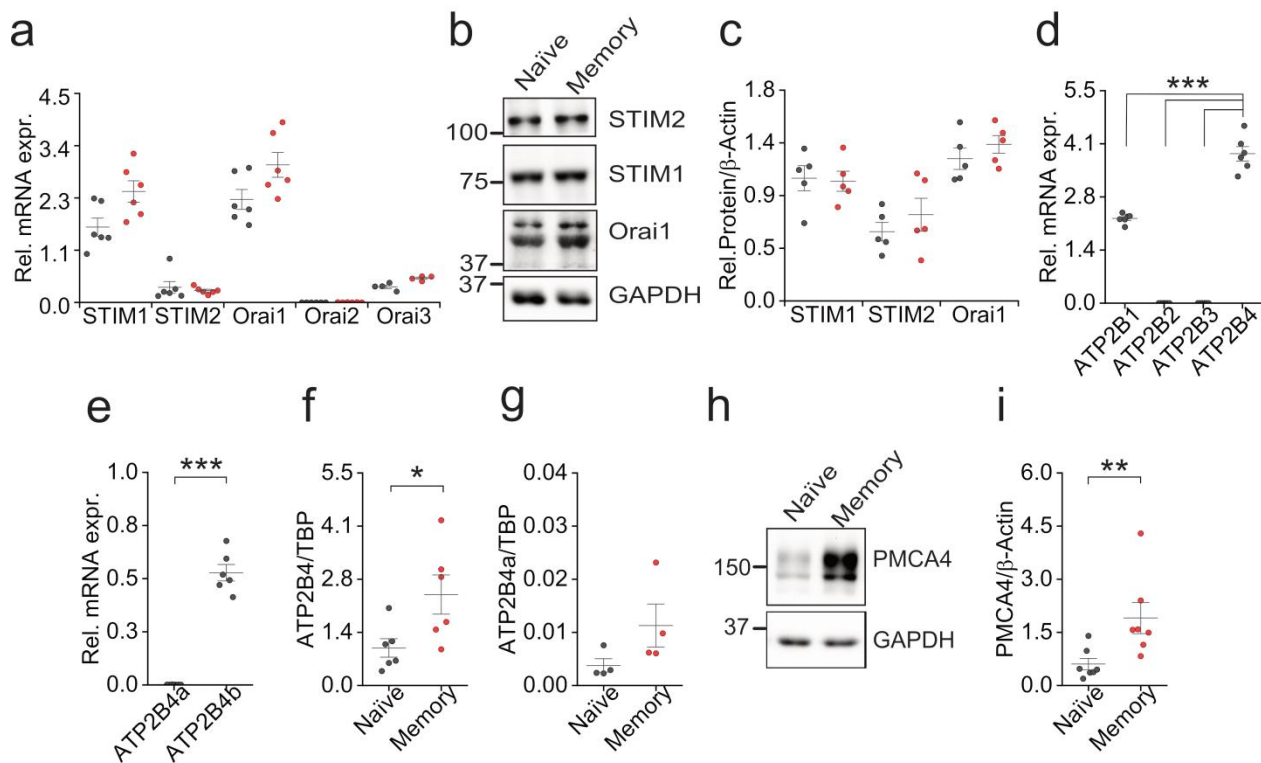

Figure 11: Upregulation of PMCA4b in memory T cells is responsible for SOCE differences.
(a) Relative expression of STIM1-2 and Orai1-3 mRNA in naïve and memory sorted CD4$^+$ T cells calculated by real time qPCR using the $2^{-\Delta Ct}$ method. **(b)** Representative of 5 independent western blots analyzing expression of STIM1-2 and Orai1 in naïve and memory CD4$^+$ T cells. **(c)** Quantification of protein expression represented in b. **(d)** Relative mRNA expression of the four isoforms of PMCAs in total CD4$^+$ T cells calculated by real time PCR using the $2^{-\Delta Ct}$ method. **(e)** Relative expression of both splices variants ATP2B4a and ATP2B4b in total CD4$^+$ T cells. **(f, g)** Relative expression of total ATP2B4 (f) or splice variant ATP2B4a (g) in naïve and memory T cells. **(h)** Representative of 7 independent WB showing expression of PMCA4 in naïve and memory T cells. **(i)** Quantification of protein expression shown in (h). Data represent mean ± SEM. Asterisks indicate significance at * p<0.05, ** p<0.01, *** p<0.001 using unpaired two-tailed Student t-test (e and f), Mann-Whitney test (i) or one-way analysis of variance (ANOVA) (d).

5.3 Pharmacological inhibition or downregulation of PMCA reverses SOCE phenotypes of memory CD4$^+$ T cells

In order to test whether PMCA has a direct role in the differences in Ca^{2+} phenotypes in naïve and memory T cells we used specific inhibitors of PMCAs known as Caloxin1C2 (C1C2). C1C2 is a short peptide that specifically inhibits PMCAs by binding to the allosteric sites of the protein and it has an isoform-selective activity depending on the used concentration (Pande et al., 2011). The reported constant of inhibition (Ki) for PMCA4 is 2-5µM while Ki values higher than 20µM have been shown to inhibit all PMCAs isoforms (Pande et al., 2011). Neither 5µM nor 20µM C1C2 applied acutely during the steady state of the Ca^{2+} re-adition protocol altered the SOCE response in naïve T cells (Figure 12a). In contrast, blocking PMCA in memory T cells not only increased its SOCE peak to the same level of the SOCE peak in naïve T cells but also increased significantly the plateau (Figure 12b and c). The Inhibition of PMCA resulted in similar inhibition with both C1C2 concentrations, however the 20 µM C1C2 resulted in significantly higher plateau/peak compared to the control cells (Figure 12c). In a second approach we downregulated ATP2B4 using a sequence-specific ATP2B4-siRNA. The efficiency of knockdown attained was 61% and 80% in the
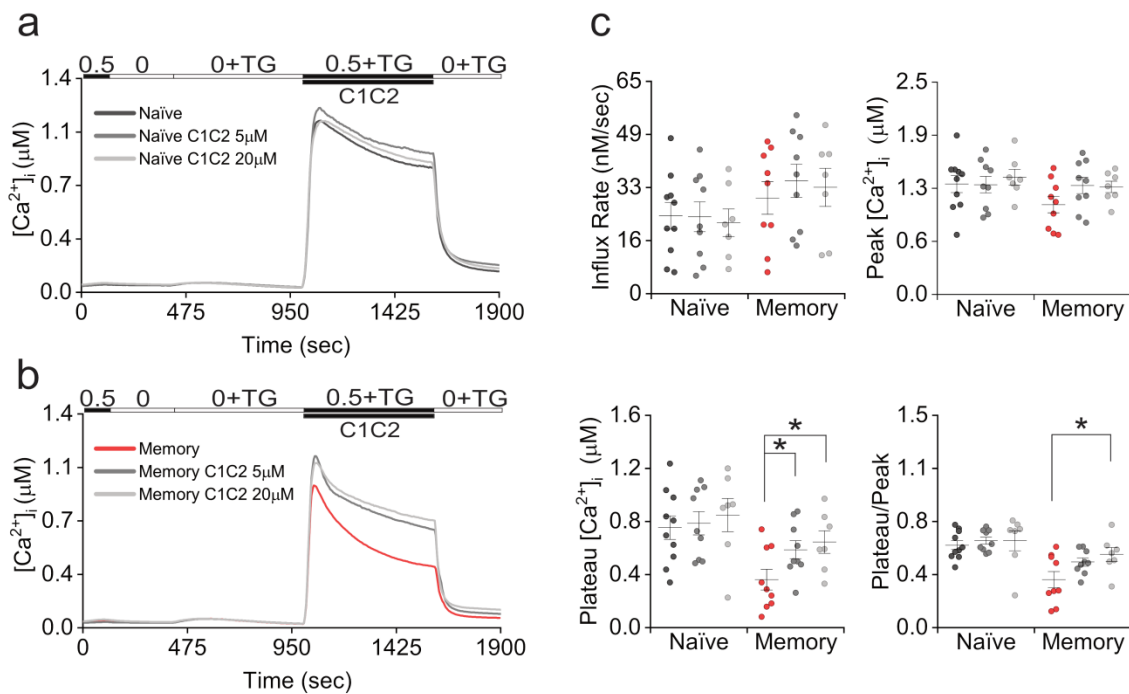

Figure 12: Pharmacological inhibition of PMCA reverses SOCE phenotype of memory cells.
(a, b) Traces showing average [Ca^{2+}]$_i$ over time of naïve (a) and memory (b) CD4$^+$ T cells in response to changes in extracellular solutions shown on the bar above in the absence (control naïve cells (black) and memory control cells (red)) or presence of 5 µM (gray) or 20 µM (dark grey) Caloxin1C2. **(c)** Bar graphs showing analyzed SOCE parameters measured in (a, b). Data represent mean ± SEM obtained from 7-10 independent measurements (~100-200 cells each) from 5 donors. Asterisks indicate significance at * p<0.05 using Kruskall-Wallis one-way analysis of variance (ANOVA).
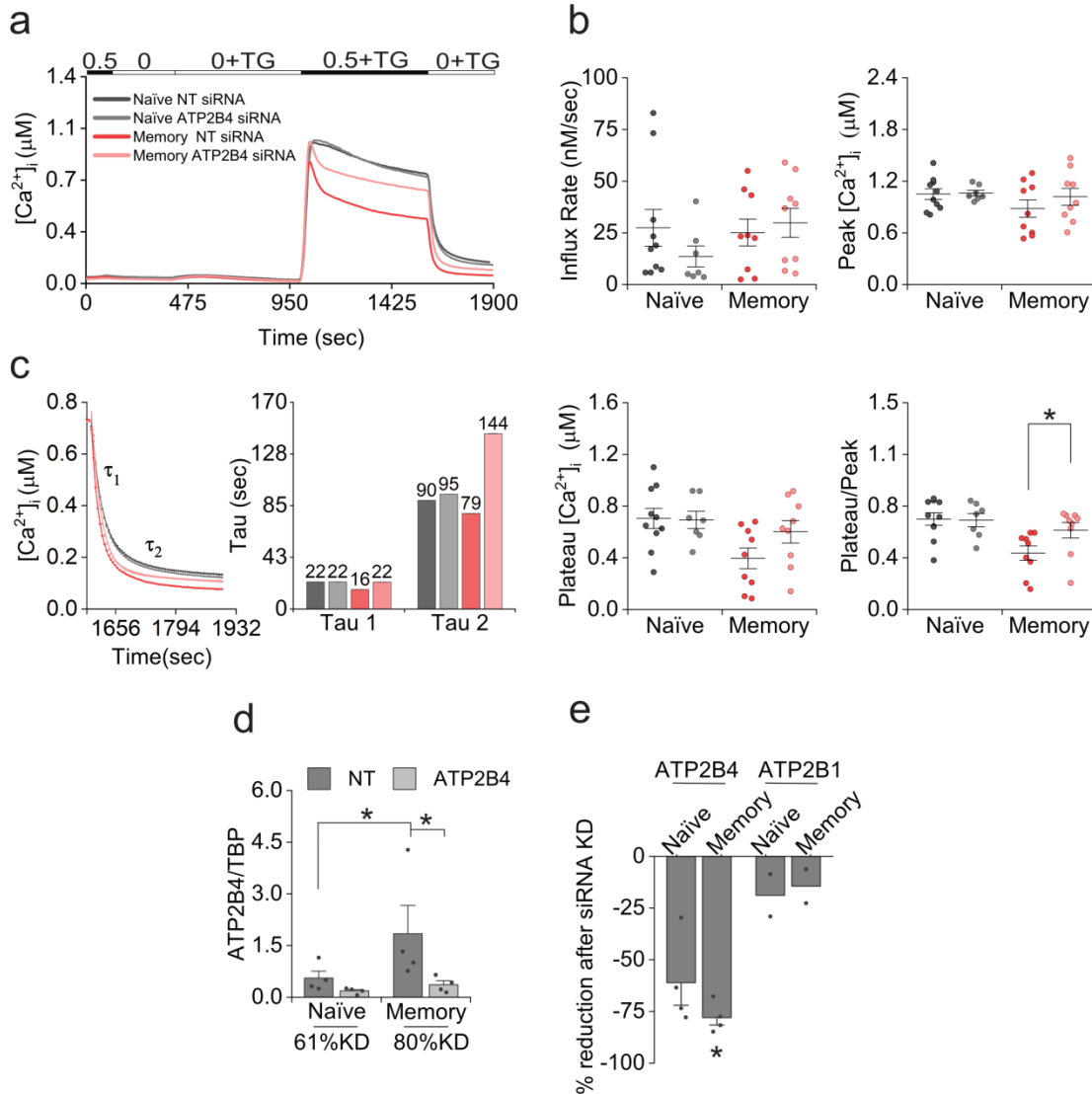
Figure 13: Downregulation of PMCA4 reverts SOCE phenotypes of memory T cells.
(a) Average $[Ca^{2+}]_i$ traces over time in response to changes of 0.5 mM Ca^{2+}_0 solution (see bar above the traces). SOCE was measured in naïve and memory CD4$^+$ T cells transfected with non-silencing RNA (dark grey or red) or transfected with ATP2B4 targeting siRNA (grey or light red). (b) Corresponding statistics of $[Ca^{2+}]_i$ influx rate, $[Ca^{2+}]_i$ peak, $[Ca^{2+}]_i$ plateau and ratio plateau/peak of SOCE measured in (a). (c) Time constants obtained from fitting a double exponential decay to the decline in $[Ca^{2+}]_i$ of average iso-cells traces measured in (a) after removal of extracellular Ca^{2+}_0. (d) mRNA expression levels of ATP2B4 in sorted naïve (CD4$^+$CD127^{high}CD25$^-$CD45RO$^-$) and memory (CD4$^+$CD127^{high}CD25$^-$CD45RO$^+$) CD4$^+$ T cells after transfecting cells with a non-targeting siRNA (control) or a siRNA targeting ATP2B4 (ATP2B4-siRNA) for 72 hours. (e) Percentage of change in ATP2B4 or ATP2B1 after ATP2B4 siRNA knockdown. Data represent mean ± SEM obtained from 7-10 independent measurements (~100-200 cells each) from 5 donors (b), 4 donors (d) and 4 and 2 donors (d and e). Asterisks indicate significance at * $p<0.05$ using Kruskall-Wallis one-way analysis of variance (ANOVA).

donors evaluated (Figure 13d), whereas ATP2B1 was in average slightly reduced (less than 18%) in the two donors evaluated (Figure 13e). While the SOCE profile of naïve cells was not altered by transfection with the ATP2B4-siRNA, the SOCE peak of memory T cells showed a 16% increase and thus became comparable to that of naïve T cells. Similarly, the plateau $[Ca^{2+}]_i$ was increased by 52% to be now not significantly different from that of naïve cells (Figure 13a and b). Furthermore, the fraction plateau/peak was significantly increased in memory T cells transfected with the ATP2B4-siRNA compared to memory control T cells (Figure 13a and b).

Next, we estimated the rates of Ca^{2+} clearance of average iso-cells by performing double-exponential curve fits to the decline phase of $[Ca^{2+}]_i$ after removal of extracellular Ca^{2+} (Figure 13c). The biphasic decay of Ca^{2+} signals after removal of extracellular Ca^{2+} shows a faster phase with a shorter time constant (tau1) and a second slower phase with a longer time constant (tau2). While the fast (tau1=22) and slow phase (tau=95) of decay were not altered in naïve T cells transfected with ATP2B4-siRNA compared to naïve control cells (tau1=22) and (tau2=90) (Figure 13c), memory T cells transfected with ATP2B4-siRNA showed a 27% and 45% increase in their fast and slow time constants respectively (Figure 13c). Noteworthy is that, control memory T cells had shorter time constants of both decay phases when compared to control naïve T cells, in agreement with analysis in (Figure 10e). Together, these results indicate that downregulation of PMCA4 in memory but not in naïve T cells changed the time course of SOCE, providing evidence that PMCA4 plays a differential role in Ca^{2+} homeostasis in memory T cells compared to naïve T cells.

5.4   PMCA4 regulates the compartment stoichiometry of the CD4^{+} T cells

Due to the differential expression of PMCA4 in naïve and memory populations, we hypothesized that PMCA is also differentially regulated upon activation of naïve T cells and differentiation into effectors and memory cells. We predict that this regulation is important to establish and maintain Ca^{2+} levels that meet requirements of long-lived memory cells after termination of the immune response. To test this hypothesis, we isolated naïve T cells out of PBMCs as shown in (Figure 10a). One day after isolation, cells were transfected either with a non-targeting RNA or an ATP2B4-specific siRNA for 3 days. After this time, naïve T cells were polyclonally stimulated with anti-CD3/antiCD28 coated beads. Medium was supplied with fresh siRNA to maintain the downregulation during the experimental procedure (Figure 14a). After 24 hours, we measured compartment distribution through changes in the surface markers CD62L and CD45RO. The former is constitutively expressed in naïve cells, needed for entry to SLC and upon TCR engagement is rapidly shed from the surface (Butcher & Picker, 1996; Hamann et al., 2000; Steeber et al., 1996). On the other hand, CD45RO is absent in naïve T cells and its expression identifies cells in transition to or already differentiated into memory cells (Deans et al., 1989; Hermiston et al., 2003). Therefore, based on the expression of these molecules, CD4^{+} T cells can be assigned into the compartments naïve (CD62L^{+}CD45RO^{-}), effector (CD62L^{-}CD45RO^{-}), effector memory (EM) (CD62L^{-}CD45RO^{+}), or central memory (CM) (CD62L^{+}CD45RO^{+}) (Figure 14a) (Sallusto et al., 1999). Downregulation of ATP2B4 followed by 24 hours of polyclonal stimulation resulted in higher fraction of cells retained in the naïve compartment and less cells undergoing

differentiation into the effector compartment (Figure 14b and c), whereas the expression of CD45RA and CCR7 were unaffected (Figure 15a and b). We also tested whether downregulation of PMCA4 affects early activation events. While the earliest activation marker CD69, a type II membrane glycoprotein involved in lymphocytes trafficking to the lymph nodes was not altered, CD154 (ligand for CD40) was up-regulated significantly (Figure 14d and e). Furthermore, CD25 (α chain of the high-affinity IL-2 receptor), important for T cell survival, was not differentially regulated (Figure 15c).
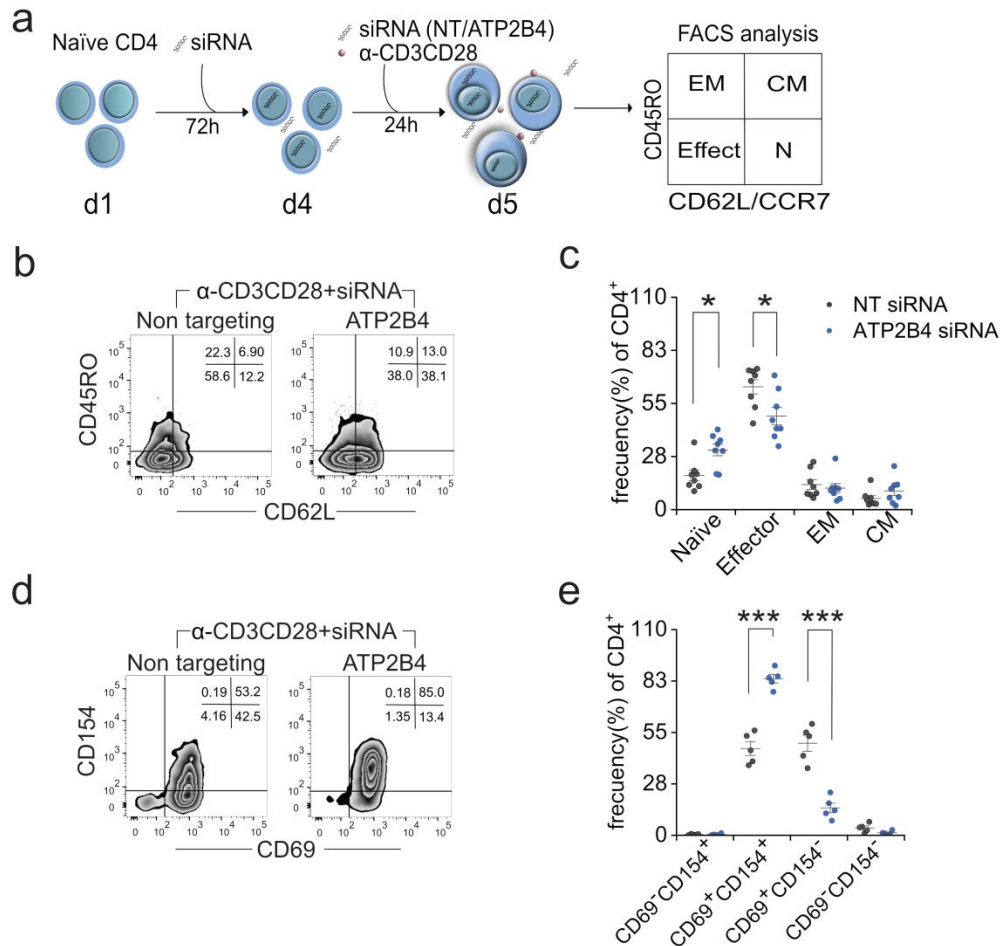

Figure 14: PMCA4 regulates the compartment stoichiometry of the CD4$^+$ T cells.
(**a**) Schematic representation of the experimental design: naïve T cells isolated from human PBMCs by flow cytometric sorting were transfected the day after with either a non-targeting siRNA (control) or with siRNA targeting ATP2B4 for 72 hours, following stimulated with anti-CD3/CD28 coated beads in the presence of fresh siRNA for 24 hours more and then analyzed by flow cytometric analysis. (**b**) Representative counter plot of activated naïve cells showing % of positive cells for the markers CD45RO and CD62L in cells treated as in (a). (**c**) Statistical analysis of cells measured in the naïve (CD62L$^+$CD45RO$^-$), Effector (CD62L$^-$CD45RO$^-$), EM (CD62L$^-$CD45RO$^+$) and CM (CD62L$^+$CD45RO$^+$) compartments. (**d**) Representative counter plot image showing % of positive cells for the markers CD69 and CD154 in cells treated as shown in (a). (**e**) Statistical analysis of cells analyzed in (d). Data represent mean ± SEM. Asterisks indicate significance at * p<0.05, *** p<0.001 using one-way analysis of variance (ANOVA).

These results indicate that PMCA4 plays an important role in compartment stoichiometry during activation and it may regulate directly or indirectly surface molecules needed to mount an efficient immune response during cognate antigen recognition.

Besides we analyzed the expression of memory markers at different time points (Figure 15d) in order to follow the compartment distribution upon our conditions of strong stimulation (1:1 bead:cell ratio), which may favor the generation of particular CD4$^+$ subtypes. From this experiment is clear that only CD62L is rapidly downregulated following activation and CD4$^+$ compartments are produced within 24 hours based on CD62L expression but not CCR7, with the former being lost at later time points. This explains why we did not detect changes on compartment distribution based on CCR7 expression in the experiment shown in (Figure 15a). On the other hand, CD45RO expression increased at 24 hours but cells still remained CD45RA, indicating early steps in the pathway of memory T cell formation.
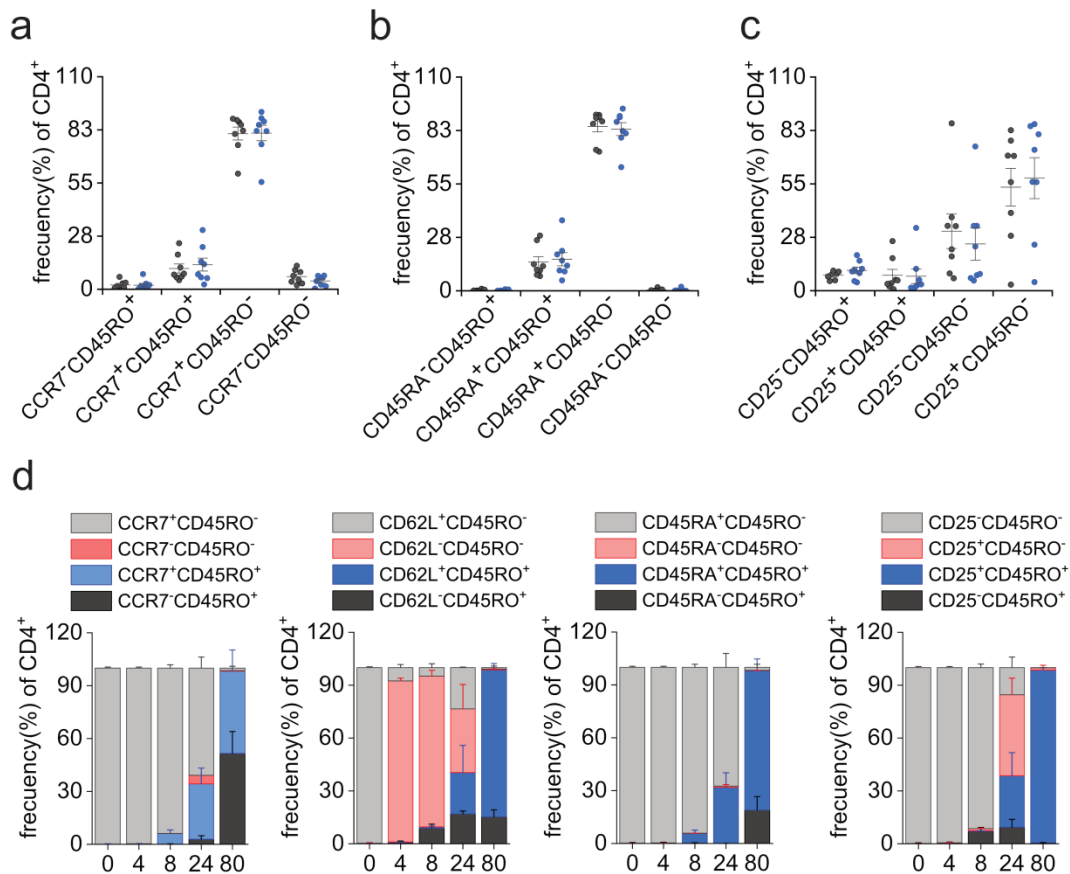

Figure 15: PMCA4 regulates the compartment stoichiometry of the CD4$^+$ T cells.
(a-c) Analysis of surface markers upon stimulation of naïve T cells with anti-CD3/CD28 beads to bead to cell ratio 1:1 for 24 hours, in the presence of a non-targeting siRNA or siRNA targeting ATP2B4. Naïve T cells were transfected either with a non-targeting siRNA or siRNA targeting ATP2B4 for 72 hours previously to activation. **(d)** Stack columns represent the expression kinetic of CCR7, CD62L, CD45RA and CD25 on naïve T cells stimulated for 4, 8, 24 and 80 hours with anti-CD3/CD28 coated beads to a bead:cell ratio of 1:1. Data represent mean ± SEM.

5.5 PMCA4 is differentially expressed in the *in vivo* differentiated CD4$^+$ T cell compartments and results in distinct SOCE profiles

The findings that reduced levels of PMCA4 affected the generation of effector cells in our *in vitro* activation model prompted us to investigate whether *in vivo* differentiated CD4$^+$ compartments express PMCA4 differentially. To answer this question, we sorted CD4$^+$ T cell compartments from human PBMCs based on the surface markers CD45RO and CCR7 as shown in (Figure 16a). Purity of the sorted populations was checked by surface marker analysis following sorting. Cells that were CD45RO$^-$CCR7$^+$CD45RA$^+$ are
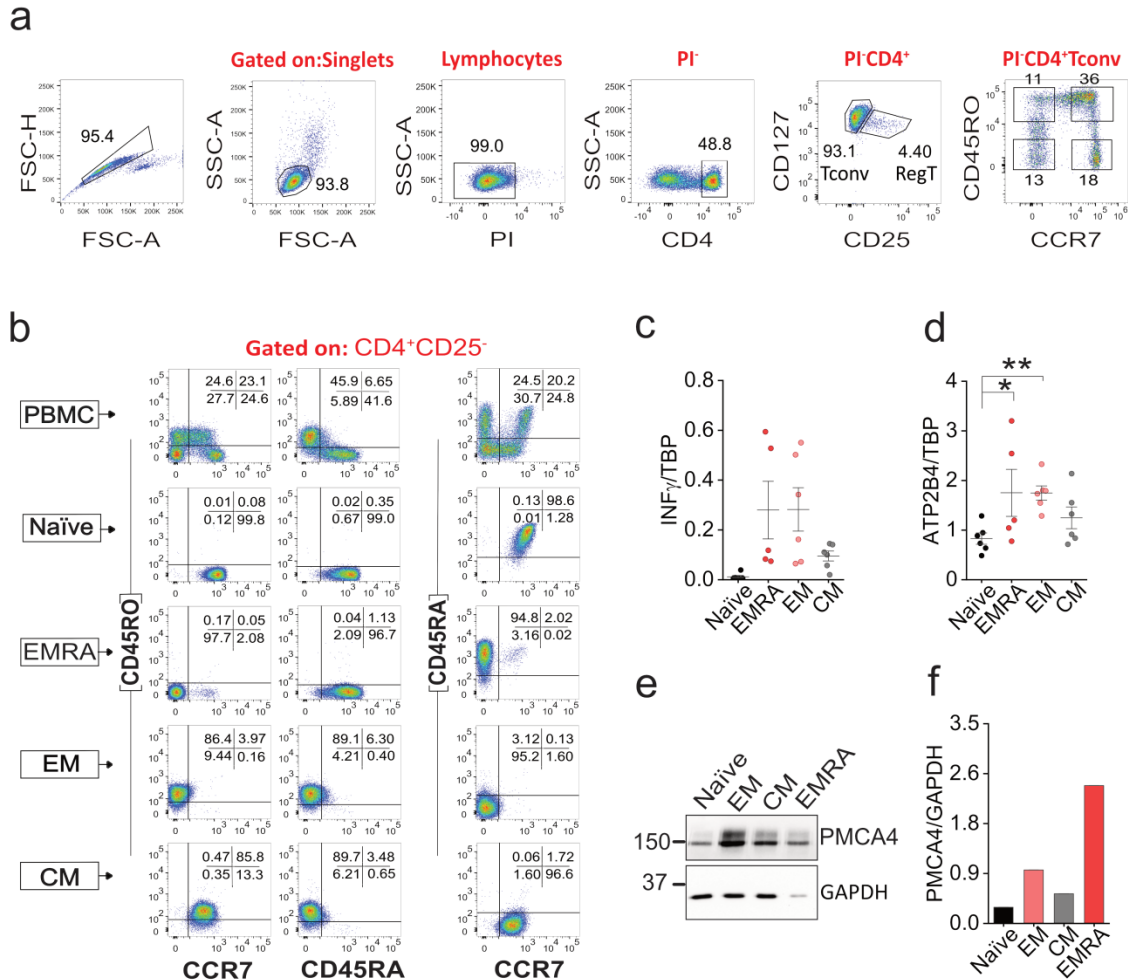

Figure 16: CD4$^+$ T cell compartments show differential expression of PMCA4.
(a) Gating strategy used to sort CD4$^+$ T cell compartments out of PBMC is shown upper the dot plots graphs in red color. CD4$^+$ T cell compartments were sorted from Conventional T cells (Tcon) population by exclusion of regulatory Tcells (regT). Naïve (CD45RO$^-$CCR7$^+$), Terminal effector cells (CD45RO$^-$CCR7$^-$), EM (CD45RO$^+$CCR7$^-$) and CM (CD45RO$^+$CCR7$^+$) T cells. **(b)** Representative post-sorting flow cytometric analysis of CD4$^+$ compartments, where CD45 positive cells are shown. **(c, d)** qRT-PCR analysis of CD4$^+$ T cell compartments sorted as in (a) showing relative expression of *IFNG* (c) and *ATP2B4* (d) normalized to *TBP*. **(e, f)** Western blot (e) and quantification (f) of PMCA4 levels in CD4$^+$ T cell compartments from one healthy donor. Data represent mean $\pm$ SEM. Asterisks indicate significance at * p<0.05, **p<0.01, using one-way analysis of variance ANOVA.

defined as naïve cells (N), CCR7$^-$CD45RO$^-$CD45RA$^+$ terminally differentiated effector memory cells (EMRA), CCR7$^-$CD45RO$^+$CD45RA$^-$ effector memory (EM) and CD45RO$^+$CCR7$^+$CD45RA$^-$ as central memory cells (CM) (Figure 16b). EMRA cells are a poorly characterized population with low frequency in human PBMC (~2-16% of the CD4$^+$ T cells) (Amyes et al., 2005), they express CD45RA and share properties with the short lived effector cells such as potent cytotoxic activity due to high INF-γ and reduced IL-2 production, show multiple signatures of senescence and end-stage differentiation (Durek et al., 2016; Henson et al., 2012; Sallusto et al., 1999). To confirm the functional properties of the sorted populations, we measured *IFNG* mRNA levels. EMRA and EM populations exhibited the higher expression of *IFNG* followed by CM, whereas it was not detectable in naïve T cells (Figure 16c). Analysis of PMCA4 expression at mRNA (Figure 16d) and protein levels (Figure 16e and f) revealed a hierarchical expression of PMCA4 with the EMRA T cells having the highest expression, followed by EM, CM and naïve T cells. In line with expression analysis, SOCE measurement after Tg-induced store depletion showed that CD4$^+$ T cell compartments have distinct SOCE profiles with comparable Ca^{2+} peaks, but distinct decay rates (Figure 17a and b). In addition, EMRA cells exhibited the lowest [Ca^{2+}]$_i$ plateau and plateau/peak ratio followed by EM, CM and naïve (Figure 17a and b), which correlates with their PMCA4 expression levels (Figure 16d-f). Furthermore, we analyzed the decay rates of iso-cells in presence of (Figure 17c) or absence of Ca^{2+}$_0$ (Figure 17d) by fitting the decline on [Ca^{2+}]$_i$ of individual iso-cells to a single exponential decay. Fitting to a single
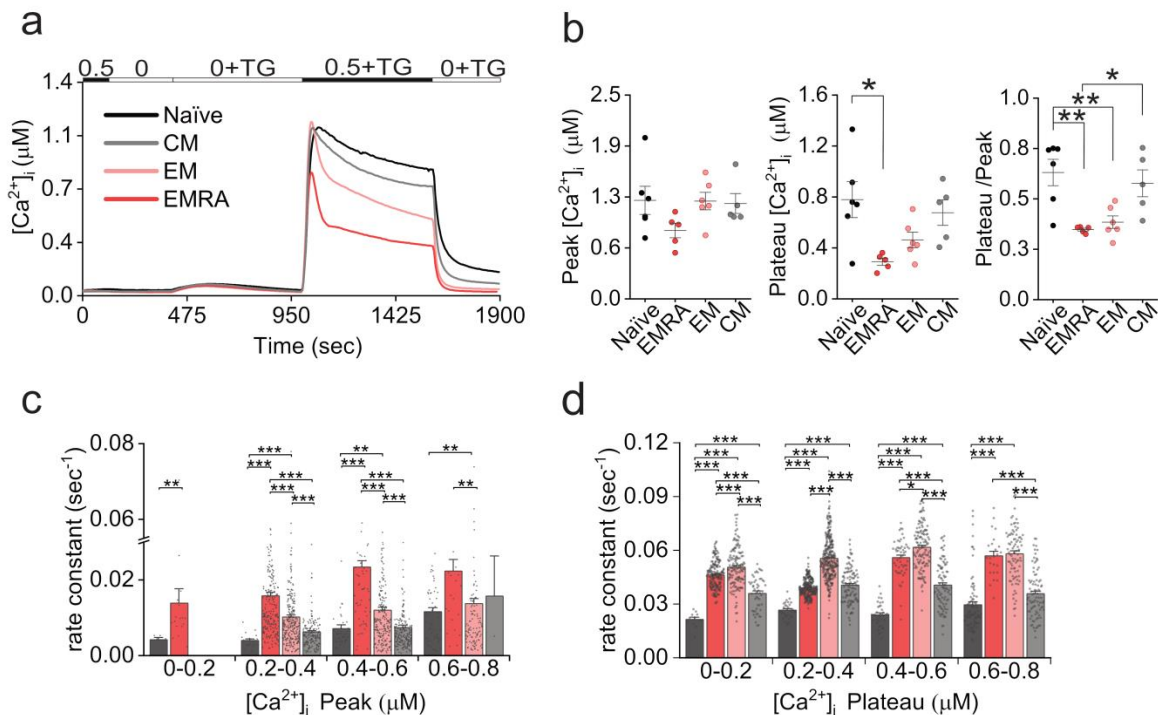

Figure 17: CD4$^+$ compartment shown distinct SOCE profiles.
(**a**) Average traces showing changes of [Ca^{2+}]$_i$ over time in response to Ca^{2+}$_0$ re-addition. (**b**) Statistical analysis of SOCE Parameters in sorted CD4$^+$ compartments shown in (a). (**c, d**) Rate constants of each individual cell analyzed in (a) plotted against their respective [Ca^{2+}]$_i$ intervals Peak (c) or Plateaus (d). Data represent mean ± SEM obtained from 6 independent measurements (~100-200 cells each) from 3 donors. Asterisks indicate significance at * p<0.05, **p<0.01, *** p<0.001 using one-way analysis of variance ANOVA (b) or Kruskall-Wallis one-way analysis of variance (ANOVA) (c and d).

exponential decay was selected over double exponential decay fitting due to not all cells (~20%) showed a two phase decay in Ca^{2+} decline, which could have impaired the final results. On the other hand, in cases where the two phases in Ca^{2+} decline were calculated (Figure 13c), iso-cell traces were average so that the effect of this small cell population lacking a two phase decay was overcome. Thus the decline of $[Ca^{2+}]_i$ after Ca^{2+} removal was calculated by fitting to a double exponential decay, reaching R^2 values higher than 99% in all curve fittings performed. Curve fitting analysis (Figure 17c and d) confirmed that $CD4^+$ T cell compartments show different efflux rates that correlate to the expression levels of PMCA4. Together, this data strongly highlights the importance of Ca^{2+}-dependent PMCA regulation in the differentiation and fate determination of naïve T cells when an immune response is elicited.

5.6 Mitochondrial contribution to Ca^{2+} homeostasis depends on the cellular compartment and activation state of $CD4^+$ T cells

Mitochondria are pivotal organelles in T cells; they are not only the main machinery of ATP production but also have an essential role in metabolism, which is programed to function accordingly to the activation of a T cell. Naïve T cells are small and quiescent and mainly use the energy derived from glucose, fatty acids and aminoacids via the tricarboxylic acid cycle (TCA), where pyruvate is converted to acetyl-CoA thereby generating reducing equivalents that fuel oxidative phosphorylation (OXPHOS) and ATP synthesis. Activated T cells, on the other hand, make preferential use of aerobic glycolysis in order to produce biomolecules required for differentiation and proliferation. Contrary to the former, memory T cells rely exclusively on fatty acid oxidation (FAO) to fuel oxidative phosphorylation (OXPHOS) (Buckler & Turner, 2015; Sena et al., 2013). In addition to their central metabolic role, mitochondrial Ca^{2+} uptake contributes to sustained Ca^{2+} signaling in activated T cells (Hoth et al., 1997; Quintana et al., 2011), as well as they can function as sinkers increasing or decreasing Ca^{2+} clearance on T cells (Bautista et al., 2002). Modulation of the mitochondrial Ca^{2+} uptake during long time activation of T cell activation is not fully understood. Therefore, we assessed the contribution of mitochondrial Ca^{2+} uptake in naïve and memory $CD4^+$ T cells in both states, resting and upon long term activation. Acute disruption of mitochondrial membrane potential ($\Delta\Psi m$) with carbonyl cyanidem chlorophenyl hydrazine (CCCP), a protonophore that dissipates $\Delta\Psi m$ and is able to block mitochondrial Ca^{2+} uptake (Hoth et al., 1997), led to significant reduction of SOCE in both resting naïve and memory cells, with naïve cells being more susceptible to immediate inhibition of the SOCE peak (Figure 18a and c) in agreement with previous results in Jurkat T cells (Hoth et al., 1997). On the other hand, in naïve T cells activated for 4 days, disruption of $\Delta\Psi m$ led to a significant enhancement of SOCE (Figure 18e), reproducing our previous observations with naïve cells polarized *in vitro* for 7 days into Th1 and regT (Kircher et al., 2018). Surprisingly, when memory T cells were activated for 4 days with anti-CD3/CD28 coated beads and acutely treated with CCCP, they showed SOCE with mild increase of the peak and mild decrease in plateau level that together result in a significant lower ratio plateau/peak compared to control, indicating an enhanced Ca^{2+} clearance (Figure 18h and i). To isolate possible effects of $[Ca^{2+}]_i$ on Ca^{2+} clearance, we analyzed the time constants of the decline in $[Ca^{2+}]_i$ of average iso-cells after Ca^{2+}_0 removal. The kinetic of Ca^{2+} clearance during Ca^{2+} removal followed a decay course characterized by a single phase of Ca^{2+} clearance in activated naïve T cells treated with CCCP, whereas two phase decay was
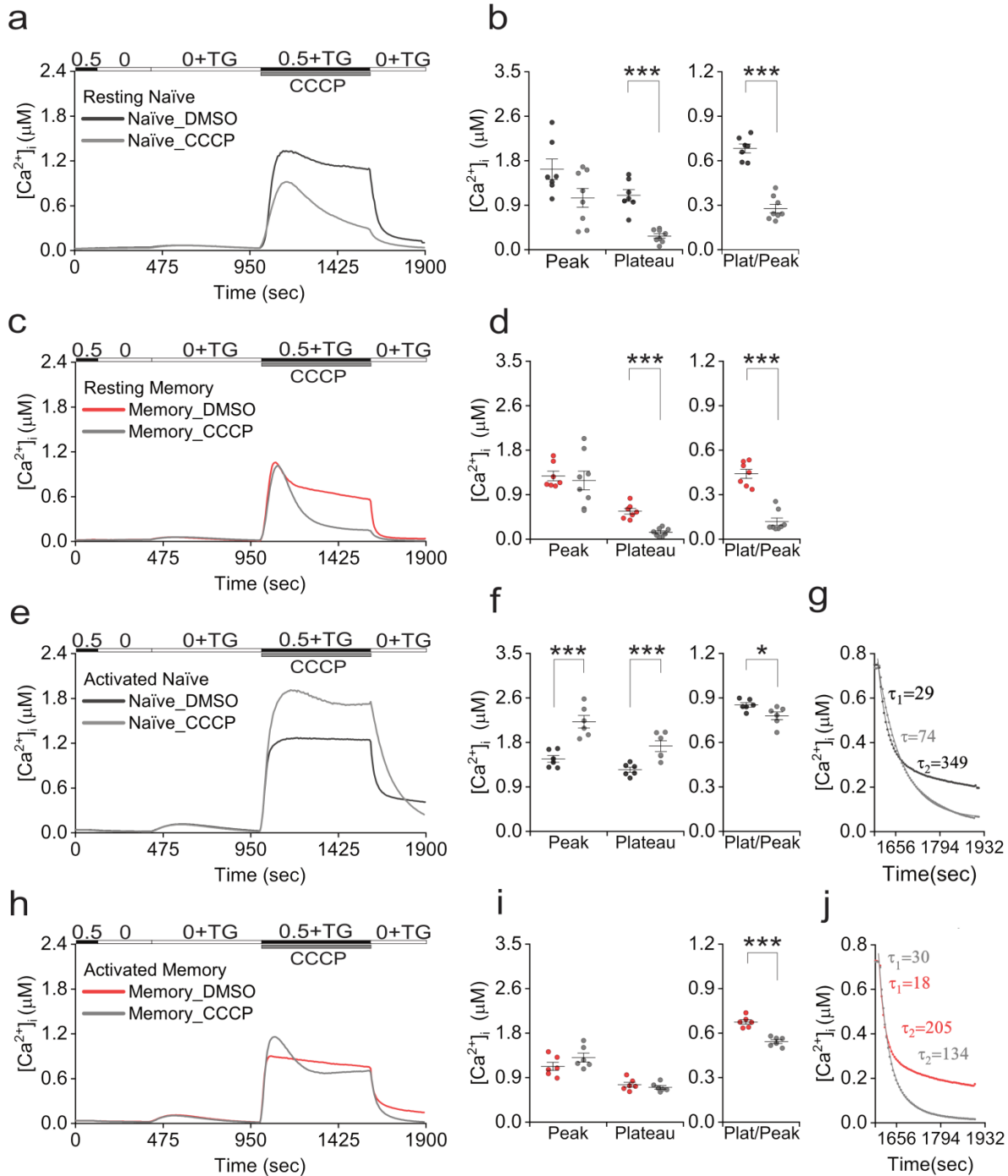
Figure 18: Mitochondrial contribution to Ca^{2+} homeostasis depends on the cellular compartment and activation state of $CD4^+$ T cells.

Average traces showing changes of $[Ca^{2+}]_i$ over time in response to Ca^{2+}_0 solution containing DMSO (control) or carbonyl cyanide chlorophenyl hydrazine (CCCP) (see bar above the traces and legends). SOCE was measured in resting naïve T cells **(a)**, resting memory T cells **(c)**, naïve T cells activated for 4 days **(e)** or memory T cells activated for 4 days **(h)**. Bar graphs showing analyzed SOCE parameters measured in a, c, e and h **(b, d, f, i)**. Time constants calculated by fitting to a single or double exponential decay the decline in $[Ca^{2+}]_i$ of average iso-cells following Ca^{2+}_0 removal **(g, j)**. Data represent mean ± SEM obtained from 6-8 independent measurements (~100-200 cells each) from 4 donors. Asterisks indicate significance at * $p<0.05$, *** $p<0.001$ using one-way analysis of variance (ANOVA).

observed in activated naïve control (Figure 18g). On the other hand, activated memory T cells treated with CCCP showed 2 phase decay, with the first time constants (t1) increasing a 40%, whereas the slow phase of decay (t2) decreased a 52% compared to memory control (Figure 18j). In parallel, we measured the effects of CCCP-induced mitochondrial depolarization in resting and activated T cells by flow cytometry. Although mitochondrial mass was measured in murine CD4$^+$ T cells (Baixauli et al., 2015), mitochondrial mass of human CD4$^+$ naïve and memory is still lacking. Therefore, we stained resting naïve and memory cells with the plasma membrane permeable mitochondria targeted dye, Mitotracker-Red. Resting naïve and memory cells showed comparable mitochondrial mass (Figure 19a and b) and shift in ΔΨm upon treatment with CCCP (Figure 19c and d). Interestingly, Mitotracker-Red staining in naïve cells activated for 4 days revealed two populations of cells, where cells with bigger mitochondrial mass were bigger in size as detected by forward scatter plots (Figure 19a) indicating that they underwent activation and became highly proliferative
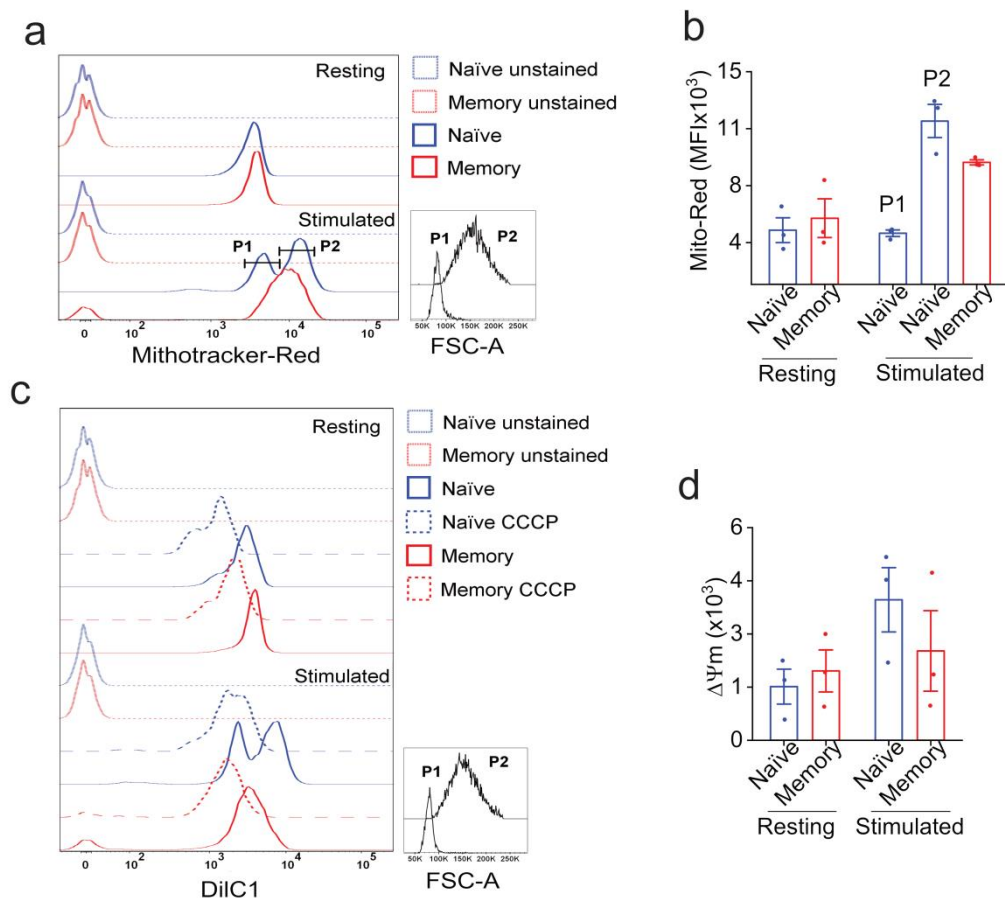

Figure 19: Mitocondria size and Mitochondrial potential in resting and activated naïve and memory T cells.
(a) Analysis of Mitochondria size in resting naïve (blue) and memory (red) human CD4$^+$ T cells stained with Mitotracker-Red and analyzed by flow cytometry. (b) Quantification of Mitochondria size in naïve and memory resting and activated T cells. (c) Analysis of Mitochondria potential (ΔΨm) in naïve (blue) and memory (red) human CD4$^+$ T cells stained with the mitochondrial membrane potential indicator DilC1, in resting or after 4 days of stimulation with anti-CD3/CD28 coated beads. Continuous lines represent control cells (DMSO treated) and dotted lines represent cells treated with CCCP preceding flow cytometry analysis (see materials and methods). (d) Quantification of ΔΨm in naïve and memory resting and activated CD4$^+$ T cells shown in b. Data represents mean ± SEM from 3donors.

blast T cells. This mitochondrial size distinction following activation was less prominent in memory cells, probably due to the fact that resting memory cells have less energetic and biosynthethic needs associated with proliferation and differentiation (Bevington et al., 2017; Desdin-Mico et al., 2018). In contrast to the resting cells, treatment of activated cells by CCCP resulted in a wider depolarization shift in naïve than memory cells (Figure 19c and d). Together, these results indicate that mitochondrial Ca^{2+} uptake differentially modulate SOCE following primary and secondary TCR stimulation.

5.7   Transcriptional control of PMCA4 results in biphasic expression following activation

The experiments performed so far showed clearly that the expression pattern of PMCA4 correlates with the activation and differentiation stage of CD4$^+$ T cells. Therefore, we asked: what are the mechanisms underlying such a tight regulation. Too little is known about transcriptional regulation of PMCA. NFAT1 has been proposed to regulate PMCA4 through a negative loop during osteoclastogenesis, where NFAT1 stimulates PMCA4 transcription and PMCA4 mediated Ca^{2+} flux prevents NFATc1 activation (Kim et al., 2012). Findings by others have shown PMCAs as negative regulators of calcineurin-mediated signaling pathways (Boczek et al., 2017; Buch et al., 2005). Therefore, we screen potential transcription factors that could bind to the promoter region of PMCA4 using available ChIP-seq information (Ambrosini et al., 2016) combined with TFBS prediction databases such as HOCOMOCO (Kulakovskiy et al., 2018) and Promo 3 (Farre et al., 2003; Messeguer et al., 2002). The resulting analysis (Figure 20a) shows the 33 transcription factors (Table 10) that were commonly predicted by all three databases. As the transcription factor YY1 was predicted with the highest, the next aim was to confirm binding of YY1 to the promoter region of PMCA4 experimentally. Because our preliminary experiments showed that a conventional protocol of chromatin immune precipitation (ChIP) experiment was prone to misleading positive results, we applied a rigorous protocol that eliminates all unspecific binding using isotype control antibody bound beads in a "pre-clearing" step (Figure 20b first lane). The efficiency of elimination of unspecific binding was demonstrated by applying the pre-cleared lysate to fresh isotype control antibody-bound beads (Figure 20b second lane). Finally, the ability of YY1 to bind to the promoter region was tested by using an YY1-specific antibody to immunoprecipitate YY1 and the bound genomic DNA, which was then amplified with specific primers, designed based on the predicted binding domains. In parallel, we used an anti-NFAT antibody to serve as an additional control for the specificity of binding. Results of the ChIP experiments showed that YY1, but not NFAT, was able to bind the promoter region of PMCA4 as visualized on agarose gels (Figure 20b). The identity of the amplicon was further confirmed by sequencing. Finally, we investigated time dependent changes in PMCA4 levels following activation in more detail. In contrast to observations made in Jurkat T cells where PMCA4 was upregulated after acute (1 to 6 h) stimulation with PHA (Ritchie et al., 2012), we observed that compared to unstimulated cells, primary human CD4$^+$ T cells stimulated for 4 h using anti-CD3/CD28 coated beads resulted in reduction of PMCA4 protein levels to 47.8% (2 donors, data not shown). This reduction was maintained upon extending stimulation time to 24h (Figure 20c and d). Interestingly, the reduction of PMCA4 levels following 24 h stimulation was accompanied by a 210% increase in YY1 protein levels (Figure 20d). Next we evaluated the expression of YY1 in resting and activated naïve and memory cells at different time points. Naïve and memory resting cells have no differences in YY1 protein levels (Figure 20e and g), but YY1 was strongly increased in both populations during the first 24 hours of activation

with anti-CD3/CD28 (Figure 20e) as seen before in total CD4$^+$ stimulated T cells (Figure 20c). Naïve cells maintained high YY1 expression up to 96 hours, thereafter YY1 levels returned to resting levels to further decrease at 168 hours of activation (Figure 20e, f and h). An inverse correlation between YY1 and PMCA4 expression patterns was found during the time course of stimulation. PMCA4 expression was decreased upon 96 hours, time at which it started to increase (Figure 20e, f and h). On the other hand, although YY1 expression increased in memory T cells at 24 hours of activation, this increase was less clear at later time points, where YY1 was detected as a faint double band, maybe product of protein degradation or translational modifications (Figure 20e and f). This double band pattern was also detected at later time points
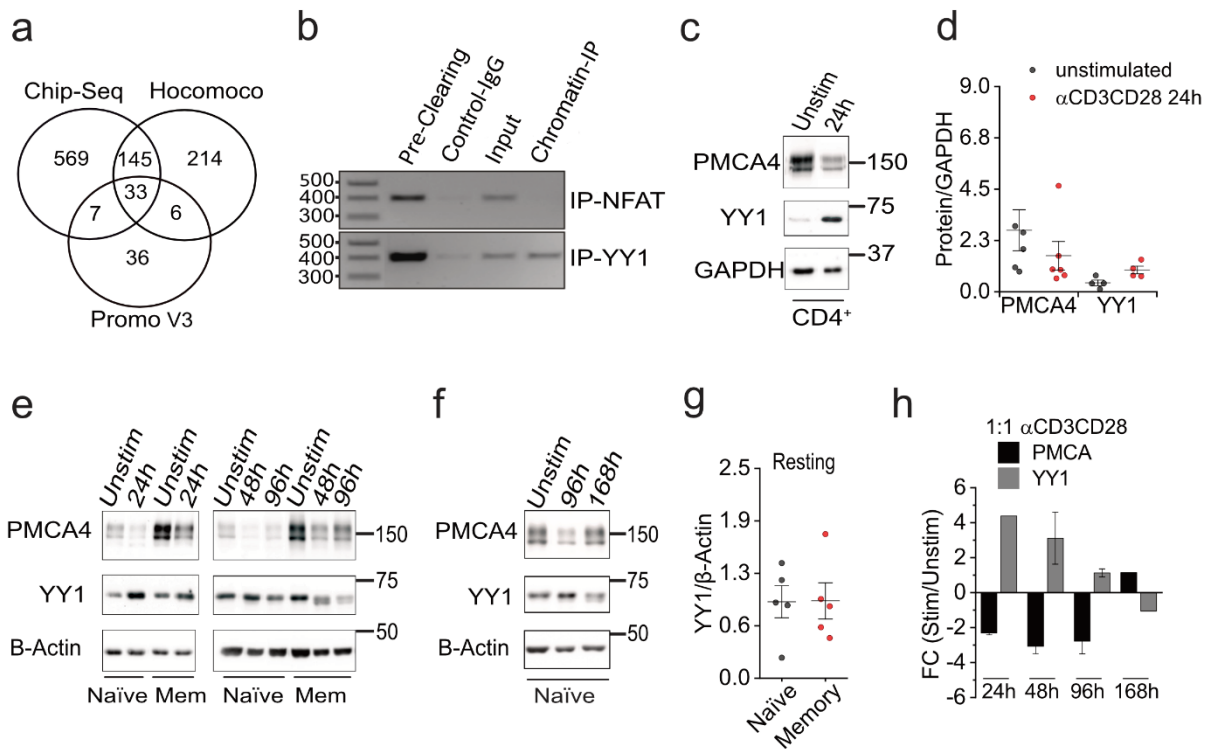

Figure 20: Transcriptional control of PMCA4 results in biphasic expression following activation.
(a) Venn diagram showing the overlapping results obtained from three databases (HOCOMOCCO, Promo V3 and ChiP-seq) used to predict transcriptional factors binding to PMCA4 promoter region. **(b)** Agarose gel showing PCR amplicons obtained with specific primers designed to amplify a 410 base pair-long fragment of ATP2B4b promoter region. Poly chain reactions (PCRs) were performed using chromatin DNA purified from total lysate (Input) or after immune precipitation by pre-clearing beads, beads bound to IgG control antibodies, beads bound to anti-NFAT (upper row, Chromatin-IP) or to anti-YY1 (lower row, Chromatin-IP). **(c)** Representative of 4-5 western blots (WB) and corresponding quantification **(d)** of total CD4$^+$ T cells stimulated for 24 hours with anti-CD3/CD28 coated beads at 1:1 bead:cell ratio. **(e)** Representative WB showing expression of PMCA4 and YY1 in naïve and memory cells left un-stimulated or stimulated for 24, 48h or 96 hours with 1:1 bead:cell ratio. **(f)** Representative WB showing expression of PMCA4 and YY1 in unstimulated or stimulated naïve and memory cells for 96h or 162h with anti-CD3/CD28 coated beads at 1:1 bead:cell ratio. **(g)** Quantification of PMCA4 and YY1 expression on resting naïve and memory of 5 donors. **(h)** Fold changes in PMCA and YY1 protein expression over time in naïve stimulated versus unstimulated ones. Naïve cells were stimulated with anti-CD3/CD28 coated beads at 1:1 bead:cell ratio for 24h (2donors), 48h (2donors), 96h (3donors) and 162h (1donor). Data in (d, g and h) represents mean ± SEM.

in naïve T cells stimulated up to 168 hours (Figure 20f), time point at which we detected a biphasic change in PMCA4 expression. Long term stimulation of naïve T cells with anti-CD3/CD28 coated beads, without inclusion of polarizing cytokines indispensable for final commitment of activated cells in terminally differentiated T helper cells, leads to generation of highly proliferative blast cells (Bevington et al., 2017). To examine possible role of PMCA4 expression in full differentiated T cells, we subjected the naïve cells to *in vitro* polarization providing stimulatory, co-stimulatory and cytokine mediated signals necessary for differentiation of naïve cells into Th1 or regT cells (Kircher et al., 2018). The polarized cells showed the expected differential expression of *IFNG* (Figure 21f) and *FOXP3* (Figure 21g), the hallmarks of Th1 and regT populations respectively. Importantly, terminally differentiated effector cells, Th1 and regT, showed an upregulation of PMCA4 that was most significant for cells polarized into Th1 or regT while the control stimulated non polarized cells (Th0) underwent milder upregulation of PMCA4 (Figure 21a and b). Strikingly, levels of YY1 followed the reverse pattern we saw before upon long term activation (168 h), thought independent of polarizing cytokines (Figure 21a and c). YY1 in polarized T cells, mainly Th1 was again seen as a double band when blot membrane were exposure for longer times, see right panel in (Figure 21a). The decrease in YY1 expression may indicate reduced transcription of YY1 gene. In order to answer
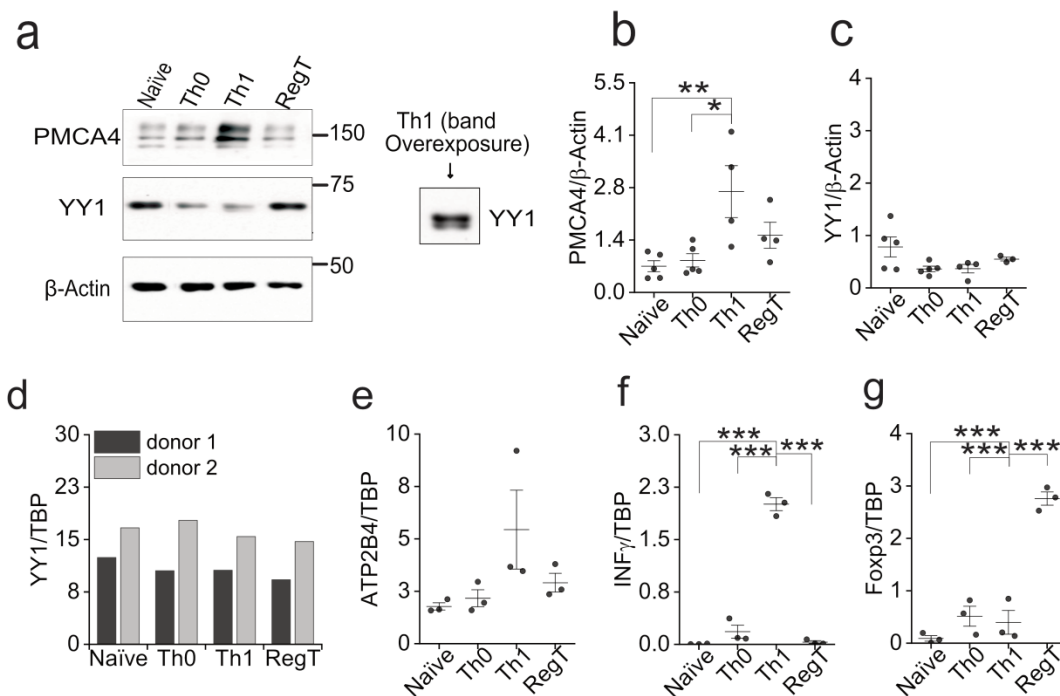

Figure 21: Cytokine signaling is needed to induce PMCA4 expression through down regulation of YY1 protein.
(a) Representative of 5 western blots showing PMCA4 and YY1 protein levels in *in vitro* polarized Th0, Th1 and Regulatory T cells (regT), to the right YY1 bands at 1800sec of overexposure time. **(b, c)** Quantification analysis shown in (a) from 5 donors normalized to ß-actin. **(d-g)** Relative mRNA expression of YY1(d), ATP2B4 (e), IFNG (f), and FOXP3 (g) in resting naïve (non-activation control), Th0 (non-polarization control), Th1 or regT cells normalized to the TATA binding protein (TBP) and calculated using the $2^{-\Delta CT}$ method. Data represent mean ± SEM. Asterisks indicate significance at * $p<0.05$, ** $p<0.01$, *** $p<0.001$ using one-way Analysis of Variance (ANOVA).

that, we measured YY1 transcripts levels in polarized T cells. Unexpectedly, YY1 mRNA levels were almost not unaltered (Figure 21d), which indicates that posttranslational modifications on YY1 can target YY1 for protein degradation.

Collectively, these results indicate that T cells may adapt the expression levels of PMCA4 during activation states under the transcriptional repressive control of YY1, probably targeting YY1 for degradation and allowing the expression of YY1 target genes, such as ATP2B4 and INFG.

Trancription factor/ Gene ID	TSS 500	Cell types	TSS 1000	Cell types	TSS 5000	Cell types	TSS 10000	Cell types
YY1 [7528]	170	13	257	13	653	13	905	13
JUN [3725]	138	7	182	7	347	7	543	11
SP1 [6667]	101	7	152	7	355	8	496	8
E2F1 [1869]	81	4	110	4	205	4	298	5
FOS [2353]	78	5	144	5	345	5	582	6
ETS1 [2113]	77	8	94	8	213	8	322	8
MAZ [4150]	73	6	111	6	244	6	317	6
TBP [6908]	70	5	102	5	189	5	276	5
IRF1 [3659]	66	3	101	3	191	3	281	4
ATF3 [467]	63	6	93	6	215	6	336	11
GATA1 [2623]	54	3	102	3	214	3	367	4
RXRA [6256]	54	3	78	5	178	5	235	6
GATA2 [2624]	42	4	65	5	149	6	273	9
PAX5 [5079]	38	5	51	6	93	6	138	7
USF2 [7392]	38	5	64	6	206	6	313	6
IRF2 [3660]	34	2	53	2	88	2	112	2
MYB [4602]	33	3	55	3	87	3	106	3
NFIC [4782]	30	2	45	2	84	2	121	2
ELK1 [2002]	29	5	49	5	145	5	226	5
SRF [6722]	29	2	36	2	107	3	147	3
LEF1 [51176]	27	2	41	2	106	2	183	2
CEBPA [1050]	24	4	46	6	79	6	89	7
HNF4A [3172]	24	2	40	3	119	4	136	5
WT1 [7490]	23	1	36	1	76	1	110	1
NFATC1/T2 [4772]	16	2	18	2	34	2	42	2
MEF2A [4205]	13	2	17	2	39	2	59	2
ETS2 [2114]	9	2	10	2	28	2	63	2
AHR [196]	8	2	9	2	15	2	26	3
HNF1A [6927]	8	1	14	1	20	1	37	1
NFKB1 [4790]	2	1	2	1	8	1	34	2
STAT4 [6775]	2	1	2	1	4	1	12	1
VDR [7421]	2	1	12	3	17	4	23	4

Table 10: Highest scored predicted transcription factors
Common Transcription factor binding to the promoter of ATP2B4 obtained from published ChiP-seq data and found in Promo V3 and Hocomoco are shown. Scores are calculated based on the probability of binding to a sequence of 500, 1000, 5000 and 10000 nucleotides long from the starting transcription site (TSS) in the ATP2B4 gene. The number of cell types in which each transcription scored are shown as well.

6 Discussion

Activation of T cells by second messenger Ca^{2+} is an indispensable step for T cells expand clonally and to mount a robust effector response against pathogens during the primary immune challenge. As result of the primary immune response, an array of memory T cells with specific effector functions and stronger potential to mount a second immune response to cognate antigen are generated. The amplitude and dynamic of Ca^{2+} signals in T cells dictate how these signals are integrated and transduced to produce functional diversity and immune specificity among T cell subtypes. Among the mechanism controlling the amplitude and kinetic of SOCE, main entry Ca^{2+} pathway in T cells, are the plasma membrane Ca^{2+} ATPases, mitochondria, endoplasmic reticulum, Ca^{2+} buffers among others. In the current work, we investigated how Ca^{2+} signals are fine-tuned during activation of $CD4^+$ T cells to regulate the stoichiometry of $CD4^+$ T cell compartments and thus the outcome of an immune response.

6.1 Characterization of Ca^{2+} profiles of human T helper subtypes and their regulatory mechanisms

The first part of this work characterizes the Ca^{2+} profiles of human *in vitro* polarized T cells (Th1, Th2, Th17, regT) and *in vivo* sorted regT, as well as investigates possible mechanisms that may contribute to the differences in Ca^{2+} phenotypes among subtypes. Human T helper subtype isolation may be challenging due to their low frequency in human blood. Hence, *in vitro* polarization of T helper subtypes using naïve $CD4^+$ T cells allows to generate a big number of T helper subtypes for further studies. *In vitro* polarization of total $CD4^+$ T cells have been already established in our group by varying both the concentration of polarizing subtype specific cytokines and stimulation intensity of TCR and CD28 co-stimulatory molecule (Kircher et al., 2018). The fact that we could only differentiate Th17 cells using memory $CD4^+$ T cells but not naïve $CD4^+$ T cells (Figure 5c) agrees with published data (van Beelen et al., 2007). The decrease in regT along with the increase in Th17 cells using the lowest TGF-ß1 concentration (Figure 5d) can be explained by the synergic role of TFG-ß and IL-6 in promoting Th17 differentiation from murine naïve T cells, while inhibiting the generation of TGF-ß-induced regT (Bettelli et al., 2006). On the other hand, while murine naïve $CD4^+$ T cells own a stronger potential to develop into Th17 effector cells, generation of human Th17 seems to be restricted to a small subset of naïve $CD4^+$ T cells bearing the cell surface marker CD161 (Cosmi et al., 2008), which explains the lack of IL-17 producing cells when polarization into Th17 starting from naïve $CD4^+$ T cells was attempted. The generation of IL-17 producing cells was also dependent on low intensity stimulation (bead: cell ratio of 1:50), as also shown by other groups (Purvis et al., 2010).

T cell fate decisions greatly depend on the TCR stimulation intensity (antigen nature, antigen load and duration of the contact between APC and T cells), which explains the fact that control cells stimulated at different bead: cell ratio (bead cell ratio 1:10, 1:20 and 1:50) produce different cytokine patterns (Figure 5b). In fact, prolonged DC-naïve T cell contact was required for Th1 polarization and by increasing the antigen load, Th1 was favored over Th2 polarization (van Panhuys et al., 2014). On the other hand, brief

stimulation was sufficient to induce Th2 differentiation independently of the Th2 cell-polarizing adjuvants used (van Panhuys et al., 2014), which explains why stimulating control Th0 cells with a bead: cell ratio of 1:20 was enough to induce a Th2-cell-differentiation program (Figure 5b). On the other hand, it has been proposed that regT induced by weak agonist peptides do not persist compared with those generated using high affinity peptides (Gottschalk et al., 2010). Despite the specificity, only a fraction of the *in vitro* polarized cells produced the signature cytokines or transcription factor, which can be explained by findings of Helmstetter and colleagues. They showed that a stimulus may induce different cell decisions with only a percentage of cells producing the specific cytokine (Helmstetter et al., 2015).

As expected, the Ca^{2+} phenotypes of *in vitro* polarized T helper subtypes using naïve $CD4^+$ T cells resembled those observed among T helper subsets polarized from total $CD4^+$ T cells (Kircher et al., 2018). Possible mechanisms leading to differences among subtypes has been already explored (Kircher et al., 2018). Therefore, in the first part of this work we explored new mechanisms that may contribute to the differential SOCE phenotypes among subtypes, based mainly in new gene expression data. Along this line, Th17 cells showed a smaller Ca^{2+} plateau than other subtypes, except for Th1, which may be a result of increased expression of PMCA4 in Th17 and Th1 (Figure 7e and f) and in accordance with published data, Th1 and Th17 phenotypes showed little specie dependent differences (Weber et al., 2008). A higher Ca^{2+} peak and plateau in regT compared to Th1 (Figure 6d) may be explained due to increased expression of ATP2B4 along with decreased expression of TRPM2 in Th1 (Figure 7e and f). Decreased expression of ATP2B4 may enhance Ca^{2+} extrusion and decrease $[Ca^{2+}]_i$, whereas downregulation of TRPM2, a non-selective and Ca^{2+} permeable channel may contribute to the decrease in $[Ca^{2+}]_i$ following TCR activation. Although some TRPC channels were expressed in T cells (TRPC1, TRPC3, TRPC6) (Figure 7f), previous data for our group showed that neither the GsMTx4 blocker nor the Sr^{2+} cation (to which TRPC are more permeable than Orai1) unmasked a TRPC contribution (Kircher et al., 2018).

Interestingly, the Ca^{2+} phenotype of *in vivo* isolated regT resembled that of the *in vitro* differentiated regT. Unlike *in vitro* differentiated regT, a decreased expression of Orai2 (Figure 8f) may explain the differences in Ca^{2+} phenotypes between regT and Tcon. Indeed, our group have previously shown that downregulating Orai2 in Jurkat T cells enhanced SOCE (Alansary et al., 2015), and naïve $CD4^+$ T cells isolated from Orai2$^{-/-}$ showed increased SOCE (Vaeth et al., 2017). A decrease in Orai2 may favor the coupling of more STIM molecules to Orai1, which possess a faster EF-hand unfolding kinetic and thus responds faster to increasing $[Ca^{2+}]_i$. On the other hand, an unaltered plateau in regT versus Tcon can be explained by a higher ratio of memory T cells versus naïve T cells in regT than Tcon. Notably, ATP2B4 was not significant upregulated at mRNA levels in regT vs Tcon (Figure 9a), probably because Tcon are also composed for naïve and memory populations, masking the differences at mRNA level. On the other hand, mitochondria contribution to SOCE has been extensively studied (Hoth et al., 1997). Our results show a role of mitochondria in SOCE in both Tcon and regT. CCCP mediated mitochondrial depolarization equally affected the Ca^{2+} Plateau of both regT and Tcon, ruling out a differential role of mitochondria to SOCE.

Cluster analysis of our microarray data showed that Th0 and regT are more similar in their gene expression pattern than Th1 (Figure 7a and d), which coincided with a higher number of genes that are uniquely differentially expressed in Th1 (836) versus 360 genes uniquely differentially expressed in regT. The results

of the microarray data confirmed that the subtypes generated showed their correspondent cytokine profiling while non-specific transcriptional programs were turned off (Figure 7c). From the gene-ontology meta-analysis of genes involved in Ca^{2+} ion homeostasis, we could identify genes that are uniquely expressed in each subtype and thus play a unique role. Interestingly, we confirmed that *in vivo* regT, as *in vitro* differentiated regT, have decreased expression of the calcium voltage-gated channel auxiliary subunit alpha2delta 2 (CACNAD2D), protein tyrosine kinase 2 (PTK2) and TMEM63C. CACNAD2D encodes the auxiliary subunit α2δ2 voltage gated Ca^{2+} channels, the direct contribution of which to Ca^{2+} signaling in T-cells is controversial, therefore unraveling the role of this subunit in regT may contribute to a better understanding of the role of voltage gated Ca^{2+} channels in T cells. PTK2 also known as FAK (focal adhesion kinase) is a cytoplasmic non-receptor mediated tyrosine kinase that acts as a kinase mediating integrin-dependent tyrosine phosphorylation. The kinase activity of FAK leads to signaling via PI3K/Akt and MAPK pathways and inhibits apoptosis (Mierke, 2013). Pharmacological inhibition of tyrosine kinases was recently shown to reduce total regT populations while leading to accumulation of naïve regT, thus introducing potential therapies for immune diseases such as graft-versus-host disease (Marinelli Busilacchi et al., 2018). On the other hand, TMEM-63 is a member of the transmembrane TMEM63 protein family representing possible candidates for osmoreceptor transduction channel (Zhao et al., 2016). Information concerning the function of this protein in $CD4^+$ cells or regT is completely lacking.

Further studies are needed to unravel the role of these candidates in the generation of subtype specific Ca^{2+} responses and to better understand the fine tuning mechanisms leading to differential Ca^{2+} phenotypes and responses among T helper subtypes.

Taking into account that control stimulated naïve Th0 and memory Th0 showed distinct SOCE phenotypes and that ATP2B4 was higher expressed in memory Th0 and Th17, the latter being polarized using memory $CD4^+$ T cells, we proceed to investigate whether unstimulated cells like Th0 have the same differences.

6.2 Differential expression of PMCA4b results in distinct SOCE profiles in naïve and memory $CD4^+$ T cells

Analysis of Ca^{2+} signals after Tg-induced SOCE in naïve and memory sorted T cells (Figure 10b), revealed a differential SOCE phenotype in both populations. Resting memory T cells not only showed a tendency to lower basal $[Ca^{2+}]_i$ (Figure 10c) but also accommodate less $[Ca^{2+}]_i$ as a result of a faster Ca^{2+} clearance mechanism, leading to significantly lower $[Ca^{2+}]_i$ plateau than in naïve T cells (Figure 10b and c). Taking into account the Ca^{2+} dependence modulation of PMCA function, a more rigorous analysis was performed. By fitting a single exponential decay to the decline of $[Ca^{2+}]_i$ of the iso-cells (cells with similar $[Ca^{2+}]_i$ peak or plateau), either after maximal CRAC channel activation (Figure 10d) or following Ca^{2+}_0 removal (Figure 10e), we confirmed that the rate constants of the decay in $[Ca^{2+}]_i$ were higher in memory than naïve T cells. This means that memory T cells independent of $[Ca^{2+}]_i$ are able to clear faster cytosolic Ca^{2+} than naïve T cells. Unaltered expression of SOCE components (Figure 11a-c) along with a dominant expression of PMCA4 over others PMCA isoforms not only in total $CD4^+$ T cells (Figure 11d), but also in sorted memory T cells (Figure 11f and h-i), indicate that the differences in the SOCE phenotypes are due to differences in

extrusion mechanisms and not to differences in the amount of incoming Ca^{2+} through CRAC channels. The differences in SOCE peak between naïve and memory T cells can be explained by the homeostatic role of PMCA maintaining low resting levels of intracellular Ca^{2+} and for the higher availability of transport sites in memory T cells (Bautista et al., 2002), that even though when PMCA is slowly modulated during maximum Ca^{2+} entry can favor the extrusion of Ca^{2+} resulting in a mild decrease in the SOCE peak.

Moreover, using primers specific for variants ATP2B4a and ATP2B4b, we demonstrated that PMCA4b is the main variant in total CD4$^+$ cells, whereas ATP2B4a is absent (Figure 11e). In line with these results, splice specific analysis in sorted naïve and memory T cells showed that the higher ATP2B4 expression in sorted memory T cells (Figure 11f) is due to ATP2B4b, because ATP2B4a was almost undetectable in sorted naïve and memory T cells (Figure 11g).

These results confirm that PMCA4b is the main isoform expressed in T cells, with a more dominant role in $[Ca^{2+}]_i$ clearance in memory than in naïve T cells.

6.3 Pharmacological inhibition or downregulation of PMCA reverses SOCE phenotypes of memory CD4$^+$ T cells

While two Ca^{2+} extrusion mechanisms operate in lymphocytes, the PMCA and the Na^+-Ca^{2+} exchanger (Balasubramanyam et al., 1993; Gardner & Balasubramanyam, 1996), other publications have shown that PMCA is the sole mechanism for Ca^{2+} clearance when SERCA and mitochondria are inhibited excluding a significant role of the Na^+-Ca^{2+} exchanger on Ca^{2+} Clearance (Bautista et al., 2002; Donnadieu et al., 1992; Donnadieu & Trautmann, 1993). In order to answer whether the increased expression of PMCA4b in memory T cells is responsible for faster $[Ca^{2+}]_i$ clearance rates after Tg-induced SOCE, we used either the allosteric inhibitor of PMCAs, Caloxin1C2 (C1C2) or we knockdown PMCA4 expression by using a PMCA4 specific siRNA. The advantage of using C1C2 over other PMCA inhibitors is its greater affinity (20 times higher affinity for PMCA4 than that of caloxin-1b1) and isoform selectivity (10 fold higher affinity for PMCA4 than for PMCA1, 2 or 3). Therefore, we decided to use 5 µM and 20 µM C1C2, due to their relative closeness to the published inhibition constants (ki) values for PMCA4 and PMCA1 in erythrocyte ghosts (Pande et al., 2011). While the SOCE phenotype in naïve T cells was not affected by inhibition of the pump activity with either C1C2 concentration (Figure 12a), the plateau in memory cells increased significantly, with the highest C1C2 concentration having a more significant effect on the decay rate compared to control memory (Figure 12b and c). Interestingly, treating memory cells with C1C2 reverted the differences in SOCE peak observed in control conditions (compare the peak values of $[Ca^{2+}]_i$ in control naïve and memory vs memory cells treated with 5 µM and 20 µM C1C2 (Figure 12c)). Therefore, we confirmed that the differences on SOCE peak between naïve and memory T cells (also seen in Figure 10b) are indeed due to differential expression of PMCA. Although effects of both C1C2 concentrations were comparable on the plateau $[Ca^{2+}]_i$ in memory T cells, only 20 µM showed significant differences versus memory control on plateau/peak fraction. Taking into account that the higher concentration blocks more than 50% of the PMCA4 pump activity (published ki for PMCA4=2.3 µM ± 0.3) and only 50% of PMCA1 pump activity (published ki for PMCA1 (21 uM ± 6) (Pande et al., 2011), we hypothesize that the significant

differences seen with 20 μM may be in part due to inhibition of PMCA4 rather than PMCA1 inhibition. Taking into account that both C1C2 concentrations affected the plateau of memory T cells to the same extent (Figure 12b and c), we conclude that PMCA4 is the main isoform responsible for Ca^{2+} extrusion during SOCE in memory T cells, whereas it plays a less important role in resting naïve T cells. In a second approach, we downregulated PMCA4 using a siRNA targeting *ATP2B4* (Figure 13d and e). The effective reduction of the ATP2B4 mRNA levels after ATP2B4-siRNA in both naïve and memory cells together with the absence of compensatory effects on ATP2B1 levels product of ATP2B4 knockdown confirmed the efficacy of the siRNA. On the other hand, the small decrease in ATP2B1 expression levels along with the functional results using C1C2 excluded possible redundancy. Again, the differences in SOCE peak between naïve and memory T cells in control conditions were reverted by ATP2B4 knockdown (Figure 13a and b), confirming that the differences in peak are due to differential expression of PMCA4. Downregulation of ATP2B4 affected only the fraction plateau/peak in memory T cells (Figure 13b) and the fast and slow phases of $[Ca^{2+}]_i$ clearance in memory T cells (Figure 13c), whereas naïve T cells remained unaffected. Interestingly, in memory T cells the effect on the slow phase was greater than that on the fast phase, probably due to secondary mechanisms influencing the slow phase of decay such as mitochondria. Mitochondrial Ca^{2+} uptake in conditions of ATP2B4 downregulation might be increased compared to control conditions, releasing it when $[Ca^{2+}]_i$ falls below 0.4 μM, therefore retarding the slow phase of Ca^{2+} clearance (Bautista et al., 2002; Hoth et al., 1997). These results strongly confirm the importance of PMCA4 as the main mechanism for Ca^{2+} extrusion in CD4^{+} T cells and the responsible for the differences in SOCE phenotypes between naïve and memory T cells.

6.4   PMCA4 regulates the compartment stoichiometry of the CD4^{+} T cells

The findings that PMCA4 plays a differential role in antigen-experienced T cells or memory T cells compared to naïve T cells, which have not been exposed to cognate-p-MHCII, led us to hypothesize that PMCA4 expression levels upon stimulation of naïve CD4^{+} T-cells with anti-CD3/CD28 coated beads could regulate the time course and generation of specific CD4^{+} subsets. While CD45RA and CD45RO are surface markers characteristics for naïve and memory respectively (Deans et al., 1989), T cells can be also classified using the differentiation markers CD62L and CCR7 as naïve (CD45RO^{-}CD62L^{+}CCR7^{+}); effector (CD45RO^{-}CD62L^{-}CCR7^{-}), central memory (CD45RO^{+}CD62L^{+}CCR7^{+}) and effector memory (CD45RO^{+}CD62L^{-}CCR7^{-}) (Sallusto et al., 1999). CD62L (ligand for L-selectin) and CCR7 (CC chemokine receptor) are constitutively co-expressed on naïve CD4^{+} T cells and are lost after TCR engagement, with a different time dependence though (Figure 15d). These differences might be explained by the different half-live expression of both molecules following activation, which guarantees a stepwise activation of downstream molecules needed for lymphocytes entry and retention into the LN. First, L-selectin mediates the tethering and rolling of naïve lymphocytes in HEVs of LN and it is cleaved from the cell surface within minutes after cellular activation by cis-acting cell surface proteases (Griffin et al., 1990; Zhao et al., 2001).This explains the rapid shedding detected as early as 4 hours after activation (Figure 15d). Subsequently, extravasation into the LN starts with the binding of chemokine CCL21 to its counter-receptor CCR7 (a G protein-coupled receptor), which triggers an intracellular signaling cascade ending in the activation of LFA1 integrin, firm arrest of lymphocytes and extravasation into the LN (Campbell et al.,

1998; Zarbock et al., 2012). This multistep fashion mechanism might explain the differences in kinetic observed between CCR7 and CD62L, with the former being lost form the surface at latter times followed activation (Figure 15d). In fact, the transition from naïve T-cells into effector memory (EM) T-cells implies L-selectin shedding, as well as transcriptional inhibition of the L-selectin gene, which mobilizes the EM cells from secondary lymphoid organs toward peripheral tissues, while CM once out of the lymph nodes are able to re-express CD62L and CCR7 allowing them the immune surveillance of peripheral lymph nodes (Galkina et al., 2003; Ivetic et al., 2019). In our *in vitro* stimulation model, activation of naïve cells after downregulation of ATP2B4 resulted in a decrease in the fraction of activated cells in the effector cell compartment (Figure 14b and c). In addition we observed a decrease in the percentage of cells in the EM compartment and an increase in the central memory compartment though to a lesser degree (Figure 14b and c). It is known that both, circulating naïve and CM T cells express high levels of CD62L, which allows trafficking to lymph nodes, while the effector and effector memory do not need CD62L and they are mainly trafficking to peripheral tissue (Ahmed et al., 2009). A possible explanation for the altered stoichiometry of cells under siRNA conditions could be that PMCA4 may regulate directly or indirectly the expression of CD62L. It is known that CaM binds to the cytoplasmic tail of L-selectin in resting lymphocytes inhibiting the shedding of CD62L and thereby protecting the extracellular domains from photolytic cleavage. After activation, it is believed that CaM induces a conformational change in the extracellular domains of L-selectin that expose the cleavage site resistant to proteolysis (Ivetic et al., 2019). It is not clear whether CaM binding to the L-selectin tail is a calcium dependent or independent process, with experiments supporting both views (Killock et al., 2009; Matala et al., 2001). Although our results indicate that CD62L is rapidly lost following activation (Figure 14c and Figure 15d), a sustained increase in $[Ca^{2+}]_i$ as result of ATP2B4 knockdown significantly reduced the fraction of cells lacking CD62L compared to control, indicating a Ca^{2+} independent mechanism.

Analysis of the expression pattern of CCR7 in the compartments after 24 hours of stimulation revealed that most of the cells remained CCR7 positive with just a few of them also positive for CD45RO (Figure 15a and d). Interestingly, the fraction of cells developing memory phenotype within 24 hours of activation remained CD45RA positive (Figure 15b) indicating that these cells are in an intermediate state of memory development, which is reached at later time points of stimulation (Figure 15d) (Birkeland et al., 1989; Deans et al., 1989). Therefore, analysis using either CD62L or CCR7 will result in different patterns of compartment stoichiometry depending on the stimulation duration, and both can be employed in order to follow the dynamic of the differentiation.

Activation of the TCR complex happens within seconds and results in the subsequent activation of gene transcription programs responsible for regulation of the cell cycle, proliferation and commitment to different T helper lineages. This process is accompanied by *de novo* protein synthesis and their insertion to the cell surface, which is a pre-requisite for signaling and lymphocyte trafficking (mobilization). In this regard, we were interested in knowing if changes in compartment distribution after PMCA knockdown are preceded by early changes during the activation process. Analysis of early activation markers such as CD69 and CD40L (CD154) are indicators of the activation stage of T cells following TCR engagement. While no changes in CD69, the earliest activation marker (Cosulich et al., 1987; Reddy et al., 2004) were detected, CD40L was significantly upregulated in naïve cells treated with ATP2B4-siRNA versus control following

24 hours of stimulation (Figure 14d and e). The differences observed can be explained by different mechanisms of regulation. CD69 is rapidly upregulated after TCR engagement at mRNA (within 30 min of activation, reaching a peak of expression to 60 min) (Ziegler et al., 1994), while protein level are detected after 2 hours (Cosulich et al., 1987), remaining elevated 24 hours and declining thereafter (Reddy et al., 2004). Due to the fact that CD69 activation and expression are regulated by the Ca^{2+} dependent activation of PKC, but not on Ca^{2+} alone (Testi et al., 1989), it is possible that an elevated $[Ca^{2+}]_i$ due to PMCA4 knockdown exceeds the threshold for PKC activation and consequent regulation of CD69 expression levels. On the other hand, CD40L mRNA expression reach a maximum after 1 to 2 h after T cell activation, and protein expression at the cell surface peaks within 4 to 6 hours, its transcription is controlled by $[Ca^{2+}]_i$ through Ca^{2+}/CaM-NFAT mediated activation and with the cooperation of activating protein 1 (AP-1) (Fuleihan et al., 1994). Thereby, a rise in $[Ca^{2+}]_i$ upon ATP2B4 downregulation might explain the increase in CD40L following stimulation. Furthermore, increased CD40L expression has been shown in patients with systemic lupus erythematosus (SLE), which has been correlated with supranormal cytoplasmic Ca^{2+} fluxes in circulating T and B cells (Liossis et al., 1998; Liossis et al., 1996). Another study revealed that rheumatoid arthritis patients have more than 10% of CD4^{+}CD40L^{+} T cells which correlated with a more active disease. (Berner et al., 2000; MacDonald et al., 1997). Thereby, tight regulation of PMCA may be essential for maintaining the immune balance. It is known that high-dose antigen or strength of TCR stimulation *in vitro* induces higher Ca^{2+} influx and CD40 upregulation on T cells, favoring Th1 polarization while blockade of CD40-CD40L interactions, as well as low dose antigen favors Th2 polarization (Ruedl et al., 2000). Therefore, CD40-CD40L interactions dictate the fate of T helper subtypes upon physiological conditions and during more pro-inflammatory conditions where aberrant CD40L expression has been detected. Therefore these results suggest a main role of PMCA4 controlling the fate of T cells through fine tuning of $[Ca^{2+}]_i$.

Last but not least, analysis of CD25 expression, which is upregulated within 24 hours and remains elevated for a few days (Laurence et al., 2007) reveled that more than the half of the cells were able to upregulate the CD25 molecule at 24 hours of stimulation, with no differences in the number of CD25^{+} cells transfected with ATP2B4-siRNA versus control (Figure 15c), meaning that cells were equally able to entry the cell cycle and proliferate.

6.5 Differential expression of PMCA4 in *in vivo* differentiated CD4^{+} compartments re-capitulates *in vitro* phenotypes and results in distinct SOCE profiles

The role of PMCA in the generation of different compartments in our *in vitro* model of CD4^{+} T cell compartment generation, prompted us to think that analysis of *in vivo* differentiated compartments not only may re-capitulate the observed phenotypes *in vitro* but also could give new insights about the role of PMCA4 during T cell differentiation. Next, we sorted CD4^{+} compartments out of PMBC as shown in (Figure 16a). Importantly, while sorting we realized that in just few donors (~8%) a negative population for CD45RO and CCR7 was found. This population showed a frequency that varied between donors from 0 to 3% of the CD4^{+} T cells, whereas this population was up to 13% of the CD4^{+} T cells in only one donor. A post sorting analysis of the compartments revealed that the scarce population was CD45RA positive, an existing memory

population known as EMRA, while EM and CM CD4^{+} T cell populations remained CD45RA negative as seen by others (Figure 16b) (Amyes et al., 2005; Roetynck et al., 2013). The EMRA population is defined as memory T cells that re-express the CD45RA markers (Amyes et al., 2005; Libri et al., 2011), which is gradually lost during the differentiation of naïve T cells to memory (Akbar et al., 1988; Deans et al., 1989). Highly differentiated populations EMRA-like CD4^{+} T cells have been shown to accumulate in older adults (Dunne et al., 2002; Libri et al., 2011), patients with persistent viral infections (Akbar & Fletcher, 2005; Appay et al., 2002) and those with inflammatory syndromes such as rheumatoid arthritis (Goronzy & Weyand, 2005) which explain the low frequency we observed. The expression levels of *INFG* mRNA in the sorted CD4^{+} compartments confirmed that the sorted populations are also functionally different. While *INFG* mRNA was lacking in naïve T cells, the effector population showed a strong increase in *INFG* followed by CM population (Figure 16c). Interestingly, and in line with our previous results, PMCA4 was differentially expressed within the memory compartments, with an increase in the order CM, EM, EMRA whereas naïve T cells showed the lowest PMCA4 expression as expected (Figure 16d-f). Next, analysis of Tg-induced SOCE phenotypes revealed a main role of PMCA4 controlling SOCE in CD4^{+} compartments, which correlated with their differential expression of PMCA4 (Figure 17a). While the EMRA and EM showed the lowest plateau and plateau/peak ratio among all subtypes (Figure 17a and b), CM T cells showed a more naïve-like SOCE phenotype with lower plateau/peak ratio (Figure 17a and b), which make them significant different to the effector populations and closer to the naïve ones. Analysis of the decline in $[Ca^{2+}]_i$ of iso-cells at relative equal $[Ca^{2+}]_i$ peak (Figure 17c) or $[Ca^{2+}]_i$ plateau (Figure 17d) confirmed our results and showed significant differences in the rate constants among subtypes. These results strongly support the role of PMCA4 in decisions of lineage commitment in an immune response. In addition, our data shed lights on the controversial memory generation theories. It has been proposed that memory T cells are generated after antigen recognition either by asymmetric cell division independently but parallel to the generation of effector cells (Bifurcative or Disparate Model) (Arsenio et al., 2014) or sequentially from effector cells (linear differentiation model) (Ahmed & Gray, 1996; Kaech et al., 2002). In line with the latter model, the finding that CM cells showed a naïve-like SOCE phenotype which correlated with an intermediate level of PMCA4 suggests that the theory of a linear differentiation model where CM T cells give rise to EM T cells and the latter to terminal differentiated or EMRA T cells may explain better the differences in PMCA expression among compartments. In fact, we saw that sorted EM T cells stimulated *in vitro* with anti-CD3/CD28 coated beads for different times were more resistant to changes in phenotypes than sorted CM T cells (data not shown) and published results (Sallusto et al., 1999). Furthermore, from Dureck and colleagues studies, sorted CD4^{+} compartments showed not only loss of partially methylated domains in the order naïve, CM, EM and EMRA but also analysis of changes in their transcriptomes grouped the samples along a progressive naïve-CM-EM-EMRA cell differentiation axis; thereby suggesting that the linear model of memory generation is the most likely one (Durek et al., 2016).

6.6 Mitochondrial contribution to Ca^{2+} homeostasis depends on the cellular compartment and activation state of CD4$^+$ T cells

It has been proposed that PMCA is the main mechanism for Ca^{2+} clearance in T cells when SERCA and mitochondria are inhibited (Bautista et al., 2002). In this line, Quintana and colleagues have shown that the sustained signaling required for efficient T cell activation is achieved by bringing in close proximity mitochondria and ORAI channels and by reorganizing PMCA close to mitochondria at the plasma membrane upon immune synapse formation. This re-distribution supports mitochondrial Ca^{2+} uptake, thus guarding against accumulation of Ca^{2+} in microdomains close to Orai channels, thereby preventing Ca^{2+}-dependent channel inactivation and reducing local Ca^{2+} dependent modulation of PMCA. This complex formation allows mitochondria to shuttle Ca^{2+} away from the plasma membrane deep into the cytosol enhancing activation of Ca^{2+} dependent transcription factors such as NFAT and thereby T cell activation (Quintana et al., 2011; Quintana et al., 2007). On the other hand, besides energy production in the form of ATP, mitochondria are important regulators of T cell metabolism and they have emerged as a signaling platform that coordinates T cell fate decisions involved in T cell activation and differentiation (Bantug et al., 2018). Although the role of mitochondria regulating SOCE upon immune synapse formation have been extensively studied (Demaurex et al., 2009; Hoth et al., 1997; Parekh, 2008; Quintana et al., 2011), its role in modulation of SOCE during T cell differentiation is much less understood. Therefore, we wanted to evaluate the role of mitochondria on SOCE in naïve and memory CD4$^+$ lymphocytes upon resting and activation conditions. While blocking mitochondrial Ca^{2+} uptake in naïve cells expressing low levels of PMCA4 (Figure 18a and b), induced immediate ORAI channels inactivation due to [Ca^{2+}]$_i$ accumulation as shown by others (Hoth et al., 1997; Zweifach & Lewis, 1995), resting memory T cells were initially more resistant to Orai channel inactivation but unable to sustained [Ca^{2+}]$_i$ signals (Figure 18c and d) likely due to the lower transport capacity of PMCA that cannot fully prevent Ca^{2+} dependent inactivation of the channel (Brini et al., 2013) and saturates to such as low [Ca^{2+}]$_i$ of 0.4 µM (Bautista et al., 2002). A sustained Ca^{2+} signal is needed for NFAT translocations and IL-2 production (Oh-hora & Rao, 2009; Quintana et al., 2011) and for signaling pathways downstream to TCR leading to synthesis of cytokines and biomolecules, as well as for supporting mitochondrial functions (Angajala et al., 2018; Gunter et al., 1994; Satrustegui et al., 2007) and is therefore essential for the differentiation of the highly proliferative T cells. Our findings indicate that to maintain sustained Ca^{2+} levels, TCR induced-activation leads to rapid downregulation of PMCA (Figure 18e and Figure 20e) to decrease Ca^{2+} efflux. In this regard, activation-induced downregulation of PMCA in activated naïve T cells or proliferating T blast induced a significant rise in [Ca^{2+}]$_i$ upon CCCP treatment (Figure 18e and f) and a more prominent decay than in control activated, which together with the higher mitochondrial mass and higher differences in mitochondrial potential versus control (Figure 19a-d) highlight the importance of mitochondria over PMCA during proliferation of blast T cells. Conversely, memory T cells after prolonged activation still have more PMCA levels than the activated naïve and less than the resting memory (Figure 20e). Due to mitochondria takes a larger amount of Ca^{2+} after immune synapse formation than after TG stimulation (Quintana et al., 2007), thereby prolonging Ca^{2+} influx and reducing the size of Ca^{2+} microdomains that inhibits Ca^{2+} dependent up-modulation of PMCA (Quintana et al., 2011; Quintana et al., 2007); activated memory T cells are now able to sustain Ca^{2+} signals better (Figure 18h) than the resting memory (Figure 18c), while CCCP-induced depolarization of mitochondria membrane in activated memory T cells restored PMCA modulation as seen by significant differences in the ratio

plateau/peak (Figure 18i). Interestingly, analysis of $[Ca^{2+}]_i$ extrusion rate in cells with similar $[Ca^{2+}]_i$ plateau after Ca^{2+}_0 removal revealed new insights. While the $[Ca^{2+}]_i$ decay in naïve T cells following activation is characterized for 2 phases (Figure 18g); inhibition of mitochondria in the almost absence of PMCA changed the time course of Ca^{2+} clearance to only one phase decay (Figure 18g). This might be explained by the differential contribution of mitochondria to different phases of Ca^{2+} clearance. In activated naïve (DMSO control) mitochondria probably accelerates the first phase of Ca^{2+} clearance by taking Ca^{2+} up when $[Ca^{2+}]_i$ rise (tau1=29 s) and retards the second phase of Ca^{2+} clearance by releasing it when $[Ca^{2+}]_i$ falls below 400 nM (tau2=349 s) (Bautista et al., 2002). This 2 phase decay mechanism changed to only one phase decay (tau=74) when mitochondria function was impaired in activated naïve T cells (Figure 18g) likely due to the absence of mitochondrial contribution to Ca^{2+} clearance that induced immediate Ca^{2+} accumulation upon conditions where PMCA4 was extremely reduced (Figure 20e) and the only mechanism for Ca^{2+} clearance in the absence of functional SERCA and mitochondria. Indeed, upon these conditions the time constant value of Ca^{2+} clearance was between the fast and slow time constant values measured under control conditions, which indicates that mitochondria changed the time recovery to a single exponential decay.

On the other hand, upon activation of memory T cells we were still able to detect 2 phases of clearance upon CCCP treatment (Figure 18j) due to Ca^{2+} clearance is mainly performed by PMCA (Figure 20e) in the absence of mitochondria and SERCA (Bautista et al., 2002). The 40% increase in tau1 along with 52% decrease in tau2 in activated memory treated with CCCP compared to activated memory control might again be explained by the mitochondrial contribution to both phases of Ca^{2+} clearance. Upon these conditions the slowdown of the faster phase of Ca^{2+} clearance can be explained due to the absence of mitochondrial Ca^{2+} uptake, while the slow phase is accelerated compared to memory control cells likely due to up-modulation of PMCA induced by Ca^{2+} accumulation during the first phase.

Interestingly, CCCP treatment in activated naïve T cells is not accompanied by Orai channel inactivation as in resting cells (Figure 18e). We reason this finding to the mitochondrial sodium-calcium-exchanger (NCX) acting in reverse mode upon CCCP, transporting Ca^{2+} into the matrix in exchange of Na^+ ions (Samanta et al., 2018). In this regard, the reverse mode was shown to operate only when mitofusin 2 was downregulated in depolarized mitochondria. Interestingly, activated T cells have been shown to have low levels of mitofusin (Dasgupta et al., 2015) and fissed mitochondria, whereas fussed mitochondria directs memory differentiation maintaining the cells in a quiescent state (Buck et al., 2016). This data highlights the importance of different mechanisms acting together in order to regulate SOCE during the establishment of an immune response. Besides stand out the solely role of mitochondria in naïve T cells and the indisputable contribution of PMCA during homeostasis and commitment to more differentiated T cells stages.

6.7 Transcriptional control of PMCA4 results in biphasic expression following activation

The differences in the expression pattern of PMCA4 among compartments, as well as the tight regulation of PMCA expression during activation, prompted us to examine possible transcriptional mechanisms regulating PMCA4. Using a combination of transcription factor databases, we scored common transcription factors in all databases able to bind to 500, 1000, 5000 and 10000 nucleotide-long sequences upstream to

the start codon of the ATP2B4 gene (Figure 20a and Table 10). Interestingly, YY1 came out with the highest score (Table 10). YY1 is a Zn finger transcription factor that can act as activator or repressor or an initiator binding protein (Krippner-Heidenreich et al., 2005). Moreover, YY1 is associated with the polycomb group (PcG) of protein complexes, important maintaining genes in a repressed state to sustain T cell fate (Otte & Kwaks, 2003). Next, ChIP assays confirmed the binding of YY1 to the ATP2B4 promoter sequence (Figure 20b). Analysis of the kinetics of PMCA4 and YY1 expression in sorted naïve and memory T cells (Figure 20e) revealed that: first YY1 is not differentially expressed in naïve and memory resting T cells (Figure 20e and g) and second that both PMCA4 and YY1 expression pattern are altered during the time course of activation in different patterns (Figure 20e and h), as also seen on total CD4$^+$ cells (Figure 20c and d). Importantly, stimulation of naïve CD4$^+$ T cells for up to 168 hours (7 days) inversed the expression level of PMCA4 and YY1 expression (Figure 20f and h). This effect was further enhanced by adding Th1 or regulatory T cell (regT) specific polarizing cytokines (Figure 21a-c), which also reduced YY1 levels in Th0 and Th1 and to a lesser extent in regT (Figure 21a and c). The finding that both Th0 cells and stimulated naïve T cells for 7 days also showed increased PMCA4 expression along with reduced YY1 expression raise the possibility that under conditions of high strong TCR signaling either by increased bead:cell ratio or prolonged TCR stimulation, T cells may become polarized even in the absence of cytokines. In this line, T-bet expression have been shown to be induced upon strong TCR signaling strength in naïve CD4$^+$ T cells in the absence of cytokines (Placek et al., 2009). Furthermore, overexposure bands together with analysis of YY1 mRNA levels, confirm that indeed YY1 downregulation is induced by protein degradation and not by transcriptional regulation in terminally differentiated Th1, regT and in Th0 (Figure 21a and d). We reason these findings to the fact that YY1 upregulation is needed to represses PMCA4 expression during activation and once the cells are committed to a certain T helper lineage, YY1 is target to degradation which allows PMCA4 upregulation and re-stablishing basal [Ca^{2+}]$_i$ levels, thereby preventing apoptosis and cell death. In fact, Smurf-2, an E3 Ubiquitin ligase, ubiquitinates YY1 and targets it to the proteosome for degradation, which suppress cell proliferation and c-Myc expression (Jeong et al., 2014; Ramkumar et al., 2013). In addition, YY1 protein levels were increased in lymphomas derived from smurf-2 knockout mice, but in contrast the transcripts were largely unchanged (Ramkumar et al., 2013). Other studies have also shown that YY1 binds to the promoter of c-Myc in ChIP assays and this binding is enough to upregulate c-Myc expression (Hsu et al., 2008; Ramkumar et al., 2013; Riggs et al., 1993). Importantly, c-Myc has been shown to bind to the PMCA4 promoter (Habib et al., 2007; Zeller et al., 2006) and c-Myc rescued B cell differentiation in the absence of pre-BCR formation by decreasing PMCA4 expression and Ca^{2+} efflux in purified B cells from Eμ-myc mice (a transgenic mouse model which express c-Myc exclusively in B lineage cells throughout development); whereas PMCA4 was increased in sorted pro-B cells deficient in both N- and c-Myc genes, both variants expressed in B-Lymphocytes (Habib et al., 2007). On the other hand, YY1 have also been shown to be target of caspases which may explain the double band detected upon long term activation of naïve and upon polarizing conditions (Krippner-Heidenreich et al., 2005). Therefore, these results are consistent with a mechanism in which YY1 upregulation-induced TCR controls c-Myc and PMCA4 expression guaranteeing proper activation and differentiation while avoiding improper immune response.

7   Conclusion and outlook

In the first part of this work we establish new conditions for the polarization of *in vitro* polarized human T helper subtypes and showed that the Ca^{2+} phenotypes of human *in vitro* polarized T helper subtypes are distinct, as it has have been previously shown in our group using similar protocols (Kircher et al., 2018) Besides, we proposed mechanisms that may differentially control Ca^{2+} signals among Th0, Th1 and regT based on gene expression data. On the other hand, we demonstrated that *in vivo* polarized regulatory T cells, as the *in vitro* polarized regulatory T cells, showed increased Ca^{2+} signals after Tg-induced store operated Ca^{2+} entry, which may be in part due to decreased expression of Orai2 in regulatory T cells versus conventional T cells. Importantly, Th0 and T17 memory T cells that were originated from memory $CD4^+$ T cells, showed increased expression of ATP2B4 compared to other subtypes, which led us to hypothesize that PMCAs play important roles in $CD4^+$ T cell fate decisions. Thus, the next step was intended to study the role of PMCAs on $CD4^+$ T cell fate decisions and compartment stoichiometry.

Our findings that PMCA4 is differentially expressed within the $CD4^+$ compartments, which correlated with its ability to regulate distinct the course and amplitude of SOCE in both resting and activated T cells, highlight a main role of PMCA4 in final T cell fate decisions. Although the role of PMCA shaping SOCE in T cells has been previously studied (Bautista et al., 2002; Quintana et al., 2011), our data indicates a more complex level of regulation, in which the T cells are able to adapt their levels of PMCA4 in accordance with the stage of differentiation and their needs during the course of the immune response. In this line, we showed that naïve T cells expressed low levels of PMCA4 and PMCA4 levels are further reduced during TCR activation, allowing prolonged Ca^{2+} signals important for NFAT nuclear retention and therefore clonal expansion and synthesis of effector molecules. Indeed, it is known that sustained TCR signaling is required to initiate effector function (Goldsmith & Weiss, 1988) and earlier disruption of p-MHC:TCR interactions yielded greater impairment of cytokine secretion (Valitutti et al., 1995) and memory formation. On the other hand, memory T cells are epigenetically different to naïve T cells; they show demethylation at the loci of several important effector molecules like IL-4 and IFN-γ and express higher NFAT protein levels than the counterpart naïve ones, all together allow them to mount a faster effector response within minutes (Dienz et al., 2007; Rogers et al., 2000). Therefore, just an initial burst of TCR in memory T cells may be enough to respond to low affinity p-MHC:TCR binding, which may induce Ca^{2+} transients rather than sustained Ca^{2+} signals. On the other hand, strong p-MHC:TCR can lead to prolonged TCR contact and sustained Ca^{2+} signals amplifying the accumulation of intracellular calcium (Rosette et al., 2001; Wulfing et al., 1997). In accordance with this, we have seen that prolonged and strong stimulation of both naïve and memory T cells induced downregulation of PMCA4 leading to prolonged Ca^{2+} signals which may preserve Ca^{2+} for intracellular processes.

Interestingly, naïve, CM, EM and EMRA cells have different patterns of PMCA4 expression, which allow them to mount different responses upon antigenic stimulation, thereby inducing different effector responses. It has been suggested that CM may need weaker TCR stimuli for their generation, whereas stronger antigenic stimuli may induce EM (Lanzavecchia & Sallusto, 2002). In this line, regulation of the magnitude and

duration of Ca^{2+} signals by PMCA4 may activate specific signaling pathways during antigen-driven responses and influence memory fate decisions.

Interestingly, while PMCA4 does not play a main role in Ca^{2+} clearance in naïve T cells, it is clear that naïve T cells are able to clear intracellular Ca^{2+} through mitochondrial Ca^{2+} uptake, which may preserve most of the calcium coming inside the cells for signaling and ATP generation to support the high energy demand of the proliferating lymphoblast.

Last but not least, our data shed lights about a possible role of YY1 on ATP2B4 promoter repression during activation of naïve T cells. We hypothesize that increased YY1 levels early during activation may induce PMCA4 downregulation to allow sustained Ca^{2+} signals required for proper activation of effector T cells. This repressive effect may revert after programing of lymphoblast under polarizing cytokine conditions leading to memory differentiation, which induces YY1 downregulation and releases its repressive effect on PMCA4 expression.

Further experiments such as a Luciferase Reporter Assay in which the PMCA4 promoter is cloned upstream the luciferase gene can help us to establish a functional connection between the presence of YY1 and the transcriptional activity of genes under the ATP2B4 promoter and therefore new insights about how YY1 dependent-modulation of PMCA4 regulates memory decisions during T cell activation.

8 Abbreviations

ADPR: ADP-ribose

AHR: Aryl hydrocarbon receptor

AHR: Hydrocarbon receptor

AICD: activation induced cell death

AP-1: Activating protein 1

APC: Antigen presenting cells

ATP: Adenosine triphosphate

BCL-2: B cell lymphoma 2

BCL-6: B cell lymphoma-6

Ca^{2+}: Ionized cytoplasmic calcium II

cADPR: Cylic ADP-ribose

CaM: Calmodulin

CaM-BD: Calmodulin binding domain

CaN: Calcineurin

CCL19: CC-chemokine ligand 19

CCL21: CC-chemokine ligand 21

CCL25: Chemokine ligand 25

CCR7: C-C chemokine receptor type 7

CCR9: C-C chemokine receptor type 9

CD25: Interleukin-2 receptor alpha chain

CD40L: Ligand for CD40

CD62L: L-selectin

CLP: Common lymphoid progenitor

CM: Central memory

CMP: Common myeloid progenitor

c-Myc: Myelocytomatosis oncogene transcription factor

CRAC: calcium release-activated Ca^{2+}

CREB: cyclic AMP-responsive element-binding protein

CsA: Cyclosporine A

CXCR3: Chemokine C-X-C motif receptor 3

DAG: Diacylglycerol

DCs: Dendritic cells

DN: Double negative

DP: Double positive

EM: Effector memory

EMRA/TE: Effector memory CD45RA positive/ terminal effector

ER: Endoplasmic reticulum

ETP: Early thymic progenitor

Abbreviations

Gal-1: Galectin-1

GATA: GATA binding protein

Glut1: Glucose transporter type 1

H2O2: Hydrogen peroxide

HEV: High endothelial venule

HK2: Hexokinase 2

HLA-DR: Human leukocyte antigen-DR isotype

HSCs: Hematopoietic stem cells

IFN-α/β: Interferon-alpha/beta

IFN-γ: Interferon-γ

Ig: Immunoglobulin

IL: Interleukin

IL-2Rα or CD25: Interleukin-2 receptor alpha chain

IL-7rα: Interleukin-7 receptor α or CD127

InsP3 or IP3: Inositol 1,4,5-trisphosphate or inositol trisphosphate

InsP3R: Inositol 1,4,5-trisphosphate receptor or Inositol trisphosphate receptor

iRegT: Induced regulatory T cells

IS: Immune synapse

LCMV: Lymphocytic choriomeningitis virus

LN: Lymph nodes

MAPKs: Mitogen-associated protein kinases

MEF2: Myocyte enhancer factor 2

mRNA: Messenger ribonucleic acid

mTEC: Medullary thymic epithelial cell

mTORc1: Mammalian target of rapamycin complex 1

NCLX: Na^{2+}/Ca^{2+} exchanger

NFAT: Nuclear factor of activated T cells

NF-kB: kappa-light-chain-enhancer of activated B cells

NLS: Nuclear localization sequence

nNOS: Nitric oxide synthase

NO: Nitric oxide

NPTN or Np: Neuroplastine

OXPHOS: Oxidative phosphorylation

PI3K: Phosphoinositide 3-kinase

PKC: Protein kinase C

PKD: Protein kinase D

PKM2: Pyruvate kinase muscle isozyme M2

PLC-γ: Phospholipase Cγ

PMCA: Plasma membrane Ca^{2+} ATPase

p-MHC: Peptide-MHC

PtdIns(3,4,5)P3 or PIP3: Phosphatidylinositol (3,4,5)-trisphosphate

Abbreviations

PtdIns-4,5-P2 or PIP2: Phosphatidylinositol-4,5-bisphosphate

RA: Rheumatoid arthritis

Rag1: Recombination activating gene 1

Rag2: Recombination activating gene 2

reg T: Regulatory T cells

ROR-$\gamma\tau$: Acid receptor-related orphan nuclear receptor $\gamma\tau$

ROS: Reactive oxygen species

S1PR: Sphingosine 1-phosphate receptor

SERCA: Sarco-endoplasmic reticulum Ca^{2+}-ATPases

SLE: Systemic lupus erythematous

SLN: Secondary lymph nodes

SLO: Secondary lymphoid organs

SOCE: Store operated Ca^{2+} entry

SP: Single positive

STAT: Signal transducer and activator of transcription

STIM: Stromal interaction molecule

TCR: T cell receptor complex

TEC: Thymic epithelial cell

Tfh: T follicular helper cells

TG: Thapsigargin

TGF-β: Transforming growth factor-β

Th: T helper

TNF-α: Tumor necrosis factor-α

YY1: Yin Yang 1

ZAP-70: Protein kinase of 70 kDa

9 References

Abraham, R. T., & Weiss, A. (2004). Jurkat T cells and development of the T-cell receptor signalling paradigm. *Nat Rev Immunol, 4*(4), 301-308. doi:10.1038/nri1330

Acuto, O., & Michel, F. (2003). CD28-mediated co-stimulation: a quantitative support for TCR signalling. *Nat Rev Immunol, 3*(12), 939-951. doi:10.1038/nri1248

Afroze, T., & Husain, M. (2000). c-Myb-binding sites mediate G(1)/S-associated repression of the plasma membrane Ca(2+)-ATPase-1 promoter. *J Biol Chem, 275*(12), 9062-9069. doi:10.1074/jbc.275.12.9062

Afroze, T., Yang, G., Khoshbin, A., Tanwir, M., Tabish, T., Momen, A., & Husain, M. (2014). Calcium efflux activity of plasma membrane Ca2+ ATPase-4 (PMCA4) mediates cell cycle progression in vascular smooth muscle cells. *J Biol Chem, 289*(10), 7221-7231. doi:10.1074/jbc.M113.533638

Ahmed, R., Bevan, M. J., Reiner, S. L., & Fearon, D. T. (2009). The precursors of memory: models and controversies. *Nat Rev Immunol, 9*(9), 662-668. doi:10.1038/nri2619

Ahmed, R., & Gray, D. (1996). Immunological memory and protective immunity: understanding their relation. *Science, 272*(5258), 54-60. doi:10.1126/science.272.5258.54

Ahsan, S., & Draghici, S. (2017). Identifying Significantly Impacted Pathways and Putative Mechanisms with iPathwayGuide. *Curr Protoc Bioinformatics, 57*, 7 15 11-17 15 30. doi:10.1002/cpbi.24

Akashi, K., Traver, D., Miyamoto, T., & Weissman, I. L. (2000). A clonogenic common myeloid progenitor that gives rise to all myeloid lineages. *Nature, 404*(6774), 193-197. doi:10.1038/35004599

Akbar, A. N., & Fletcher, J. M. (2005). Memory T cell homeostasis and senescence during aging. *Curr Opin Immunol, 17*(5), 480-485. doi:10.1016/j.coi.2005.07.019

Akbar, A. N., Terry, L., Timms, A., Beverley, P. C., & Janossy, G. (1988). Loss of CD45R and gain of UCHL1 reactivity is a feature of primed T cells. *J Immunol, 140*(7), 2171-2178.

Alansary, D., Bogeski, I., & Niemeyer, B. A. (2015). Facilitation of Orai3 targeting and store-operated function by Orai1. *Biochim Biophys Acta, 1853*(7), 1541-1550. doi:10.1016/j.bbamcr.2015.03.007

Alexa, A., Rahnenfuhrer, J., & Lengauer, T. (2006). Improved scoring of functional groups from gene expression data by decorrelating GO graph structure. *Bioinformatics, 22*(13), 1600-1607. doi:10.1093/bioinformatics/btl140

Ambrosini, G., Dreos, R., Kumar, S., & Bucher, P. (2016). The ChIP-Seq tools and web server: a resource for analyzing ChIP-seq and other types of genomic data. *BMC Genomics, 17*(1), 938. doi:10.1186/s12864-016-3288-8

Amezcua Vesely, M. C., Pallis, P., Bielecki, P., Low, J. S., Zhao, J., Harman, C. C. D., . . . Flavell, R. A. (2019). Effector TH17 Cells Give Rise to Long-Lived TRM Cells that Are Essential for an Immediate Response against Bacterial Infection. *Cell, 178*(5), 1176-1188 e1115. doi:10.1016/j.cell.2019.07.032

Amyes, E., McMichael, A. J., & Callan, M. F. (2005). Human CD4+ T cells are predominantly distributed among six phenotypically and functionally distinct subsets. *J Immunol, 175*(9), 5765-5773. doi:10.4049/jimmunol.175.9.5765

Anderson, G., & Takahama, Y. (2012). Thymic epithelial cells: working class heroes for T cell development and repertoire selection. *Trends Immunol, 33*(6), 256-263. doi:10.1016/j.it.2012.03.005

Angajala, A., Lim, S., Phillips, J. B., Kim, J. H., Yates, C., You, Z., & Tan, M. (2018). Diverse Roles of Mitochondria in Immune Responses: Novel Insights Into Immuno-Metabolism. *Front Immunol, 9*, 1605. doi:10.3389/fimmu.2018.01605

Anuradha, R., George, P. J., Hanna, L. E., Chandrasekaran, V., Kumaran, P., Nutman, T. B., & Babu, S. (2013). IL-4-, TGF-beta-, and IL-1-dependent expansion of parasite antigen-specific Th9 cells is associated with clinical pathology in human lymphatic filariasis. *J Immunol, 191*(5), 2466-2473. doi:10.4049/jimmunol.1300911

References

Appay, V., Dunbar, P. R., Callan, M., Klenerman, P., Gillespie, G. M., Papagno, L., . . . Rowland-Jones, S. L. (2002). Memory CD8+ T cells vary in differentiation phenotype in different persistent virus infections. *Nat Med, 8*(4), 379-385. doi:10.1038/nm0402-379

Armesilla, A. L., Williams, J. C., Buch, M. H., Pickard, A., Emerson, M., Cartwright, E. J., . . . Neyses, L. (2004). Novel functional interaction between the plasma membrane Ca2+ pump 4b and the proapoptotic tumor suppressor Ras-associated factor 1 (RASSF1). *J Biol Chem, 279*(30), 31318-31328. doi:10.1074/jbc.M307557200

Arsenio, J., Kakaradov, B., Metz, P. J., Kim, S. H., Yeo, G. W., & Chang, J. T. (2014). Early specification of CD8+ T lymphocyte fates during adaptive immunity revealed by single-cell gene-expression analyses. *Nat Immunol, 15*(4), 365-372. doi:10.1038/ni.2842

Artyomov, M. N., Lis, M., Devadas, S., Davis, M. M., & Chakraborty, A. K. (2010). CD4 and CD8 binding to MHC molecules primarily acts to enhance Lck delivery. *Proc Natl Acad Sci U S A, 107*(39), 16916-16921. doi:10.1073/pnas.1010568107

Atchison, L., Ghias, A., Wilkinson, F., Bonini, N., & Atchison, M. L. (2003). Transcription factor YY1 functions as a PcG protein in vivo. *EMBO J, 22*(6), 1347-1358. doi:10.1093/emboj/cdg124

Attali, B., Romey, G., Honore, E., Schmid-Alliana, A., Mattei, M. G., Lesage, F., . . . Lazdunski, M. (1992). Cloning, functional expression, and regulation of two K+ channels in human T lymphocytes. *J Biol Chem, 267*(12), 8650-8657.

Badou, A., Jha, M. K., Matza, D., Mehal, W. Z., Freichel, M., Flockerzi, V., & Flavell, R. A. (2006). Critical role for the beta regulatory subunits of Cav channels in T lymphocyte function. *Proc Natl Acad Sci U S A, 103*(42), 15529-15534. doi:10.1073/pnas.0607262103

Baggott, R. R., Alfranca, A., Lopez-Maderuelo, D., Mohamed, T. M., Escolano, A., Oller, J., . . . Armesilla, A. L. (2014). Plasma membrane calcium ATPase isoform 4 inhibits vascular endothelial growth factor-mediated angiogenesis through interaction with calcineurin. *Arterioscler Thromb Vasc Biol, 34*(10), 2310-2320. doi:10.1161/ATVBAHA.114.304363

Baixauli, F., Acin-Perez, R., Villarroya-Beltri, C., Mazzeo, C., Nunez-Andrade, N., Gabande-Rodriguez, E., . . . Mittelbrunn, M. (2015). Mitochondrial Respiration Controls Lysosomal Function during Inflammatory T Cell Responses. *Cell Metab, 22*(3), 485-498. doi:10.1016/j.cmet.2015.07.020

Bajnok, A., Ivanova, M., Rigo, J., Jr., & Toldi, G. (2017). The Distribution of Activation Markers and Selectins on Peripheral T Lymphocytes in Preeclampsia. *Mediators Inflamm, 2017*, 8045161. doi:10.1155/2017/8045161

Balasubramanyam, M., Kimura, M., Aviv, A., & Gardner, J. P. (1993). Kinetics of calcium transport across the lymphocyte plasma membrane. *Am J Physiol, 265*(2 Pt 1), C321-327. doi:10.1152/ajpcell.1993.265.2.C321

Bankovich, A. J., Shiow, L. R., & Cyster, J. G. (2010). CD69 suppresses sphingosine 1-phosophate receptor-1 (S1P1) function through interaction with membrane helix 4. *J Biol Chem, 285*(29), 22328-22337. doi:10.1074/jbc.M110.123299

Bantug, G. R., Galluzzi, L., Kroemer, G., & Hess, C. (2018). The spectrum of T cell metabolism in health and disease. *Nat Rev Immunol, 18*(1), 19-34. doi:10.1038/nri.2017.99

Bautista, D. M., Hoth, M., & Lewis, R. S. (2002). Enhancement of calcium signalling dynamics and stability by delayed modulation of the plasma-membrane calcium-ATPase in human T cells. *J Physiol, 541*(Pt 3), 877-894. doi:10.1113/jphysiol.2001.016154

Bautista, D. M., & Lewis, R. S. (2004). Modulation of plasma membrane calcium-ATPase activity by local calcium microdomains near CRAC channels in human T cells. *J Physiol, 556*(Pt 3), 805-817. doi:10.1113/jphysiol.2003.060004

Bautista, J. L., Lio, C. W., Lathrop, S. K., Forbush, K., Liang, Y., Luo, J., . . . Hsieh, C. S. (2009). Intraclonal competition limits the fate determination of regulatory T cells in the thymus. *Nat Immunol, 10*(6), 610-617. doi:10.1038/ni.1739

Beals, C. R., Sheridan, C. M., Turck, C. W., Gardner, P., & Crabtree, G. R. (1997). Nuclear export of NF-ATc enhanced by glycogen synthase kinase-3. *Science, 275*(5308), 1930-1934. doi:10.1126/science.275.5308.1930

References

Beeton, C., Wulff, H., Standifer, N. E., Azam, P., Mullen, K. M., Pennington, M. W., . . . Chandy, K. G. (2006). Kv1.3 channels are a therapeutic target for T cell-mediated autoimmune diseases. *Proc Natl Acad Sci U S A, 103*(46), 17414-17419. doi:10.1073/pnas.0605136103

Bending, D., De la Pena, H., Veldhoen, M., Phillips, J. M., Uyttenhove, C., Stockinger, B., & Cooke, A. (2009). Highly purified Th17 cells from BDC2.5NOD mice convert into Th1-like cells in NOD/SCID recipient mice. *J Clin Invest, 119*(3), 565-572. doi:10.1172/JCI37865

Berner, B., Wolf, G., Hummel, K. M., Muller, G. A., & Reuss-Borst, M. A. (2000). Increased expression of CD40 ligand (CD154) on CD4+ T cells as a marker of disease activity in rheumatoid arthritis. *Ann Rheum Dis, 59*(3), 190-195. doi:10.1136/ard.59.3.190

Berridge, M. J., & Dupont, G. (1994). Spatial and temporal signalling by calcium. *Curr Opin Cell Biol, 6*(2), 267-274. doi:10.1016/0955-0674(94)90146-5

Bettelli, E., Carrier, Y., Gao, W., Korn, T., Strom, T. B., Oukka, M., . . . Kuchroo, V. K. (2006). Reciprocal developmental pathways for the generation of pathogenic effector TH17 and regulatory T cells. *Nature, 441*(7090), 235-238. doi:10.1038/nature04753

Bevington, S. L., Cauchy, P., Withers, D. R., Lane, P. J., & Cockerill, P. N. (2017). T Cell Receptor and Cytokine Signaling Can Function at Different Stages to Establish and Maintain Transcriptional Memory and Enable T Helper Cell Differentiation. *Front Immunol, 8*, 204. doi:10.3389/fimmu.2017.00204

Beyersdorf, N., Kerkau, T., & Hunig, T. (2015). CD28 co-stimulation in T-cell homeostasis: a recent perspective. *Immunotargets Ther, 4*, 111-122. doi:10.2147/ITT.S61647

Biedermann, T., Rocken, M., & Carballido, J. M. (2004). TH1 and TH2 lymphocyte development and regulation of TH cell-mediated immune responses of the skin. *J Investig Dermatol Symp Proc, 9*(1), 5-14. doi:10.1111/j.1087-0024.2004.00829.x

Birkeland, M. L., Johnson, P., Trowbridge, I. S., & Pure, E. (1989). Changes in CD45 isoform expression accompany antigen-induced murine T-cell activation. *Proc Natl Acad Sci U S A, 86*(17), 6734-6738. doi:10.1073/pnas.86.17.6734

Blattman, J. N., Antia, R., Sourdive, D. J., Wang, X., Kaech, S. M., Murali-Krishna, K., . . . Ahmed, R. (2002). Estimating the precursor frequency of naive antigen-specific CD8 T cells. *J Exp Med, 195*(5), 657-664. doi:10.1084/jem.20001021

Boczek, T., Lisek, M., Ferenc, B., & Zylinska, L. (2017). Cross talk among PMCA, calcineurin and NFAT transcription factors in control of calmodulin gene expression in differentiating PC12 cells. *Biochim Biophys Acta Gene Regul Mech, 1860*(4), 502-515. doi:10.1016/j.bbagrm.2017.01.012

Bohm, J., Chevessier, F., Maues De Paula, A., Koch, C., Attarian, S., Feger, C., . . . Laporte, J. (2013). Constitutive activation of the calcium sensor STIM1 causes tubular-aggregate myopathy. *Am J Hum Genet, 92*(2), 271-278. doi:10.1016/j.ajhg.2012.12.007

Boyman, O., Letourneau, S., Krieg, C., & Sprent, J. (2009). Homeostatic proliferation and survival of naive and memory T cells. *Eur J Immunol, 39*(8), 2088-2094. doi:10.1002/eji.200939444

Bradley, L. M., Duncan, D. D., Yoshimoto, K., & Swain, S. L. (1993). Memory effectors: a potent, IL-4-secreting helper T cell population that develops in vivo after restimulation with antigen. *J Immunol, 150*(8 Pt 1), 3119-3130.

Brandman, O., Liou, J., Park, W. S., & Meyer, T. (2007). STIM2 is a feedback regulator that stabilizes basal cytosolic and endoplasmic reticulum Ca2+ levels. *Cell, 131*(7), 1327-1339. doi:10.1016/j.cell.2007.11.039

Brenchley, J. M., Karandikar, N. J., Betts, M. R., Ambrozak, D. R., Hill, B. J., Crotty, L. E., . . . Koup, R. A. (2003). Expression of CD57 defines replicative senescence and antigen-induced apoptotic death of CD8+ T cells. *Blood, 101*(7), 2711-2720. doi:10.1182/blood-2002-07-2103

Brini, M., Cali, T., Ottolini, D., & Carafoli, E. (2013). The plasma membrane calcium pump in health and disease. *FEBS J, 280*(21), 5385-5397. doi:10.1111/febs.12193

Brini, M., Di Leva, F., Ortega, C. K., Domi, T., Ottolini, D., Leonardi, E., . . . Carafoli, E. (2010). Deletions and mutations in the acidic lipid-binding region of the plasma membrane Ca2+ pump: a study on

different splicing variants of isoform 2. *J Biol Chem, 285*(40), 30779-30791. doi:10.1074/jbc.M110.140475

Brodin, P., Falchetto, R., Vorherr, T., & Carafoli, E. (1992). Identification of two domains which mediate the binding of activating phospholipids to the plasma-membrane Ca2+ pump. *Eur J Biochem, 204*(2), 939-946. doi:10.1111/j.1432-1033.1992.tb16715.x

Bryant, V. L., Ma, C. S., Avery, D. T., Li, Y., Good, K. L., Corcoran, L. M., . . . Tangye, S. G. (2007). Cytokine-mediated regulation of human B cell differentiation into Ig-secreting cells: predominant role of IL-21 produced by CXCR5+ T follicular helper cells. *J Immunol, 179*(12), 8180-8190. doi:10.4049/jimmunol.179.12.8180

Buch, M. H., Pickard, A., Rodriguez, A., Gillies, S., Maass, A. H., Emerson, M., . . . Armesilla, A. L. (2005). The sarcolemmal calcium pump inhibits the calcineurin/nuclear factor of activated T-cell pathway via interaction with the calcineurin A catalytic subunit. *J Biol Chem, 280*(33), 29479-29487. doi:10.1074/jbc.M501326200

Buck, M. D., O'Sullivan, D., Klein Geltink, R. I., Curtis, J. D., Chang, C. H., Sanin, D. E., . . . Pearce, E. L. (2016). Mitochondrial Dynamics Controls T Cell Fate through Metabolic Programming. *Cell, 166*(1), 63-76. doi:10.1016/j.cell.2016.05.035

Buckler, K. J., & Turner, P. J. (2015). Functional Properties of Mitochondria in the Type-1 Cell and Their Role in Oxygen Sensing. *Adv Exp Med Biol, 860*, 69-80. doi:10.1007/978-3-319-18440-1_9

Butcher, E. C., & Picker, L. J. (1996). Lymphocyte homing and homeostasis. *Science, 272*(5258), 60-66. doi:10.1126/science.272.5258.60

Cahalan, M. D., & Chandy, K. G. (2009). The functional network of ion channels in T lymphocytes. *Immunol Rev, 231*(1), 59-87. doi:10.1111/j.1600-065X.2009.00816.x

Campbell, J. J., Hedrick, J., Zlotnik, A., Siani, M. A., Thompson, D. A., & Butcher, E. C. (1998). Chemokines and the arrest of lymphocytes rolling under flow conditions. *Science, 279*(5349), 381-384. doi:10.1126/science.279.5349.381

Cano R, L., & Lopera H, D. (2013). Introduction to T and B lymphocytes. In J. Manuel Anaya, Y. Shoenfeld, A. Rojas-Villarraga, R. Levy, & R. Cervera (Eds.), *AUTOIMMUNITY From Bench to Bedside* (Vol. 15, pp. 77-95). Colombia: El Rosario University Press.

Carafoli, E. (1994). Biogenesis: plasma membrane calcium ATPase: 15 years of work on the purified enzyme. *FASEB J, 8*(13), 993-1002.

Carafoli, E., Kessler, F., Falchetto, R., Heim, R., Quadroni, M., Krebs, J., . . . Vorherr, T. (1992). The molecular basis of the modulation of the plasma membrane calcium pump by calmodulin. *Ann N Y Acad Sci, 671*, 58-68; discussion 68-59. doi:10.1111/j.1749-6632.1992.tb43784.x

Caride, A. J., Penheiter, A. R., Filoteo, A. G., Bajzer, Z., Enyedi, A., & Penniston, J. T. (2001). The plasma membrane calcium pump displays memory of past calcium spikes. Differences between isoforms 2b and 4b. *J Biol Chem, 276*(43), 39797-39804. doi:10.1074/jbc.M104380200

Carpenter, A. C., & Bosselut, R. (2010). Decision checkpoints in the thymus. *Nat Immunol, 11*(8), 666-673. doi:10.1038/ni.1887

Cedeno-Laurent, F., Opperman, M., Barthel, S. R., Kuchroo, V. K., & Dimitroff, C. J. (2012). Galectin-1 triggers an immunoregulatory signature in Th cells functionally defined by IL-10 expression. *J Immunol, 188*(7), 3127-3137. doi:10.4049/jimmunol.1103433

Celli, S., Lemaitre, F., & Bousso, P. (2007). Real-time manipulation of T cell-dendritic cell interactions in vivo reveals the importance of prolonged contacts for CD4+ T cell activation. *Immunity, 27*(4), 625-634. doi:10.1016/j.immuni.2007.08.018

Chami, M., Ferrari, D., Nicotera, P., Paterlini-Brechot, P., & Rizzuto, R. (2003). Caspase-dependent alterations of Ca2+ signaling in the induction of apoptosis by hepatitis B virus X protein. *J Biol Chem, 278*(34), 31745-31755. doi:10.1074/jbc.M304202200

Champagne, D. P., Hatle, K. M., Fortner, K. A., D'Alessandro, A., Thornton, T. M., Yang, R., . . . Rincon, M. (2016). Fine-Tuning of CD8(+) T Cell Mitochondrial Metabolism by the Respiratory Chain Repressor MCJ Dictates Protection to Influenza Virus. *Immunity, 44*(6), 1299-1311. doi:10.1016/j.immuni.2016.02.018

References

Chang, C. H., Curtis, J. D., Maggi, L. B., Jr., Faubert, B., Villarino, A. V., O'Sullivan, D., . . . Pearce, E. L. (2013). Posttranscriptional control of T cell effector function by aerobic glycolysis. *Cell, 153*(6), 1239-1251. doi:10.1016/j.cell.2013.05.016

Chang, J. T., Palanivel, V. R., Kinjyo, I., Schambach, F., Intlekofer, A. M., Banerjee, A., . . . Reiner, S. L. (2007). Asymmetric T lymphocyte division in the initiation of adaptive immune responses. *Science, 315*(5819), 1687-1691. doi:10.1126/science.1139393

Chi, H. (2012). Regulation and function of mTOR signalling in T cell fate decisions. *Nat Rev Immunol, 12*(5), 325-338. doi:10.1038/nri3198

Choi, Y. S., Yang, J. A., Yusuf, I., Johnston, R. J., Greenbaum, J., Peters, B., & Crotty, S. (2013). Bcl6 expressing follicular helper CD4 T cells are fate committed early and have the capacity to form memory. *J Immunol, 190*(8), 4014-4026. doi:10.4049/jimmunol.1202963

Chu, H. H., Moon, J. J., Kruse, A. C., Pepper, M., & Jenkins, M. K. (2010). Negative selection and peptide chemistry determine the size of naive foreign peptide-MHC class II-specific CD4+ T cell populations. *J Immunol, 185*(8), 4705-4713. doi:10.4049/jimmunol.1002276

Cibrian, D., Saiz, M. L., de la Fuente, H., Sanchez-Diaz, R., Moreno-Gonzalo, O., Jorge, I., . . . Sanchez-Madrid, F. (2016). CD69 controls the uptake of L-tryptophan through LAT1-CD98 and AhR-dependent secretion of IL-22 in psoriasis. *Nat Immunol, 17*(8), 985-996. doi:10.1038/ni.3504

Cogliati, S., Enriquez, J. A., & Scorrano, L. (2016). Mitochondrial Cristae: Where Beauty Meets Functionality. *Trends Biochem Sci, 41*(3), 261-273. doi:10.1016/j.tibs.2016.01.001

Colegrove, S. L., Albrecht, M. A., & Friel, D. D. (2000). Dissection of mitochondrial Ca2+ uptake and release fluxes in situ after depolarization-evoked [Ca2+](i) elevations in sympathetic neurons. *J Gen Physiol, 115*(3), 351-370. doi:10.1085/jgp.115.3.351

Cosmi, L., De Palma, R., Santarlasci, V., Maggi, L., Capone, M., Frosali, F., . . . Annunziato, F. (2008). Human interleukin 17-producing cells originate from a CD161+CD4+ T cell precursor. *J Exp Med, 205*(8), 1903-1916. doi:10.1084/jem.20080397

Cosulich, M. E., Rubartelli, A., Risso, A., Cozzolino, F., & Bargellesi, A. (1987). Functional characterization of an antigen involved in an early step of T-cell activation. *Proc Natl Acad Sci U S A, 84*(12), 4205-4209. doi:10.1073/pnas.84.12.4205

Crabtree, G. R., & Olson, E. N. (2002). NFAT signaling: choreographing the social lives of cells. *Cell, 109 Suppl*, S67-79. doi:10.1016/s0092-8674(02)00699-2

Crompton, J. G., Sukumar, M., Roychoudhuri, R., Clever, D., Gros, A., Eil, R. L., . . . Restifo, N. P. (2015). Akt inhibition enhances expansion of potent tumor-specific lymphocytes with memory cell characteristics. *Cancer Res, 75*(2), 296-305. doi:10.1158/0008-5472.CAN-14-2277

D'Ambrosio, D., Cantrell, D. A., Frati, L., Santoni, A., & Testi, R. (1994). Involvement of p21ras activation in T cell CD69 expression. *Eur J Immunol, 24*(3), 616-620. doi:10.1002/eji.1830240319

Dang, C. V., Le, A., & Gao, P. (2009). MYC-induced cancer cell energy metabolism and therapeutic opportunities. *Clin Cancer Res, 15*(21), 6479-6483. doi:10.1158/1078-0432.CCR-09-0889

Dasgupta, A., Chen, K. H., Munk, R. B., Sasaki, C. Y., Curtis, J., Longo, D. L., & Ghosh, P. (2015). Mechanism of Activation-Induced Downregulation of Mitofusin 2 in Human Peripheral Blood T Cells. *J Immunol, 195*(12), 5780-5786. doi:10.4049/jimmunol.1501023

de la Fuente, H., Cruz-Adalia, A., Martinez Del Hoyo, G., Cibrian-Vera, D., Bonay, P., Perez-Hernandez, D., . . . Sanchez-Madrid, F. (2014). The leukocyte activation receptor CD69 controls T cell differentiation through its interaction with galectin-1. *Mol Cell Biol, 34*(13), 2479-2487. doi:10.1128/MCB.00348-14

Dean, W. L., Chen, D., Brandt, P. C., & Vanaman, T. C. (1997). Regulation of platelet plasma membrane Ca2+-ATPase by cAMP-dependent and tyrosine phosphorylation. *J Biol Chem, 272*(24), 15113-15119. doi:10.1074/jbc.272.24.15113

Deans, J. P., Boyd, A. W., & Pilarski, L. M. (1989). Transitions from high to low molecular weight isoforms of CD45 (T200) involve rapid activation of alternate mRNA splicing and slow turnover of surface CD45R. *J Immunol, 143*(4), 1233-1238.

References

Deans, J. P., Shaw, J., Pearse, M. J., & Pilarski, L. M. (1989). CD45R as a primary signal transducer stimulating IL-2 and IL-2R mRNA synthesis by CD3-4-8- thymocytes. *J Immunol, 143*(8), 2425-2430.

DeHaven, W. I., Smyth, J. T., Boyles, R. R., & Putney, J. W., Jr. (2007). Calcium inhibition and calcium potentiation of Orai1, Orai2, and Orai3 calcium release-activated calcium channels. *J Biol Chem, 282*(24), 17548-17556. doi:10.1074/jbc.M611374200

Deknuydt, F., Bioley, G., Valmori, D., & Ayyoub, M. (2009). IL-1beta and IL-2 convert human Treg into T(H)17 cells. *Clin Immunol, 131*(2), 298-307. doi:10.1016/j.clim.2008.12.008

Demaurex, N., Poburko, D., & Frieden, M. (2009). Regulation of plasma membrane calcium fluxes by mitochondria. *Biochim Biophys Acta, 1787*(11), 1383-1394. doi:10.1016/j.bbabio.2008.12.012

Desai-Mehta, A., Lu, L., Ramsey-Goldman, R., & Datta, S. K. (1996). Hyperexpression of CD40 ligand by B and T cells in human lupus and its role in pathogenic autoantibody production. *J Clin Invest, 97*(9), 2063-2073. doi:10.1172/JCI118643

Desdin-Mico, G., Soto-Heredero, G., & Mittelbrunn, M. (2018). Mitochondrial activity in T cells. *Mitochondrion, 41*, 51-57. doi:10.1016/j.mito.2017.10.006

Di, A., Gao, X. P., Qian, F., Kawamura, T., Han, J., Hecquet, C., . . . Malik, A. B. (2011). The redox-sensitive cation channel TRPM2 modulates phagocyte ROS production and inflammation. *Nat Immunol, 13*(1), 29-34. doi:10.1038/ni.2171

Di Leva, F., Domi, T., Fedrizzi, L., Lim, D., & Carafoli, E. (2008). The plasma membrane Ca2+ ATPase of animal cells: structure, function and regulation. *Arch Biochem Biophys, 476*(1), 65-74. doi:10.1016/j.abb.2008.02.026

Di Mitri, D., Azevedo, R. I., Henson, S. M., Libri, V., Riddell, N. E., Macaulay, R., . . . Akbar, A. N. (2011). Reversible senescence in human CD4+CD45RA+CD27- memory T cells. *J Immunol, 187*(5), 2093-2100. doi:10.4049/jimmunol.1100978

Dienz, O., Eaton, S. M., Krahl, T. J., Diehl, S., Charland, C., Dodge, J., . . . Rincon, M. (2007). Accumulation of NFAT mediates IL-2 expression in memory, but not naive, CD4+ T cells. *Proc Natl Acad Sci U S A, 104*(17), 7175-7180. doi:10.1073/pnas.0610442104

Doetze, A., Satoguina, J., Burchard, G., Rau, T., Loliger, C., Fleischer, B., & Hoerauf, A. (2000). Antigen-specific cellular hyporesponsiveness in a chronic human helminth infection is mediated by T(h)3/T(r)1-type cytokines IL-10 and transforming growth factor-beta but not by a T(h)1 to T(h)2 shift. *Int Immunol, 12*(5), 623-630. doi:10.1093/intimm/12.5.623

Dolmetsch, R. E., & Lewis, R. S. (1994). Signaling between intracellular Ca2+ stores and depletion-activated Ca2+ channels generates [Ca2+]i oscillations in T lymphocytes. *J Gen Physiol, 103*(3), 365-388. doi:10.1085/jgp.103.3.365

Dolmetsch, R. E., Xu, K., & Lewis, R. S. (1998). Calcium oscillations increase the efficiency and specificity of gene expression. *Nature, 392*(6679), 933-936. doi:10.1038/31960

Donnadieu, E., Bismuth, G., & Trautmann, A. (1992). Calcium fluxes in T lymphocytes. *J Biol Chem, 267*(36), 25864-25872.

Donnadieu, E., & Trautmann, A. (1993). Is there a Na+/Ca2+ exchanger in macrophages and in lymphocytes? *Pflugers Arch, 424*(5-6), 448-455. doi:10.1007/BF00374907

Donohoe, M. E., Zhang, X., McGinnis, L., Biggers, J., Li, E., & Shi, Y. (1999). Targeted disruption of mouse Yin Yang 1 transcription factor results in peri-implantation lethality. *Mol Cell Biol, 19*(10), 7237-7244. doi:10.1128/mcb.19.10.7237

Dontje, W., Schotte, R., Cupedo, T., Nagasawa, M., Scheeren, F., Gimeno, R., . . . Blom, B. (2006). Delta-like1-induced Notch1 signaling regulates the human plasmacytoid dendritic cell versus T-cell lineage decision through control of GATA-3 and Spi-B. *Blood, 107*(6), 2446-2452. doi:10.1182/blood-2005-05-2090

Dooms, H., Wolslegel, K., Lin, P., & Abbas, A. K. (2007). Interleukin-2 enhances CD4+ T cell memory by promoting the generation of IL-7R alpha-expressing cells. *J Exp Med, 204*(3), 547-557. doi:10.1084/jem.20062381

References

Duchen, M. R., Verkhratsky, A., & Muallem, S. (2008). Mitochondria and calcium in health and disease. *Cell Calcium, 44*(1), 1-5. doi:10.1016/j.ceca.2008.02.001

Duhen, T., Geiger, R., Jarrossay, D., Lanzavecchia, A., & Sallusto, F. (2009). Production of interleukin 22 but not interleukin 17 by a subset of human skin-homing memory T cells. *Nat Immunol, 10*(8), 857-863. doi:10.1038/ni.1767

Dunne, P. J., Faint, J. M., Gudgeon, N. H., Fletcher, J. M., Plunkett, F. J., Soares, M. V., . . . Akbar, A. N. (2002). Epstein-Barr virus-specific CD8(+) T cells that re-express CD45RA are apoptosis-resistant memory cells that retain replicative potential. *Blood, 100*(3), 933-940. doi:10.1182/blood-2002-01-0160

Durek, P., Nordstrom, K., Gasparoni, G., Salhab, A., Kressler, C., de Almeida, M., . . . Polansky, J. K. (2016). Epigenomic Profiling of Human CD4(+) T Cells Supports a Linear Differentiation Model and Highlights Molecular Regulators of Memory Development. *Immunity, 45*(5), 1148-1161. doi:10.1016/j.immuni.2016.10.022

Ecker, C., Guo, L., Voicu, S., Gil-de-Gomez, L., Medvec, A., Cortina, L., . . . Riley, J. L. (2018). Differential Reliance on Lipid Metabolism as a Salvage Pathway Underlies Functional Differences of T Cell Subsets in Poor Nutrient Environments. *Cell Rep, 23*(3), 741-755. doi:10.1016/j.celrep.2018.03.084

Elgueta, R., Benson, M. J., de Vries, V. C., Wasiuk, A., Guo, Y., & Noelle, R. J. (2009). Molecular mechanism and function of CD40/CD40L engagement in the immune system. *Immunol Rev, 229*(1), 152-172. doi:10.1111/j.1600-065X.2009.00782.x

Endo, Y., Noguchi, S., Hara, Y., Hayashi, Y. K., Motomura, K., Miyatake, S., . . . Nishino, I. (2015). Dominant mutations in ORAI1 cause tubular aggregate myopathy with hypocalcemia via constitutive activation of store-operated Ca(2)(+) channels. *Hum Mol Genet, 24*(3), 637-648. doi:10.1093/hmg/ddu477

Enyedi, A., Flura, M., Sarkadi, B., Gardos, G., & Carafoli, E. (1987). The maximal velocity and the calcium affinity of the red cell calcium pump may be regulated independently. *J Biol Chem, 262*(13), 6425-6430.

Eyerich, S., Eyerich, K., Pennino, D., Carbone, T., Nasorri, F., Pallotta, S., . . . Cavani, A. (2009). Th22 cells represent a distinct human T cell subset involved in epidermal immunity and remodeling. *J Clin Invest, 119*(12), 3573-3585. doi:10.1172/JCI40202

Falchetto, R., Vorherr, T., Brunner, J., & Carafoli, E. (1991). The plasma membrane Ca2+ pump contains a site that interacts with its calmodulin-binding domain. *J Biol Chem, 266*(5), 2930-2936.

Fanger, C. M., Neben, A. L., & Cahalan, M. D. (2000). Differential Ca2+ influx, KCa channel activity, and Ca2+ clearance distinguish Th1 and Th2 lymphocytes. *J Immunol, 164*(3), 1153-1160. doi:10.4049/jimmunol.164.3.1153

Farber, D. L., Yudanin, N. A., & Restifo, N. P. (2014). Human memory T cells: generation, compartmentalization and homeostasis. *Nat Rev Immunol, 14*(1), 24-35. doi:10.1038/nri3567

Farre, D., Roset, R., Huerta, M., Adsuara, J. E., Rosello, L., Alba, M. M., & Messeguer, X. (2003). Identification of patterns in biological sequences at the ALGGEN server: PROMO and MALGEN. *Nucleic Acids Res, 31*(13), 3651-3653. doi:10.1093/nar/gkg605

Fazilleau, N., Eisenbraun, M. D., Malherbe, L., Ebright, J. N., Pogue-Caley, R. R., McHeyzer-Williams, L. J., & McHeyzer-Williams, M. G. (2007). Lymphoid reservoirs of antigen-specific memory T helper cells. *Nat Immunol, 8*(7), 753-761. doi:10.1038/ni1472

Feske, S. (2007). Calcium signalling in lymphocyte activation and disease. *Nat Rev Immunol, 7*(9), 690-702. doi:10.1038/nri2152

Feske, S. (2010). CRAC channelopathies. *Pflugers Arch, 460*(2), 417-435. doi:10.1007/s00424-009-0777-5

Feske, S., Prakriya, M., Rao, A., & Lewis, R. S. (2005). A severe defect in CRAC Ca2+ channel activation and altered K+ channel gating in T cells from immunodeficient patients. *J Exp Med, 202*(5), 651-662. doi:10.1084/jem.20050687

Feske, S., Skolnik, E. Y., & Prakriya, M. (2012). Ion channels and transporters in lymphocyte function and immunity. *Nat Rev Immunol, 12*(7), 532-547. doi:10.1038/nri3233

References

Fontenot, J. D., Gavin, M. A., & Rudensky, A. Y. (2003). Foxp3 programs the development and function of CD4+CD25+ regulatory T cells. *Nat Immunol, 4*(4), 330-336. doi:10.1038/ni904

Fornes, O., Castro-Mondragon, J. A., Khan, A., van der Lee, R., Zhang, X., Richmond, P. A., . . . Mathelier, A. (2020). JASPAR 2020: update of the open-access database of transcription factor binding profiles. *Nucleic Acids Res, 48*(D1), D87-D92. doi:10.1093/nar/gkz1001

Forster, R., Mattis, A. E., Kremmer, E., Wolf, E., Brem, G., & Lipp, M. (1996). A putative chemokine receptor, BLR1, directs B cell migration to defined lymphoid organs and specific anatomic compartments of the spleen. *Cell, 87*(6), 1037-1047. doi:10.1016/s0092-8674(00)81798-5

Frauwirth, K. A., Riley, J. L., Harris, M. H., Parry, R. V., Rathmell, J. C., Plas, D. R., . . . Thompson, C. B. (2002). The CD28 signaling pathway regulates glucose metabolism. *Immunity, 16*(6), 769-777. doi:10.1016/s1074-7613(02)00323-0

Frieden, M., James, D., Castelbou, C., Danckaert, A., Martinou, J. C., & Demaurex, N. (2004). Ca(2+) homeostasis during mitochondrial fragmentation and perinuclear clustering induced by hFis1. *J Biol Chem, 279*(21), 22704-22714. doi:10.1074/jbc.M312366200

Fuleihan, R., Ramesh, N., Horner, A., Ahern, D., Belshaw, P. J., Alberg, D. G., . . . Geha, R. S. (1994). Cyclosporin A inhibits CD40 ligand expression in T lymphocytes. *J Clin Invest, 93*(3), 1315-1320. doi:10.1172/JCI117089

Furtado, G. C., Curotto de Lafaille, M. A., Kutchukhidze, N., & Lafaille, J. J. (2002). Interleukin 2 signaling is required for CD4(+) regulatory T cell function. *J Exp Med, 196*(6), 851-857. doi:10.1084/jem.20020190

Fuse, S., Zhang, W., & Usherwood, E. J. (2008). Control of memory CD8+ T cell differentiation by CD80/CD86-CD28 costimulation and restoration by IL-2 during the recall response. *J Immunol, 180*(2), 1148-1157. doi:10.4049/jimmunol.180.2.1148

Galkina, E., Tanousis, K., Preece, G., Tolaini, M., Kioussis, D., Florey, O., . . . Ager, A. (2003). L-selectin shedding does not regulate constitutive T cell trafficking but controls the migration pathways of antigen-activated T lymphocytes. *J Exp Med, 198*(9), 1323-1335. doi:10.1084/jem.20030485

Galvin, K. M., & Shi, Y. (1997). Multiple mechanisms of transcriptional repression by YY1. *Mol Cell Biol, 17*(7), 3723-3732. doi:10.1128/mcb.17.7.3723

Gamberucci, A., Giurisato, E., Pizzo, P., Tassi, M., Giunti, R., McIntosh, D. P., & Benedetti, A. (2002). Diacylglycerol activates the influx of extracellular cations in T-lymphocytes independently of intracellular calcium-store depletion and possibly involving endogenous TRP6 gene products. *Biochem J, 364*(Pt 1), 245-254. doi:10.1042/bj3640245

Gao, P., Tchernyshyov, I., Chang, T. C., Lee, Y. S., Kita, K., Ochi, T., . . . Dang, C. V. (2009). c-Myc suppression of miR-23a/b enhances mitochondrial glutaminase expression and glutamine metabolism. *Nature, 458*(7239), 762-765. doi:10.1038/nature07823

Gardner, J. P., & Balasubramanyam, M. (1996). Na-Ca exchange in circulating blood cells. *Ann N Y Acad Sci, 779*, 502-514. doi:10.1111/j.1749-6632.1996.tb44824.x

Garris, C. S., Wu, L., Acharya, S., Arac, A., Blaho, V. A., Huang, Y., . . . Han, M. H. (2013). Defective sphingosine 1-phosphate receptor 1 (S1P1) phosphorylation exacerbates TH17-mediated autoimmune neuroinflammation. *Nat Immunol, 14*(11), 1166-1172. doi:10.1038/ni.2730

Garson, J. A., Huggett, J. F., Bustin, S. A., Pfaffl, M. W., Benes, V., Vandesompele, J., & Shipley, G. L. (2009). Unreliable real-time PCR analysis of human endogenous retrovirus-W (HERV-W) RNA expression and DNA copy number in multiple sclerosis. *AIDS Res Hum Retroviruses, 25*(3), 377-378; author reply 379-381. doi:10.1089/aid.2008.0270

Gasper, D. J., Tejera, M. M., & Suresh, M. (2014). CD4 T-cell memory generation and maintenance. *Crit Rev Immunol, 34*(2), 121-146. doi:10.1615/critrevimmunol.2014010373

Gattinoni, L., Lugli, E., Ji, Y., Pos, Z., Paulos, C. M., Quigley, M. F., . . . Restifo, N. P. (2011). A human memory T cell subset with stem cell-like properties. *Nat Med, 17*(10), 1290-1297. doi:10.1038/nm.2446

Gattinoni, L., Speiser, D. E., Lichterfeld, M., & Bonini, C. (2017). T memory stem cells in health and disease. *Nat Med, 23*(1), 18-27. doi:10.1038/nm.4241

References

Geginat, J., Lanzavecchia, A., & Sallusto, F. (2003). Proliferation and differentiation potential of human CD8+ memory T-cell subsets in response to antigen or homeostatic cytokines. *Blood, 101*(11), 4260-4266. doi:10.1182/blood-2002-11-3577

Gerlach, C., Rohr, J. C., Perie, L., van Rooij, N., van Heijst, J. W., Velds, A., . . . Schumacher, T. N. (2013). Heterogeneous differentiation patterns of individual CD8+ T cells. *Science, 340*(6132), 635-639. doi:10.1126/science.1235487

Gerriets, V. A., Kishton, R. J., Nichols, A. G., Macintyre, A. N., Inoue, M., Ilkayeva, O., . . . Rathmell, J. C. (2015). Metabolic programming and PDHK1 control CD4+ T cell subsets and inflammation. *J Clin Invest, 125*(1), 194-207. doi:10.1172/JCI76012

Gesbert, F., Moreau, J. L., & Theze, J. (2005). IL-2 responsiveness of CD4 and CD8 lymphocytes: further investigations with human IL-2Rbeta transgenic mice. *Int Immunol, 17*(8), 1093-1102. doi:10.1093/intimm/dxh289

Giacomello, M., Drago, I., Bortolozzi, M., Scorzeto, M., Gianelle, A., Pizzo, P., & Pozzan, T. (2010). Ca2+ hot spots on the mitochondrial surface are generated by Ca2+ mobilization from stores, but not by activation of store-operated Ca2+ channels. *Mol Cell, 38*(2), 280-290. doi:10.1016/j.molcel.2010.04.003

Girard, J. P., Moussion, C., & Forster, R. (2012). HEVs, lymphatics and homeostatic immune cell trafficking in lymph nodes. *Nat Rev Immunol, 12*(11), 762-773. doi:10.1038/nri3298

Glatman Zaretsky, A., Taylor, J. J., King, I. L., Marshall, F. A., Mohrs, M., & Pearce, E. J. (2009). T follicular helper cells differentiate from Th2 cells in response to helminth antigens. *J Exp Med, 206*(5), 991-999. doi:10.1084/jem.20090303

Glendenning, P., Ratajczak, T., Dick, I. M., & Prince, R. L. (2001). Regulation of the 1b isoform of the plasma membrane calcium pump by 1,25-dihydroxyvitamin D3 in rat osteoblast-like cells. *J Bone Miner Res, 16*(3), 525-534. doi:10.1359/jbmr.2001.16.3.525

Goldberg, J., Nairn, A. C., & Kuriyan, J. (1996). Structural basis for the autoinhibition of calcium/calmodulin-dependent protein kinase I. *Cell, 84*(6), 875-887. doi:10.1016/s0092-8674(00)81066-1

Goldsmith, M. A., & Weiss, A. (1988). Early signal transduction by the antigen receptor without commitment to T cell activation. *Science, 240*(4855), 1029-1031. doi:10.1126/science.3259335

Gonzalez-Amaro, R., Cortes, J. R., Sanchez-Madrid, F., & Martin, P. (2013). Is CD69 an effective brake to control inflammatory diseases? *Trends Mol Med, 19*(10), 625-632. doi:10.1016/j.molmed.2013.07.006

Gordon, S., Akopyan, G., Garban, H., & Bonavida, B. (2006). Transcription factor YY1: structure, function, and therapeutic implications in cancer biology. *Oncogene, 25*(8), 1125-1142. doi:10.1038/sj.onc.1209080

Goronzy, J. J., & Weyand, C. M. (2005). Rheumatoid arthritis. *Immunol Rev, 204*, 55-73. doi:10.1111/j.0105-2896.2005.00245.x

Gottschalk, R. A., Corse, E., & Allison, J. P. (2010). TCR ligand density and affinity determine peripheral induction of Foxp3 in vivo. *J Exp Med, 207*(8), 1701-1711. doi:10.1084/jem.20091999

Griffin, J. D., Spertini, O., Ernst, T. J., Belvin, M. P., Levine, H. B., Kanakura, Y., & Tedder, T. F. (1990). Granulocyte-macrophage colony-stimulating factor and other cytokines regulate surface expression of the leukocyte adhesion molecule-1 on human neutrophils, monocytes, and their precursors. *J Immunol, 145*(2), 576-584.

Grissmer, S., Dethlefs, B., Wasmuth, J. J., Goldin, A. L., Gutman, G. A., Cahalan, M. D., & Chandy, K. G. (1990). Expression and chromosomal localization of a lymphocyte K+ channel gene. *Proc Natl Acad Sci U S A, 87*(23), 9411-9415. doi:10.1073/pnas.87.23.9411

Grissmer, S., Nguyen, A. N., & Cahalan, M. D. (1993). Calcium-activated potassium channels in resting and activated human T lymphocytes. Expression levels, calcium dependence, ion selectivity, and pharmacology. *J Gen Physiol, 102*(4), 601-630. doi:10.1085/jgp.102.4.601

References

Groux, H., O'Garra, A., Bigler, M., Rouleau, M., Antonenko, S., de Vries, J. E., & Roncarolo, M. G. (1997). A CD4+ T-cell subset inhibits antigen-specific T-cell responses and prevents colitis. *Nature, 389*(6652), 737-742. doi:10.1038/39614

Gunter, T. E., Gunter, K. K., Sheu, S. S., & Gavin, C. E. (1994). Mitochondrial calcium transport: physiological and pathological relevance. *Am J Physiol, 267*(2 Pt 1), C313-339. doi:10.1152/ajpcell.1994.267.2.C313

Gunter, T. E., & Pfeiffer, D. R. (1990). Mechanisms by which mitochondria transport calcium. *Am J Physiol, 258*(5 Pt 1), C755-786. doi:10.1152/ajpcell.1990.258.5.C755

Guo, B., Aslam, F., van Wijnen, A. J., Roberts, S. G., Frenkel, B., Green, M. R., . . . Stein, J. L. (1997). YY1 regulates vitamin D receptor/retinoid X receptor mediated transactivation of the vitamin D responsive osteocalcin gene. *Proc Natl Acad Sci U S A, 94*(1), 121-126. doi:10.1073/pnas.94.1.121

Habib, T., Park, H., Tsang, M., de Alboran, I. M., Nicks, A., Wilson, L., . . . Iritani, B. M. (2007). Myc stimulates B lymphocyte differentiation and amplifies calcium signaling. *J Cell Biol, 179*(4), 717-731. doi:10.1083/jcb.200704173

Hale, J. S., & Ahmed, R. (2015). Memory T follicular helper CD4 T cells. *Front Immunol, 6*, 16. doi:10.3389/fimmu.2015.00016

Hamann, A., Klugewitz, K., Austrup, F., & Jablonski-Westrich, D. (2000). Activation induces rapid and profound alterations in the trafficking of T cells. *Eur J Immunol, 30*(11), 3207-3218. doi:10.1002/1521-4141(200011)30:11<3207::AID-IMMU3207>3.0.CO;2-L

Harigai, M., Hara, M., Nakazawa, S., Fukasawa, C., Ohta, S., Sugiura, T., . . . Kashiwazaki, S. (1999). Ligation of CD40 induced tumor necrosis factor-alpha in rheumatoid arthritis: a novel mechanism of activation of synoviocytes. *J Rheumatol, 26*(5), 1035-1043.

Harris, S. J., Parry, R. V., Westwick, J., & Ward, S. G. (2008). Phosphoinositide lipid phosphatases: natural regulators of phosphoinositide 3-kinase signaling in T lymphocytes. *J Biol Chem, 283*(5), 2465-2469. doi:10.1074/jbc.R700044200

Hashimoto, S., Ogoshi, K., Sasaki, A., Abe, J., Qu, W., Nakatani, Y., . . . Matsushima, K. (2013). Coordinated changes in DNA methylation in antigen-specific memory CD4 T cells. *J Immunol, 190*(8), 4076-4091. doi:10.4049/jimmunol.1202267

Hay, N. (2011). Interplay between FOXO, TOR, and Akt. *Biochim Biophys Acta, 1813*(11), 1965-1970. doi:10.1016/j.bbamcr.2011.03.013

Hedrick, S. M. (2009). The cunning little vixen: Foxo and the cycle of life and death. *Nat Immunol, 10*(10), 1057-1063. doi:10.1038/ni.1784

Hegazy, A. N., Peine, M., Helmstetter, C., Panse, I., Frohlich, A., Bergthaler, A., . . . Lohning, M. (2010). Interferons direct Th2 cell reprogramming to generate a stable GATA-3(+)T-bet(+) cell subset with combined Th2 and Th1 cell functions. *Immunity, 32*(1), 116-128. doi:10.1016/j.immuni.2009.12.004

Helmstetter, C., Flossdorf, M., Peine, M., Kupz, A., Zhu, J., Hegazy, A. N., . . . Lohning, M. (2015). Individual T helper cells have a quantitative cytokine memory. *Immunity, 42*(1), 108-122. doi:10.1016/j.immuni.2014.12.018

Hemmings, B. A., & Restuccia, D. F. (2012). PI3K-PKB/Akt pathway. *Cold Spring Harb Perspect Biol, 4*(9), a011189. doi:10.1101/cshperspect.a011189

Henson, S. M., & Akbar, A. N. (2009). KLRG1--more than a marker for T cell senescence. *Age (Dordr), 31*(4), 285-291. doi:10.1007/s11357-009-9100-9

Henson, S. M., Riddell, N. E., & Akbar, A. N. (2012). Properties of end-stage human T cells defined by CD45RA re-expression. *Curr Opin Immunol, 24*(4), 476-481. doi:10.1016/j.coi.2012.04.001

Hermiston, M. L., Xu, Z., & Weiss, A. (2003). CD45: a critical regulator of signaling thresholds in immune cells. *Annu Rev Immunol, 21*, 107-137. doi:10.1146/annurev.immunol.21.120601.140946

Hogan, P. G., Lewis, R. S., & Rao, A. (2010). Molecular basis of calcium signaling in lymphocytes: STIM and ORAI. *Annu Rev Immunol, 28*, 491-533. doi:10.1146/annurev.immunol.021908.132550

Hoth, M., Fanger, C. M., & Lewis, R. S. (1997). Mitochondrial regulation of store-operated calcium signaling in T lymphocytes. *J Cell Biol, 137*(3), 633-648. doi:10.1083/jcb.137.3.633

References

Hoth, M., & Niemeyer, B. A. (2013). The neglected CRAC proteins: Orai2, Orai3, and STIM2. *Curr Top Membr, 71*, 237-271. doi:10.1016/B978-0-12-407870-3.00010-X

Hsu, K. W., Hsieh, R. H., Lee, Y. H., Chao, C. H., Wu, K. J., Tseng, M. J., & Yeh, T. S. (2008). The activated Notch1 receptor cooperates with alpha-enolase and MBP-1 in modulating c-myc activity. *Mol Cell Biol, 28*(15), 4829-4842. doi:10.1128/MCB.00175-08

Huang, J., & Manning, B. D. (2009). A complex interplay between Akt, TSC2 and the two mTOR complexes. *Biochem Soc Trans, 37*(Pt 1), 217-222. doi:10.1042/BST0370217

Iezzi, G., Scheidegger, D., & Lanzavecchia, A. (2001). Migration and function of antigen-primed nonpolarized T lymphocytes in vivo. *J Exp Med, 193*(8), 987-993. doi:10.1084/jem.193.8.987

Infante-Duarte, C., Horton, H. F., Byrne, M. C., & Kamradt, T. (2000). Microbial lipopeptides induce the production of IL-17 in Th cells. *J Immunol, 165*(11), 6107-6115. doi:10.4049/jimmunol.165.11.6107

Ivanov, II, McKenzie, B. S., Zhou, L., Tadokoro, C. E., Lepelley, A., Lafaille, J. J., . . . Littman, D. R. (2006). The orphan nuclear receptor RORgammat directs the differentiation program of proinflammatory IL-17+ T helper cells. *Cell, 126*(6), 1121-1133. doi:10.1016/j.cell.2006.07.035

Ivetic, A., Hoskins Green, H. L., & Hart, S. J. (2019). L-selectin: A Major Regulator of Leukocyte Adhesion, Migration and Signaling. *Front Immunol, 10*, 1068. doi:10.3389/fimmu.2019.01068

Jackson, A. L., Matsumoto, H., Janszen, M., Maino, V., Blidy, A., & Shye, S. (1990). Restricted expression of p55 interleukin 2 receptor (CD25) on normal T cells. *Clin Immunol Immunopathol, 54*(1), 126-133. doi:10.1016/0090-1229(90)90012-f

James, P. H., Pruschy, M., Vorherr, T. E., Penniston, J. T., & Carafoli, E. (1989). Primary structure of the cAMP-dependent phosphorylation site of the plasma membrane calcium pump. *Biochemistry, 28*(10), 4253-4258. doi:10.1021/bi00436a020

Jeltsch, K. M., & Heissmeyer, V. (2016). Regulation of T cell signaling and autoimmunity by RNA-binding proteins. *Curr Opin Immunol, 39*, 127-135. doi:10.1016/j.coi.2016.01.011

Jenkins, M. K., & Moon, J. J. (2012). The role of naive T cell precursor frequency and recruitment in dictating immune response magnitude. *J Immunol, 188*(9), 4135-4140. doi:10.4049/jimmunol.1102661

Jeong, H. M., Choi, Y. H., Lee, S. H., & Lee, K. Y. (2014). YY1 represses the transcriptional activity of Runx2 in C2C12 cells. *Mol Cell Endocrinol, 383*(1-2), 103-110. doi:10.1016/j.mce.2013.12.001

Jeong, H. M., Lee, S. H., Yum, J., Yeo, C. Y., & Lee, K. Y. (2014). Smurf2 regulates the degradation of YY1. *Biochim Biophys Acta, 1843*(9), 2005-2011. doi:10.1016/j.bbamcr.2014.04.023

Josefowicz, S. Z., & Rudensky, A. (2009). Control of regulatory T cell lineage commitment and maintenance. *Immunity, 30*(5), 616-625. doi:10.1016/j.immuni.2009.04.009

Kaech, S. M., Wherry, E. J., & Ahmed, R. (2002). Effector and memory T-cell differentiation: implications for vaccine development. *Nat Rev Immunol, 2*(4), 251-262. doi:10.1038/nri778

Katsiari, C. G., Liossis, S. N., Souliotis, V. L., Dimopoulos, A. M., Manoussakis, M. N., & Sfikakis, P. P. (2002). Aberrant expression of the costimulatory molecule CD40 ligand on monocytes from patients with systemic lupus erythematosus. *Clin Immunol, 103*(1), 54-62. doi:10.1006/clim.2001.5172

Katzav, S. (2004). Vav1: an oncogene that regulates specific transcriptional activation of T cells. *Blood, 103*(7), 2443-2451. doi:10.1182/blood-2003-08-2834

Kawasaki, T., Lange, I., & Feske, S. (2009). A minimal regulatory domain in the C terminus of STIM1 binds to and activates ORAI1 CRAC channels. *Biochem Biophys Res Commun, 385*(1), 49-54. doi:10.1016/j.bbrc.2009.05.020

Khakh, B. S. (2001). Molecular physiology of P2X receptors and ATP signalling at synapses. *Nat Rev Neurosci, 2*(3), 165-174. doi:10.1038/35058521

Killock, D. J., Parsons, M., Zarrouk, M., Ameer-Beg, S. M., Ridley, A. J., Haskard, D. O., . . . Ivetic, A. (2009). In Vitro and in Vivo Characterization of Molecular Interactions between Calmodulin, Ezrin/Radixin/Moesin, and L-selectin. *J Biol Chem, 284*(13), 8833-8845. doi:10.1074/jbc.M806983200

References

Kim, H. J., Prasad, V., Hyung, S. W., Lee, Z. H., Lee, S. W., Bhargava, A., . . . Kim, H. H. (2012). Plasma membrane calcium ATPase regulates bone mass by fine-tuning osteoclast differentiation and survival. *J Cell Biol, 199*(7), 1145-1158. doi:10.1083/jcb.201204067

Kim, M. H., Lee, G. S., Jung, E. M., Choi, K. C., & Jeung, E. B. (2009). The negative effect of dexamethasone on calcium-processing gene expressions is associated with a glucocorticoid-induced calcium-absorbing disorder. *Life Sci, 85*(3-4), 146-152. doi:10.1016/j.lfs.2009.05.013

Kinashi, T., & Katagiri, K. (2005). Regulation of immune cell adhesion and migration by regulator of adhesion and cell polarization enriched in lymphoid tissues. *Immunology, 116*(2), 164-171. doi:10.1111/j.1365-2567.2005.02214.x

Kip, S. N., & Strehler, E. E. (2004). Vitamin D3 upregulates plasma membrane Ca2+-ATPase expression and potentiates apico-basal Ca2+ flux in MDCK cells. *Am J Physiol Renal Physiol, 286*(2), F363-369. doi:10.1152/ajprenal.00076.2003

Kircher, S., Merino-Wong, M., Niemeyer, B. A., & Alansary, D. (2018). Profiling calcium signals of in vitro polarized human effector CD4(+) T cells. *Biochim Biophys Acta Mol Cell Res, 1865*(6), 932-943. doi:10.1016/j.bbamcr.2018.04.001

Koguchi, Y., Buenafe, A. C., Thauland, T. J., Gardell, J. L., Bivins-Smith, E. R., Jacoby, D. B., . . . Parker, D. C. (2012). Preformed CD40L is stored in Th1, Th2, Th17, and T follicular helper cells as well as CD4+ 8- thymocytes and invariant NKT cells but not in Treg cells. *PLoS One, 7*(2), e31296. doi:10.1371/journal.pone.0031296

Komori, H. K., Hart, T., LaMere, S. A., Chew, P. V., & Salomon, D. R. (2015). Defining CD4 T cell memory by the epigenetic landscape of CpG DNA methylation. *J Immunol, 194*(4), 1565-1579. doi:10.4049/jimmunol.1401162

Kondo, M., Weissman, I. L., & Akashi, K. (1997). Identification of clonogenic common lymphoid progenitors in mouse bone marrow. *Cell, 91*(5), 661-672. doi:10.1016/s0092-8674(00)80453-5

Koppenol, W. H., Bounds, P. L., & Dang, C. V. (2011). Otto Warburg's contributions to current concepts of cancer metabolism. *Nat Rev Cancer, 11*(5), 325-337. doi:10.1038/nrc3038

Koretzky, G. A., Abtahian, F., & Silverman, M. A. (2006). SLP76 and SLP65: complex regulation of signalling in lymphocytes and beyond. *Nat Rev Immunol, 6*(1), 67-78. doi:10.1038/nri1750

Korthals, M., Langnaese, K., Smalla, K. H., Kahne, T., Herrera-Molina, R., Handschuh, J., . . . Thomas, U. (2017). A complex of Neuroplastin and Plasma Membrane Ca(2+) ATPase controls T cell activation. *Sci Rep, 7*(1), 8358. doi:10.1038/s41598-017-08519-4

Kosiorek, M., Zylinska, L., Zablocki, K., & Pikula, S. (2014). Calcineurin/NFAT signaling represses genes Vamp1 and Vamp2 via PMCA-dependent mechanism during dopamine secretion by Pheochromocytoma cells. *PLoS One, 9*(3), e92176. doi:10.1371/journal.pone.0092176

Kotturi, M. F., & Jefferies, W. A. (2005). Molecular characterization of L-type calcium channel splice variants expressed in human T lymphocytes. *Mol Immunol, 42*(12), 1461-1474. doi:10.1016/j.molimm.2005.01.014

Koziel, K., Lebiedzinska, M., Szabadkai, G., Onopiuk, M., Brutkowski, W., Wierzbicka, K., . . . Wieckowski, M. R. (2009). Plasma membrane associated membranes (PAM) from Jurkat cells contain STIM1 protein is PAM involved in the capacitative calcium entry? *Int J Biochem Cell Biol, 41*(12), 2440-2449. doi:10.1016/j.biocel.2009.07.003

Krippner-Heidenreich, A., Walsemann, G., Beyrouthy, M. J., Speckgens, S., Kraft, R., Thole, H., . . . Luscher, B. (2005). Caspase-dependent regulation and subcellular redistribution of the transcriptional modulator YY1 during apoptosis. *Mol Cell Biol, 25*(9), 3704-3714. doi:10.1128/MCB.25.9.3704-3714.2005

Kulakovskiy, I. V., Vorontsov, I. E., Yevshin, I. S., Sharipov, R. N., Fedorova, A. D., Rumynskiy, E. I., . . . Makeev, V. J. (2018). HOCOMOCO: towards a complete collection of transcription factor binding models for human and mouse via large-scale ChIP-Seq analysis. *Nucleic Acids Res, 46*(D1), D252-D259. doi:10.1093/nar/gkx1106

Lanzavecchia, A., & Sallusto, F. (2002). Progressive differentiation and selection of the fittest in the immune response. *Nat Rev Immunol, 2*(12), 982-987. doi:10.1038/nri959

References

Launay, S., Bobe, R., Lacabaratz-Porret, C., Bredoux, R., Kovacs, T., Enouf, J., & Papp, B. (1997). Modulation of endoplasmic reticulum calcium pump expression during T lymphocyte activation. *J Biol Chem, 272*(16), 10746-10750. doi:10.1074/jbc.272.16.10746

Laurence, A., Tato, C. M., Davidson, T. S., Kanno, Y., Chen, Z., Yao, Z., . . . O'Shea J, J. (2007). Interleukin-2 signaling via STAT5 constrains T helper 17 cell generation. *Immunity, 26*(3), 371-381. doi:10.1016/j.immuni.2007.02.009

Leonard, R. J., Garcia, M. L., Slaughter, R. S., & Reuben, J. P. (1992). Selective blockers of voltage-gated K+ channels depolarize human T lymphocytes: mechanism of the antiproliferative effect of charybdotoxin. *Proc Natl Acad Sci U S A, 89*(21), 10094-10098. doi:10.1073/pnas.89.21.10094

Lewis, R. S. (2001). Calcium signaling mechanisms in T lymphocytes. *Annu Rev Immunol, 19*, 497-521. doi:10.1146/annurev.immunol.19.1.497

Li, X., McKinstry, K. K., Swain, S. L., & Dalton, D. K. (2007). IFN-gamma acts directly on activated CD4+ T cells during mycobacterial infection to promote apoptosis by inducing components of the intracellular apoptosis machinery and by inducing extracellular proapoptotic signals. *J Immunol, 179*(2), 939-949. doi:10.4049/jimmunol.179.2.939

Liao, W., Lin, J. X., & Leonard, W. J. (2013). Interleukin-2 at the crossroads of effector responses, tolerance, and immunotherapy. *Immunity, 38*(1), 13-25. doi:10.1016/j.immuni.2013.01.004

Libri, V., Azevedo, R. I., Jackson, S. E., Di Mitri, D., Lachmann, R., Fuhrmann, S., . . . Akbar, A. N. (2011). Cytomegalovirus infection induces the accumulation of short-lived, multifunctional CD4+CD45RA+CD27+ T cells: the potential involvement of interleukin-7 in this process. *Immunology, 132*(3), 326-339. doi:10.1111/j.1365-2567.2010.03386.x

Lindsten, T., June, C. H., & Thompson, C. B. (1988). Multiple mechanisms regulate c-myc gene expression during normal T cell activation. *EMBO J, 7*(9), 2787-2794.

Link, A., Vogt, T. K., Favre, S., Britschgi, M. R., Acha-Orbea, H., Hinz, B., . . . Luther, S. A. (2007). Fibroblastic reticular cells in lymph nodes regulate the homeostasis of naive T cells. *Nat Immunol, 8*(11), 1255-1265. doi:10.1038/ni1513

Liossis, S. N., Ding, X. Z., Dennis, G. J., & Tsokos, G. C. (1998). Altered pattern of TCR/CD3-mediated protein-tyrosyl phosphorylation in T cells from patients with systemic lupus erythematosus. Deficient expression of the T cell receptor zeta chain. *J Clin Invest, 101*(7), 1448-1457. doi:10.1172/JCI1457

Liossis, S. N., Kovacs, B., Dennis, G., Kammer, G. M., & Tsokos, G. C. (1996). B cells from patients with systemic lupus erythematosus display abnormal antigen receptor-mediated early signal transduction events. *J Clin Invest, 98*(11), 2549-2557. doi:10.1172/JCI119073

Liou, J., Kim, M. L., Heo, W. D., Jones, J. T., Myers, J. W., Ferrell, J. E., Jr., & Meyer, T. (2005). STIM is a Ca2+ sensor essential for Ca2+-store-depletion-triggered Ca2+ influx. *Curr Biol, 15*(13), 1235-1241. doi:10.1016/j.cub.2005.05.055

Lioudyno, M. I., Kozak, J. A., Penna, A., Safrina, O., Zhang, S. L., Sen, D., . . . Cahalan, M. D. (2008). Orai1 and STIM1 move to the immunological synapse and are up-regulated during T cell activation. *Proc Natl Acad Sci U S A, 105*(6), 2011-2016. doi:10.1073/pnas.0706122105

Lis, A., Peinelt, C., Beck, A., Parvez, S., Monteilh-Zoller, M., Fleig, A., & Penner, R. (2007). CRACM1, CRACM2, and CRACM3 are store-operated Ca2+ channels with distinct functional properties. *Curr Biol, 17*(9), 794-800. doi:10.1016/j.cub.2007.03.065

Liu, S. K., Fang, N., Koretzky, G. A., & McGlade, C. J. (1999). The hematopoietic-specific adaptor protein gads functions in T-cell signaling via interactions with the SLP-76 and LAT adaptors. *Curr Biol, 9*(2), 67-75. doi:10.1016/s0960-9822(99)80017-7

Livak, K. J., & Schmittgen, T. D. (2001). Analysis of relative gene expression data using real-time quantitative PCR and the 2(-Delta Delta C(T)) Method. *Methods, 25*(4), 402-408. doi:10.1006/meth.2001.1262

Lohning, M., Hegazy, A. N., Pinschewer, D. D., Busse, D., Lang, K. S., Hofer, T., . . . Hengartner, H. (2008). Long-lived virus-reactive memory T cells generated from purified cytokine-secreting T helper type 1 and type 2 effectors. *J Exp Med, 205*(1), 53-61. doi:10.1084/jem.20071855

References

Lorenz, U. (2009). SHP-1 and SHP-2 in T cells: two phosphatases functioning at many levels. *Immunol Rev, 228*(1), 342-359. doi:10.1111/j.1600-065X.2008.00760.x

Lu, S. Y., Rodriguez, M., & Liao, W. S. (1994). YY1 represses rat serum amyloid A1 gene transcription and is antagonized by NF-kappa B during acute-phase response. *Mol Cell Biol, 14*(9), 6253-6263. doi:10.1128/mcb.14.9.6253

Lugli, E., Goldman, C. K., Perera, L. P., Smedley, J., Pung, R., Yovandich, J. L., . . . Roederer, M. (2010). Transient and persistent effects of IL-15 on lymphocyte homeostasis in nonhuman primates. *Blood, 116*(17), 3238-3248. doi:10.1182/blood-2010-03-275438

Luik, R. M., Wang, B., Prakriya, M., Wu, M. M., & Lewis, R. S. (2008). Oligomerization of STIM1 couples ER calcium depletion to CRAC channel activation. *Nature, 454*(7203), 538-542. doi:10.1038/nature07065

Luik, R. M., Wu, M. M., Buchanan, J., & Lewis, R. S. (2006). The elementary unit of store-operated Ca2+ entry: local activation of CRAC channels by STIM1 at ER-plasma membrane junctions. *J Cell Biol, 174*(6), 815-825. doi:10.1083/jcb.200604015

Ma, J., McCarl, C. A., Khalil, S., Luthy, K., & Feske, S. (2010). T-cell-specific deletion of STIM1 and STIM2 protects mice from EAE by impairing the effector functions of Th1 and Th17 cells. *Eur J Immunol, 40*(11), 3028-3042. doi:10.1002/eji.201040614

Macallan, D. C., Borghans, J. A., & Asquith, B. (2017). Human T Cell Memory: A Dynamic View. *Vaccines (Basel), 5*(1). doi:10.3390/vaccines5010005

MacDonald, K. P., Nishioka, Y., Lipsky, P. E., & Thomas, R. (1997). Functional CD40 ligand is expressed by T cells in rheumatoid arthritis. *J Clin Invest, 100*(9), 2404-2414. doi:10.1172/JCI119781

Mach, F., Schonbeck, U., & Libby, P. (1998). CD40 signaling in vascular cells: a key role in atherosclerosis? *Atherosclerosis, 137 Suppl*, S89-95. doi:10.1016/s0021-9150(97)00309-2

Macian, F., Lopez-Rodriguez, C., & Rao, A. (2001). Partners in transcription: NFAT and AP-1. *Oncogene, 20*(19), 2476-2489. doi:10.1038/sj.onc.1204386

MacIver, N. J., Michalek, R. D., & Rathmell, J. C. (2013). Metabolic regulation of T lymphocytes. *Annu Rev Immunol, 31*, 259-283. doi:10.1146/annurev-immunol-032712-095956

Mackenzie, K. J., Nowakowska, D. J., Leech, M. D., McFarlane, A. J., Wilson, C., Fitch, P. M., . . . Anderton, S. M. (2014). Effector and central memory T helper 2 cells respond differently to peptide immunotherapy. *Proc Natl Acad Sci U S A, 111*(8), E784-793. doi:10.1073/pnas.1316178111

MacLeod, M. K., Clambey, E. T., Kappler, J. W., & Marrack, P. (2009). CD4 memory T cells: what are they and what can they do? *Semin Immunol, 21*(2), 53-61. doi:10.1016/j.smim.2009.02.006

MacLeod, M. K., Kappler, J. W., & Marrack, P. (2010). Memory CD4 T cells: generation, reactivation and re-assignment. *Immunology, 130*(1), 10-15. doi:10.1111/j.1365-2567.2010.03260.x

Mahnke, Y. D., Brodie, T. M., Sallusto, F., Roederer, M., & Lugli, E. (2013). The who's who of T-cell differentiation: human memory T-cell subsets. *Eur J Immunol, 43*(11), 2797-2809. doi:10.1002/eji.201343751

Malherbe, L., Hausl, C., Teyton, L., & McHeyzer-Williams, M. G. (2004). Clonal selection of helper T cells is determined by an affinity threshold with no further skewing of TCR binding properties. *Immunity, 21*(5), 669-679. doi:10.1016/j.immuni.2004.09.008

Maraskovsky, E., O'Reilly, L. A., Teepe, M., Corcoran, L. M., Peschon, J. J., & Strasser, A. (1997). Bcl-2 can rescue T lymphocyte development in interleukin-7 receptor-deficient mice but not in mutant rag-1-/- mice. *Cell, 89*(7), 1011-1019. doi:10.1016/s0092-8674(00)80289-5

Marinelli Busilacchi, E., Costantini, A., Viola, N., Costantini, B., Olivieri, J., Butini, L., . . . Olivieri, A. (2018). Immunomodulatory Effects of Tyrosine Kinase Inhibitor In Vitro and In Vivo Study. *Biol Blood Marrow Transplant, 24*(2), 267-275. doi:10.1016/j.bbmt.2017.10.039

Marrack, P., & Kappler, J. (2004). Control of T cell viability. *Annu Rev Immunol, 22*, 765-787. doi:10.1146/annurev.immunol.22.012703.104554

Martin, P., Gomez, M., Lamana, A., Cruz-Adalia, A., Ramirez-Huesca, M., Ursa, M. A., . . . Sanchez-Madrid, F. (2010). CD69 association with Jak3/Stat5 proteins regulates Th17 cell differentiation. *Mol Cell Biol, 30*(20), 4877-4889. doi:10.1128/MCB.00456-10

References

Massullo, P., Sumoza-Toledo, A., Bhagat, H., & Partida-Sanchez, S. (2006). TRPM channels, calcium and redox sensors during innate immune responses. *Semin Cell Dev Biol, 17*(6), 654-666. doi:10.1016/j.semcdb.2006.11.006

Matala, E., Alexander, S. R., Kishimoto, T. K., & Walcheck, B. (2001). The cytoplasmic domain of L-selectin participates in regulating L-selectin endoproteolysis. *J Immunol, 167*(3), 1617-1623. doi:10.4049/jimmunol.167.3.1617

Matza, D., Badou, A., Kobayashi, K. S., Goldsmith-Pestana, K., Masuda, Y., Komuro, A., . . . Flavell, R. A. (2008). A scaffold protein, AHNAK1, is required for calcium signaling during T cell activation. *Immunity, 28*(1), 64-74. doi:10.1016/j.immuni.2007.11.020

McCarl, C. A., Khalil, S., Ma, J., Oh-hora, M., Yamashita, M., Roether, J., . . . Feske, S. (2010). Store-operated Ca2+ entry through ORAI1 is critical for T cell-mediated autoimmunity and allograft rejection. *J Immunol, 185*(10), 5845-5858. doi:10.4049/jimmunol.1001796

McKinstry, K. K., Strutt, T. M., Bautista, B., Zhang, W., Kuang, Y., Cooper, A. M., & Swain, S. L. (2014). Effector CD4 T-cell transition to memory requires late cognate interactions that induce autocrine IL-2. *Nat Commun, 5*, 5377. doi:10.1038/ncomms6377

Mekahli, D., Bultynck, G., Parys, J. B., De Smedt, H., & Missiaen, L. (2011). Endoplasmic-reticulum calcium depletion and disease. *Cold Spring Harb Perspect Biol, 3*(6). doi:10.1101/cshperspect.a004317

Messeguer, X., Escudero, R., Farre, D., Nunez, O., Martinez, J., & Alba, M. M. (2002). PROMO: detection of known transcription regulatory elements using species-tailored searches. *Bioinformatics, 18*(2), 333-334. doi:10.1093/bioinformatics/18.2.333

Mierke, C. T. (2013). The role of focal adhesion kinase in the regulation of cellular mechanical properties. *Phys Biol, 10*(6), 065005. doi:10.1088/1478-3975/10/6/065005

Misceo, D., Holmgren, A., Louch, W. E., Holme, P. A., Mizobuchi, M., Morales, R. J., . . . Frengen, E. (2014). A dominant STIM1 mutation causes Stormorken syndrome. *Hum Mutat, 35*(5), 556-564. doi:10.1002/humu.22544

Missiaen, L., Raeymaekers, L., Wuytack, F., Vrolix, M., de Smedt, H., & Casteels, R. (1989). Phospholipid-protein interactions of the plasma-membrane Ca2+-transporting ATPase. Evidence for a tissue-dependent functional difference. *Biochem J, 263*(3), 687-694. doi:10.1042/bj2630687

Miyamoto, S., Murphy, A. N., & Brown, J. H. (2008). Akt mediates mitochondrial protection in cardiomyocytes through phosphorylation of mitochondrial hexokinase-II. *Cell Death Differ, 15*(3), 521-529. doi:10.1038/sj.cdd.4402285

Mold, J. E., Venkatasubrahmanyam, S., Burt, T. D., Michaelsson, J., Rivera, J. M., Galkina, S. A., . . . McCune, J. M. (2010). Fetal and adult hematopoietic stem cells give rise to distinct T cell lineages in humans. *Science, 330*(6011), 1695-1699. doi:10.1126/science.1196509

Mora, J. R., & von Andrian, U. H. (2006). T-cell homing specificity and plasticity: new concepts and future challenges. *Trends Immunol, 27*(5), 235-243. doi:10.1016/j.it.2006.03.007

Morin, G., Bruechle, N. O., Singh, A. R., Knopp, C., Jedraszak, G., Elbracht, M., . . . Rochette, J. (2014). Gain-of-Function Mutation in STIM1 (P.R304W) Is Associated with Stormorken Syndrome. *Hum Mutat, 35*(10), 1221-1232. doi:10.1002/humu.22621

Moulton, V. R., Bushar, N. D., Leeser, D. B., Patke, D. S., & Farber, D. L. (2006). Divergent generation of heterogeneous memory CD4 T cells. *J Immunol, 177*(2), 869-876. doi:10.4049/jimmunol.177.2.869

Muller, M. R., & Rao, A. (2010). NFAT, immunity and cancer: a transcription factor comes of age. *Nat Rev Immunol, 10*(9), 645-656. doi:10.1038/nri2818

Mullins, F. M., Park, C. Y., Dolmetsch, R. E., & Lewis, R. S. (2009). STIM1 and calmodulin interact with Orai1 to induce Ca2+-dependent inactivation of CRAC channels. *Proc Natl Acad Sci U S A, 106*(36), 15495-15500. doi:10.1073/pnas.0906781106

Nakayama, T., & Yamashita, M. (2009). Critical role of the Polycomb and Trithorax complexes in the maintenance of CD4 T cell memory. *Semin Immunol, 21*(2), 78-83. doi:10.1016/j.smim.2009.02.001

References

Niggli, V., Adunyah, E. S., & Carafoli, E. (1981). Acidic phospholipids, unsaturated fatty acids, and limited proteolysis mimic the effect of calmodulin on the purified erythrocyte Ca2+ - ATPase. *J Biol Chem, 256*(16), 8588-8592.

Niggli, V., Adunyah, E. S., Penniston, J. T., & Carafoli, E. (1981). Purified (Ca2+-Mg2+)-ATPase of the erythrocyte membrane. Reconstitution and effect of calmodulin and phospholipids. *J Biol Chem, 256*(1), 395-401.

Odumade, O. A., Knight, J. A., Schmeling, D. O., Masopust, D., Balfour, H. H., Jr., & Hogquist, K. A. (2012). Primary Epstein-Barr virus infection does not erode preexisting CD8(+) T cell memory in humans. *J Exp Med, 209*(3), 471-478. doi:10.1084/jem.20112401

Oestreich, K. J., & Weinmann, A. S. (2012). Master regulators or lineage-specifying? Changing views on CD4+ T cell transcription factors. *Nat Rev Immunol, 12*(11), 799-804. doi:10.1038/nri3321

Oh-hora, M., & Rao, A. (2008). Calcium signaling in lymphocytes. *Curr Opin Immunol, 20*(3), 250-258. doi:10.1016/j.coi.2008.04.004

Oh-hora, M., & Rao, A. (2009). The calcium/NFAT pathway: role in development and function of regulatory T cells. *Microbes Infect, 11*(5), 612-619. doi:10.1016/j.micinf.2009.04.008

Okunade, G. W., Miller, M. L., Pyne, G. J., Sutliff, R. L., O'Connor, K. T., Neumann, J. C., . . . Shull, G. E. (2004). Targeted ablation of plasma membrane Ca2+-ATPase (PMCA) 1 and 4 indicates a major housekeeping function for PMCA1 and a critical role in hyperactivated sperm motility and male fertility for PMCA4. *J Biol Chem, 279*(32), 33742-33750. doi:10.1074/jbc.M404628200

Oliveros. (2007). "VENNY. An interactive tool for comparing lists with Venn Diagrams" https://bioinfogp.cnb.csic.es/tools/venny/index.html.

Orkin, S. H., & Zon, L. I. (2008). Hematopoiesis: an evolving paradigm for stem cell biology. *Cell, 132*(4), 631-644. doi:10.1016/j.cell.2008.01.025

Otte, A. P., & Kwaks, T. H. (2003). Gene repression by Polycomb group protein complexes: a distinct complex for every occasion? *Curr Opin Genet Dev, 13*(5), 448-454. doi:10.1016/s0959-437x(03)00108-4

Ouyang, W., & Li, M. O. (2011). Foxo: in command of T lymphocyte homeostasis and tolerance. *Trends Immunol, 32*(1), 26-33. doi:10.1016/j.it.2010.10.005

Ozaki, K., Spolski, R., Ettinger, R., Kim, H. P., Wang, G., Qi, C. F., . . . Leonard, W. J. (2004). Regulation of B cell differentiation and plasma cell generation by IL-21, a novel inducer of Blimp-1 and Bcl-6. *J Immunol, 173*(9), 5361-5371. doi:10.4049/jimmunol.173.9.5361

Pallard, C., Stegmann, A. P., van Kleffens, T., Smart, F., Venkitaraman, A., & Spits, H. (1999). Distinct roles of the phosphatidylinositol 3-kinase and STAT5 pathways in IL-7-mediated development of human thymocyte precursors. *Immunity, 10*(5), 525-535. doi:10.1016/s1074-7613(00)80052-7

Palmgren, M. G., & Nissen, P. (2011). P-type ATPases. *Annu Rev Biophys, 40*, 243-266. doi:10.1146/annurev.biophys.093008.131331

Palty, R., Silverman, W. F., Hershfinkel, M., Caporale, T., Sensi, S. L., Parnis, J., . . . Sekler, I. (2010). NCLX is an essential component of mitochondrial Na+/Ca2+ exchange. *Proc Natl Acad Sci U S A, 107*(1), 436-441. doi:10.1073/pnas.0908099107

Pande, J., Szewczyk, M. M., & Grover, A. K. (2011). Allosteric inhibitors of plasma membrane Ca pumps: Invention and applications of caloxins. *World J Biol Chem, 2*(3), 39-47. doi:10.4331/wjbc.v2.i3.39

Pannabecker, T. L., Chandler, J. S., & Wasserman, R. H. (1995). Vitamin-D-dependent transcriptional regulation of the intestinal plasma membrane calcium pump. *Biochem Biophys Res Commun, 213*(2), 499-505. doi:10.1006/bbrc.1995.2159

Parekh, A. B. (2008). Mitochondrial regulation of store-operated CRAC channels. *Cell Calcium, 44*(1), 6-13. doi:10.1016/j.ceca.2007.12.006

Parekh, A. B., & Penner, R. (1997). Store depletion and calcium influx. *Physiol Rev, 77*(4), 901-930. doi:10.1152/physrev.1997.77.4.901

Park, C. Y., Hoover, P. J., Mullins, F. M., Bachhawat, P., Covington, E. D., Raunser, S., . . . Lewis, R. S. (2009). STIM1 clusters and activates CRAC channels via direct binding of a cytosolic domain to Orai1. *Cell, 136*(5), 876-890. doi:10.1016/j.cell.2009.02.014

References

Partiseti, M., Choquet, D., Diu, A., & Korn, H. (1992). Differential regulation of voltage- and calcium-activated potassium channels in human B lymphocytes. *J Immunol, 148*(11), 3361-3368.

Partiseti, M., Le Deist, F., Hivroz, C., Fischer, A., Korn, H., & Choquet, D. (1994). The calcium current activated by T cell receptor and store depletion in human lymphocytes is absent in a primary immunodeficiency. *J Biol Chem, 269*(51), 32327-32335.

Paszty, K., Antalffy, G., Hegedus, L., Padanyi, R., Penheiter, A. R., Filoteo, A. G., . . . Enyedi, A. (2007). Cleavage of the plasma membrane Ca+ATPase during apoptosis. *Ann N Y Acad Sci, 1099*, 440-450. doi:10.1196/annals.1387.003

Pearce, E. L., Walsh, M. C., Cejas, P. J., Harms, G. M., Shen, H., Wang, L. S., . . . Choi, Y. (2009). Enhancing CD8 T-cell memory by modulating fatty acid metabolism. *Nature, 460*(7251), 103-107. doi:10.1038/nature08097

Pearce, S. C., Gabler, N. K., Ross, J. W., Escobar, J., Patience, J. F., Rhoads, R. P., & Baumgard, L. H. (2013). The effects of heat stress and plane of nutrition on metabolism in growing pigs. *J Anim Sci, 91*(5), 2108-2118. doi:10.2527/jas.2012-5738

Penniston, J. T., & Enyedi, A. (1998). Modulation of the plasma membrane Ca2+ pump. *J Membr Biol, 165*(2), 101-109. doi:10.1007/s002329900424

Pepper, M., & Jenkins, M. K. (2011). Origins of CD4(+) effector and central memory T cells. *Nat Immunol, 12*(6), 467-471. doi:10.1038/ni.2038

Pepper, M., Linehan, J. L., Pagan, A. J., Zell, T., Dileepan, T., Cleary, P. P., & Jenkins, M. K. (2010). Different routes of bacterial infection induce long-lived TH1 memory cells and short-lived TH17 cells. *Nat Immunol, 11*(1), 83-89. doi:10.1038/ni.1826

Perraud, A. L., Fleig, A., Dunn, C. A., Bagley, L. A., Launay, P., Schmitz, C., . . . Scharenberg, A. M. (2001). ADP-ribose gating of the calcium-permeable LTRPC2 channel revealed by Nudix motif homology. *Nature, 411*(6837), 595-599. doi:10.1038/35079100

Peschon, J. J., Morrissey, P. J., Grabstein, K. H., Ramsdell, F. J., Maraskovsky, E., Gliniak, B. C., . . . Davison, B. L. (1994). Early lymphocyte expansion is severely impaired in interleukin 7 receptor-deficient mice. *J Exp Med, 180*(5), 1955-1960. doi:10.1084/jem.180.5.1955

Phan, A. T., Doedens, A. L., Palazon, A., Tyrakis, P. A., Cheung, K. P., Johnson, R. S., & Goldrath, A. W. (2016). Constitutive Glycolytic Metabolism Supports CD8(+) T Cell Effector Memory Differentiation during Viral Infection. *Immunity, 45*(5), 1024-1037. doi:10.1016/j.immuni.2016.10.017

Philipp, S., Strauss, B., Hirnet, D., Wissenbach, U., Mery, L., Flockerzi, V., & Hoth, M. (2003). TRPC3 mediates T-cell receptor-dependent calcium entry in human T-lymphocytes. *J Biol Chem, 278*(29), 26629-26638. doi:10.1074/jbc.M304044200

Placek, K., Gasparian, S., Coffre, M., Maiella, S., Sechet, E., Bianchi, E., & Rogge, L. (2009). Integration of distinct intracellular signaling pathways at distal regulatory elements directs T-bet expression in human CD4+ T cells. *J Immunol, 183*(12), 7743-7751. doi:10.4049/jimmunol.0803812

Plum, J., De Smedt, M., Leclercq, G., Verhasselt, B., & Vandekerckhove, B. (1996). Interleukin-7 is a critical growth factor in early human T-cell development. *Blood, 88*(11), 4239-4245.

Porstmann, T., Santos, C. R., Griffiths, B., Cully, M., Wu, M., Leevers, S., . . . Schulze, A. (2008). SREBP activity is regulated by mTORC1 and contributes to Akt-dependent cell growth. *Cell Metab, 8*(3), 224-236. doi:10.1016/j.cmet.2008.07.007

Powell, J. D., & Delgoffe, G. M. (2010). The mammalian target of rapamycin: linking T cell differentiation, function, and metabolism. *Immunity, 33*(3), 301-311. doi:10.1016/j.immuni.2010.09.002

Prakriya, M., & Lewis, R. S. (2015). Store-Operated Calcium Channels. *Physiol Rev, 95*(4), 1383-1436. doi:10.1152/physrev.00020.2014

Prasad, V., Okunade, G., Liu, L., Paul, R. J., & Shull, G. E. (2007). Distinct phenotypes among plasma membrane Ca2+-ATPase knockout mice. *Ann N Y Acad Sci, 1099*, 276-286. doi:10.1196/annals.1387.029

References

Premack, B. A., McDonald, T. V., & Gardner, P. (1994). Activation of Ca2+ current in Jurkat T cells following the depletion of Ca2+ stores by microsomal Ca(2+)-ATPase inhibitors. *J Immunol, 152*(11), 5226-5240.

Preston, G. C., Sinclair, L. V., Kaskar, A., Hukelmann, J. L., Navarro, M. N., Ferrero, I., . . . Cantrell, D. A. (2015). Single cell tuning of Myc expression by antigen receptor signal strength and interleukin-2 in T lymphocytes. *EMBO J, 34*(15), 2008-2024. doi:10.15252/embj.201490252

Purvis, H. A., Stoop, J. N., Mann, J., Woods, S., Kozijn, A. E., Hambleton, S., . . . Hilkens, C. M. (2010). Low-strength T-cell activation promotes Th17 responses. *Blood, 116*(23), 4829-4837. doi:10.1182/blood-2010-03-272153

Quintana, A., Pasche, M., Junker, C., Al-Ansary, D., Rieger, H., Kummerow, C., . . . Hoth, M. (2011). Calcium microdomains at the immunological synapse: how ORAI channels, mitochondria and calcium pumps generate local calcium signals for efficient T-cell activation. *EMBO J, 30*(19), 3895-3912. doi:10.1038/emboj.2011.289

Quintana, A., Schwindling, C., Wenning, A. S., Becherer, U., Rettig, J., Schwarz, E. C., & Hoth, M. (2007). T cell activation requires mitochondrial translocation to the immunological synapse. *Proc Natl Acad Sci U S A, 104*(36), 14418-14423. doi:10.1073/pnas.0703126104

Radulovic, K., Manta, C., Rossini, V., Holzmann, K., Kestler, H. A., Wegenka, U. M., . . . Niess, J. H. (2012). CD69 regulates type I IFN-induced tolerogenic signals to mucosal CD4 T cells that attenuate their colitogenic potential. *J Immunol, 188*(4), 2001-2013. doi:10.4049/jimmunol.1100765

Ramkumar, C., Cui, H., Kong, Y., Jones, S. N., Gerstein, R. M., & Zhang, H. (2013). Smurf2 suppresses B-cell proliferation and lymphomagenesis by mediating ubiquitination and degradation of YY1. *Nat Commun, 4*, 2598. doi:10.1038/ncomms3598

Razvi, E. S., Jiang, Z., Woda, B. A., & Welsh, R. M. (1995). Lymphocyte apoptosis during the silencing of the immune response to acute viral infections in normal, lpr, and Bcl-2-transgenic mice. *Am J Pathol, 147*(1), 79-91.

Reddy, M., Eirikis, E., Davis, C., Davis, H. M., & Prabhakar, U. (2004). Comparative analysis of lymphocyte activation marker expression and cytokine secretion profile in stimulated human peripheral blood mononuclear cell cultures: an in vitro model to monitor cellular immune function. *J Immunol Methods, 293*(1-2), 127-142. doi:10.1016/j.jim.2004.07.006

Reinhardt, R. L., Khoruts, A., Merica, R., Zell, T., & Jenkins, M. K. (2001). Visualizing the generation of memory CD4 T cells in the whole body. *Nature, 410*(6824), 101-105. doi:10.1038/35065111

Reinhardt, R. L., Liang, H. E., & Locksley, R. M. (2009). Cytokine-secreting follicular T cells shape the antibody repertoire. *Nat Immunol, 10*(4), 385-393. doi:10.1038/ni.1715

Riggs, K. J., Saleque, S., Wong, K. K., Merrell, K. T., Lee, J. S., Shi, Y., & Calame, K. (1993). Yin-yang 1 activates the c-myc promoter. *Mol Cell Biol, 13*(12), 7487-7495. doi:10.1128/mcb.13.12.7487

Riha, P., & Rudd, C. E. (2010). CD28 co-signaling in the adaptive immune response. *Self Nonself, 1*(3), 231-240. doi:10.4161/self.1.3.12968

Riman, S., Rizkallah, R., Kassardjian, A., Alexander, K. E., Luscher, B., & Hurt, M. M. (2012). Phosphorylation of the transcription factor YY1 by CK2alpha prevents cleavage by caspase 7 during apoptosis. *Mol Cell Biol, 32*(4), 797-807. doi:10.1128/MCB.06466-11

Ritchie, M. F., Samakai, E., & Soboloff, J. (2012). STIM1 is required for attenuation of PMCA-mediated Ca2+ clearance during T-cell activation. *EMBO J, 31*(5), 1123-1133. doi:10.1038/emboj.2011.495

Ritchie, M. F., Zhou, Y., & Soboloff, J. (2011). Transcriptional mechanisms regulating Ca(2+) homeostasis. *Cell Calcium, 49*(5), 314-321. doi:10.1016/j.ceca.2010.10.001

Rizzuto, R., Brini, M., Murgia, M., & Pozzan, T. (1993). Microdomains with high Ca2+ close to IP3-sensitive channels that are sensed by neighboring mitochondria. *Science, 262*(5134), 744-747. doi:10.1126/science.8235595

Rizzuto, R., De Stefani, D., Raffaello, A., & Mammucari, C. (2012). Mitochondria as sensors and regulators of calcium signalling. *Nat Rev Mol Cell Biol, 13*(9), 566-578. doi:10.1038/nrm3412

Roetynck, S., Olotu, A., Simam, J., Marsh, K., Stockinger, B., Urban, B., & Langhorne, J. (2013). Phenotypic and functional profiling of CD4 T cell compartment in distinct populations of healthy

adults with different antigenic exposure. *PLoS One, 8*(1), e55195. doi:10.1371/journal.pone.0055195

Rogers, P. R., Dubey, C., & Swain, S. L. (2000). Qualitative changes accompany memory T cell generation: faster, more effective responses at lower doses of antigen. *J Immunol, 164*(5), 2338-2346. doi:10.4049/jimmunol.164.5.2338

Romero, P., Zippelius, A., Kurth, I., Pittet, M. J., Touvrey, C., Iancu, E. M., . . . Rufer, N. (2007). Four functionally distinct populations of human effector-memory CD8+ T lymphocytes. *J Immunol, 178*(7), 4112-4119. doi:10.4049/jimmunol.178.7.4112

Rosette, C., Werlen, G., Daniels, M. A., Holman, P. O., Alam, S. M., Travers, P. J., . . . Jameson, S. C. (2001). The impact of duration versus extent of TCR occupancy on T cell activation: a revision of the kinetic proofreading model. *Immunity, 15*(1), 59-70. doi:10.1016/s1074-7613(01)00173-x

Ruedl, C., Bachmann, M. F., & Kopf, M. (2000). The antigen dose determines T helper subset development by regulation of CD40 ligand. *Eur J Immunol, 30*(7), 2056-2064. doi:10.1002/1521-4141(200007)30:7<2056::AID-IMMU2056>3.0.CO;2-S

Sakaguchi, S., Sakaguchi, N., Asano, M., Itoh, M., & Toda, M. (1995). Immunologic self-tolerance maintained by activated T cells expressing IL-2 receptor alpha-chains (CD25). Breakdown of a single mechanism of self-tolerance causes various autoimmune diseases. *J Immunol, 155*(3), 1151-1164.

Sallusto, F. (2016). Heterogeneity of Human CD4(+) T Cells Against Microbes. *Annu Rev Immunol, 34*, 317-334. doi:10.1146/annurev-immunol-032414-112056

Sallusto, F., & Lanzavecchia, A. (2001). Exploring pathways for memory T cell generation. *J Clin Invest, 108*(6), 805-806. doi:10.1172/JCI14005

Sallusto, F., Lenig, D., Forster, R., Lipp, M., & Lanzavecchia, A. (1999). Two subsets of memory T lymphocytes with distinct homing potentials and effector functions. *Nature, 401*(6754), 708-712. doi:10.1038/44385

Samanta, K., Mirams, G. R., & Parekh, A. B. (2018). Sequential forward and reverse transport of the Na(+) Ca(2+) exchanger generates Ca(2+) oscillations within mitochondria. *Nat Commun, 9*(1), 156. doi:10.1038/s41467-017-02638-2

Santo-Domingo, J., & Demaurex, N. (2010). Calcium uptake mechanisms of mitochondria. *Biochim Biophys Acta, 1797*(6-7), 907-912. doi:10.1016/j.bbabio.2010.01.005

Satrustegui, J., Pardo, B., & Del Arco, A. (2007). Mitochondrial transporters as novel targets for intracellular calcium signaling. *Physiol Rev, 87*(1), 29-67. doi:10.1152/physrev.00005.2006

Scharenberg, A. M., Humphries, L. A., & Rawlings, D. J. (2007). Calcium signalling and cell-fate choice in B cells. *Nat Rev Immunol, 7*(10), 778-789. doi:10.1038/nri2172

Schmidt, N., Kollewe, A., Constantin, C. E., Henrich, S., Ritzau-Jost, A., Bildl, W., . . . Schulte, U. (2017). Neuroplastin and Basigin Are Essential Auxiliary Subunits of Plasma Membrane Ca(2+)-ATPases and Key Regulators of Ca(2+) Clearance. *Neuron, 96*(4), 827-838 e829. doi:10.1016/j.neuron.2017.09.038

Schonbeck, U., & Libby, P. (2001). CD40 signaling and plaque instability. *Circ Res, 89*(12), 1092-1103. doi:10.1161/hh2401.101272

Schuh, K., Uldrijan, S., Telkamp, M., Rothlein, N., & Neyses, L. (2001). The plasmamembrane calmodulin-dependent calcium pump: a major regulator of nitric oxide synthase I. *J Cell Biol, 155*(2), 201-205. doi:10.1083/jcb.200104131

Schulze-Luehrmann, J., & Ghosh, S. (2006). Antigen-receptor signaling to nuclear factor kappa B. *Immunity, 25*(5), 701-715. doi:10.1016/j.immuni.2006.10.010

Schwab, B. L., Guerini, D., Didszun, C., Bano, D., Ferrando-May, E., Fava, E., . . . Nicotera, P. (2002). Cleavage of plasma membrane calcium pumps by caspases: a link between apoptosis and necrosis. *Cell Death Differ, 9*(8), 818-831. doi:10.1038/sj.cdd.4401042

Sena, L. A., Li, S., Jairaman, A., Prakriya, M., Ezponda, T., Hildeman, D. A., . . . Chandel, N. S. (2013). Mitochondria are required for antigen-specific T cell activation through reactive oxygen species signaling. *Immunity, 38*(2), 225-236. doi:10.1016/j.immuni.2012.10.020

References

Shaw, P. J., & Feske, S. (2012). Regulation of lymphocyte function by ORAI and STIM proteins in infection and autoimmunity. *J Physiol, 590*(17), 4157-4167. doi:10.1113/jphysiol.2012.233221

Sher, A., & Coffman, R. L. (1992). Regulation of immunity to parasites by T cells and T cell-derived cytokines. *Annu Rev Immunol, 10*, 385-409. doi:10.1146/annurev.iy.10.040192.002125

Shi, Y., Seto, E., Chang, L. S., & Shenk, T. (1991). Transcriptional repression by YY1, a human GLI-Kruppel-related protein, and relief of repression by adenovirus E1A protein. *Cell, 67*(2), 377-388. doi:10.1016/0092-8674(91)90189-6

Shiow, L. R., Rosen, D. B., Brdickova, N., Xu, Y., An, J., Lanier, L. L., . . . Matloubian, M. (2006). CD69 acts downstream of interferon-alpha/beta to inhibit S1P1 and lymphocyte egress from lymphoid organs. *Nature, 440*(7083), 540-544. doi:10.1038/nature04606

Sinclair, L. V., Finlay, D., Feijoo, C., Cornish, G. H., Gray, A., Ager, A., . . . Cantrell, D. A. (2008). Phosphatidylinositol-3-OH kinase and nutrient-sensing mTOR pathways control T lymphocyte trafficking. *Nat Immunol, 9*(5), 513-521. doi:10.1038/ni.1603

Smallwood, J. I., Gugi, B., & Rasmussen, H. (1988). Regulation of erythrocyte Ca2+ pump activity by protein kinase C. *J Biol Chem, 263*(5), 2195-2202.

Solle, M., Labasi, J., Perregaux, D. G., Stam, E., Petrushova, N., Koller, B. H., . . . Gabel, C. A. (2001). Altered cytokine production in mice lacking P2X(7) receptors. *J Biol Chem, 276*(1), 125-132. doi:10.1074/jbc.M006781200

Sommer, K., Guo, B., Pomerantz, J. L., Bandaranayake, A. D., Moreno-Garcia, M. E., Ovechkina, Y. L., & Rawlings, D. J. (2005). Phosphorylation of the CARMA1 linker controls NF-kappaB activation. *Immunity, 23*(6), 561-574. doi:10.1016/j.immuni.2005.09.014

Srivastava, S., Ko, K., Choudhury, P., Li, Z., Johnson, A. K., Nadkarni, V., . . . Skolnik, E. Y. (2006). Phosphatidylinositol-3 phosphatase myotubularin-related protein 6 negatively regulates CD4 T cells. *Mol Cell Biol, 26*(15), 5595-5602. doi:10.1128/MCB.00352-06

Stafford, N., Wilson, C., Oceandy, D., Neyses, L., & Cartwright, E. J. (2017). The Plasma Membrane Calcium ATPases and Their Role as Major New Players in Human Disease. *Physiol Rev, 97*(3), 1089-1125. doi:10.1152/physrev.00028.2016

Stathopulos, P. B., Zheng, L., & Ikura, M. (2009). Stromal interaction molecule (STIM) 1 and STIM2 calcium sensing regions exhibit distinct unfolding and oligomerization kinetics. *J Biol Chem, 284*(2), 728-732. doi:10.1074/jbc.C800178200

Staudt, V., Bothur, E., Klein, M., Lingnau, K., Reuter, S., Grebe, N., . . . Bopp, T. (2010). Interferon-regulatory factor 4 is essential for the developmental program of T helper 9 cells. *Immunity, 33*(2), 192-202. doi:10.1016/j.immuni.2010.07.014

Steeber, D. A., Green, N. E., Sato, S., & Tedder, T. F. (1996). Lyphocyte migration in L-selectin-deficient mice. Altered subset migration and aging of the immune system. *J Immunol, 157*(3), 1096-1106.

Stoll, S., Delon, J., Brotz, T. M., & Germain, R. N. (2002). Dynamic imaging of T cell-dendritic cell interactions in lymph nodes. *Science, 296*(5574), 1873-1876. doi:10.1126/science.1071065

Strehler, E. E. (2013). Plasma membrane calcium ATPases as novel candidates for therapeutic agent development. *J Pharm Pharm Sci, 16*(2), 190-206. doi:10.18433/j3z011

Strehler, E. E., & Zacharias, D. A. (2001). Role of alternative splicing in generating isoform diversity among plasma membrane calcium pumps. *Physiol Rev, 81*(1), 21-50. doi:10.1152/physrev.2001.81.1.21

Sui, Y., Wu, T., Li, F., Wang, F., Cai, Y., & Jin, J. (2019). YY1/BCCIP Coordinately Regulates P53-Responsive Element (p53RE)-Mediated Transactivation of p21(Waf1/Cip1). *Int J Mol Sci, 20*(9). doi:10.3390/ijms20092095

Sukumar, M., Liu, J., Ji, Y., Subramanian, M., Crompton, J. G., Yu, Z., . . . Gattinoni, L. (2013). Inhibiting glycolytic metabolism enhances CD8+ T cell memory and antitumor function. *J Clin Invest, 123*(10), 4479-4488. doi:10.1172/JCI69589

Surh, C. D., & Sprent, J. (2008). Homeostasis of naive and memory T cells. *Immunity, 29*(6), 848-862. doi:10.1016/j.immuni.2008.11.002

References

Swanson, B. J., Murakami, M., Mitchell, T. C., Kappler, J., & Marrack, P. (2002). RANTES production by memory phenotype T cells is controlled by a posttranscriptional, TCR-dependent process. *Immunity, 17*(5), 605-615. doi:10.1016/s1074-7613(02)00456-9

Tan, J. T., Dudl, E., LeRoy, E., Murray, R., Sprent, J., Weinberg, K. I., & Surh, C. D. (2001). IL-7 is critical for homeostatic proliferation and survival of naive T cells. *Proc Natl Acad Sci U S A, 98*(15), 8732-8737. doi:10.1073/pnas.161126098

Testi, R., Phillips, J. H., & Lanier, L. L. (1989). T cell activation via Leu-23 (CD69). *J Immunol, 143*(4), 1123-1128.

Thomas, M. J., & Seto, E. (1999). Unlocking the mechanisms of transcription factor YY1: are chromatin modifying enzymes the key? *Gene, 236*(2), 197-208. doi:10.1016/s0378-1119(99)00261-9

Tidow, H., Poulsen, L. R., Andreeva, A., Knudsen, M., Hein, K. L., Wiuf, C., . . . Nissen, P. (2012). A bimodular mechanism of calcium control in eukaryotes. *Nature, 491*(7424), 468-472. doi:10.1038/nature11539

Tough, D. F., & Sprent, J. (1994). Turnover of naive- and memory-phenotype T cells. *J Exp Med, 179*(4), 1127-1135. doi:10.1084/jem.179.4.1127

Toyoshima, C., Nakasako, M., Nomura, H., & Ogawa, H. (2000). Crystal structure of the calcium pump of sarcoplasmic reticulum at 2.6 A resolution. *Nature, 405*(6787), 647-655. doi:10.1038/35015017

Trifari, S., Kaplan, C. D., Tran, E. H., Crellin, N. K., & Spits, H. (2009). Identification of a human helper T cell population that has abundant production of interleukin 22 and is distinct from T(H)-17, T(H)1 and T(H)2 cells. *Nat Immunol, 10*(8), 864-871. doi:10.1038/ni.1770

Tubo, N. J., Pagan, A. J., Taylor, J. J., Nelson, R. W., Linehan, J. L., Ertelt, J. M., . . . Jenkins, M. K. (2013). Single naive CD4+ T cells from a diverse repertoire produce different effector cell types during infection. *Cell, 153*(4), 785-796. doi:10.1016/j.cell.2013.04.007

Uehara, S., Song, K., Farber, J. M., & Love, P. E. (2002). Characterization of CCR9 expression and CCL25/thymus-expressed chemokine responsiveness during T cell development: CD3(high)CD69+ thymocytes and gammadeltaTCR+ thymocytes preferentially respond to CCL25. *J Immunol, 168*(1), 134-142. doi:10.4049/jimmunol.168.1.134

Vaeth, M., Yang, J., Yamashita, M., Zee, I., Eckstein, M., Knosp, C., . . . Feske, S. (2017). ORAI2 modulates store-operated calcium entry and T cell-mediated immunity. *Nat Commun, 8*, 14714. doi:10.1038/ncomms14714

Valitutti, S., Dessing, M., Aktories, K., Gallati, H., & Lanzavecchia, A. (1995). Sustained signaling leading to T cell activation results from prolonged T cell receptor occupancy. Role of T cell actin cytoskeleton. *J Exp Med, 181*(2), 577-584. doi:10.1084/jem.181.2.577

van Beelen, A. J., Zelinkova, Z., Taanman-Kueter, E. W., Muller, F. J., Hommes, D. W., Zaat, S. A., . . . de Jong, E. C. (2007). Stimulation of the intracellular bacterial sensor NOD2 programs dendritic cells to promote interleukin-17 production in human memory T cells. *Immunity, 27*(4), 660-669. doi:10.1016/j.immuni.2007.08.013

van der Windt, G. J., & Pearce, E. L. (2012). Metabolic switching and fuel choice during T-cell differentiation and memory development. *Immunol Rev, 249*(1), 27-42. doi:10.1111/j.1600-065X.2012.01150.x

van Herwijnen, M. J., Wieten, L., van der Zee, R., van Kooten, P. J., Wagenaar-Hilbers, J. P., Hoek, A., . . . Broere, F. (2012). Regulatory T cells that recognize a ubiquitous stress-inducible self-antigen are long-lived suppressors of autoimmune arthritis. *Proc Natl Acad Sci U S A, 109*(35), 14134-14139. doi:10.1073/pnas.1206803109

van Panhuys, N., Klauschen, F., & Germain, R. N. (2014). T-cell-receptor-dependent signal intensity dominantly controls CD4(+) T cell polarization In Vivo. *Immunity, 41*(1), 63-74. doi:10.1016/j.immuni.2014.06.003

Venken, K., Thewissen, M., Hellings, N., Somers, V., Hensen, K., Rummens, J. L., & Stinissen, P. (2007). A CFSE based assay for measuring CD4+CD25+ regulatory T cell mediated suppression of auto-antigen specific and polyclonal T cell responses. *J Immunol Methods, 322*(1-2), 1-11. doi:10.1016/j.jim.2007.01.025

<div style="text-align: center;">References</div>

Vig, M., DeHaven, W. I., Bird, G. S., Billingsley, J. M., Wang, H., Rao, P. E., . . . Kinet, J. P. (2008). Defective mast cell effector functions in mice lacking the CRACM1 pore subunit of store-operated calcium release-activated calcium channels. *Nat Immunol, 9*(1), 89-96. doi:10.1038/ni1550

von Boehmer, H., & Fehling, H. J. (1997). Structure and function of the pre-T cell receptor. *Annu Rev Immunol, 15*, 433-452. doi:10.1146/annurev.immunol.15.1.433

von Boehmer, H., & Melchers, F. (2010). Checkpoints in lymphocyte development and autoimmune disease. *Nat Immunol, 11*(1), 14-20. doi:10.1038/ni.1794

Waldeck-Weiermair, M., Malli, R., Parichatikanond, W., Gottschalk, B., Madreiter-Sokolowski, C. T., Klec, C., . . . Graier, W. F. (2015). Rearrangement of MICU1 multimers for activation of MCU is solely controlled by cytosolic Ca(2.). *Sci Rep, 5*, 15602. doi:10.1038/srep15602

Wang, A., Chandran, S., Shah, S. A., Chiu, Y., Paria, B. C., Aghamolla, T., . . . Kammula, U. S. (2012). The stoichiometric production of IL-2 and IFN-gamma mRNA defines memory T cells that can self-renew after adoptive transfer in humans. *Sci Transl Med, 4*(149), 149ra120. doi:10.1126/scitranslmed.3004306

Wang, R., Dillon, C. P., Shi, L. Z., Milasta, S., Carter, R., Finkelstein, D., . . . Green, D. R. (2011). The transcription factor Myc controls metabolic reprogramming upon T lymphocyte activation. *Immunity, 35*(6), 871-882. doi:10.1016/j.immuni.2011.09.021

Warnock, R. A., Askari, S., Butcher, E. C., & von Andrian, U. H. (1998). Molecular mechanisms of lymphocyte homing to peripheral lymph nodes. *J Exp Med, 187*(2), 205-216. doi:10.1084/jem.187.2.205

Weber, K. S., Li, Q. J., Persaud, S. P., Campbell, J. D., Davis, M. M., & Allen, P. M. (2012). Distinct CD4+ helper T cells involved in primary and secondary responses to infection. *Proc Natl Acad Sci U S A, 109*(24), 9511-9516. doi:10.1073/pnas.1202408109

Weber, K. S., Miller, M. J., & Allen, P. M. (2008). Th17 cells exhibit a distinct calcium profile from Th1 and Th2 cells and have Th1-like motility and NF-AT nuclear localization. *J Immunol, 180*(3), 1442-1450. doi:10.4049/jimmunol.180.3.1442

Weill, L., Shestakova, E., & Bonnefoy, E. (2003). Transcription factor YY1 binds to the murine beta interferon promoter and regulates its transcriptional capacity with a dual activator/repressor role. *J Virol, 77*(5), 2903-2914. doi:10.1128/jvi.77.5.2903-2914.2003

Whitmire, J. K., Asano, M. S., Kaech, S. M., Sarkar, S., Hannum, L. G., Shlomchik, M. J., & Ahmed, R. (2009). Requirement of B cells for generating CD4+ T cell memory. *J Immunol, 182*(4), 1868-1876. doi:10.4049/jimmunol.0802501

Williams, J. C., Armesilla, A. L., Mohamed, T. M., Hagarty, C. L., McIntyre, F. H., Schomburg, S., . . . Neyses, L. (2006). The sarcolemmal calcium pump, alpha-1 syntrophin, and neuronal nitric-oxide synthase are parts of a macromolecular protein complex. *J Biol Chem, 281*(33), 23341-23348. doi:10.1074/jbc.M513341200

Williams, M. A., Ravkov, E. V., & Bevan, M. J. (2008). Rapid culling of the CD4+ T cell repertoire in the transition from effector to memory. *Immunity, 28*(4), 533-545. doi:10.1016/j.immuni.2008.02.014

Wise, D. R., DeBerardinis, R. J., Mancuso, A., Sayed, N., Zhang, X. Y., Pfeiffer, H. K., . . . Thompson, C. B. (2008). Myc regulates a transcriptional program that stimulates mitochondrial glutaminolysis and leads to glutamine addiction. *Proc Natl Acad Sci U S A, 105*(48), 18782-18787. doi:10.1073/pnas.0810199105

Woehrle, T., Yip, L., Elkhal, A., Sumi, Y., Chen, Y., Yao, Y., . . . Junger, W. G. (2010). Pannexin-1 hemichannel-mediated ATP release together with P2X1 and P2X4 receptors regulate T-cell activation at the immune synapse. *Blood, 116*(18), 3475-3484. doi:10.1182/blood-2010-04-277707

Wofford, J. A., Wieman, H. L., Jacobs, S. R., Zhao, Y., & Rathmell, J. C. (2008). IL-7 promotes Glut1 trafficking and glucose uptake via STAT5-mediated activation of Akt to support T-cell survival. *Blood, 111*(4), 2101-2111. doi:10.1182/blood-2007-06-096297

Wu, X., Chang, B., Blair, N. S., Sargent, M., York, A. J., Robbins, J., . . . Molkentin, J. D. (2009). Plasma membrane Ca2+-ATPase isoform 4 antagonizes cardiac hypertrophy in association with calcineurin inhibition in rodents. *J Clin Invest, 119*(4), 976-985. doi:10.1172/JCI36693

References

Wulfing, C., Rabinowitz, J. D., Beeson, C., Sjaastad, M. D., McConnell, H. M., & Davis, M. M. (1997). Kinetics and extent of T cell activation as measured with the calcium signal. *J Exp Med, 185*(10), 1815-1825. doi:10.1084/jem.185.10.1815

Xia, X. M., Fakler, B., Rivard, A., Wayman, G., Johnson-Pais, T., Keen, J. E., . . . Adelman, J. P. (1998). Mechanism of calcium gating in small-conductance calcium-activated potassium channels. *Nature, 395*(6701), 503-507. doi:10.1038/26758

Yang, S., Liu, F., Wang, Q. J., Rosenberg, S. A., & Morgan, R. A. (2011). The shedding of CD62L (L-selectin) regulates the acquisition of lytic activity in human tumor reactive T lymphocytes. *PLoS One, 6*(7), e22560. doi:10.1371/journal.pone.0022560

Yang, X. O., Pappu, B. P., Nurieva, R., Akimzhanov, A., Kang, H. S., Chung, Y., . . . Dong, C. (2008). T helper 17 lineage differentiation is programmed by orphan nuclear receptors ROR alpha and ROR gamma. *Immunity, 28*(1), 29-39. doi:10.1016/j.immuni.2007.11.016

Yang, X. P., Ghoreschi, K., Steward-Tharp, S. M., Rodriguez-Canales, J., Zhu, J., Grainger, J. R., . . . Laurence, A. (2011). Opposing regulation of the locus encoding IL-17 through direct, reciprocal actions of STAT3 and STAT5. *Nat Immunol, 12*(3), 247-254. doi:10.1038/ni.1995

Ye, J., Cippitelli, M., Dorman, L., Ortaldo, J. R., & Young, H. A. (1996). The nuclear factor YY1 suppresses the human gamma interferon promoter through two mechanisms: inhibition of AP1 binding and activation of a silencer element. *Mol Cell Biol, 16*(9), 4744-4753. doi:10.1128/mcb.16.9.4744

Yip, L., Woehrle, T., Corriden, R., Hirsh, M., Chen, Y., Inoue, Y., . . . Junger, W. G. (2009). Autocrine regulation of T-cell activation by ATP release and P2X7 receptors. *FASEB J, 23*(6), 1685-1693. doi:10.1096/fj.08-126458

Yu, X., Carpenter, P., & Anasetti, C. (2001). Advances in transplantation tolerance. *Lancet, 357*(9272), 1959-1963. doi:10.1016/s0140-6736(00)05068-6

Zarbock, A., Kempf, T., Wollert, K. C., & Vestweber, D. (2012). Leukocyte integrin activation and deactivation: novel mechanisms of balancing inflammation. *J Mol Med (Berl), 90*(4), 353-359. doi:10.1007/s00109-011-0835-2

Zeller, K. I., Zhao, X., Lee, C. W., Chiu, K. P., Yao, F., Yustein, J. T., . . . Wei, C. L. (2006). Global mapping of c-Myc binding sites and target gene networks in human B cells. *Proc Natl Acad Sci U S A, 103*(47), 17834-17839. doi:10.1073/pnas.0604129103

Zerbino, D. R., Wilder, S. P., Johnson, N., Juettemann, T., & Flicek, P. R. (2015). The ensembl regulatory build. *Genome Biol, 16*, 56. doi:10.1186/s13059-015-0621-5

Zhang, D. H., Cohn, L., Ray, P., Bottomly, K., & Ray, A. (1997). Transcription factor GATA-3 is differentially expressed in murine Th1 and Th2 cells and controls Th2-specific expression of the interleukin-5 gene. *J Biol Chem, 272*(34), 21597-21603. doi:10.1074/jbc.272.34.21597

Zhang, S. L., Yu, Y., Roos, J., Kozak, J. A., Deerinck, T. J., Ellisman, M. H., . . . Cahalan, M. D. (2005). STIM1 is a Ca2+ sensor that activates CRAC channels and migrates from the Ca2+ store to the plasma membrane. *Nature, 437*(7060), 902-905. doi:10.1038/nature04147

Zhang, W., Sloan-Lancaster, J., Kitchen, J., Trible, R. P., & Samelson, L. E. (1998). LAT: the ZAP-70 tyrosine kinase substrate that links T cell receptor to cellular activation. *Cell, 92*(1), 83-92. doi:10.1016/s0092-8674(00)80901-0

Zhang, W. J., Wu, X. N., Shi, T. T., Xu, H. T., Yi, J., Shen, H. F., . . . Liu, W. (2016). Regulation of Transcription Factor Yin Yang 1 by SET7/9-mediated Lysine Methylation. *Sci Rep, 6*, 21718. doi:10.1038/srep21718

Zhang, Y., Joe, G., Hexner, E., Zhu, J., & Emerson, S. G. (2005). Host-reactive CD8+ memory stem cells in graft-versus-host disease. *Nat Med, 11*(12), 1299-1305. doi:10.1038/nm1326

Zhao, L., Shey, M., Farnsworth, M., & Dailey, M. O. (2001). Regulation of membrane metalloproteolytic cleavage of L-selectin (CD62l) by the epidermal growth factor domain. *J Biol Chem, 276*(33), 30631-30640. doi:10.1074/jbc.M103748200

Zhao, X., Yan, X., Liu, Y., Zhang, P., & Ni, X. (2016). Co-expression of mouse TMEM63A, TMEM63B and TMEM63C confers hyperosmolarity activated ion currents in HEK293 cells. *Cell Biochem Funct, 34*(4), 238-241. doi:10.1002/cbf.3185

References

Zhou, L., Lopes, J. E., Chong, M. M., Ivanov, II, Min, R., Victora, G. D., . . . Littman, D. R. (2008). TGF-beta-induced Foxp3 inhibits T(H)17 cell differentiation by antagonizing RORgammat function. *Nature, 453*(7192), 236-240. doi:10.1038/nature06878

Ziegler, S. F., Ramsdell, F., & Alderson, M. R. (1994). The activation antigen CD69. *Stem Cells, 12*(5), 456-465. doi:10.1002/stem.5530120502

Zlotoff, D. A., Sambandam, A., Logan, T. D., Bell, J. J., Schwarz, B. A., & Bhandoola, A. (2010). CCR7 and CCR9 together recruit hematopoietic progenitors to the adult thymus. *Blood, 115*(10), 1897-1905. doi:10.1182/blood-2009-08-237784

Zweifach, A., & Lewis, R. S. (1993). Mitogen-regulated Ca2+ current of T lymphocytes is activated by depletion of intracellular Ca2+ stores. *Proc Natl Acad Sci U S A, 90*(13), 6295-6299. doi:10.1073/pnas.90.13.6295

Zweifach, A., & Lewis, R. S. (1995). Slow calcium-dependent inactivation of depletion-activated calcium current. Store-dependent and -independent mechanisms. *J Biol Chem, 270*(24), 14445-14451. doi:10.1074/jbc.270.24.14445

10 List of figures

11 List of tables and equations

Publications

Merino-Wong, M., Niemeyer, B. A., & Alansary, D**.** Plasma Membrane Calcium ATPase Regulates Stoichiometry of CD4$^+$ T-cell Compartments under Transcriptional Repression by YY1 (under revision)

Kircher, S., **Merino-Wong, M**., Niemeyer, B. A., & Alansary, D. (2018). Profiling calcium signals of in vitro polarized human effector CD4(+) T cells. Biochim Biophys Acta Mol Cell Res, 1865(6), 932-943. doi:10.1016/j.bbamcr.2018.04.001Sarah

Dorvignit, D., Palacios, J. L., **Merino, M**., Hernandez, T., Sosa, K., Casaco, A., . . . Mateo de Acosta, C. (2012). Expression and biological characterization of an anti-CD20 biosimilar candidate antibody: a case study. MAbs, 4(4), 488-496. doi:10.4161/mabs.20761

Declaration of Academic Integrity

Declaration in accordance with Section 7 Paragraph 1 No. 4

I hereby declare in lieu of oath that I have researched and written this thesis myself, no passages of text have been taken from third parties without having been identified as such and that all tools, personal notifications, and sources used by the applicant have been indicated in the thesis.

The assistance of a professional consultant has not been utilized and no third parties have either directly or indirectly received monetary benefits from the candidate for work related to the contents of the submitted thesis.

The persons who have supported this work are listed below:

1. The isolation of total $CD4^+$ T cells using total $CD4^+$ Kit Isolation (Miltenyi) was performed by Carmen Hässig.
2. The RNA isolation and qRT-PCR shown in (Figure 6d and e) was done by Kathrin Förderer.
3. A list of transcription factors binding to the promoter of ATP2B4 obtained from published ChiP-seq data was provided by Dr. Martin Hart, Institute of Human Genetics, Saarland University with the help of Tim Kehl, Center for Bioinformatics, Saarland University
4. The Chromatin Immunoprecipitation (ChIP) experiments shown in (Figure 16b) was done by Dr. Dalia Alansary.
5. The microarray hybridization was performed at the Department of Human Genetics of the University Hospital of Saarland, Prof. Dr. Eckart Meese's lab with the help of Dr. Nicole Ludwig and the hierarchical cluster of genes and sample replicates shown in (Figure 7a) was done in collaboration with the Department of Clinical Bioinformatics, University of Saarland, Prof. Dr. Andreas Keller's lab with the help of Dr. Mustafa Kahraman.

No other people were involved in the preparation of the content of this thesis. In particular, I do not have the paid help from placement or Consultation services (doctoral advisors or other people) taken. Except for those specified.

The thesis has not been submitted to another examination authority in the same or a similar form in another procedure to obtain the doctoral degree, either in Germany or abroad. I affirm in lieu of an oath that I have told the truth to the best of my knowledge and have not concealed anything.

………………………………………..

Ort, Datum

Declaration of Academic Integrity

…………………………………………………..

Signature of the doctoral candidate

…………………………………………………

Signature of the official accepting the declaration in lieu of oath

Acknowledgments

I hereby want to thank to my supervisors Dr. Dalia Alansary and Prof. Barbara Niemeyer for the opportunity of working on an interesting immunological project and their supervision, support, enthusiasm and feedback throughout this project. I am also thankful for the opportunities to present my data at international meetings and for the ability to participate in immunological seminars and bioinformatics training schools.

Many thanks to Prof. Markus Hoth for his support and advice throughout the project.

I also want to thank all the members of the department of Biophysics at the University of Saarland for nicely introducing me into the group, helping me with experimental issues and supporting me in hard times. Thanks for the nice talks, laughs, coffees after lunch and all the fun in social events, which have made my instance at the university really pleasant and unforgettable.

I would also like to express my acknowledgement to all the assistance I received during my time in the department of Molecular Biophysics. I want to thank to Kathrin Förderer, Cora Hoxha, Carmen Hessig, Gertrud Schwär and Susanne Renno for their technical assistance, as well as Ute Luger and Regine Kaleja for their support with the paper work.

Thanks to Dr. Krause from the FACS Facility of the Institute of Physiology (DFG grant 207087572) for help with the FACSAria III sorter.

Last but not least, I would like to express my gratitude to my parents for always supporting me in any possible way. This work would not have been possible without their guidance and love.

Die experimentellen Arbeiten der vorliegenden Dissertation wurden im Institut für Biophysik am Zentrum für integrative Physiologie und Medizin der Universität des Saarlandes durchgeführt.

Dekan: Prof. Dr. Michael D. Menger

Berichterstatter: Prof. Dr. Barbara Anne Niemeyer-Hoth

                Prof. Dr. Robert Ernst

                Prof. Dr. Stephan Philipp

Tag der mündlichen Prüfung: 03.12.2021